A Multiscale and Multifunctional Design Method for Mesoscale Lattice Structures Fabricated by Additive Manufacturing Processes

by

Yunlong Tang

Doctor of Philosophy

Department of Mechanical Engineering

Faculty of Engineering

McGill University, Montreal

2017 June

A thesis submitted to McGill University in partial fulfillment of the requirements of the degree of Doctor of Philosophy

Abstract

Mesoscale lattice structures with different desired physical properties are promising for a broad spectrum of applications. However, intricate geometric features of these structures are usually difficult to be directly fabricated by traditional manufacturing processes. The availability of Additive Manufacturing (AM) technology has significantly relaxed the fabricating limitation of mesoscale lattice structures. It enables the fabrication of the tailored heterogeneous lattice structures which generally show a better performance than its homogeneous counterpart. However, the lack of suitable design methods and tools for heterogeneous lattice structures seriously hinders its wide application.

In this thesis, a general multiscale and multifunctional design methodology is presented to solve the issue mentioned above. This proposed design methodology aims to help designers to take advantages of multiscale design freedom provided by existing AM technologies. The general design flow of the proposed design methodology can be divided into three major design stages: initial design, design optimization and multiscale geometric modeling. In the first design stage, detailed design steps and their related design guidelines are developed to help designers to build the initial design space. Based on this design space, three different optimization methods are proposed, which can find the optimal design parameters for desired functional performance. At the end, the proposed multiscale geometric modeling method can be applied to construct the geometric model of optimized structures which can be directly fabricated by AM processes. This novel design methodology has been implemented in a computer-aided design tool. A design case has been conducted using this computer-aided design tool to validate the efficiency of the proposed design methodology. This proposed design methodology lays a foundation for the wide applications of mesoscale lattice structures fabricated by AM processes.

Résumé

Les structures en treillis de méso-échelle avec différentes propriétés physiques souhaitées sont prometteuses pour un large éventail d'applications. Cependant, les caractéristiques géométriques complexes de ces structures sont généralement difficiles à fabriquer directement par les procédés de fabrication traditionnels. La disponibilité de la technologie de fabrication additive a considérablement réduit la limitation de la fabrication des structures en treillis de méso-échelle. Elle permet la fabrication de structures en treillis hétérogènes sur mesure qui performent généralement mieux que leur homologue homogène. Cependant, le manque de méthodes et d'outils de conception appropriés pour les structures de treillis hétérogènes entrave gravement sa large application.

Dans cette thèse, une méthodologie générale de conception multiscalaire et multifonctionnelle est présentée pour résoudre le problème mentionné ci-dessus. Cette méthodologie de conception proposée vise à aider les concepteurs à tirer profit des avantages de la liberté de conception multiscalaire qui vient avec les technologies de fabrication additive existantes. La démarche générale de la méthodologie de conception proposée peut être divisée en trois grands stades: conception initiale, optimisation de conception et modélisation géométrique multiscalaire. Au premier stade de la conception, des étapes de conception détaillées et leurs directives de conception connexes sont développées pour aider les concepteurs à construire l'espace de conception initial. En se basant sur cet espace de conception, trois méthodes d'optimisation différentes sont proposées, ce qui permet de trouver les paramètres de conception optimum pour les performances fonctionnelles souhaitées. À la fin, la méthode de modélisation géométrique multiscalaire proposée peut être appliquée pour construire le modèle géométrique de structures optimisées qui peuvent

être directement fabriquées par des processus de fabrication additive. Cette nouvelle méthodologie de conception a été implémentée dans un outil de conception assisté par ordinateur. Plusieurs cas de conception ont été menés à l'aide de cet outil (conception assistée par ordinateur) pour valider l'efficacité de la méthodologie de conception proposée. Cette méthodologie de conception proposée établit une base pour les applications étendues des structures de treillis de méso-échelle fabriquées par des procédés de fabrication additive.

Acknowledgement

First and foremost, I want to thank my Ph.D. advisor Prof. Yaoyao Fiona Zhao. It has been an honor to be her first Ph.D. student. Dr. Zhao is open-minded and always encourages me to think freely. The insightful discussion with her always keeps me in the right direction of research. Moreover, Prof. Zhao also provides a timely feedback from industry to my research, which instills more practical value to my research. I appreciate all her contributions of time, ideas, and funding that make my Ph.D. experience productive and stimulating. Her enthusiasm on research motivates me in the pursuit Ph.D during hard time. Generally, I cannot accomplish this thesis without her kind help.

Besides my advisor, I would like to thank the rest of my thesis committee: Prof. Jorge Angeles, Prof. Francois Barthelat, for their insightful comments and encouragement, but also for the critical question which incents me to widen my research from various perspectives.

The members of Additive Manufacturing and Design Lab (ADML) have contributed immensely to my personal and professional time at McGill. The group has been a source of friendships as well as advice and collaboration. I would like to express my gratitude to those colleagues in ADML including, Sheng Yang, Zhibo Luo, Guoying Dong, Xin Xu, Han Chen, Yuhaowei Zhou, Fan Yang, Aidan Kurtz and Marc Wang etc., for everything they have done to help me along the study. Especially for the implementation of geometric modeling algorithms for lattice structures, Aidan provides a great help. He always brings me the latest geometric modeling techniques which refresh my mind.

I would also like to extend my gratitude to Natural Science and Engineering Research Council of Canada (NSERC) Discovery Grant (RGPIN 436055-2013), and China Scholarship Council

(CSC 201306020032), Rio Tinto – Richard Evans Graduate Fellowship, for the financial assistance of my research.

Importantly, I would express my great gratitude to my family who are always here to support my life and research. I would like to express my sincere thanks to my parents, Jinghua Shen and Jiancheng Tang, for their unselfishness dedication and support for my life. Throughout my life, my parents have done their uttermost to provide me a good environment. I would also like to show my special thanks to my wife, Qianqian, Ding, who has given up her career in China to accompany me in Canada. I am forever grateful for what she has done for me. Moreover, I would like to share this thesis with my one-year daughter, Tina Yuqing Tang. She has brought a lot of happiness to the family during my Ph.D. study period.

At the end, I would like to thank all my friends and relatives for their great support in my life.

Yunlong Tang

May 30, 2017

Claim of Originality

The author claims the originality of the main ideas and research results reported in this thesis. The most significant contributions are listed below:

1) A general design methodology for mesoscale lattice structures is proposed in this thesis. This general design methodology can be applied to take advantages of design freedom enabled by additive manufacturing technologies for multifunctional purposes.

2) The concepts of Functional Volumes and Function Surfaces are proposed. Guidelines for FV division are summarized. These concepts and guidelines assist designers to design a hybrid lattice-solid structure with a better functional performance.

3) The manufacturability of existing AM processes is considered during the design process of lattice structures based on the proposed manufacturability analysis model. This manufacturability analysis model can deal with lattice structures with different cell topology and relative densities.

4) Three different design optimization methods: BESO based method, heuristic optimization method and generalized relative density based optimization method are developed in this thesis. A comparison and guidelines are provided in this thesis to help designers select the suitable optimization method for their design.

5) An innovative multiscale geometric modeling method is proposed in this thesis. Compared to existing geometric modeling method, the proposed method can efficiently generate different types of lattice structures. It also supports the lattice structures with heterogeneous material distribution.

Some contents of this thesis have already been published in some journal and conference papers. The abstracts of these papers are listed in Appendix D.

List of Abbreviations

AM	**A**dditive **M**anufacturing
ANN	**A**rtificial **N**eural **N**etwork
ASTM	**A**merican **S**ociety **for T**esting **M**aterials
BESO	**B**idirectional **E**volutionary **S**tructural **O**ptimization
B-Rep	**B**oundary **R**epresentation
CAD	**C**omputer **A**ided-**D**esign
CAM	**C**omputer **A**ided **M**anufacturing
CNC	**C**omputer **N**umerical **C**ontrol
CSG	**C**onstructive **S**olid **G**eometry
CT	**C**omputed **T**omography
DDoF	**D**esign **D**egree of **F**reedom
DFAM	**D**esign **f**or **A**dditive **M**anufacturing
DFM	**D**esign **f**or **M**anufacutring
DSP	**D**ecision **S**upport **P**rogramming
ESO	**E**volutionary **S**tructural **O**ptimization
FDM	**F**used **D**eposition **M**odeling
FGM	**F**unctional **G**raded **M**aterial
FEA	**F**inite **E**lement **A**nalaysis
F-P-P-D	**F**unction-**P**erformance-**Pr**operty-**D**esign parameter
FS	**F**unctional **S**urface
F-Rep	**F**unctional **R**epresentation

FV	**F**unctional **V**olume
IDE	**I**ntegrated **D**evelopment **E**nvironment
IO	**I**nput/**o**utput
MMA	**M**ethod **of M**oving **A**symptotes
NC	**N**umerical **C**ontrol
PAMP	**P**orous **A**nisotropic **M**aterial with **P**enalization
PBC	**P**eriodic **B**oundary **C**ondition
PBG	**P**hononic/**P**hotonic **B**and **G**ap
PFA	**P**roduct **F**amily **A**rchitecture
P-HGM	**P**refabrication- **H**ybrid **G**eometric **M**odeling
PI	**P**erformance **I**ndex
RBE	**R**igid **B**ody **E**lement
SDK	**S**oftware **D**eveloper **K**it
SHM	**S**tructural **H**ealth **M**onitoring
SIMP	**S**olid **I**sotropic **M**aterial **P**enalization
SLM	**S**elective **L**aser **M**elting
SLS	**S**elective **L**aser **S**intering
SPL	**S**oftware **P**roduct **L**ine
SQP	**S**equential **Q**uadratic **P**rogramming
STL	**St**ereo **L**ithography
UAV	**U**nmanned **A**ero **V**ehicle
UI	**U**ser **I**nterface

Table of Contents

List of Figures

List of Tables

List of Algorithms, Rules and Guidelines

Algorithms

Rules

Design Guidelines

Chapter 1 Introduction

Design is the creation of a plan or convention for the construction of an object, system or human interactions [1], while manufacturing can be regarded as a process to implement the result of design into a real product. These two processes are closely related to each other and mutually promoted. On the one hand, the increasing complexity of a designed product requires the development of advanced manufacturing technologies. For example, the first prototype of Numerical Control (NC) machine was developed by John T. Parsons to produce the rotor blades with complex outline which is difficult to be manufactured with traditional milling machines [2]. On the other hand, the development of manufacturing technologies also drives the innovation of new design methods and their related tools. The rapid development 3-Dimensional (3D) Computer-Aided Design (CAD) software is a good example. The urgent demand of design tools which can deal with complex three-dimensional curved surfaces fabricated by advanced 5-axis Computer Numerical Control (CNC) machine drives the evolution of CAD technology from 2-Dimensional (2D) into the 3D era.

Like the case of 3D CAD techniques mentioned above, this thesis is dedicated to developing an innovative design method which takes advantages of the new design freedom enabled by the advancement of Additive Manufacturing (AM) technologies. The proposed design method specially focuses on the design and optimization of mesoscale lattice structures fabricated by AM processes. It aims to assist designers to take advantage of these structures to further improve the functional performance of the designed product.

In this chapter, the research background of this thesis is introduced. A detailed introduction on lattice structures is firstly provided, which is followed by a brief review of available manufacturing

methods on lattice structures. In this review, design freedom and challenges enabled by AM processes on mesoscale lattice structures are emphasized. To deal with the summarized challenges, the objectives of this research are proposed in Section 1.3. In Section 1.4, the organization of this thesis is introduced. At the end, a summary is made.

1.1 Lattice structures

The word 'lattice' originally means a framework or structure of crossed wood or metal strips and can be extended to a regular geometric arrangement of points or objects over an area or in space [3]. This word can be used to describe different objects with the same characteristics. For example, in crystallography, 'lattice' is used to describe the arrangement of atoms on a microscale. In this thesis, the lattice structure is defined as a type structure which consists of interconnected struts or walls with a certain repeated arrangement in 3D space. It can be considered as a type of cellular structures [4]. Compared to other types of cellular structures, such as foams and woods, lattice structures are more flexible to achieve a wide range of desired physical properties including high stiffness-weight ratio [5], low thermal expansion coefficient [6], negative Poisson ratio [7], and high heat dissipation rate accompanied with active cooling [8]. Moreover, it can also be used to design a bio-implant to enhance the ossesointegration as well as alleviating stress-shielding effect. Due to its outstanding performance, lattice structures have been used in a broad spectrum of applications, including bone and dental implants [9-11], ultralight structures [12, 13], energy absorbers[14], low thermal expansion structures [15], and conformal cooling [16].

Based on the size of a lattice unit cell, lattice structures are classified into three major design scales. They are microscale(<0.1mm), mesoscale (0.1mm to 100mm) and macroscale (>100mm) lattice structures. In this thesis, the lattice structure on mesoscale is the focus, since it can be easily fabricated by existing AM processes. Thus, otherwise stated, the lattice structures mentioned in

the following contents of this thesis all indicate mesoscale lattice structures.

Lattice structures can be classified into two groups based on their geometric configurations. They are 2D lattice and 3D lattice. 2D lattice structures are also widely known as honeycomb structures. It is made of two-dimensional cells which have been extruded in the third direction to fill a 3D space. As to 3D lattice structures, it can be considered as a structure with cells made of space truss. 3D lattice structures on mesoscale can also be called as mesoscale truss structures. The difference between these two types of lattice structures is shown in Figure 1-1. It is obvious that 2D lattice structures can be regarded as a special type of 3D lattice structures where the struts of cells are stacked along a certain direction into solid walls.

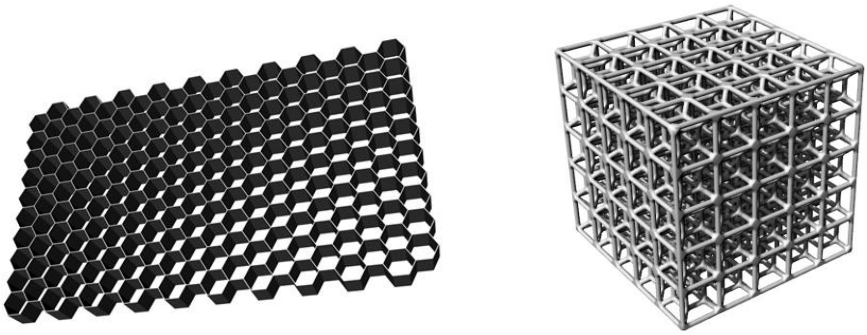

(a) An example of 2D lattice (b) An example of 3D lattice

Figure 1-1 Comparison between 2D and 3D lattice structures

Based on the degree of order, lattice structures can be further divided into three types. They are randomized lattice structures, uniform lattice structures and pseudo-periodic lattice structures. In randomized lattice structures, the shape and size of lattice cell are randomly distributed in the design domain. The typical randomized lattice generated based on Voronoi cells is shown in Figure 1-2(a). This type of lattice structures is usually used in the bio-related applications to simulate the microstructure of human bone [17].

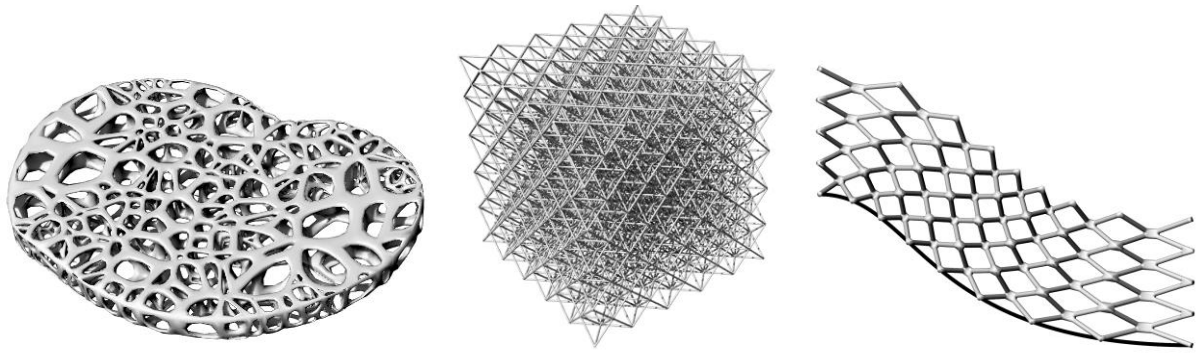

(a) Randomized lattice (b) Uniform lattice (c)Pseudo-periodic lattice

Figure 1-2 Three different types of lattice structures

The second type of lattice structures is called uniform lattice structure. This type of lattice structures can be regarded as a structure created by a regular periodic repetition of unit cells with a certain shape, topology and size in a 3D Euclidean space. Thus, every cell in this type of lattice structures has the same topology and size. A typical uniform lattice structure with octahedron cell topology is shown in Figure 1-2(b). Since cell is periodically distributed, this type of lattice can be also called as periodic lattice structures. The uniform lattice structures can be further divided into two types: homogeneous uniform lattice structures and heterogeneous uniform lattice structures. The homogeneous lattice structure means all the struts (3D lattice) or walls (2D lattice) have the same thickness, while the thickness of the strut or wall inside heterogeneous lattice varies over the entire structure. The difference between these two types of lattice structures is shown in Figure 1-3. By optimizing the strut's thickness distribution, the performance of designed lattice structures can be further improved [12].

(a) Heterogeneous lattice (b) Homogeneous lattice

Figure 1-3 Difference between two types of uniform lattice structures

The third type of lattice structures is called pseudo-periodic lattice structures (shown in Figure 1-2(c)). In this type of lattice structures, lattice cell only shares the same topology but with different size and shape. By changing the size and shape of lattice cells in the design space, this type of lattice structures can achieve some special properties. For example, the conformal lattice structure which is firstly proposed by Wang and Rosen [20] is a typical pseudo-periodic lattice structure. In a conformal lattice structure, the shape and size of each unit cell is varied to adapt to the macro-shape of its design space. Compared to periodic lattice structures, all cells on the boundary of conformal lattice structures keep their integrity, and there is no partial cell located on its boundary. Generally, pseudo periodic lattice can be viewed as a type of lattice structures located between disordered lattice structures and periodic lattice structures. If lattice cell is small enough, the lattice structure in each local region can be viewed as a periodic lattice structure. However, it cannot be considered as a pure periodic lattice structure globally, since the size and shape of cell vary globally in the design space of lattice structures. Moreover, like uniform lattice structures discussed above, pseudo-periodic lattice structures can also be divided into two sub-types based on the distribution of strut's thickness. They are homogenous pseudo-periodic lattice structures and heterogenous pseudo-periodic lattice structures. For simplicity, in this thesis, both homogeneous pseudo-periodic lattice and homogeneous uniform lattice are collectively called as homogeneous lattice structures. Similar naming rule is also used for heterogeneous lattice structures.

1.2 Manufacturing methods of lattice structures

The manufacturing methods which are available to fabricate lattice structures are divided into two categories: traditional manufacturing methods and AM processes. These two categories of manufacturing methods will be discussed in the following two sub-sections respectively.

1.2.1 Traditional manufacturing methods

Traditionally, lattice structures are mainly used as the core of sandwich panels or columns. To manufacture these structures, several traditional manufacturing methods are available. For example, metallic lattice structures can be made by investment casting using volatile wax or polymer patterns [18]. In this process, the pattern can be prefabricated either by AM processes [19] or injection molding [20]. Besides investment casting, lattice structures can also be fabricated by the combination of sheet metal forming and material joining processes. The fabricated lattice core of each layer can be joined together by welding process. Compared to the investment casting process, the sheet metal forming process is more efficient. It is suitable for mass production of lattice cores of sandwich panels. In addition to sheet metal forming, the weaving and braiding process of metallic wires is another option for lattice structures fabrication. Both solid wire and hollow wire can be used to fabricate lattice structures. Compared to sheet metal forming, this method is also cheaper since only simple tools are needed [21].

However, it should be noted that all the traditional manufacturing methods discussed above can only be applied to fabricate lattice structures with few simple cell topologies in a design domain of regular macro-shape. In the following sub-section, detailed information of AM process and its application on mesoscale lattice structures will be discussed.

1.2.2 Additive Manufacturing

Traditional manufacturing methods seriously limits the complexity of lattice structure that they can fabricate. AM technologies produce parts by adding materials at desired place. It is a young manufacturing technique with about 30 years of history [22]. This process is formally defined by American Society for Testing Materials (ASTM) as a “process of joining materials to make objects from 3D model data, usually layer upon layer, as opposed to subtractive manufacturing

methodologies" [23]. AM processes are classified into several categories according to ASTM standard [23]. The comparison between different types of AM process is summarized in Appendix A of this thesis.

Generally, AM technologies can be used to fabricate parts made of a wide range of materials. Compared to traditional manufacturing methods, such as CNC machining, casting and sheet metal forming, AM has many unique advantages [24]. Firstly, it enables the fabrication of structures with multiscale complexities, and provides a great design freedom for designers to further improve product's functional performance. Secondly, several types of AM technologies [25-27] can process multiple materials either simultaneously or sequentially. Materials can be processed at each point or at each layer at a time enabling the manufacturing of parts with complex material compositions and designed property gradients. Thirdly, this manufacturing process can significantly decrease the lead time between design and manufacturing process because no additional tools, such as casting mode or forming die, are needed. The design can be directly fabricated from a 3D digital model. Moreover, AM processes can also reduce the generation of waste materials compared to traditional subtractive manufacturing methods. Thus, it is more environmentally friendly [28].

Due to these unique capabilities, AM technology is an ideal candidate for the fabrication of complex mesoscale lattice structures, especially those structure that are designed for tailored unique physical properties. Figure 1-4(a) shows the AM fabricated lattice structures whose thermal expansion coefficient is negative. Figure 1-4(b) presents a bio-implant of cranial bone which is fabricated by Selective Laser Melting (SLM) one of widely used AM processes. To fit the fracture region of patient's cranial bone, the macro shape of lattice structures is reconstructed from Computed Tomography (CT) scan on the surrounding cranial bone. Moreover, lattice structures made of multi-materials can also be fabricated by certain types of AM processes such as Poly-Jet

technique[29]. This process can be used to fabricate lattice structures which are made of Functional Graded Materials (FGM).

(a) 3D-printed lattice cell with negative thermal expansion coefficient[30]

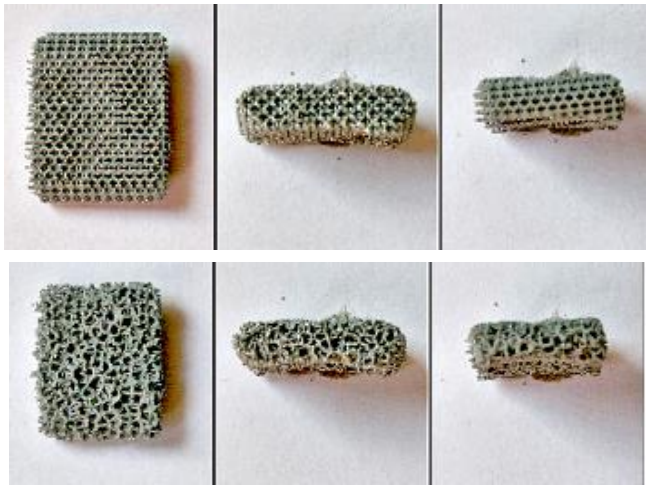

(b) Bio-implant for cranial bone with mesoscale lattice structures

Figure 1-4 Examples of mesoscale lattice structures fabricated by AM process

To summarize, AM technologies significantly increase the design freedom of lattice structures. It enables designers to further tailor the physical properties of designed lattice structures to achieve better functional performance. However, it should also be noted that every manufacturing process has limitations, even for AM process. There are still certain manufacturing limitations on the complexity of lattice structures which AM process can achieve [31]. Thus, designers should also consider these limitations during the design process.

1.3 Research objectives

To take full advantage of those unique capabilities brought by AM processes on mesoscale lattice structures, an efficient design method which can consider both AM enabled design freedom and manufacturing constraints is needed. Based on the careful review of existing design methods in Chapter 2, it is found that most related research only focuses on a single design scale or a single function. There is no valid multiscale and multifunctional design method to help designer design the combination of solid and lattice structure to achieve multifunction. Such method is greatly needed to support innovative product design. The review discussed in Chapter 2 also shows the lack of efficient geometric modeling method for lattice structures with multiscale complexity which is another obstacle for designers. To solve these issues, the research objectives of this thesis are summarized below.

1) To develop a multiscale design method for parts with hierarchical complexity on both macro and mesoscale. Although, in aerospace and automobile industries, parts with mesoscale structures, such as sandwich panels, have already been widely used, there is no theoretical design method which simultaneously considers the design on macro and mesoscale. In another word, the design optimization of solid structures is usually neglected when a certain optimization method is applied on lattice structures. The developed design method takes advantages of both solid and lattice structures, which can further improve the functional performance of designed products.
2) To develop a design method which can deal with the part for multifunctional purposes. The design freedom enabled by AM technology allows the integration of multifunction in a single part. Thus, it is imperative to develop a design method which can simultaneously improve performances for multiple functions.

3) To develop an efficient geometric modeling method which can directly generate the digital model of lattice structures with multiscale complexities. Moreover, this method should be flexible enough to deal with different type of lattice structures.
4) To integrate those developed methods into a general design methodology. This general design methodology can be used by designers who want to take advantages of lattice structures for different functional purposes. A CAD tool needs to be implemented to support this general design methodology, and can assist designers to design and generate lattice structures.

1.4 Thesis organization

To detailed describe the developed design methodology, the following contents of this thesis are organized as below. Its graphical view is shown in Figure 1-5.

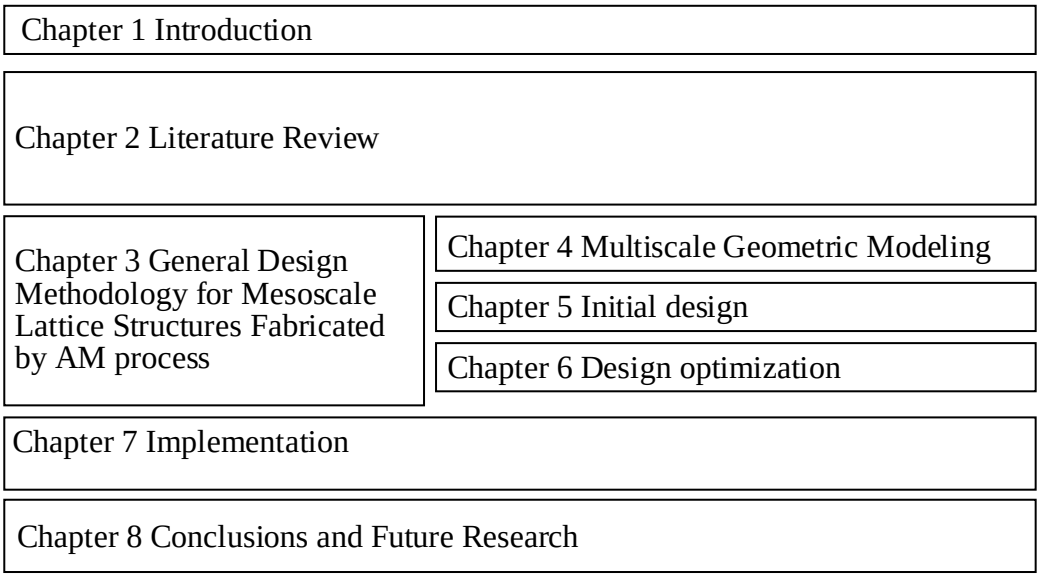

Figure 1-5 The graphical view of the thesis organization

Chapter 2 gives a thorough survey of design methods for additive manufacturing to improve the functional performance of parts. This survey specially focuses on the mesoscale lattice structures. The existing design and optimization methods for mesoscale lattice structures have been

discussed and compared. A conclusion of the issues of current research is summarized. Based on this conclusion, several future research perspectives are pointed out. This chapter can be used as an informative source for designers and researchers working in this field.

To solve the summarized issues from Chapter 2, a general multiscale and multifunctional design methodology for mesoscale lattice structures is proposed in Chapter 3. In this chapter, several basic concepts of the proposed design methodology are firstly introduced. Then the overall framework of developed design methodology is provided. The design flow of the proposed design methodology can be mainly divided into three stages: initial design, design optimization and geometric modeling. The functions of each major design stage are discussed in detail. At the end of this chapter, a summary is made to emphasize the difference between the proposed design methodology and other existing design methods.

To further introduce the details of the proposed design methodology, each design stage of the proposed design methodology will be discussed in the following three chapters respectively. Among them, the multiscale geometric modeling method is introduced at first in Chapter 4, since some terminologies defined in this chapter will be used in the introduction of the design methods for other two design stages. In this chapter, the basic concepts and terminologies used in the proposed geometric modeling methods are formally defined at the beginning. Then, the general geometric modeling process is introduced. Detailed algorithms for each major step of the geometric modeling process are discussed. At the end of this chapter, several case studies have been provided to prove the effectiveness and efficiency of the proposed method.

After the detailed discussion of geometric modeling process of lattice structures, Chapter 5 mainly focuses on the design methods and its related techniques used in the initial design stage. In this chapter, the general design flow is given. Some design guidelines are summarized to assist

designers for decision making during the initial design stage. These detailed design process and guidelines are illustrated with selected design cases.

In Chapter 6, detailed discussion on the developed optimization methods is presented. In this chapter, a design case is used to illustrate the procedures to construct F-P-P-D model at the beginning. This developed model can be used to help designers to analyze complex relations between functions and the selected design parameters. Then, three developed optimization methods for mesoscale lattice structures are introduced respectively. At the end of this chapter, design cases are provided to validate the proposed method. A comparison is made between the developed optimization methods. Based on this comparison, a guideline is summarized to help designers to select suitable optimization methods for their design tasks.

To implement the proposed general design methodology and the optimization methods introduced above, a software tool called Intralattice is developed and carefully introduced in Chapter 7. In this chapter, the software development environment is presented at first. Then, a detailed discussion is made on the framework of software and its operation flow. At the end of this chapter, a design case is made to further illustrate how to use this developed design tool during the design process. The result of this case study also shows the efficiency of the proposed design methodology.

At the end of this thesis, a general conclusion is given. The future research perspectives are also pointed out in Chapter 8.

There are four Appendences attached at the end of this thesis. Appendix A contains a table which summarizes different types of AM processes. Appendix B illustrates the detailed steps and formulations to evaluate the gradient of functional performance parameters. Appendix C summaries developed User Interface (UI) for Intralattice. Appendix D includes a list of

publications during Ph.D. period. This list includes five published journal papers, one submitted journal paper, one book chapter, and four peer reviewed conference papers. The abstracts of five published journal papers are also attached at the end of Appendix D.

1.5 Summary

In this chapter, a brief introduction of research background and research objectives are given. At the beginning, the definition of a lattice structure and its classification method are discussed. Then, available manufacturing methods for lattice structures are reviewed. Unique capabilities of AM processes on lattice structures are emphasized. To take full advantages of AM enabled design freedom, a general design methodology on mesoscale lattice structures is needed. To develop this method, four research objectives are summarized. At the end of this chapter, the overview of the entire thesis structure is presented

Chapter 2 Literature Review

Additive Manufacturing is defined as a material joining process whereby a product can be directly fabricated from its 3D model [23]. Compared to other manufacturing methods, such as machining or casting, AM processes have the following unique capabilities. Firstly, parts with complex shape can be built by AM processes without additional tools or fixtures. Secondly, some AM techniques are suitable for processing multiple materials either simultaneously or sequentially; therefore, parts with complex material compositions can be easily achieved. Thirdly, lead time between design and manufacturing can be substantially reduced, since the part is directly fabricated from its 3D model. These unique capabilities of AM technologies have brought great application potentials in several major industries such as aerospace [32] and medical implants manufacturers [33]. For example, in the aerospace industry, lightweight, strong and sometimes electrically conductive parts are more desired. AM process can produce lightweight components by replacing solid material with lattice structures. Gradient electrical conductivity can also be achieved by changing the composition of materials at each fabrication point or each fabrication layer. Major airplane manufacturers such as Boeing, Airbus, and Northrop Grumman have all identified AM to be an emerging and revolutionary manufacturing method [34].

However, it is a challenge for most designers to fully take advantage of the unique capabilities brought by AM for two main reasons. Firstly, design rules or guidelines for traditional manufacturing methods are deeply rooted in designers' mind. These design rules and guidelines restrict designers to further improve the performance of products by designing an intricate part fabricated by AM processes. Secondly, the lack of design and analysis tool for complex structure is another obstacle for designers to take use of AM technologies. For example, even though the

lattice structure fabricated by AM process has been proved to have a better weight-stiffness ratio, it is difficult to model this type of structure with most existing commercial featured-based CAD systems.

To overcome those difficulties mentioned above, the design methods which can consider the unique capabilities of AM technologies are needed. These design methods are not only required to improve the manufacturability of products fabricated by AM processes, but also should consider how to improve the overall functional performance of designed products with the unique capabilities brought by AM. To achieve the above objectives, in this thesis, a concept called as Design for Additive Manufacturing (DFAM) is proposed.

"Design for Additive Manufacturing is a type of design methods whereby functional performance and (or) other key product life-cycle considerations such as manufacturability, reliability and cost can be optimized subjected to the capabilities of additive manufacturing technologies."

This concept provides a broader perspective of design techniques which can take advantages of the design freedom enabled by AM technologies. It has intersections between many traditional DFX methodologies such as Design for Manufacturing, Design for Maintenance and Design for Cost. However, unlike most traditional Design for Manufacturing and Cost methods which mainly aims at tailoring designs to minimize manufacturing difficulties and cost, DFAM also provides an opportunity for designers to take use of the unique capabilities of AM technologies in the design process to improve functional performance. To emphasize this unique opportunity brought by AM technologies, this chapter mainly focuses on those DFAM methods for the improvement of functional performance. Thus, unless otherwise specified, the narrow perspective of DFAM is used to indicate those DFAM which are developed for the improvement of functional performance.

Some of these DFAM methods have already been employed in several different fields. For example, in the aerospace industry, topology optimization, one of the DFAM methods, serves to reduce the weight of products and increase their stiffness. Complex optimized shapes of products can only be fabricated by AM techniques. In bioengineering, the bio-implant with mesoscale structures can be designed by DFAM methods. This type of bio-implant can achieve the same mechanical properties of real human bone, which avoids stress shielding after surgery. Due to its wide application, DFAM has recently attracted a great interest from different application fields.

This chapter aims to provide a comprehensive review of state of the art DFAM methods. This review can provide a guide for designers who want to take advantages of AM technologies to further improve the products' performance, as well as the foundation for the developing of new DFAM methods. To achieve this goal, existing DFAM methods are classified into three categories based on their design scales. The design methods on each scale will be respectively reviewed in the next three sections. At the end of this chapter, the discussion and summary will be made based on the reviewed DFAM methods. Then some future research perspectives will be pointed out.

2.1 Macroscale design methods

Available DFAM methods on macroscale are further divided into two categories. The first category mainly includes those DFAM methods focusing on the improvement of functional performance based on structural optimization methods, while the second category of design methods mainly contains those DFAM method for customized part design. These two categories of design methods will be reviewed in the following two sub-sections respectively.

2.1.1 Structural optimization methods for AM

On macroscale, different types of structural optimization methods can be directly applied to improve the structural performance of parts fabricated by AM processes. Generally, structural

optimization methods can be divided into three groups: size optimization, shape optimization and topology optimization. Compared with other two types of structural optimization methods, topology optimization does not only optimize the boundary shape of a structure but also changes its topology, which can offer better performance under certain requirements [35]. Thus, topology optimization has received extensive attentions from designers, especially in the conceptual design stage. Initially, topology optimization methods are proposed to only focus on structural performance. Now, this type of optimization methods has spread to a wide range of disciplines, including fluid [36], acoustic [37], control [38], optics [39].

Table 2-1 Comparison between different types of topology optimization techniques

Method Name	Advantages	Disadvantages
Ground Structure	• Easy to be implemented; • Suitable for low volume truss structure	• Initial configuration of ground structure has a significant impact on the result. • Not suitable for the optimization of continuum structure
SIMP	• Easy to be implemented; • Requires less storage as well as computational time.	• Optimization result depends on the penalty factor; • Difficult to interpret the region with intermediate density
Level Set	• No checkerboard effects of SIMP methods	• Solution may be different for different starting point
Homogenization	• It can be used to optimize structures with intermediate density;	• It takes more time and storage space to calculate the effective properties of materials with intermediate density
Evolution	• Non-gradient based method	• The rate of convergence depends on the parameters used in the algorithm
Genetic Algorithm	• Non-gradient based method	• large computation load is needed even for simple problem;

Several different topology optimization techniques including ground structure method [40, 41], homogenization method [42], Solid Isotropic Material with Penalization (SIMP) method [43], level set method [44, 45], evolutionary method [46, 47] and genetic method [48, 49] have been developed. Each of them has its own advantages and disadvantages. A brief comparison between these methods is summarized and shown in Table 2-1. The detailed technical review of each type

of topology optimization method is beyond the scope of this chapter. In this chapter, we are focusing on the application of topology optimization method on the design process for AM technologies. For more detailed information, there are some comprehensive review papers [50, 51] which readers can refer to.

Among those different types of topology optimization technique listed in Table 2-1, ground structure method is the most suitable approach for truss like structure. It can be applied for both macroscale and mesoscale truss like structures, such as lattice structures. For example, the lattice structure fabricated by Selective Laser Sintering (SLS) process is designed for the wing of Unmanned Aerial Vehicle (UAV) by Navasivayam and Seepersad [52] to decrease the deviation from intending surface profile. In the design process, ground structure based topology optimization technique is used to determine the detailed configuration of the lattice structure under the skin of a wing. Besides ground structure method, SIMP techniques can also be applied on macroscale to improve the structural performance of the designed part. Lin et al. [53] take use of SIMP method to design adaptive cores of the structure for a uniform beam which is capable of large deflection while simultaneously processing load carrying capabilities. Another SIMP based method has recently been used by Gaynor et al. [25] to design multi-material compliant mechanisms fabricated via PolyJet technique. In this design method, the SIMP approach is modified by combination with a combinatorial SIMP approach and multiphase SIMP approach to design the multi-material topology for compliant mechanisms. In addition to SIMP, Bidirectional Evolutionary Structural Optimization (BESO) method is also used by Aremu et al. [54] to optimize an aerospace component. This research shows evolutionary optimization methods can steer the solution to an optimum with features suitable for AM process by careful selection of a suitable set of optimization parameters.

To further consider the manufacturability of selected AM process during the design optimization process on macroscale, several design methods have been developed. For example, Leary et al. [55] has proposed a design method to seek the optimal topology of designed parts which can be printed without support structures. In this design method, the theoretically optimal topology is modified to ensure the manufacturing process without requiring additional support material. Another design method technique is proposed by Gardan and Schneider [56] to seek the optimized internal pattern fabricated by SLS process. In this method, manufacturing constraints and considerations generated from the knowledge management of SLS process are integrated into the topology optimization process. In addition to that, some pre-designed cleaning channels are added to the final optimized result to ensure the powders cleaning inside the internal cavity.

Besides those methods mentioned above which only focus on improving the functional performance related to a single function, Brackett et al. [57] has proposed a topology optimization based design framework for multi-functional 3D printing. In this design framework, the automated placement and routing of electrical systems are integrated into the topology optimization process for Structural Health Monitoring (SHM) product. This framework has recently been extended to 3D design by Panesar et al.[58].

Besides those academic efforts mentioned above, some commercial software like OptiStruct [59] have also been developed to help designers with less knowledge and experience on structural optimization. This software has been successfully applied to optimize parts fabricated by AM processes [60, 61]. However, more developing work should be done to further integrate the unique manufacturing capabilities and constraints of AM in the structural optimization process.

2.1.2 DFAM methods for customized products

Another notable type of DFAM methods on macroscale is the design of customized products.

This type of DFAM methods has a wide application on customized medical devices and personal products. Compared to standard medical devices, customized devices can provides an individual fitting and adequate match which will further improve the surgical outcome [62]. The general design and manufacturing flow of customized medical devices is summarized and shown in Figure 2-1. This general flow mainly consists of five steps: image acquisition, image post-processing, surgical planning, customized devices design and AM fabrication. Now several customized prostheses, such as cranial bone [63-65], hip joint [66] and femoral joint [67], have already been successfully designed and fabricated. The results of these successful cases foresee the brilliant future of customized medical devices fabricated via AM processes. Besides customized medical devices, some consumer goods, such as customized shoes [68], are also successfully designed to address the individual requirements of customers. These customized products can further improve user experience compared to their original designs.

Besides those successful cases of customized products mentioned above, several research has recently been done to further facilitate the efficiency of current customized design process for AM technologies. For example, a template based design method for customized products is proposed by Ariadi and Rennie [69]. In this design method, a product template provided by Product Family Architecture (PFA) is generated to allow consumers to develop a customized product. An investigation has been done by Ariadi et al. [70] to further study the potential for consumers who will design their own products. The result of this investigation shows the possibility that consumers can be involved in the design procedure of customized products. Moreover, the result of this research also suggests that a careful attention must be paid on consumers' product preferences and their ability to use software. A specific CAD tool for computer mice is developed by Zhou [71]. In this design tool, a co-design method is used to enable customers to decide the size and shape of

mouse. In order to establish a connection between customization design for AM and software product line (SPL) engineering, an exploratory study [72] has been done on the popular 3D printing customization website called "Thingiverse"[73]. This research provides hints that SPL-alike techniques can be also used in the design process of customized products fabricated by AM processes. To summarize current research on DFAM methods for product customization, it can be concluded that most studies are focusing on co-design methods which enable customers to participate in a design process. However, how to share the design knowledge and information between designers and customers is still an issue for this type of design methods. Moreover, the role of surgeon or other people with specialized knowledge is also needed to consider in the design process of customized products.

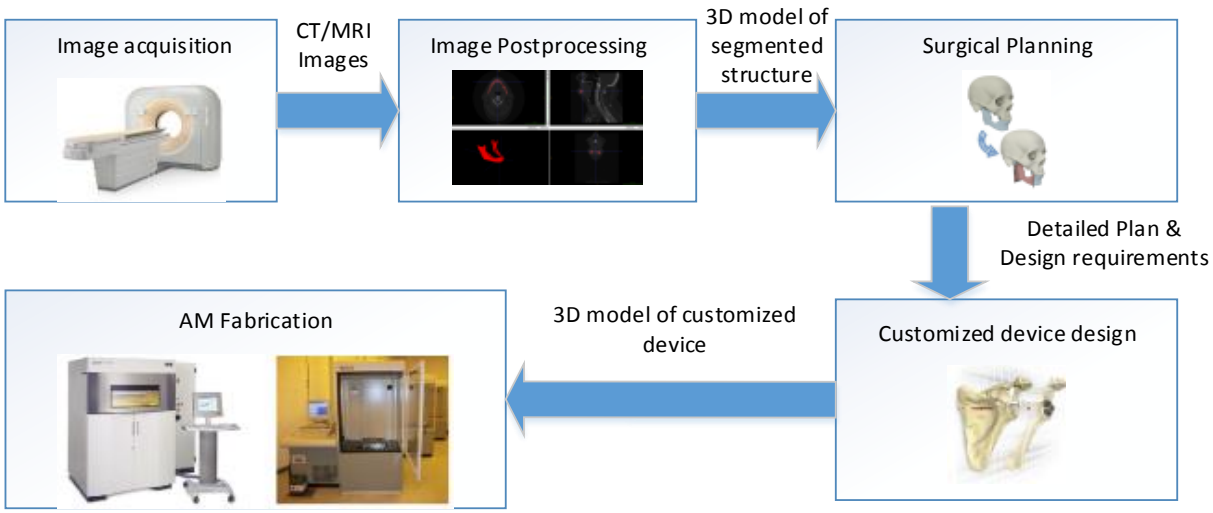

Figure 2-1 General design and manufacturing flow of customized medical device

2.2 Mesoscale design methods

On mesoscale, cellular structures are widely used to achieve an excellent performance and multi-capabilities while reducing weight. The word 'cell' derives from the Latin cella which means a small room [74]. Cellular structure can be regarded as a kind of structure that consists of an interconnected network of solid struts or plates which form the edges and faces of cells [75]. This

kind of structure is common in nature, such as wood, bone and coral. It can bear a long-term static or cyclical load. These natural cellular structures have been used by humans for centuries. Recently, some man-made cellular structures have been designed and fabricated for their multi-functionalities such as weight reduction, energy absorption, heat transfer, thermal protection and insulation [75-79]. Among those available man-made cellular structures, a lattice structure which consists of interconnected struts or walls exhibit excellent performance. Comparing to other types of cellular structures including woods and metal foams, lattice structures are easier to be tailored for the desired properties. Moreover, as it is summarized in Chapter 1, the rapid development of AM processes also significantly enlarges the design freedom of lattice structures. To takes advantages of these design freedoms, several available design methods can be used. In this section, a comprehensive review will be made on the design methods which can be applied on mesoscale lattice structures. The available design methods will be divided into two portions for different types of lattice structures and reviewed respectively in the next two sub-sections. Besides DFAM methods for mesoscale lattice structures, their available geometric modeling methods are also summarized in this section, since it plays an imperative role in the design and manufacturing process of mesoscale lattice structures. Some issues of existing geometric modeling methods for mesoscale lattice structures are summarized at the end.

2.2.1 DFAM methods for homogeneous lattice structures

For material scientists and engineering designers, homogeneous uniform lattice structures on mesoscale can be regarded as homogeneous materials on macroscale. The effective properties of lattice structure on macroscale can be calculated by several homogenization methods [80]. Based on the calculated effective properties, the macro shape of homogeneous lattice structure can be designed by macroscale design methods such as structural optimization methods. On mesoscale,

material selection strategy [81] shown in Figure 2-2 can be applied to select an appropriate mesoscale cell topology with respect to design requirements. Besides directly selecting existing lattice topologies in a material chart, sometimes, designers can also design a lattice structure with new cell topology on a meso or microscale to fill the blank area of material chart for some desired properties. The technique called as "inverse homogenization" is first proposed by Sigmund [82, 83] to optimize material distribution in each unit cell for desired material properties. Based on pioneering works of Sigmund, various structural optimization techniques have been applied to design the geometry of each unit cell on meso or microscale. So far, three types of topology optimization methods including ground structure optimization method, SIMP and BESO have been successfully applied to design a lattice unit cell for desired mechanical properties [82-87]. Besides mechanical properties, some computational methods are developed to design cell's topology and structure for other types of desired properties, such as thermal conductivity [88], electromagnetic property [89], or combination of several properties at the same time [90-92]. Readers should be noted that the inverse homogenization technique can also be used for micro-cell design, which will be detailed discussed in Section 2.3.

There is a certain limitation of homogenization method on the effective physical properties of lattice structures which are related to non-local, scalable dependent governed phenomenon[93]. For example, it cannot be directly used to calculate the effective Nusselt number on macroscale when lattice structures are used under forced convective cooling condition. To solve this issue, the innovative multifunctional design method for the topology of 2D homogenous lattice cell are developed by Seepersad et al. [93]. This design method generally considers two different functions: ultralight load bearing and active cooling. The performance related to these two functions are sequentially optimized by a two-stage topology design approach.

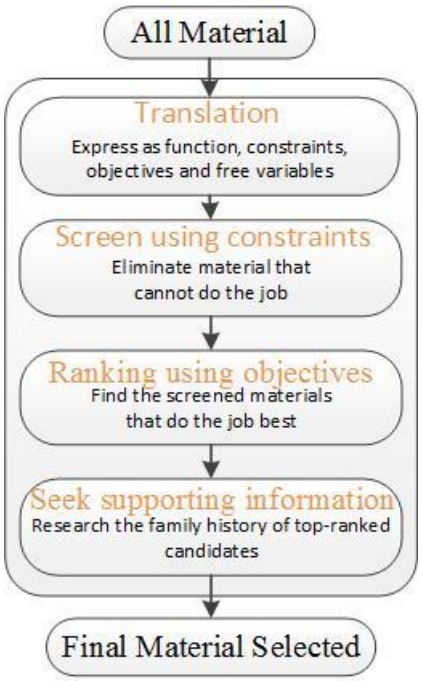

Figure 2-2 Strategy of material selection for design [81]

Besides directly using the available design methods on macroscale based on the homogenized effective properties, some design methods are proposed for the specific weight efficient parts with meso-lattice core, such as sandwich panels and beams. Strictly speaking, these design methods cannot be fully considered as DFAM, since they are not developed to take unique capabilities of AM processes. However, these methods are still included in this chapter, since they can also be applied to the design process of lattice structures fabricated by AM processes. Among them, a design method for sandwich panels has been developed by Desphande and Fleck [94]. This method aims at the design and analysis of truss core sandwich structures with either solid face or triangulated face-sheets. By modeling triangular truss as pin-jointed assemblies, effective properties of triangular truss core and face are calculated. Based on the calculation result, a collapse mechanism map is generated. With this map, an optimization procedure can be performed graphically based on equations of failure modes for the faces and core. Then, the optimal sandwich beam of minimum weight for a given structural load index can be selected. The result of their

research shows that sandwich beams with lattice cores are significantly lighter than competing concept with foam cores. Another weight minimization of sandwich panels with truss cores is proposed by Wicks and Hutchinson [95, 96]. In their design method, two different loading conditions: shear-bending and compression are considered with [96] or without [95] crushing stresses applied to the face. Instead of calculating effective properties of truss cores, the relationship between external load and stress in each structural member is established by analysis of the truss structure. This method assumes that the faces and core are made of the same material and design is only subjected to strength constraints based on four failure modes of lattice. Sequential Quadratic Programming (SQP) method is used to solve this optimization problem. The result of their method also shows that solid sheet faces and truss cores are highly efficient from a weight standpoint. Another generalized closed form optimization procedure for sandwich structures with a truss core is proposed by Rathbum et al [97]. It also takes minimum weight of sandwich panels as the design objective. However, instead of using optimization algorithm, design parameters are solved directly by three in-active strength constraints. Then the fourth strength constraint is used to check whether the previous solution is admissible. This method can deal with four types of lattice topologies: tetrahedral, pyramidal, 2D square cell and corrugated sheets.

Compared to those design methods for sandwich panels which only focuses on a single loading condition, a multi-objective and multi-loading optimization method for sandwich panels with lattice core are presented by Liu and Lu [98]. A systematic method is developed based on the concept of parameter profiles which can be used to evaluate structure's overall performance under multi-loading conditions. Based on this method, sandwich structures can be simultaneously designed and optimized for multi-objectives including weight, stress and fundamental frequency. The same group of authors proposes another optimization design method [99] for sandwich

structure with lattice core. In this method, a homogenization method is used to calculate the effective properties of a lattice core. Compared with their previous method, the new method can significantly reduce the computational load. Besides bearing load with lightweight, other functions such as active cooling, energy absorption, internal actuation can also be achieved by careful design sandwich's homogeneous lattice core [21, 100-102]. However, it shows that most existing design methods for the lattice cores used in sandwich structures are focusing on the structural performance such as weight and strength. Only few of them [98, 102] can consider multi-objectives for multifunctional purposes. Moreover, some simplification and assumptions are used in these methods for sandwich panels, which makes them cannot be directly extended to more complex applications where lattice is not in a regular shape as the core of panels.

2.2.2 DFAM methods for customized lattice structures

To further improve the performance of a designed lattice structure, lattice strut's thickness and its frame can also be optimized. In this review paper, this type of optimized lattice structure is called as customized lattice structure. Based on the classification method of lattice structures introduced in Chapter 1, customized lattice structure mainly includes two major types of lattice structures. They are heterogeneous lattice and pseudo-periodic lattice. Because of its high complexity on mesoscale, customized lattice structures are preferred candidates for AM processes. In the following two paragraphs, DFAM methods for two major types of customized lattice structures will be reviewed respectively.

The key design parameter of most design method of heterogenous lattice structures is the distribution of thickness of struts. To obtain the optimized distribution of strut's thickness. Several structural optimization methods can be applied for the heterogeneous lattice on mesoscale. Among different structural optimization methods, the size optimization method can be directly applied to

the design of heterogeneous lattice structures. In this optimization method, the thickness of each lattice strut is regarded as a design variable, and key performance indexes such as displacement or maximum Von-Mises stress can be regarded as a design objective. Compared to other design methods for heterogeneous lattice design, the size optimization method is the easiest one for implementation, since there is no complex conversion on design requirements and optimization parameters. Although some standard programming methods can be applied to solve this optimization problem, a large number of design variables and a heavy computational load for direct analysis on mesoscale make this method impractical. In order to reduce optimization parameters, topology optimization methods based on SIMP [103] or homogenization theory [104] are proposed to design heterogeneous lattice structure. Among them, Sundararajan's proposed a method where homogenization approach and interpolation scheme are firstly used to establish the relationship between the lattice unit cell's relative density and its mechanical properties. Based on this relationship, topology optimization method is used to obtain optimized relative density distribution in the design domain. The result of topology optimization can be directly converted to the thickness of lattice struts. Compared to size optimization method, the number of design variables can be reduced from $n \times m$ to n, where n is the number of unit cells in the whole structure and m is the number of struts in each unit cell. Moreover, a macroscale analysis can be used to obtain the response of structures for this optimization method. Thus, a heavy computation load for size optimization is avoided. Rezaie et al. [103] has proposed another design method for lattice structures based on topology optimization. Compared to Sundararajan's method, the SIMP approach is used instead of homogenization based topology optimization. A mapping function is used to find lattice structure on mesoscale to represent intermediate relative density from the result of topology optimization. This method does not consider the stress distribution of the optimal

solution from a topology optimization process. The performance of designed result can be further improved.

Compared to size optimization methods, topology optimization methods mentioned above shows great advantages. However, there are still some room for the improvement. Firstly, none of the aforementioned design methods considers the effect of parameters used in the optimization process on the final design result. For example, in topology optimization for structural part, FEA is usually used to calculate displacement response of the structure under a certain load. Different size or types of elements in FEA will lead to the different results for topology optimization. Thus, more research needs to be done on how to select parameters for topology optimization based on given lattice cell size and topology. Secondly, current design methods only consider simple design objectives and constraints. However, for some more complex design tasks, multiple design objectives and constraints should be considered. Thus, the research on how to convert these complex multiple design objectives and constraints into topology optimization is necessary. Thirdly, almost all current design methods assume that thicknesses of struts in each unit cell are equal. However, no research has been done to show the lattice structure designed under this assumption is optimal. Thus, some further research should be done to find whether anisotropic lattice unit cell can achieve better structural performance.

Besides heterogeneous lattice structures mentioned above, another type of customized lattice structure called pseudo-periodic lattice structure has also attracted a lot of researchers' attention. Generally, design methods for pseudo-periodic lattice structure can be divided into two types. They are geometry conformal lattice and load adaptive lattice. The concept and design method of geometry conformal lattice is first proposed by Wang and Rosen [105-107]. The difference between conformal lattice and uniform lattice is shown in Figure 2-3. It is manifested that the

shape of each unit cell is no longer the same. It changes to adapt the macro shape of the design domain. Compared to the periodic lattice structure, their research shows that the conformal lattice structure usually has a better performance for lightweight structure and compliance mechanism design [107]. The analysis and design method for conformal lattice structure is first proposed by Wang [107]. In his approach, the conformal lattice frame is first generated based on structure's macro shape. Then the effective stiffness matrix for a unit cell is established to describe the relationship between the nodal displacement and force. Based on this analysis method, size optimization on thickness of lattice struts can be done to achieve desired performance of a structure. Based on Wang's method, a general DFAM method for lattice structure is proposed by Rosen [13]. In this method, a process-structure-property-behavior model is used to analyze and design lattice structures on a mesoscale. Unlike Wang's method, struts of lattice are divided into ten groups and in each group, thicknesses of struts are equal. Although this method can dramatically reduce the number of design parameters, the principle of dividing struts into 10 clusters is still unclear.

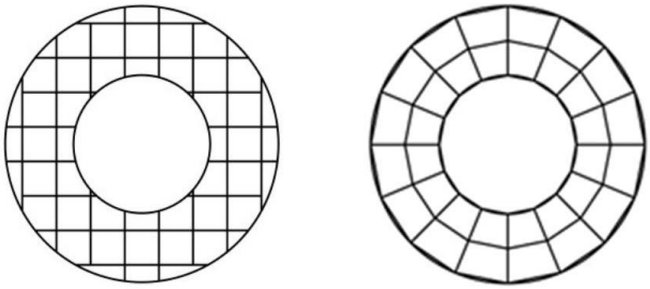

(a) uniform lattice (b) conformal lattice

Figure 2-3 Difference between uniform lattice and conformal lattice

More recently, another conformal lattice design method is presented by Nguyen et al.[108]. The design process of this proposed method consists of two main steps. The first step is to generate conformal hexahedral mesh for cells in a cell library, and then to populate the mesh with selected cells. After generating conformal lattice frame, in the second step, the optimization algorithm is

developed to determine the diameter of each strut. Unlike traditional ground structure methods, the optimization process presented in this research removes the rigorous large-scale multivariable topology optimization by utilizing a heuristic algorithm. This optimization only has two design variables which are the largest and smallest diameter of lattice strut. Local stress for each lattice unit cell is computed by FEA. And the diameter of each strut in lattice unit cell is determined by local stress and the range of diameter determined by two design variables. For load adaptive pseudo-periodic lattice structure, Chen [109] has proposed a design method based on 3D texturing mapping. In his method, a space warping technique is used to distribute materials based on stress distribution. The unit cells are stretched from low stress place to high stress place. The lattice structure designed by this method is shown in Figure 2-4. Another similar load-adaptive lattice structure design method is developed by Brackett et al [110]. Instead of using space warping technique in Chen's method, a dithering method is used to represent a gray scale stress fringe with variably spaced black dots. These spaced black dots can be also used as the lattice cell's vertices. Like Chen's approach, this design method also enables the variation of lattice size and shape according to stress distribution inside the design space. It is obvious that both Chen and Brackett's design methods are computationally efficient, since they do not need any iteration for an optimization. However, there are two obvious disadvantages for these two design methods. Firstly, to evaluate the performance of generated pseudo-periodic lattice structures has a huge computational burden, since homogenization theory is no longer suitable to analyze this type of structures. Secondly, it is also skeptical to use the stress distribution of initial design domain with solid material to represent the stress distribution of the design domain filled with lattice structures. Recently, Teufelhart and Reignhart [111-113] proposed a design method for load adaptive lattice structures (shown in Figure 2-5) based on force flux. In their method, customized lattice frame is

firstly established based on the force flux in a design domain under a given load. The size optimization method is applied to the thickness of lattice struts. Based on this method, it is possible to achieve equal stresses in the whole structure for each strut and gain a better lightweight performance. However, to generate force flux for a design domain with complex geometric shape and the boundary condition is still a very difficult task for both designers and software.

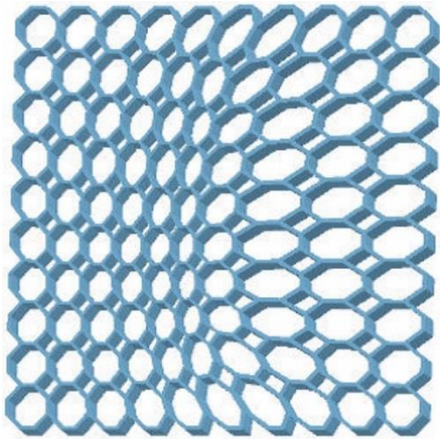

Figure 2-4 Pseudo-periodic lattice structure generated by 3d text mapping technique [109]

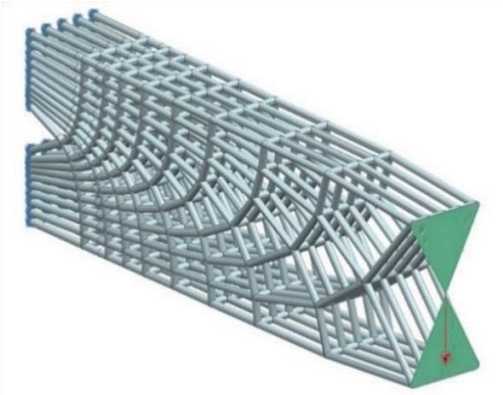

Figure 2-5 Pseudo-periodic lattice structure generated based on the force flux [111]

To summarize those available DFAM methods for customized lattice structures, it can be concluded that most recent developed DFAM methods are trying to integrate lattice frame design and struts' thickness optimization into their design process to further optimize the performance of design. Although remarkable progress has been achieved, there still existing some design

difficulties especially in the design domain with complex geometry and design requirements involves multifunction. Thus, multifunctional design method which can deal with intricated design domain on macroscale is still in need.

2.2.3 Geometric modeling method for mesoscale lattice structures

To represent geometric configurations of lattice structures, geometric modeling process is needed. This process is crucial in the entire design and fabrication process of lattice structures. It is the link between design, simulation and manufacturing. This process is typically done by designers with the help of CAD tools. However, to build the geometric model of lattice structures with multiscale complexity is not an easy task with conventional CAD tool. It is mainly due to the underlying methods used by those tools cannot efficiently handle and manipulate complex geometric information on multiple design scales [114]. To deal with this issue, several geometric modeling methods have been proposed to generate the geometric model of lattice structures. In this sub-section, these methods have been summarized. A brief comparison is made to address both advantages and disadvantages of each geometric modeling method. Future research trends for this field has been wrapped up at the end of this section.

Generally, the existing lattice geometric modeling methods can be categorized into three groups according its underlying geometric representation methods. They are voxel based methods[114], Functional Representation (FRep) based methods[115, 116] and hybrid methods[117, 118]. Among them, volumetric representation method has been applied to describe a complex shape of lattice structures on a meso or micro scale. In this representation method, the shape of geometric model has been described based on a set of values defined on a regular grid in 3D space. Based on the value of each grid point, one can easily determine whether this point is inside or outside of the geometric model. Compared to other representation techniques including

polygon mesh and Boundary Representation (B-Rep), the voxel based modeling method has following advantages. Firstly, efficient Boolean operation can be easily implemented. For example, the union of two complex geometries can be quickly achieved by applying 'OR' gate between their corresponding voxels. Thus, this method enables the efficient trimming of lattice structures with the complex macro shape of its design space[114]. Secondly, the construction speed of voxel model for periodic lattice structures is fast. Designers only need to build the voxel model of one unit cell. Then the entire lattice structures can be easily obtained by copying and transforming this unit cell into the whole design space. Thirdly, voxel based modeling methods can directly output the slice file for a AM process. It can save the time for slicing the polygon mesh. More importantly, voxel based method also provides a potential capability to represent multi-material or functional graded material [119]. Each voxel point can associate multiple values to represent the material compositions. However, it should be noted that voxel based modeling methods also has some disadvantages. Firstly, voxel model may lose the topology information of lattice structure. This information is important for the construction of a FEA model, when lattice structures is modeled with beam elements. Secondly, current voxel based modeling method is only limited to a certain type of lattice structures with periodically distribution of unit cells in the three-dimensional space. It cannot be applied to those lattice structures without strictly periodical behavior such as geometric conformal lattice or load adaptive lattice[112, 120]. Another obvious drawback of voxel based modeling method is its fixed resolution. Hence, it needs to be rebuilt for different AM machines with different resolutions. This process is usually time consuming.

Besides voxel based modeling, Functional Representation method has also been used to represent the geometric model of lattice structures recently. In the FRep method[121], the geometric objects are considered as closed subsets in the n-dimensional Euclidean space E_n with

the definition:

$$f(x_1, x_2, \dots, x_n) \geq 0 \tag{2.1}$$

Where f is a real continuous function defined on E_n. This function can also be called as a defining function. Based on this definition of geometric object, different types of operations and relations [121] have been developed to help designers to construct complex three dimensional geometries. Particularly for lattice structures discussed in this section, a procedural functional-based modelling technique has been developed by Pasko et al. [115]. In this method, the modelling process of periodic lattice structures consists of two steps. First, the geometric object for the unit cell is prepared. Then, a periodic replicating function $g(t)$ can be applied on the unit cell and map it into the whole design space. This process can be further extended to build geometric model of lattice structures with random of irregular microstructures by introducing the pseudo-random variations. This work has been further developed by Fryazinov et al. [116]. Several methods of generating spatial variations in microstructures have been proposed. It enables user to realize parameterization with point coordinates, metamorphosis between different unit cells, transfinite interpolation between different lattice types with given space partitions and recursive multi-scale replications [116]. Compared to voxel based modeling methods, F-Rep based methods provide a great freedom for designers to generate lattice structure with multiscale complexity. It generally provides an accurate and concise representation on a lattice structure with multiscale complexity. The result of this type of modeling methods can be directly rendered [122] and fabricated by AM process without auxiliary format [116]. Thus, it significantly shortens the model preparation time between design and manufacturing. However, it should be noted this method has the similar issue like voxel based modeling method. The topology information of lattice structures is not preserved. Besides this, to construct the function which can represents and controls the desired shape of unit

cell is not intuitive. Moreover, this group of methods is not compatible with B-Rep used in most existing CAD & CAE tools. If users want to use this method to generate the lattice inside the design domain represented by B-Rep, the format conversion needs to be done at first.

The last group of lattice geometric modeling method is called hybrid modeling methods. This type of methods generally combines several different geometric representation methods to accelerate the generation speed of lattice structures. For example, Wang and et al [117] has proposed a hybrid geometric modeling methods for large-scale conformal lattice structures. In this method, a concept of unit truss is proposed to avoid the calculation of overlap region between two neighbored primitives. Based on this concept, the solid model (B-Rep) of each unit truss is constructed at first. Then the faceted model (polygon mesh) of each unit truss is generated based on obtained B-Rep model. By assembling faceted models of all unit cells, the geometric model of the entire lattice structure can be obtained. It is clear that this hybrid method generally considers the advantages of both solid modeling and polygonal representation. Compared to other geometric modeling methods, this method can be applied to several different types of lattice structures including uniform lattice structures as well as geometric conformal lattice structures. Recently, another similar method called Prefabrication- Hybrid Geometric Modeling (P-HGM) has been proposed by Vongbunyong and Kara [118], the solid model of lattice unit cell is prefabricated. Based on cell's position, certain surface of prefabricated cell is removed. Then those prefabricated cells can be assembled into the whole geometric model of lattice structures. Compared to Wang's method, P-HGM method can generally achieve a better speed since it only need to construct the solid unit cell once. However, this method can only be applied to uniform and homogeneous lattice, which seriously limits the design freedom of lattice structure fabricated by AM process. Besides those two hybrid geometric modeling methods mentioned above, another type of hybrid geometric

model methods [17, 123] has been developed. Instead of construction of solid model for lattice unit cell, the polygonal boundary (including edges and faces) of each lattice cell is obtained first. Based on its polygonal boundary, the algorithm has been developed to directly generate the triangular mesh of each unit cell. By pending the generated mesh for each cell, the entire lattice structures can be obtained. This method can only deal with those lattice cell in the polygonal shape without internal struts. It is widely used to generate those randomized lattice structures constructed based on randomized Voronoi cells. Compared to voxel based methods and F-Rep based method, hybrid geometric modeling methods generally provides more intuitive way for designers to build lattice structures. And it is also share some common features with existing CAD tools. Thus, it is easy to be implemented and can seamlessly work with existing CAD tools [124]. However, the generated mesh model is difficult to be modified, since it usually contains the large number of triangular faces. To trim the generated mesh model with a design space in a complex shape is another time-consuming process which is not considered in most existing hybrid geometric modelling methods.

To summarize those geometric modeling methods mentioned above, Table 2-2 is provided to compare the different groups of geometric modeling methods. Each group of method has their own merits. Thus, further research on hybrid modeling technique needs to be done to overcome the shortcomings of existing geometric modeling methods.

Table 2-2 Comparison between geometric modelling methods of lattice structures

Method name	Speed	Size of model	Direct fabrication	Morphed lattice cells	Topology information	Compatibility *
Voxel based modeling	fast	big	yes	no	no	good
F-Rep based modeling	Very fast	small	yes	yes	no	bad
Hybrid modeling	fast	big	no	yes	yes	good

* compatibility between lattice modeling methods and existing commercial CAD tools

2.3 Microscale design methods

On microscale, by controlling the fabrication parameters of some AM processes, a certain microstructure can be fabricated to enhance the performance of the part. For example, Functionally Graded Materials (FGMs) can be realized by gradually changing the microstructure of one or several different compositions over the design domain [125], which can improve the parts' performance or add new functions. In this section, the DFAM methods related to microstructure design and optimization are divided into two major categories. They are DFAM methods for homogeneous microstructure and DFAM methods for heterogeneous microstructure. The design methods of these two categories are respectively reviewed in the following content. Like structural optimization methods, some design methods included in this chapter on microscale have also been studied for several decades. However, they can also be used to improve the performance of parts fabricated by AM. Thus, they are also included in this chapter.

2.3.1 DFAM for homogenous microstructure

For the design of homogenous microstructure, the key is to design a material with the certain microstructure which can achieve the desired properties. Among design methods for different types of microstructure, the design method of composite materials consisting of a periodic microstructure has drawn a great interest for researchers, since the properties of this type of material are easy to control. Designers can easily tailor different physical properties by modifying the shape of micro unit cell like the cellular structures discussed on mesoscale. Compared to cellular structures on mesoscale, the periodic microstructures are more suitable for those parts with a small characteristic dimension. However, it should also be noted that both the fabrication cost and difficulty may increase for periodic microstructures even by AM processes.

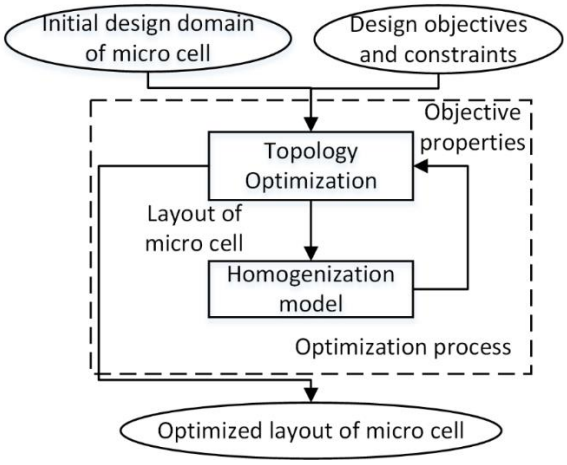

Figure 2-6 General scheme and procedure of inverse homogenization technique

To design a microstructure for tailored material properties, a technique commonly termed "inverse homogenization" is firstly proposed by Sigmund [82] and its general flow is shown in Figure 2-6. This technique has already been discussed in the previous section for the design methods of homogenous lattice structures. In this section, some applications of this technique on a microscale design will be discussed. On microscale, existing inverse homogenization based design methods have already covered a full range of different disciplines including material stiffness[86], Poisson ratio[83], electronic or heat conductivity [126], fluidic properties of permeability and diffusivity [127], thermal expansion coefficient [128] and Phononic/Photonic Band Gap (PBG) [129]. Instead of only focusing on a single material property, some design methods are developed to simultaneously consider multiple competing material properties including stiffness/permeability [127, 130] and stiffness/conductivity [131, 132]. In these design methods, a Pareto front can be generated to visually help designers to keep balance of different properties depending on their specific needs. Generally, these multifunction design methods for microstructure are suitable for the products with multifunctional requirements. For the detailed techniques and processes of these design methods on micro cells, there is a comprehensive review [133] which readers can refer to.

Besides the design methods mentioned above which only focus on microscale design, some design methods have been proposed to update the structures on both macro and microscale. A hierarchical numerical scheme is proposed by Rodrigues et al. [134] for optimizing material distribution as well as the point-wise material microstructures concurrently. In this approach, the design process uncouples the topology optimization into two related sub problems. The outer problem deal with the spatial distribution of material, which can be regarded as the design on macroscale. The inner problem is to solve the question of optimal choice of material microstructure. Compared to those single scale design methods, Rodrigues's method can further improve the functional performance of products. However, the connection between different optimized microstructures is not considered in this design method, which makes the optimized structures are difficult to fabricate even with advanced AM processes. A two-stage method for fusion cage design is developed by Lin et al. [135]. In this design method, topology optimization method on macro scale is firstly used to divide the design domain into several different regions with different porosities. Then, inverse homogenization technique is used to find micro cell which can achieve the better stiffness under the porosity constraint for each region. The final design is generated by integrating design of the two-scaled structures. Liu et al. [136] has proposed a Porous Anisotropic Material with Penalization (PAMP) method to deal with macro and micro design simultaneously. In this design method, the microstructures are assumed to be uniformly distributed in the design domain. This assumption can guarantee the connection between different micro cells. Liu's method has also been successfully been applied to the multi-objective design of lightweight thermoplastic structures with maximum fundamental frequencies [137]. Another concurrent design method is proposed by Yan et al. [138]. Like Liu's method, Yan's method also assumes the microstructures are uniformly distributed in the design domain. Moreover, in Yan's method, BESO based

optimization is used for both macro and microscale design. Recently, another multi-scale design method is proposed by Xu et al. [139]. Compared to those design methods mentioned above, this multiscale design method can deal with unknown-but-bounded load with a robust concurrent optimization method. This optimization can consider the worst-case scenario in a confident way. To summarize these available multi-scale design methods, it is clear most of them assume the microstructures are homogenously distributed in the design domain. Even though this simple assumption can guarantee the manufacturability of designed structures, it also restricts the design freedom of using heterogeneous microstructures to further improve the functional performance.

2.3.2 DFAM for heterogeneous microstructure

Compared to the design methods for homogeneous microstructure, the design methods for heterogeneous microstructures are more complex. One way to design this type microstructure is to obtain the distribution of different types of microstructures directly from the 3D scanning of some existing objects. For example, in tissue engineering, the scaffold with heterogeneous microstructures [140, 141] is designed from the CT scanning data. The scaffolds designed by this method can interface better with the surrounding tissue and facilitate more efficient rehabilitation for patients.

Another way to design heterogeneous microstructures is based on those design methods for FGMs. Generally, for FGMs, there are two types of design variables. The first type of design variables is the topology of FGMs' microstructure. For those FGMs fabricated by traditional manufacturing methods, there is little design freedom for designers. Thus, designers usually cannot directly optimize the topology of microstructures. Only some typical microstructures shown in Figure 2-7 can be selected to meet their design requirements.

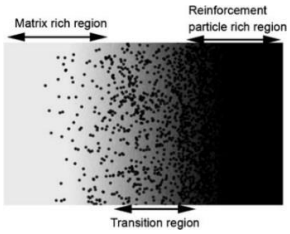

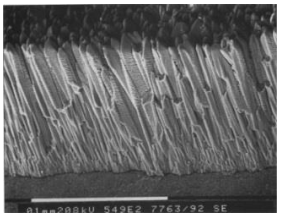
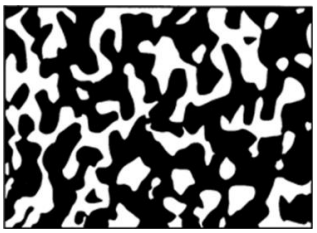

(a) Particulate FGMs [142] **(b) Columnar FGMs [143]** **(c) Skeletal FGMs [144]**

Figure 2-7 Typical types of microstructures of FGMs

Thanks to AM technologies, parts with optimized and tailored microstructures can be realized. Thus, some research has been done to optimize the microstructures of FGMs for the certain material properties gradient. For example, a design method for two-phase (avoid and solid) microstructures of FGMs has been proposed by Zhou and Li [145]. Like design methods of microstructures for homogenous materials, the inverse homogenization technique is also used in this method to design the Periodic Base Cells (PBCs) on a microscale. The designed PBCs vary in the direction parallel to the property gradient but periodically repeat themselves in the perpendicular direction. Moreover, to preserve the connectivity between two adjacent micro cells, three different methods, namely connective constraint, pseudo load, and unified formulation with nonlinear diffusion are proposed in this design method. Another inverse homogenization techniques based design method is proposed by Radman et al. [146]. Like Zhou and Li's [145] design method, the microstructure of FGMs in Radman's design method is also composed of a series of PBCs in the direction of properties variation and self-repeated in other directions. However, instead of using SIMP for topology optimization in Zhou and Li's method, BESO is used in Radman's method to obtain the optimized microstructures of each cell. Moreover, in Radman's method, the PBCs are optimized progressively by considering three base cells at each stage. This innovative technique guarantees the connections between adjacent PBCs with high computational efficiency. More recently, another inverse homogenization based microstructure is developed by

Radman et al. [147]. Two different functions are considered in their latest design method. In this design method, the overall stiffness of FGMs can be maximized with a prescribed variation of thermal conductivity. This design method is more useful for the design of multifunctional parts.

The second type of design variables of FGMs includes spatial distributions of volume fractions for different material phases, orientation distribution for reinforcement fibers and other parameters of microstructure. In terms of the design parameterization scheme of the second type of design variables, existing methods can be categorized into two main types: discrete modeling and functional modeling. In the first type, different types of discrete models are used to divide the design space into sub-regions or elements whose parameters of material microstructure are assumed to be homogenous or can be interpolated from discrete control points. In most one-dimensional FGMs optimal design methods (also known as unidirectional FGMs design) where the parameters of microstructure only vary along a single direction, a design domain is usually divided into several homogenous layers [148-150]. For two-dimensional FGMs optimal design methods (also known as bidirectional FGMs design) where the parameters of microstructure of constituents vary inside a two-dimensional plane or surfaces, rectangular elements are usually used to separate the dimensional design space [151]. For the three-dimensional FGMs optimal design (also known as tri-variate FGMs design) where the parameters of microstructure of constituents vary inside three-dimensional space, tetrahedron elements are used by Hu et al.[152] to maximize the stiffness of 3-dimentional “I” shaped beam as well as minimizing the structural weight. The advantage of discrete modeling methods is its flexibility. This type of parameterization scheme can represent an arbitrary complex distribution of design parameters inside the design domain. However, the disadvantage of the discrete model is the non-trivial computational load when the number of discrete elements is very large. This is simply due to the large number of design

variables of discrete modeling methods [153].

Instead of modeling FGMs distributions of spatial discrete elements, functional modeling methods [119] are also available in the optimal design of FGMs. In the functional modeling methods, the distributions of parameters of microstructure can be depicted by the given analytical functions. In one-dimensional FGMs design, power-law based functions are most widely used to represent the distribution of volume fractions in some one-dimensional FGMs design methods [154, 155]. Besides power-law based functions, other types of analytical functions, such as exponential and parabolic functions [156], parametric Bezier curve function [157] and generalized Tylor expansion [158] are also used to represent the distributions of FGMs' constituents. Similar functions are also used to represent the distributions of parameters of microstructure in the two and three dimensional designs. For example, multivariate polynomial functions are used to model the heterogeneities of 2-dimentional FGMs [159, 160]. As to three-dimensional problems, trivariate spline functions are used to describe the heterogeneous constituents' distribution in three-dimensional space [161, 162]. Besides using a single function to describe the material distribution, a procedural model is developed by Kou and et al. [153] to model material distributions with multiple functions. In Kou's method, multiple distribution functions are modeled in a tree structure. The parameters of microstructure at any given point can be evaluated by execution of a collection of procedures. In each procedure, a single analytical function is used to evaluate the material distribution. Compared to those functional modeling methods with a single function, this procedure modeling method is more flexible to express a complex distribution inside the design domain. Generally, compared to the discrete modeling method, the functional modeling can significantly reduce the number of design variables in the optimization process, since only several coefficients of a distribution function are regarded as the design variables. Despite the obvious

advantage of functional modeling, it should be noted that this modeling method still has some limitations. For example, the choice of a distribution function is largely depending on the designers' experience. It is obvious that different distribution functions may lead to different optimal performance. Thus, the quality of distribution functions is important for functional modeling methods.

Table 2-3 Optimization method for FGMs

APPLICATION FIELD	One dimension	Two dimension	Three dimension
THERMAL PERFORMANCE	Ootao et al. [155]; Nadeau and Ferrari [148]; Cho and Ha [149]; Cho and Shin [163]; Vel and Pelletier [164]; Zhang, et al [165]; Fereidoon, et al [166]; Parashkevova et al. [167]; Chen and Jie [168]; Na and Kim [154]; Na and Kim [150]; Mazafari et al [169]; Xu [170];Noh et al. [171]	Goupee and Vel [172];Cho and Ha.[151]; Turteltaub [173]; Turteltaub[174]; Cho and Park [175]; Vel and Coupee [176]; Nemat-Alla [177]; Maciejewski[178]; Kou et al [153];	
STATIC RESPONSE		Lipton [179]; Stump et al. [180];	Hu et al.[152];
DYNAMIC RESPONSE	Batra and Jin [181]; Rubio and et al.[182]	Qian and Batra [183]	
ACTUATORS AND SENSORS	Rubio and Silva [184] ; Carbonari and Silva [185]; Rubio et al. [186]; Amigo[187];	Carbonari et al. [188]	
BIOMEDICAL APPLICATION	Lin et al.[189]; Lin et al.[190]; Sadollah and Bahreininejad [191], Bahraminasab et al. [192], Cui and Sun [193]; Gasik et al.[194]; Hedia and Founda [195];		Lin et al.[135]

The objective functions of the second types of design variables of FGMs also vary dependant on the tasks and application considered, but usually include mass, thermal stresses, fracture resistance, static and dynamic responses, heat transfer and insulation. Table 2-3 is presented to categorize the existing optimization methods of FGMs into five different application fields. For each application field, the design methods are further divided into three sub-groups according to their design dimension. From this table, it is obvious that most existing optimization methods of

FGMs are related to its thermal performance. This is simply due to the outstanding performance of FGMs on heat resistant. Moreover, it can also be concluded that most optimization methods can only deal with one or two-dimensional design. One reason to explain this is that the limitation of conventional manufacturing methods. Furthermore, the heavy computational load for the optimization process is another obstacle to explore the optimal distributions of parameters of microstructure in a three-dimensional space.

Besides those design methods reviewed above which mainly focus on a single design scale, some design methods are proposed which can take advantage on both macro and micro scale. A general computer-aided FGMs method is proposed by Chen and Feng [196, 197]. In this design method, a design process of heterogeneous material is decoupled into a sequence of steps to find the optimal macro geometric parameters as well as the distribution of material constituents. This design methods can deal with the optimization in macro and microscale sequentially. Thus, it can be considered as a multiscale design method. Besides this method, there are also few other multiscale methods [182, 185] available for FGMs. In these methods, the macro shape and microstructure distribution are sequentially optimized. More specifically, topology optimization is used to design the macro shape of structure. Then the distribution of material constitutions inside the macro shape of part is optimized based on existing optimization methods for FGM. However, most of these existing multiscale design methods can only deal the one-dimensional FGMs optimization due to the heavy computational load.

2.4 Discussion and Summary

Admittedly, DFAM methods which are used for functional purposes are divided into three groups according to its related design scale in this chapter. It does not mean that there is always a strict and clear boundary between them. Some DFAM methods can be used for more than one

design scale. For example, the inverse homogenization technique can be applied to the unit cell on both micro and mesoscale. But, there is only a few DFAM methods considering the design with multiscale complexity. Moreover, most multiscale DFAM methods also assume the microstructures are uniformly distributed, which may limit designers to further improve parts' performance. These issues inherit from the available design methods for traditional manufacturing processes. To further improve the efficiency of DFAM methods and take full advantage of the capabilities of AM processes, it is necessary to have a DFAM method to support multiple design scales, and integrate them into a multiscale design framework.

Moreover, it is also found that most of existing design methods for mesoscale lattice are focusing on a single function. Few of them can deal with multiple functions. None of them can generate heterogeneous lattice structures for multifunctional purposes. Based on the design result of existing heterogeneous lattice structures for a single function, it can be inferred that the performances for multiple function can also be improved by the same manner. Thus, it needs a method which can deal with coupled relations between functions and design parameters for those lattice structures play multifunctional roles.

Another interest fact can be summarized from this review is the drawback of existing CAD tools. Most commercial CAD tools only focus on macroscale design. Their geometric modeling kernels are usually based on B-Rep or Constructive Solid Geometry (CSG) techniques. These modeling techniques are not efficient to deal with structures with multiscale complexities. In addition to geometric modeling method, a lack of generative CAD-tool to guide designers who are not familiar with the unique capabilities of AM processes is another issue for current CAD software. The design constraints of traditional manufacturing methods are deeply rooted in the designers' mind. Such generative design tool can help designers think freely and to explore the potential

opportunities provided by AM process on design.

Based on the above discussion and summary, several research perspectives are pointed out.

1) To synthesize design methods of different design scales. Compared to the design methods on a single scale, multiscale design methods may further improve the products functionality. However, there are only a few multiscale design methods, and most of them can only deal with homogenous lattice structures. Thus, to further improve the functional performance of designed parts, a novel multiscale design methods for heterogenous lattice structures is needed.

2) To develop a DFAM method enabling multifunctional and multidisciplinary design. Most of the current DFAM methods for functional improvement focus on optimization of a single function or multi-function in a single discipline. However, in some design cases, parts need to have several functions. Thus, it is necessary to develop a DFAM method which can simultaneously consider multiple functions in multiple disciplines.

3) To develop a user-friendly CAD tool enabling the design of products with multi-scale complexity. Based on existing feature-based CAD software, it is difficult to build and modify the model with complex multi-scale features. This issue restricts the design innovation on hierarchical structure with high functional performance. To solve this problem, a user-friendly CAD tool is needed to help designers build model with multiscale complexity.

Chapter 3 General Design Methodology for Mesoscale Lattice Structures Fabricated by Additive Manufacturing Processes

In this chapter, a general framework of multiscale and multifunctional design methodology for mesoscale lattice structures is proposed. The proposed design methodology aims to provide a guide for designers to take advantage of the mesoscale lattice structures enabled by AM technologies. By following its design flow, the functional performance and other product's key life cycle factors can be further improved. To make the proposed design methodology easier to understand, several basic concepts of the proposed design methodology are introduced at the beginning of this chapter. Based on these basic concepts, a general framework of the proposed design methodology is presented in Section 3.2. This general framework is divided into three major design stages. The role and functions of each design stage are briefly introduced, which provides an overall understanding of the proposed design methodology. The design steps and related design techniques used in each design stage will be discussed in detail in the following chapters of this thesis. At the end of this chapter, a summary is made to address the differences between the proposed design methodology and other existing design methods for AM processes.

3.1 Basic concepts

3.1.1 Functional and physical entity

The concept of functional entity is given to describe the result of the functional analysis in the proposed design methodology. This concept is defined as an abstract entity which is constructed to realize a given set of functions to fulfill a set of prescribed design requirements. Based on this definition, it can be concluded that the defined functional entity should include two types of information. They are a set of targeted functions and a set of design requirements. Functions is the

kernel of functional entity which describes the major physical behavior designers want to achieve through this abstract entity. Besides functions, design requirements represent another important portion of a functional entity. They describe the requirements on the behavior of a designed part. The design requirements of a functional entity are generally divided into two categories according to its relation to the defined functions of the functional entity. If the design requirement is defined based on the behavior which directly links to the defined function, this design requirement is considered as a functional related design requirement. Otherwise, the design requirement is called as non-functional related design requirement. For example, in the design process of a kettle to boil water, the design requirement defined on the boiling speed can be considered as a functional related design requirements, since this parameter directly decide whether the required function can be achieved. But the design requirement defined on the weight of a kettle is a non-functional related requirement, since the behavior which this requirement describes is not directly linked to functions. Both types of requirements are important to a designed part. The weight of the designed kettle is not crucial for its major function – boil water. However, if this kettle is used for the outdoor purpose, the weight is an important factor to be considered during the design process. Thus, both functional and non-functional related design requirements should be carefully considered during the design process.

Based on the definition of a functional entity, the concept of a physical entity is defined as a physical implementation of a functional entity which can achieve the set of defined functions under given design requirements. To consider the design freedom enabled by AM, the physical entity defined in this thesis should include three types of information: geometric information, material information and the information of mesoscale structures. To satisfy this requirement, a mathematical model of a physical entity is proposed based on a general model of object [198]. Its

mathematical representation is stated as:

$$M_P = M_G \times M_c(M_G) \times M_s(M_G) \tag{3.1}$$

Where M_P represents the model of a physical entity. M_G denotes the geometric model of a physical entity. It is defined in 3D Euclidean space E^3 (or a subspace). Specifically, it can be represented by an r-set. M_c and M_s are two attributes models which describe material compositions and mesoscale lattice structures of a physical entity respectively. These two attribute models are both defined based on geometric model M_G. For a physical model, a set of functions $F = \{F_i\}$ can be specified to map the geometry model M_G to its related attribute models M_c and M_s. The symbol "×" used in the Equation 3.1 can be precisely defined as topological products [198]. Thus, the model of a physical entity expends the modeling space from pure E^3 to a trivial fiber bundle [199], which enable designers to further control the material distribution as well as mesoscale structures during the design process.

3.1.2 Functional Surfaces and Functional Volume

To geometrically characterize the common features of those feasible physical entity, the concepts of Functional Surface (FS) and Functional Volume (FV) are proposed. Particularly, FS is defined as a key surface of a physical entity which is used to implement certain functions described by a functional entity, while FV is referred to as a volumetric region which incorporates the geometric shapes of all feasible physical entities. Based on these definitions, it can be concluded that FSs describes the common boundaries that shared by feasible physical entities which may in different shapes. As to FV, it can be simply considered as the body which contains the union of all possible physical entities. Generally, FV should establish the physical connections between the given FSs. Thus, the relation between FSs and FVs is expressed as:

$$s_f \subseteq \partial\Omega_{FV} \tag{3.2}$$

Where Ω_{FV} represents the domain of FV and s_f is a given FS. A typical example of FSs and FVs is provided to further illustrate these two concepts, which are shown in Figure 3-1. In Figure 3-1(a), a triple clamp of a motor cycle is given. Its major function is to link the steering handle with front fork and the main frame of a motorcycle. To achieve this function, five cylindrical surfaces are extracted and shown in Figure 3-1(b). Among them, FS1 and FS2 provide a solid connection between the designed part with the front fork. The shape of these two FSs is determined based on the shape of the front fork. Likewise, FS3 and FS4 offer a support for steering handle. Their shapes should conform to the steering handle. The last FS is FS5 which connects the main frame of a motorcycle and provides a rotational center of the front wheel of a motorcycle. To connect those five FSs, the FV is constructed and shown Figure 3-1(b). Generally, FSs and FVs provide a rough description of physical entity. Based on this information, the design space and its related design parameters are figured out, which provides a foundation for the following optimization processes.

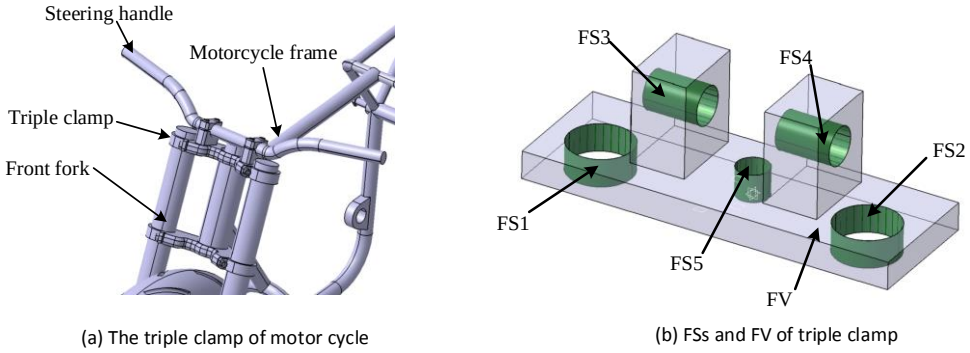

(a) The triple clamp of motor cycle

(b) FSs and FV of triple clamp

Figure 3-1 FSs and FV of a triple clamp of a motor cycle

3.1.3 Design space and design parameters

In the proposed design methodology, the design space of a physical entity indicates a set of physical entities which are considered as candidates to implement its corresponding functional entity. It should be noticed that not every candidate inside the design space is a feasible physical entity for its corresponding functional entity. However, the design space itself should be big

enough to incorporate as many feasible solutions as possible. An example is given in Figure 3-2 which shows the different design results with respect to their corresponding design spaces. In this example, a structure is designed to support the given pressure on the top of design space. To achieve the maximum stiffness with respect to a given weight, topology optimization technique has been used. According to its functional requirements mentioned above, three potential design spaces are constructed for topology optimization under the same loading condition. These three design spaces are all in the cuboid shape with the same thickness (20mm), but with the different width and height (shown in Figure 3-2).

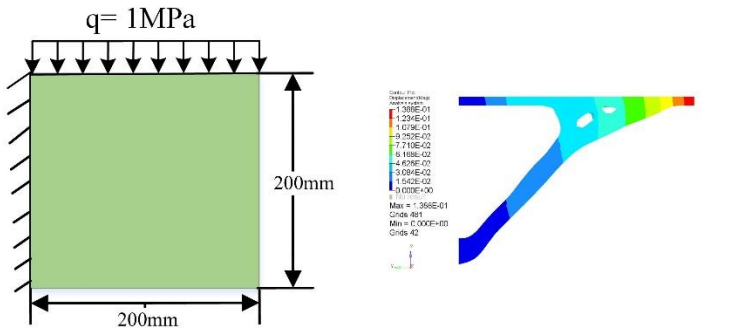

(a) Volume fraction 5%

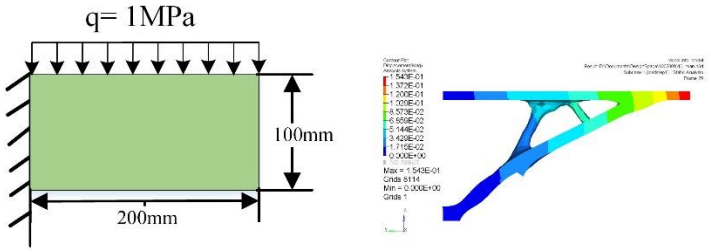

(b) Volume fraction 10%

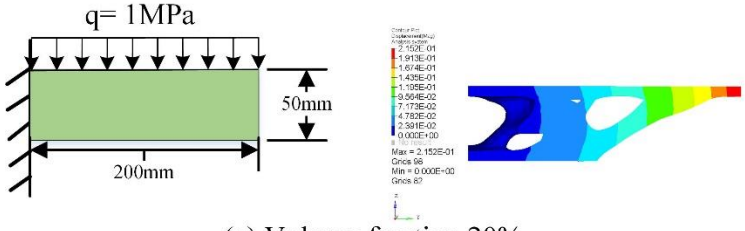

(c) Volume fraction 20%

Figure 3-2 The effects of design space on the optimization result

Different volume fraction constraints are applied on those design space shown in Figure 3-2 to

guarantee the optimized structures have the same weight. The FEA based simulation results are given in Figure 3-2 which shows that with the increase of design space, the maximum displacement of designed structures is reduced. This example illustrates the fact that the design space which designers constructed in the earlier design stage may have a profound effect on the performance of the final design result.

Traditionally, design space can be represented by defining its boundary in three-dimensional Euclidean space. Thus, the FV described previously can be considered as the design space of a given physical entity. However, this representation method is no longer valid for the proposed design methodology in this thesis, because mesoscale structures information should be considered during the subsequent design and optimization process. To solve this problem, a set of design parameters has been used to describe the design space of the physical entity. In this thesis, design parameters generally refer to the design configurations that designers can directly control during the design optimization process. To select suitable design parameters, designers should consider the manufacturability of selected AM process as well as available design optimization methods. Different design optimization methods may use different types of design parameters during the optimization process. The detailed process of design parameters selection is introduced in Chapter 5. The feasible values of these design parameters construct a domain which is a subset of vector space. It is expressed as:

$$S_D = S_{D1} \times S_{D2} \cdots \times S_{Dn} \tag{3.3}$$

Where S_D represents a domain of design parameters. S_{Di} $(i = 1,2 \ldots, n)$ is the feasible domain of i^{th} design parameter. The construction process of a domain of design parameters is called as design parameterization. Detailed information of design parametrization process will also be discussed in Chapter 5. The relation between the design space and the domain of selected design parameters

can be described by a one to one mapping function g.

$$M_P = g(D_p), M_P \in S_M, D_p \in S_D \tag{3.4}$$

Where M_P refers to model of physical entity, D_p is a vector which contains a collection of selected design parameters. S_M represents the design space of a physical entity. It should be noted that there is usually more than one design parametrization method for a given physical entity. Thus, the size of design space also depends on its related parametrization methods. To quantitatively measure the design freedom of design space, a concept of Design Degree of Freedom (DDoF) is provided. This concept is referred to as the number of parameters defined in the domain of design parameters. Generally, the larger DDoF is, the more design freedom designers may have, but it also increases the difficulty in the following design optimization stage. In the earlier design stages, it is recommended to construct the design space with a larger DDoF since lack of enough information and knowledge of the design. During the process of design, the number of DDoF should decrease with the increase of design knowledge and information. In the proposed design methodology, several proposed design optimization techniques can be applied to determine the values of all design parameters in the defined space. Thus, the final designed physical entity can be considered as a special design space whose DDoF equals to zero.

3.1.4 F-P-P-D model

To represent the complex relationship between functions and its related design parameters, F-P-P-D (Function-Performance-Property-Design Parameter) model has been proposed in this thesis. This model is built for a physical entity based on its related functional entity and design requirements. The general graphic view of this model is given in Figure 3-3. It mainly consists of four domains and their linked relations.

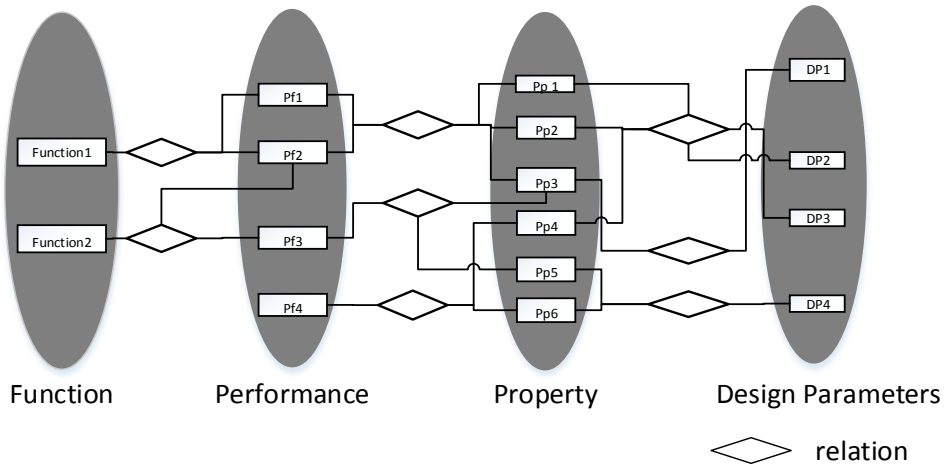

Figure 3-3 Graphic view of F-P-P-D model

The first domain of F-P-P-D model is called as a functional domain. In this domain, the functions of designed parts should be clearly stated. Generally, function of each part can be easily analyzed based on its corresponding functional entity. They are usually expressed in a natural language which describe the existing purpose of designed part. In most cases, they can be expressed in an active verb with a noun, such as "cut beams" or "boil water" [200]. It should be noticed that the same function may be illustrated in different ways by different people. For example, the function of "boil water" can also be described as the "heat the water" or "increase the temperature of water". Thus, in this domain, functions are only defined in an informal way, which cannot be directly computed.

To formalize the functions defined in the functional domain and characterize those non-functional related design requirements, the performance domain is defined in the F-P-P-D model. In this domain, the performance parameters are applied to quantitatively describe and evaluate the performance of each function as well as those non-functional design requirements such as weight and cost. Generally, the performance parameters defined in this domain can be roughly classified into three categories. In the first category, the performance parameters are directly related to the

defined functions described in the functional domain. For example, to evaluate the performance of function “boil water”, the time which is taken to heat the water of a unit volume from room temperature (20 °C) to boiling temperature (100 °C) can be regarded as the performance parameters in this domain. This performance parameter directly determines whether the defined function can be successfully achieved, and describes how well the function can be achieved to satisfy the customer needs and design requirements. For example, if it takes infinite time to boil water, it can be inferred that the product is malfunctioning. In practical terms, some threshold values may be provided on this type of performance parameters to judge whether the function is working or not. The second category of performance parameters mainly includes those parameters which have indirect effects on the defined functions. These parameters directly determine the value of parameter defined in the first category. They are usually state variables for each discipline. From this point of view, it can be considered as an indirect relation to given functions. For example, in the design of a structure for heat conduction purpose, heat conduction rate is considered as the first type of performance parameter which is linked to its function. To calculate its value, the temperature distribution inside the designed structure should be firstly calculated. This distribution is not directly linked to the function of a structure. But it represents the state of structure which is closely related to its function. Thus, the distribution of temperature is considered as the second category of performance parameters. The last type of performance parameters is not directly or indirectly related to any specific functions of the designed structure or part. However, they are still important, since they are mainly summarized based on those non-functional related design requirements such as mass, volume, ergonomic factors and cost of designed parts.

To achieve the performance parameters defined in the performance domain, the related properties of designed part such as elastic modulus, heat conduction coefficient should be clarified

in the third domain of the F-P-P-D model. It should be noted that these properties may non-uniformly distribute inside the given geometric boundary of design space. Thus, instead of using constant value, a mapping function is defined in the design space to describe the distribution of each property which can be stated as:

$$P_i = p_i(x), x \in D \subseteq \mathbb{R}^3 \tag{3.5}$$

Where P_i represents a specific ith property defined in the properties domain; $p_i(x)$ is its distribution function; D is the entire design space which is sub-space of 3D Euclidean space. The relationship between the properties and defined performance parameters can be expressed based on the governing equation in different disciplines. For example, in the design of a load bearing structure, the Hook's law can be used to describe the relationship between elastic modulus and displacement distribution under a given load condition.

The last domain of the F-P-P-D model is the design parameter domain. The formal definition of design parameters has already been provided in Section 3.1.3. It can be considered as the alternative configurations which the designer has a direct control over in the given design space. Generally, design parameters for mesoscale lattice structures are mainly divided into three types: geometric parameters, material parameters and mesoscale parameters. These three types of design parameters directly correspond to three models defined in Section 3.1.2 for a physical entity. Some of these design parameters are determined at the earlier initial designs stage, while others are regarded as the design variables during the optimization process. Once the value of certain parameters has been decided, it can no longer be considered as a design parameter since its value is fixed. These design parameters will directly affect the properties defined the property domain. Some property may rely on several design parameters at the same time. For example, the normalized effective elastic modulus of homogeneous lattice structure will be determined by both

cell topology as well its relative density. It should also be noticed that one design parameter may also affect more than one type of property. For instance, the change of the relative density of lattice structures will have both impacts on its effective elastic modulus and effective heat conductivity.

Generally, the F-P-P-D model proposed in this thesis provides a general tool for designers to analyze the relations between each function and their related design parameters. It establishes the foundation for the proposed multifunctional optimization method.

3.2 General framework of the proposed design methodology

Based on those basic concepts mentioned above, the general framework of the proposed design methodology is presented in this section. Its general graphic view is shown in Figure 3-4.

As it is shown in Figure 3-4, the proposed design methodology can generally take two types of design inputs. However, these two types of inputs are not simultaneously necessary for all design cases. For those innovative design cases, only the design and functional requirements are needed. These requirements can be directly summarized based on customers' needs or obtained from the requirements of its higher-level system. However, for those redesign cases, both two types of design inputs are needed. The original design result provides both geometric and material information of the old design, which may be used as a reference during the redesign process and help designers to get more design knowledge during the earlier design stage.

Besides these two design inputs discussed above, there are also another two external data sources which can provide the needed information during the design process of the proposed design methodology. They are the database of AM enabled mesoscale features and manufacturability model of selected AM process on the mesoscale structures. The information provided by these two external sources is important during the initial design stage. Particularly, the database of AM enabled mesoscale structures can help designers to quickly find a suitable type

of lattice structures to achieve the given functions and its related design requirements, while the manufacturability model is used to determine the range of each design parameters. It can guarantee the final design result is manufacturable.

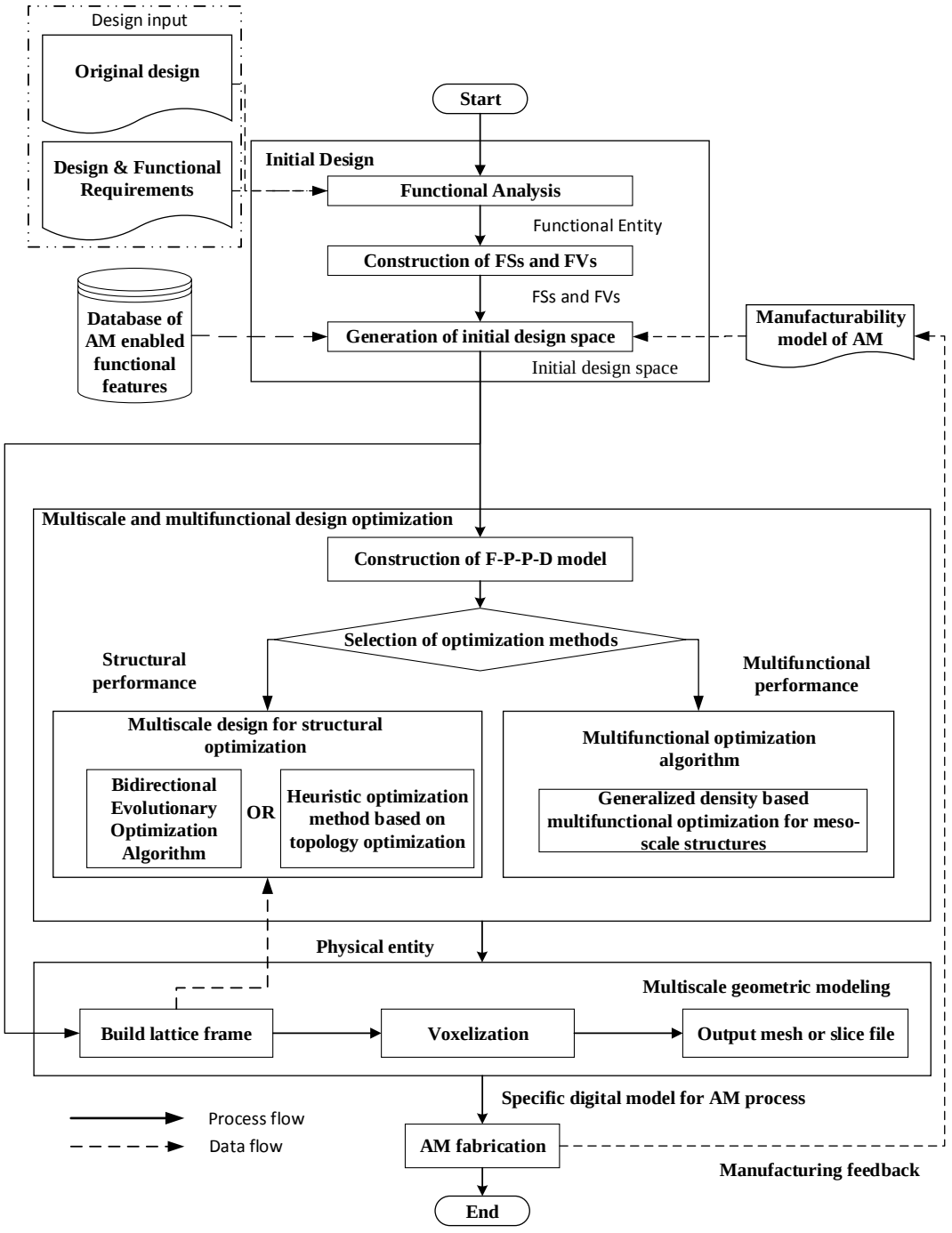

Figure 3-4 Graphic view of the proposed multiscale and multifunctional design methodology

The output of the proposed design methodology is the digital model of the designed physical entity which can be directly fabricated by a AM process. Unlike those widely used format of digital model such as STL (STereoLithography) file, the output digital model of the proposed design methodology does not require the postprocessing. It can output the sliced file which can be directly used for fabrication purposes. Thus, it further shortens the lead time between design and manufacturing.

To link the defined design inputs and outputs, the entire design process is mainly divided into three stages. They are initial design, design optimization and geometric modeling. Among these three design stages, the initial design is the first design stage which mainly focuses on the generation of the initial design space based on the given design input. In this design stage, the input functions and design requirements need to be formalized at first. Based on the formalized function and design requirements, functional entities are built to describe the functions and the required physical behaviors of designed parts. Based on the defined functional entities, the FSs and FVs can be constructed by designers. For those redesign cases, FSs can be directly extracted from its original design, but relations between the defined functions in a functional entity and extracted FSs need to be established. Based on the extracted FSs, the FVs which connect FSs and incorporate all possible geometric shape of a physical entity are built. As to those innovative design cases, FSs are constructed by analyzing the defined functions and its related material, energy and information flow to other functional entities. Based on the constructed FSs, FVs can be manually built to connect those FSs and assist FSs to achieve the given functions. The third step of the initial design stage is to divide the generated FV into several small sub-regions which are called as sub-FVs in this thesis. Different sub-FVs may be filled with different types of structures including lattice structures and solid material. The sub-FV is mainly divided into two types: sub-FVs with solid

materials and sub-FV with lattice structures. The decomposition process of FV is mainly based on the initial analysis which aims to identify the desired material behavior in each region. Based on the obtained sub-FVs, the last step of initial design is to construct the initial design space of each sub-FV. In this step, a set of parameters will be selected as the design parameters. The range of design parameter is generally decided based on the manufacturability model of the selected AM process. The design parameters with their corresponding domains construct an initial design space which is the foundation for the next design stage. Detailed techniques and processes used for initial design stage are going to be discussed in Chapter 5.

Based on the initial design space constructed in the first stage, the goal of the second design stage is to determine the value of design parameters defined in the initial design space by using the numerical optimization methods. To achieve this purpose, the F-P-P-D model needs to be built at the beginning to analyze the relations between defined function and design requirements. Based on this model, the numerical optimization formulation of design problem is built and solved. Specifically, for those applications focused on the structural performance, two different optimization methods are proposed which can efficiently improve the stiffness of designed structures without increasing its weight. As to those multifunctional applications, a generalized density based multifunctional optimization framework is proposed. In this method, the performances for different functions are simultaneously considered during the optimization process. Detailed information of those optimization processes will be presented in Chapter 6.

The last stage of the proposed design methodology is to construct the digital model of designed physical entity obtained from the previous design stage. The constructed digital model can be directly fabricated by different types of AM processes. To achieve this goal, a multiscale geometric modeling method is developed in this thesis. This geometric modeling method is a hybrid method

which combines implicit modeling, B-Rep modeling and voxel based modeling techniques together. It enables the construction of the physical entity which contains both solid and mesoscale lattice structures with a given material distribution in an efficient way. Besides building a digital model for the fabrication process, the proposed geometric modeling method also plays the role as a data support for design simulation and manufacturability evaluation in the previous two major design stages. Moreover, some terminologies defined in the lattice geometric modeling process will be also used to describe the design processes of another two design stages. Thus, the detailed data structure and algorithms used in the geometric modeling stage will be firstly discussed in the next chapter of this thesis.

3.3 Summary

In this chapter, a general design framework of multiscale and multifunctional design methodology for mesoscale lattice structures is proposed. This design methodology mainly focuses on the design freedom enabled by AM processes. It aims to help designers to achieve the design with better functional performance under the given design and functional requirements by using the mesoscale lattice structures fabricated by AM process. Compared to most existing design methods for lattice structures, the proposed design methodology has the following characteristics.

1) The proposed design methodology enables the designers to consider both solid and mesoscale lattice structures during the design process. It expanses the application potentials of lattice structures.

2) The proposed design methodology can generally consider several different types of mesoscale structures which include uniform, conformal and randomized lattice structures during the design process. Several guidelines are summarized to help designers select suitable type of lattice structures for their design.

3) Manufacturing constraints of mesoscale lattice structures are considered during the design process, which guarantees the designed structures is fabricatable.

4) The proposed design methodology can deal with lattice structures which play a multifunctional role. Specifically, the proposed F-P-P-D model can be used by designers to analyze the relations between each functions and the defined design parameters in the design space. The proposed relative density based multifunctional optimization method that will be discussed in detail in Chapter 5 can be used for the design of multifunctional purposes.

5) A unique hybrid multiscale geometric modeling process is proposed for lattice-solid structures. Compared to existing methods, this hybrid geometric modeling method can directly output the digital models for both manufacturing process and simulation process in an efficient manner. It shortens the lead time between the design and fabrication process. It also provides a seamless interface between design and simulation, which plays an important role in the design optimization stage.

Chapter 4 Multiscale Geometric Modeling for Mesoscale Lattice

In the proposed design methodology, the geometric modeling method plays a crucial role. On the one hand, it links the design and manufacturing process by providing a digital model of the physical entity which is directly fabricated by a selected AM process. On the other hand, it also provides the required geometric information for the FEA simulation of the design optimization stage. To achieve these desired functions, an efficient and flexible geometric modeling method which can deal with the structures with multiscale complexity is needed. However, according to the survey of existing geometric modeling methods for lattice structures presented in Chapter 2, it can be concluded that most existing methods cannot satisfy those requirements of the proposed design methodology. They are either time consuming or lack of flexibility for the different types of mesoscale lattice structures. The lack of suitable geometric modeling method severely prevents the design and wide application of mesoscale lattice structures.

To solve those issues and support the proposed design methodology, a multiscale geometric modeling method is developed and discussed in this chapter. Compared to the existing geometric modeling methods for mesoscale lattice structures, the proposed method can efficiently generate geometric model of lattice-solid structures by combining the advantages from several different solid modeling techniques including B-Rep implicitly modeling and voxel based modeling. Based on its unique data structures, the proposed method can be applied to generate several different types of lattice structures including uniform lattice, conformal lattice and randomized lattice. Moreover, this proposed geometric modeling method also allows a complex material distribution defined inside the designed lattice structures. Thus, it also helps designers to generate multi-materials lattice structures.

To introduce the detailed information of the proposed geometric modeling method, the subsequent contents of this chapter are organized as follows. First, the basic concepts and their data structures used in the proposed multiscale geometric modeling method are presented. Based on these defined concepts. General working flow of proposed method is briefly introduced in Section 4.2. This general working flow is divided into three steps. They are lattice frame generation, implicit function construction and voxelization. The detailed algorithms used for each step will be discussed in detail in the next three sections. After that, in Section 4.6, several case studies are presented and a comparison between existing geometric methods and the proposed method is made. At the end of this chapter, a summary is concluded.

4.1 Basic concepts

4.1.1 Lattice frame

In the proposed multiscale geometric modeling method, lattice frame is defined as the topological skeleton of a designed lattice structure. A relationship between a lattice structure and its frame is shown in Figure 4-1. Generally, the lattice frame is represented by a unidirectional graph G_s:

$$G_s = (P, E) \tag{4.1}$$

Where P is a set of points in the 3D Euclidean space. The points defined in this set are denoted as lattice nodes. E represents the set of lattice struts which is expressed as:

$$E = (p_i, p_j) \quad p_i, p_j \subseteq P, i \neq j \tag{4.2}$$

This proposed concept of lattice frame does not limit to any type of lattice structures. It can be broadly used for different types of lattice. Thus, the universal data structure which is used for lattice generation is proposed in this thesis. The graphic view of this data structure is shown in Figure 4-2.

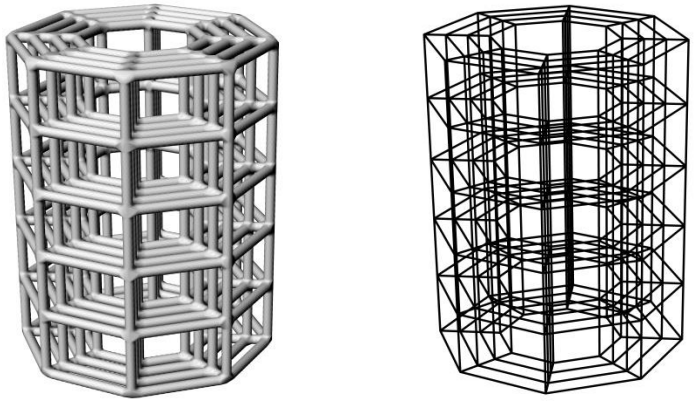

(a) Lattice structure **(b) Lattice frame**

Figure 4-1 The relationship between a lattice structure and a lattice frame

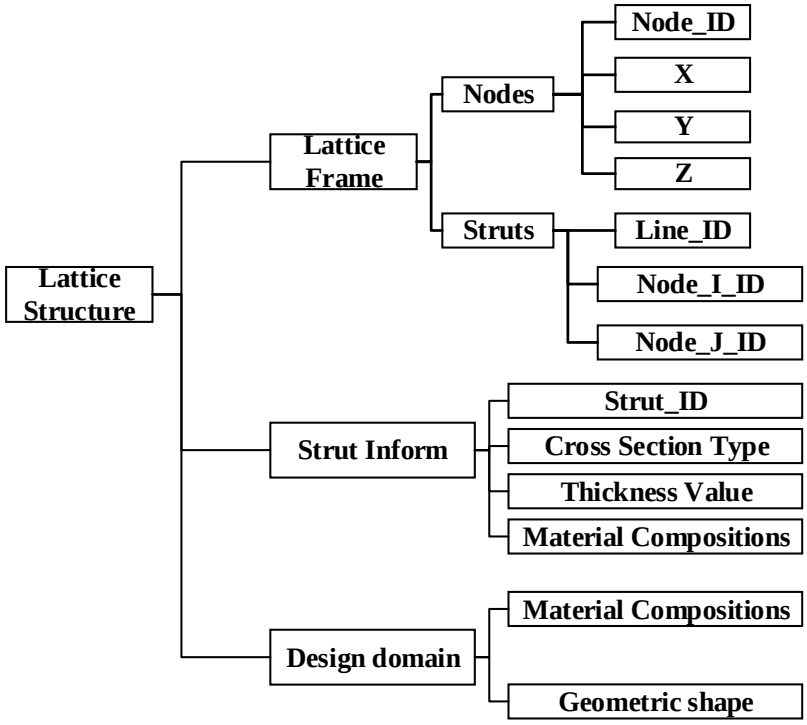

Figure 4-2 Graphic view of data structure of lattice structure

It is shown in Figure 4-2 that the data structure of lattice structure mainly consists of three parts. They are lattice frame, lattice struts and design domain. Among them, the design domain mainly describes the information of generated lattice structures on a macroscale which includes its

macro shape and macroscale material distributions. The lattice frame connects the geometric data between macroscale and mesoscale. It is generated based on several proposed algorithms discussed in Section 4.3. As to information of strut, it mainly relates to the mesoscale geometric information including shape of lattice strut and its material distribution. This information is the input to the second step of proposed method, and it will be discussed in detail in Section 4.4.

4.1.2 Lattice unit cell

In this thesis, the lattice unit cell is generally referred to as the minimal unit which is defined to describe the characteristic of designed lattice structures. The definitions of lattice unit cell are different for different types of lattice structures considered in this thesis. Thus, in this sub-section, the definitions of lattice unit cells for three different types of lattice structures are discussed respectively.

Uniform lattice

The frame of uniform lattice structure is composed of periodically distributed unit. The simplest repeating unit in the uniform lattice structure is defined as its unit cell. Due to the periodicity of uniform lattice frame, classical notion of crystal structures is used to describe this type of unit cell. Specifically, the primitive cell of a lattice unit cell is formulated based on the lattice translational symmetry primitive bases $\overrightarrow{a_k}$ where $k = 1,2$ for 2D lattice, and $k = 1,2,3$ for 3D cases. The defined primitive cell should contain the minimal number of lattice nodes. The defined primitive cells can be considered as a translational tiling of the entire space. In Figure 4-3, several different 2D lattice structures are given. The general shape of primitive cell of 2D lattice is parallelogram. Two translational base vectors are regarded as the two-adjacent edge of parallelogram. The size of 2D lattice cell is defined based on the length its primitive cell's edges which equal to the length of two translational base vectors. The geometric center of primitive cell

is referred to as the kernel point. It represents the position of each unit primitive cell.

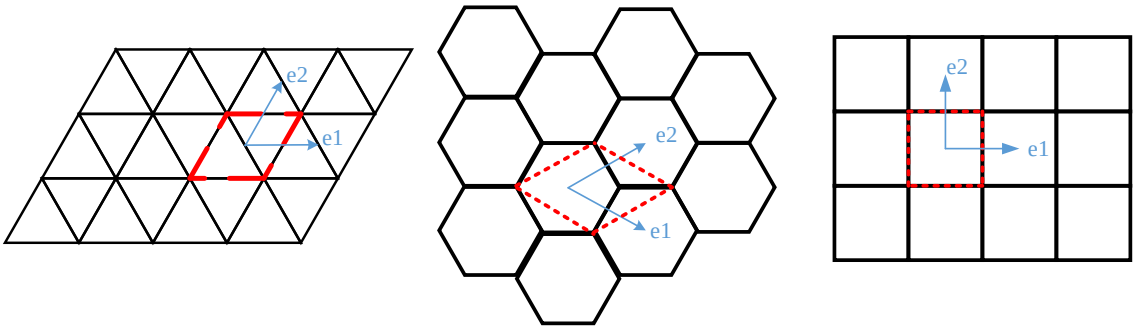

(a) 2d-triangular lattice frame (b) 2d-hexagon lattice frame (c) 2d-square lattice frame

Figure 4-3 Examples of 2D uniform lattice structures

In 3D cases, the primitive cell of uniform lattice structures is generally defined as a parallelepiped. The three translational base vectors of a uniform lattice structure form the three edges of a parallelepiped that meet at one vertex. Like 2D lattice structures, the length of three translational base vectors is defined as the size of 3D lattice unit cell. If the three translational base vectors are orthogonal to each other, the shape of primitive cell will become cuboid. This type of uniform lattice structures is called as a cuboid lattice structure. Due to its unique symmetric properties, it is the most widely used type of uniform lattice structures. Thus, unless otherwise stated, the uniform lattice structures mentioned in this thesis all indicate cuboid lattice structures. Several examples of unit cell of cuboid lattice are provided in Figure 4-4.

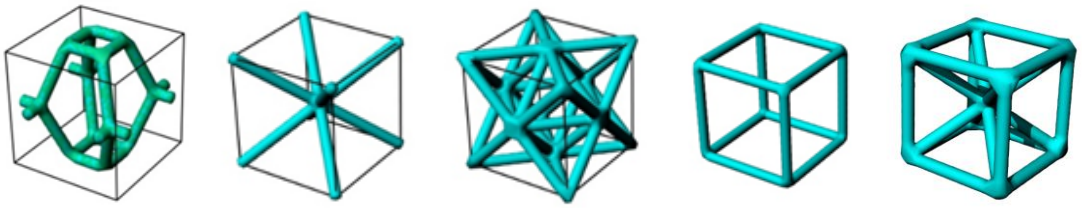

(a) 3d Hexagon (b) "X" shape cell (c) Octahedron Cell (d) Cubic cell (d) Body center cubic cell

Figure 4-4 Examples of unit cells of cuboid lattice

Generally, the lattice node defined in each unit cell can also be described by the local

coordinate system which is constructed by translational bases vectors. Particularly, the centroid of each cell primitive is considered as the origin of the local coordinate system. The translational bases vectors are considered as its axes. If the primitive cell is defined in a rectangular or cuboid shape, the local coordinate system of lattice cell is orthogonal. Otherwise, it is an oblique coordinate system. The relation between cell local coordinate system and global coordinate system is shown in Figure 4-5.

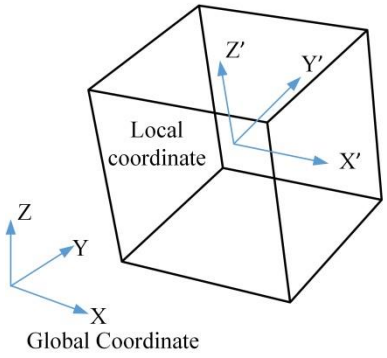

Figure 4-5 A relation between local coordinate and global coordinate

For cuboid lattice structures, the concept of lattice orientation is proposed. The lattice orientation can be described as a triplet Euler angles (α,β,γ) defined between lattice local system and global coordinate system in ZYZ order. An example is demonstrated in Figure 4-6. In this example, the lattice local coordinate system is regarded as a reference coordinate system, while the global coordinate system which is used for the design of FV is considered as the derived coordinate system.

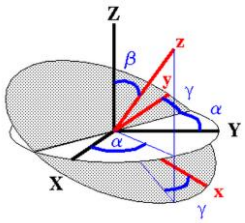

XYZ: Lattice local coordinate system
xyz: Global coordinate system

Figure 4-6 Lattice orientation

Based on the concept of lattice orientation, for any lattice node $p = (x, y, z)$ defined in the local coordinate system of cuboid lattice unit cell, its position $p' = (x', y', z')$ defined in the global coordinate system is calculated by the following equation:

$$\begin{bmatrix} x' \\ y' \\ z' \end{bmatrix} = T + \mathbf{L}\begin{bmatrix} x \\ y \\ z \end{bmatrix} = \begin{bmatrix} t_x \\ t_y \\ t_z \end{bmatrix} + \begin{bmatrix} l_{11} & l_{12} & l_{13} \\ l_{21} & l_{22} & l_{23} \\ l_{31} & l_{32} & l_{33} \end{bmatrix}\begin{bmatrix} x \\ y \\ z \end{bmatrix} \tag{4.3}$$

Where (t_x, t_y, t_z) is the centroid of lattice unit cell defined in the global coordinate system. l_{ij} is the component of transformation matrix **L**. The value of l_{ij} is calculated based on the defined Euler angle (α,β,γ) which represents the orientation of unit cell. Its formulation is expressed as:

$$\mathbf{L} = \begin{bmatrix} \cos\alpha\cos\beta\cos\gamma - \sin\alpha\sin\gamma & \sin\alpha\cos\beta\cos\gamma + \cos\alpha\sin\gamma & -\sin\beta\cos\gamma \\ -\cos\alpha\cos\beta\sin\gamma - \sin\alpha\cos\gamma & -\sin\alpha\cos\beta\sin\gamma + \cos\alpha\cos\gamma & \sin\beta\sin\gamma \\ \cos\alpha\sin\beta & \sin\alpha\sin\beta & \cos\beta \end{bmatrix} \tag{4.4}$$

For those uniform lattice structures with non-cuboid unit cell, the concept of lattice orientation angle cannot be used to describe their orientation during the design process. But Equation 4.3 can also be used to convert the vector defined in unit cell's local coordinate systems to global coordinate system. However, the transformation matrix **L** for this type of lattice structures cannot be calculated by Equation 4.4, since this equation can be only applied to the transformation between two orthogonal coordinate systems. For a general case, a new equation is given to calculate this transformation matrix which is expressed as:

$$\mathbf{L} = \begin{bmatrix} i_x & i_y & i_z \\ j_x & j_y & j_z \\ k_x & k_y & k_z \end{bmatrix} \tag{4.5}$$

Where (i_x, i_y, i_z) (j_x, j_y, j_z) (k_x, k_y, k_z) are components defined in global coordinates to describe three unit base vectors of the local coordinate of a lattice unit cell.

To describe the topology of lattice unit cell, cell topology model is developed. In this model, a regular parent primitive cell is defined in the reference coordinate. In 2D lattice structures, it is a

square, while in 3D cases, it is defined as a cube which is shown in Figure 4-7(a). Each lattice node is presented as a point defined in the parent primitive described by the reference coordinate system as:

$$p_c = (\xi, \eta, \mu) \in P_c \subseteq [-1,1]^3 \tag{4.6}$$

Where P_c is a set of all the nodes defined in the lattice unit cell. Based on the lattice nodes, the topology of lattice unit cell is described by a unidirectional G_c, This graph is defined as:

$$G_c = (E_c, P_c) \tag{4.7}$$

Where E_c represent a set of struts which is defined between two nodes. Specifically, the edge e_c in the set E_c is represented by an unordered pair of nodes:

$$e_c = \{p_i, p_j\}, p_i, p_j \in P_c \tag{4.8}$$

Once the topology of lattice cell is determined, the frame of lattice unit cell can be built based on the mapping function defined between reference coordinate and the local coordinate of the unit cell. In this thesis, a trilinear mapping function is built by linking corresponding corner points of parent primitive cell and the primitive cell defined in the local coordinate of a lattice unit cell, which is shown in Figure 4-7 (b). The general form of this mapping function is expressed as:

$$\begin{bmatrix} x \\ y \\ z \end{bmatrix} = \begin{bmatrix} x_1 & x_2 & x_3 & x_4 & x_5 & x_6 & x_7 & x_8 \\ y_1 & y_2 & y_3 & y_4 & y_5 & y_6 & y_7 & y_8 \\ z_1 & z_2 & z_3 & z_4 & z_5 & z_6 & z_7 & z_8 \end{bmatrix} \begin{bmatrix} N_1^c(\xi, \eta, \mu) \\ N_2^c(\xi, \eta, \mu) \\ N_3^c(\xi, \eta, \mu) \\ N_4^c(\xi, \eta, \mu) \\ N_5^c(\xi, \eta, \mu) \\ N_6^c(\xi, \eta, \mu) \\ N_7^c(\xi, \eta, \mu) \\ N_8^c(\xi, \eta, \mu) \end{bmatrix} \tag{4.9}$$

Where (x, y, z) is the point defined in the local coordinate of lattice unit cell, while (ξ, η, μ) represents its position in the reference coordinate system. (x_i, y_i, z_i) is the position of ith corner of the primitive cell defined in the local coordinate of lattice unit cell. $N_i^c(\xi, \eta, \mu)$ is the shape

function. The general form of shape function is expressed as:

$$N_i^c(\xi,\eta,\mu) = \frac{1}{8}(1-\xi_i\xi)(1-\eta_i\eta)(1-\mu_i\mu) \tag{4.10}$$

Where (ξ_i, η_i, μ_i) is the position of i[th] corner of the parent primitive cell defined in the reference coordinate system.

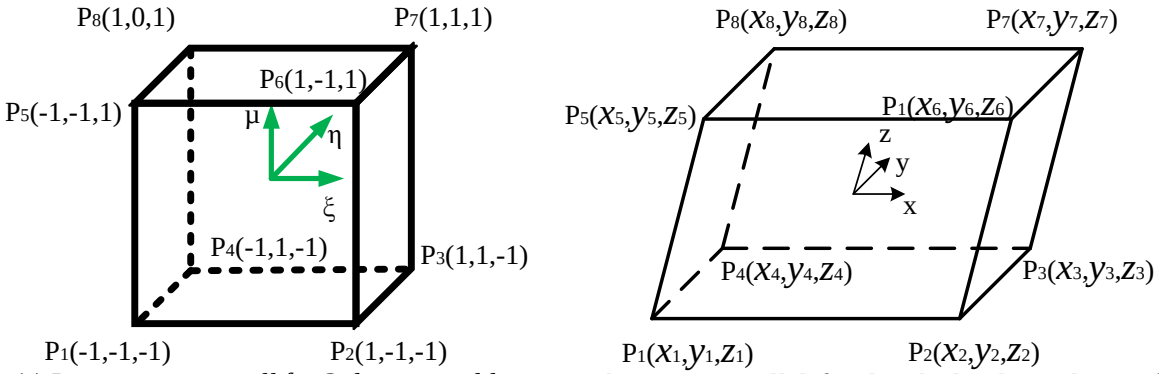

(a) Parent primitive cell for 3-dimensional lattice defined in the reference coordinate

(b) primitive cell defined in the local coordinate of lattice unit cell

Figure 4-7 The reference coordinate systems used to describe cell topology

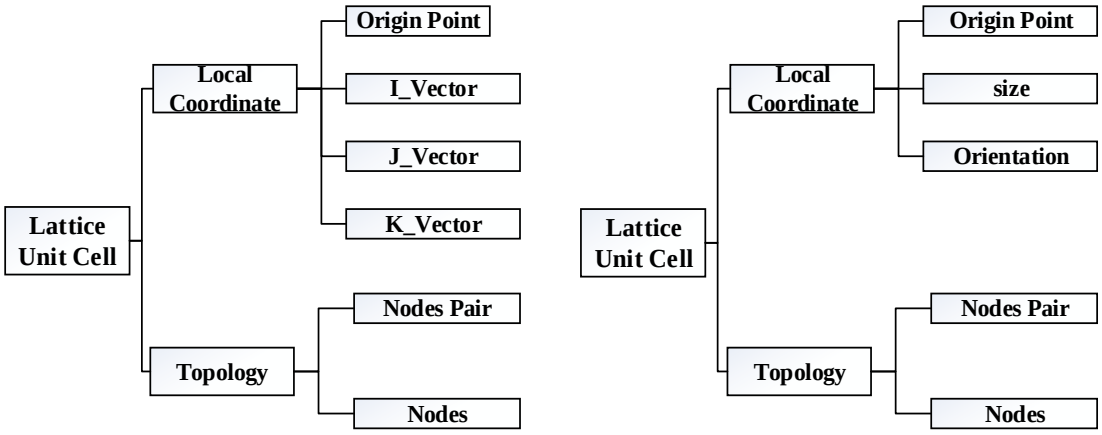

(a) general data structure for lattice unit cell

(b) simplified data structure for cuboid unit cell

Figure 4-8 Graphic view of the data structure of a lattice unit cell for uniform lattice structures

To summarize the lattice unit cell model discussed above, the unit cell defined for uniform

lattice structures in this thesis mainly includes two types of information. They are cell topology model and the shape of its primitive cell. Thus, the data structure of lattice unit cell is developed. its graphic view is given in Figure 4-8 (a). Particularly for the cuboid lattice focused in this thesis, this general data structure is simplified into Figure 4-8 (b), where lattice orientation angle and size are used instead of three translational base vectors.

Conformal lattice structures

The definition of lattice unit cell of uniform lattice structures cannot be directly applied on the conformal lattice structures, since there is no periodically distributed unit pattern in the design space of conformal lattice structures. However, by carefully analyzing the topology of conformal lattice's frame, it can be found that the lattice frames can be classified into a group of units which share the same topology. This unit which contains the smallest number of lattice nodes is referred to as unit cell for conformal lattice structures. Based on this definition, it can be inferred that the shape of each unit cell defined in the conformal lattice may change, but its topology should be the same. An example of the unit cell of conformal lattice is provided in Figure 4-9. It is manifest that each cell defined in the conformal lattice generally shares the same "x" topology. However, the shapes and orientations of lattice unit cells in different region of design domain are different.

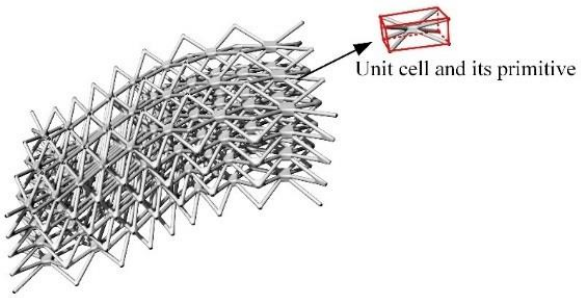

Figure 4-9 Unit cell of conformal lattice structures

Like uniform lattice structures, the unit cell of conformal lattice structures can also be

described by its topology and cell shape. As to the topology of unit cell, the topology model discussed above for uniform lattice structures can be used. For the cell shape, since the cells of conformal lattice no longer satisfy the periodic condition, their shape cannot be described in a parallelepiped primitive cell. Thus, in this thesis, a more general hexahedron primitive cell is used to describe the shape of the unit cell for conformal lattice structures. Specifically, the shape of a hexahedron primitive is described by the eight corners which are sequentially defined in the global coordinate system. Their sequence should be defined based on the following rule:

Rule 4-1 Lattice node sequencing rule:

1) Choose a starting corner point with the minimum coordinate value with respect to lexicographic order along x, y and z axis. This point is numbered as 1.

2) There are three corner points linked to the point 1. Choose the point which has maximum value on x axis as the point 2.

3) Choose a point which has the maximum value on y axis from three linked points of point 1 as the point 4

4) The last corner point on the plane defined by points 1,2,4 is numbered as point 3.

5) The corner point which is linked to point 1 and on the opposite side of the plane defined by point 1,2,4 is numbered as point 5

6) On the opposite plane of plane defined by point 1,2,4, another three corner nodes are numbered anticlockwise.

The example of numbered hexahedron primitive is provided and shown in Figure 4-10. Unlike the uniform lattice structures discussed above, it is usually difficult to directly characterize the size of the unit cell of conformal lattice structures. For each cell, its cell size is defined as the largest diameter of circumscribed sphere defined by any four corner points of the cell. This parameter

helps designers to control the average cell size during the lattice frame generation.

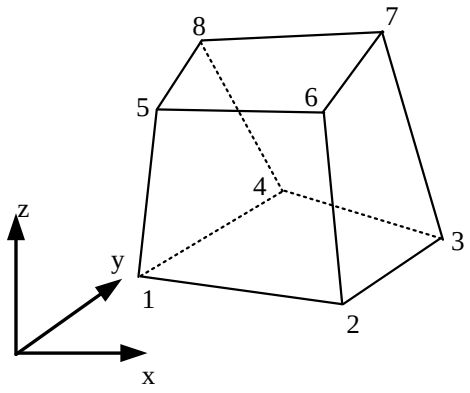

Figure 4-10 Numbering order of hexahedron primitive for a unit cell

Based on the defined hexahedron primitive and the topology model of lattice unit cell, the frame of each lattice cell in the conformal lattice structures can be easily obtained. The graphic view of unit cell defined for conformal lattice structures is shown in Figure 4-11.

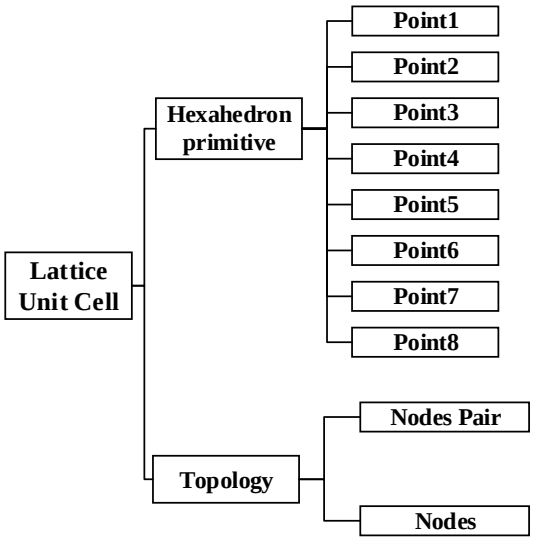

Figure 4-11 Graphic view of the data structure of a unit cell of conformal lattice

Randomized lattice structures

Compared to uniform and conformal lattice structures discussed above, both the cell type and its topology of randomized lattice structure vary in the design space. In this thesis, the unit cell of

randomized lattice is defined based on the polyhedron whose edges are the struts of randomized lattice structures. If all the unit cells in the designed randomized lattice are in the tetrahedron shape, this type of randomized lattice is called as tetrahedron-based lattice structures. Otherwise, for those randomized lattice structures which are built based on Voronoi cell, they are generally referred to as Voronoi-based lattice structures. Difference between Voronoi-based lattice and tetrahedron-based lattice is shown in Figure 4-12. It is obvious that compared to tetrahedron lattice, the cells of Voronoi lattice usually combines several different types of polyhedrons. They are more like natural randomized foam structures.

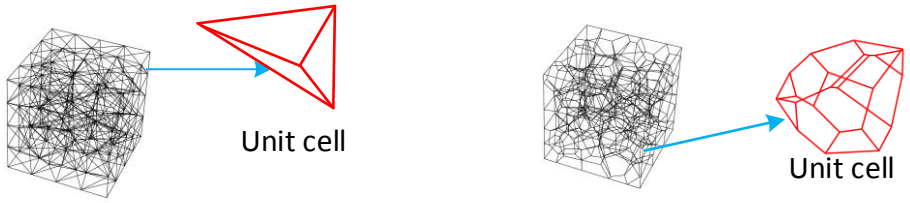

(a) Unit cell of tetrahedron based randomized lattice

(a) Unit cell of Voronoi based randomized lattice

Figure 4-12 Unit cells for two different types of randomized lattice structures

Like the conformal lattice structures discussed above, the size of randomized lattice is also difficult to be directly characterized. For tetrahedron based randomized lattice, the diameter of its circumscribed sphere is considered as the factor to evaluate its size. For Voronoi lattice, the size of the cube which has the same volume of the Voronoi polyhedron cell is considered as its size. Based on this definition, the size of Voronoi lattice is efficiently controlled.

Unit cell of both types of randomized lattice can be expressed as their defined polyhedron. Thus, the general data structure of the unit cell of randomized lattice structures is developed and shown in Figure 4-13.

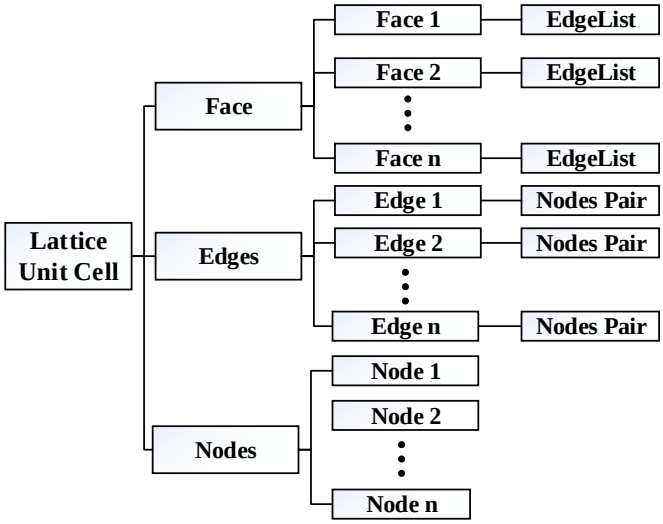

Figure 4-13 Graphic view of defined data structure of unit cell in randomized lattice

4.1.3 Conformal surface

In this thesis, the concept of conformal surface is proposed to represent the surface which is used to control the shape of unit cell near the conformal surface. Specifically, the shape of each cell should be deformed to keep integrity on the boundary defined by the conformal surface. An example of conformal surface and its related conformal lattice structure is provided in Figure 4-14(a). Compared to the uniform lattice structures designed in the same shape of design domain which is shown in Figure 4-14(b), each unit cell located on the defined conformal surface is complete which can adapt to the shape of the selected surface.

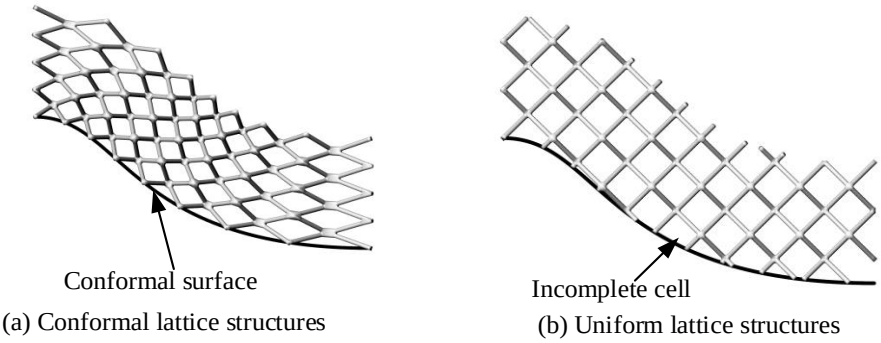

Figure 4-14 Example of conformal surface

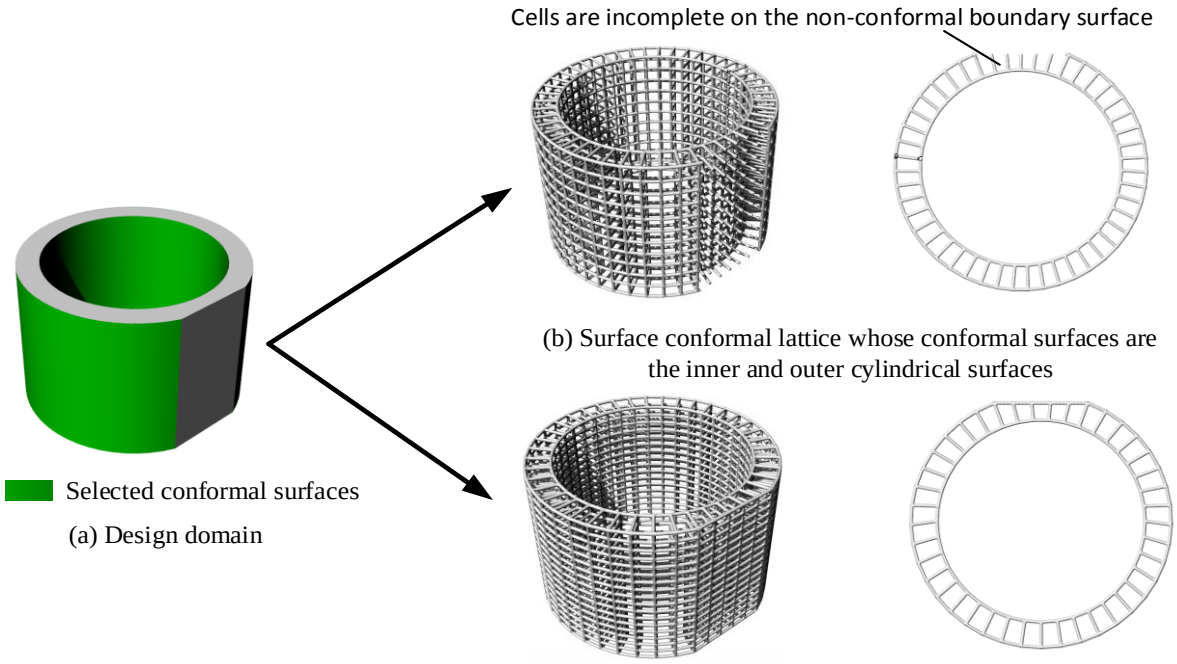

Figure 4-15 Comparison between two types of conformal lattice structures

In most design cases, conformal surfaces can be selected from the boundary of the design domain of a lattice structure. It can be used to control the trend of the shape change of cells. It should be noted there is a difference between the defined conformal lattice in this thesis and conformal lattice introduced in some existing literatures [107]. In this thesis, conformal lattice structures only need to vary the shape for the selected conformal surfaces. They are not required to adapt to all the boundary surfaces of a given design domain. To differentiate the conformal lattice defined by Wang [107], the conformal lattice structures proposed in this thesis are also called as surface conformal lattice structures. If all the boundary surfaces of a design domain are selected as conformal surfaces, then this type of conformal lattice structures is as the same as the conformal structures defined by Wang[107]. In this thesis, this type of conformal lattice structures is called as volume conformal lattice structures, since it adapts to all the boundary surfaces of a design domain. The difference between these two types of conformal lattice is shown in Figure

4-15. It is manifest that there are several incomplete cells located on the front flat surface of cylinder for the surface conformal lattice structure shown in Figure 4-15(b), since this surface is not selected as conformal surface. However, all the cells are completely defined in the volume conformal lattice structure shown in Figure 4-15(c), as all the boundary surfaces of this design domain have been selected as conformal surfaces for the volume conformal lattice structures.

4.2 General working flow

Based on those basic concepts introduced in the previous section, the general working flow of multiscale lattice geometric modeling method is presented in this section. As it is shown in Figure 4-16, this general working flow is mainly divided into three steps. They are lattice frame generation, construction of geometry and materials functions, and voxelization.

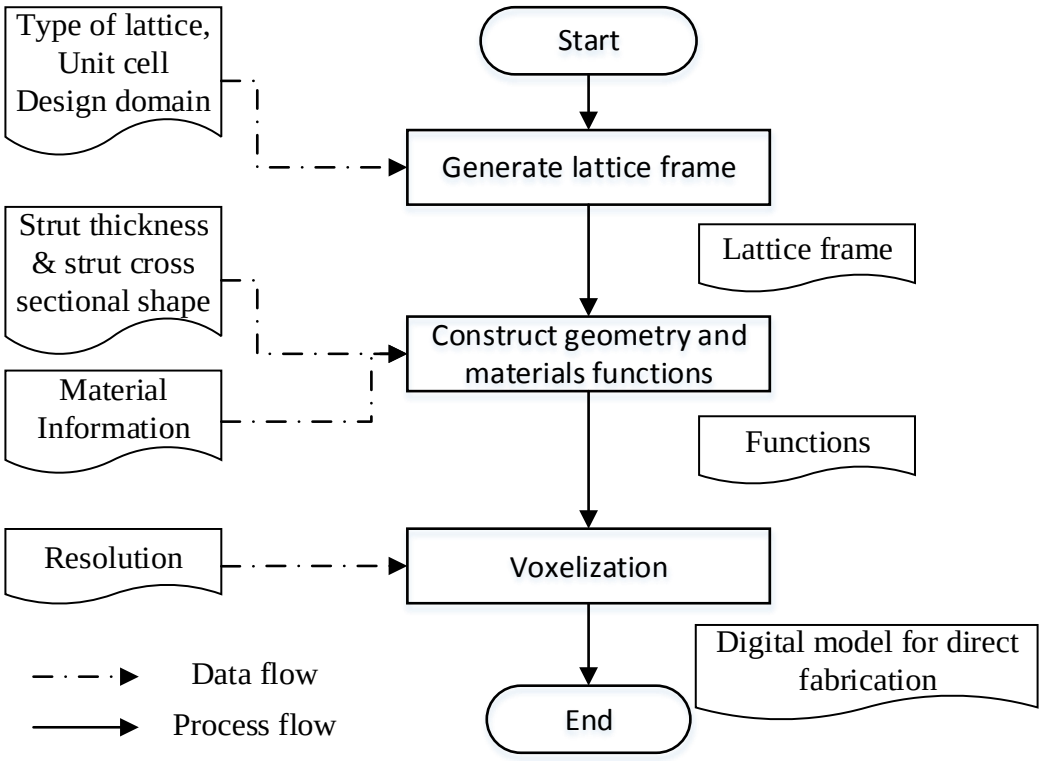

Figure 4-16 General working flow of multiscale geometric modeling of lattice structures

Lattice frame is going to be generated in the first step. To generate lattice frame, the

information related to the lattice type, unit cell model and design domain is needed. Different frame generation methods are proposed for different types of lattice structures. Then, based on the generated lattice frame and selected cross-section shape of lattice structures, implicit functions are established to describe the geometry of lattice struts defined in the lattice frame. Moreover, materials distribution of the lattice structures can be also described as a set of functions defined on macro and mesoscale. Finally, the voxelization process will be done to evaluate the value of implicit function for geometry as well as the materials distribution functions at each grid point in the design domain. Then, the digital model including slice image or slice contour is directly output for fabrication process. These three major steps will be discussed respectively in the following contents of this chapter.

4.3 Lattice frame generation

The first step of multiscale geometric modeling process is to construct lattice frame. Different types of lattice frames are generated using different methods. In this section, the lattice frame generation methods for uniform lattice, conformal lattice and randomized lattice structures will be introduced respectively. Even though the details for each type of lattice frame generation method are different, they share the common working flow which is shown in Figure 4-17.

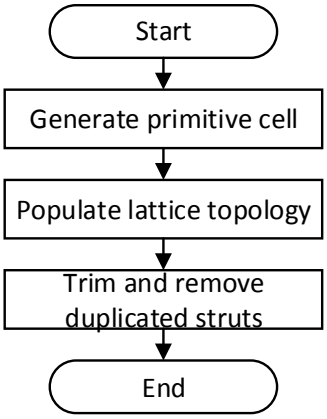

Figure 4-17 Common working flow for lattice frame generation

4.3.1 Uniform lattice structures

The detailed steps of the frame generation of a uniform lattice structure are shown in Figure 4-18. It is generally divided into 6 sub-steps. At the beginning, the primitive cells of uniform lattice structures should be generated. In the proposed method, the center of each primitive cell which is denoted as its kernel point is used to represent its position. To obtain the kernel points shown in Figure 4-18, the following developed algorithm is applied.

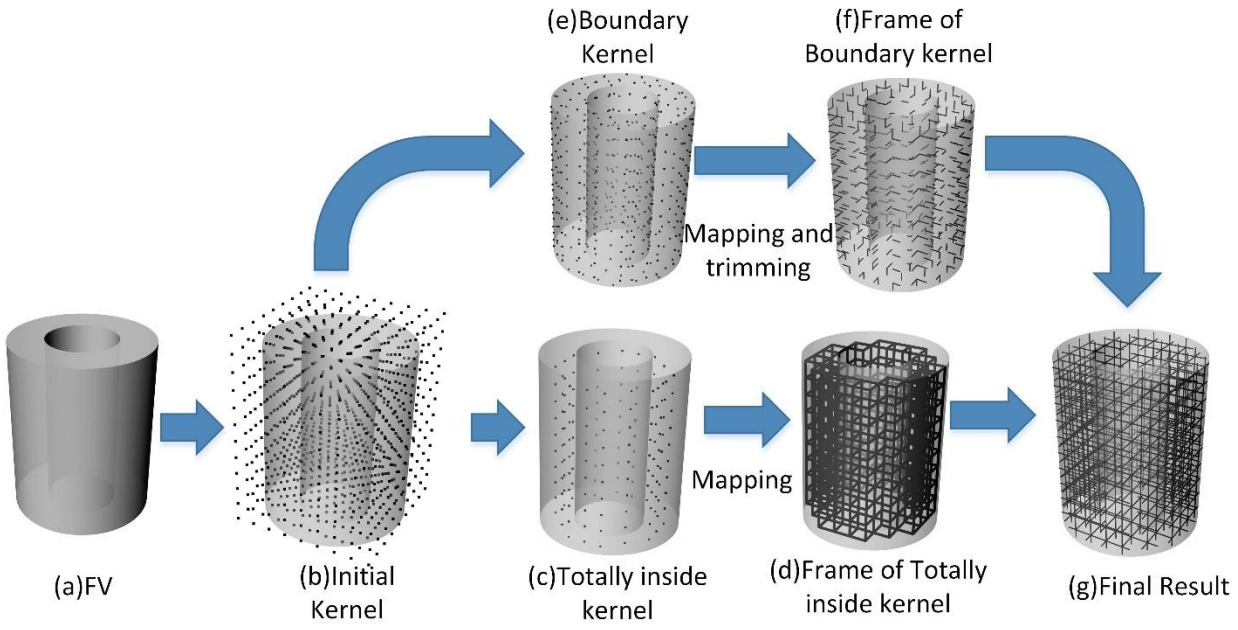

Figure 4-18 Frame generation of uniform lattice structures

Algorithm 4-1: kernel points generation algorithm

1) Based on the lattice orientation, construct the bounding box of design domain which is denoted as B_d. The base of bounding box should be parallel to the XOY plane of lattice unit cell's local coordinate system.

2) Build a kernel point p_i based on the following equation:

$$p_i = (x_{min} + \frac{l_x}{2}, y_{min} + \frac{l_y}{2}, z_{min} + \frac{l_z}{2}) \tag{4.11}$$

Where $(x_{min}, y_{min}, z_{min})$ is the point inside the bounding box with minimum coordinate values

along each global design coordinate system. (l_x, l_y, l_z) refers to lattice cell size.

4) Calculate other kennel points inside the bounding box with the equation:

$$p_{(a,b,c)} = \left(x_i + al_x, y_i + bl_y, z_i + cl_z\right), \;\; a, b, c \in Z^+, p_{(a,b,c)} \in B_d \tag{4.12}$$

Where (x_i, y_i, z_i) denotes the coordinate values of initial kernel point p_i.

Based on the above algorithm, the kernel points of uniform lattice structures are generated. The example is shown in Figure 4-18(b).

After obtaining all the initial kernel points of designed uniform lattice structures based on the algorithm presented above, the second sub-step is to differentiate kernel points according to their positions. Rather than generating a lattice frame for the entire grid of kernel points, which would need significant trimming time, the kernel points are categorized to the following sets:

1) Internal kernel points set P_i – Kernel points are located inside the design domain;

2) External kernel points set P_e – Kernel points are located outside the design domain;

3) Boundary kernel points set P_b – Points are neighboring the boundary of the design domain. Its represented cell is partially located inside the design domain;

4) Totally Inside points set P_{ti} – Points are in P_i which are not in P_b, which can be expressed as $P_{ti} = \{p | \, p \in P_i \wedge p \notin P_b\}$;

To recognize the boundary kernel points set P_b and totally inside points set P_{ti}, the following rules are developed.

Rule 4-2: Boundary kernel points recognition rule

Suppose points k_1 and k_2 are two adjacent kernel points in the kernel grid of design domain, if $(k_1 \in P_i) \oplus (k_2 \in P_i)$, then both k_1 and k_2 are boundary kernel points, denoted as $k_b \in P_b$. In this rule, the symbol "$\oplus$" means "exclusive or". The boundary kernel points are shown in Figure 4-18(e).

Rule 4-3: Totally inside kernel points recognition rule

Suppose point k_1 is a kernel point of FV f, if $k_1 \in P_i \wedge k_1 \notin P_b$, then k_1 is a totally inside kernel point, which is denoted as $k_{ti} \in P_{ti}$. The totally inside kernel points are shown in Figure 4-18(c).

After classification of kernel points based on these two rules, the lattice topology model is used to generate the frame of lattice unit cell. For the uniform lattice structures discussed in this sub-section, the shapes of all the unit cell are the same. Thus, the mapping function defined in Equation 4.9 only needs to be applied once. Then, the frame of each unit cell is be obtained. This frame is transformed to the location of each primitive cell based on transformation matrix defined in Equation 4.3 where the kernel points will be generally considered as the origin of each cell's local coordinate. By applying Equation 4.3 to all kernel points totally inside the design domain, the frame of totally inside kernel points is obtained which is shown in Figure 4-18(d).

Besides totally inside kernel points P_{ti}, the frame of boundary kernel points also needs to be constructed. For these kernel points, the frame of each point is also built based on Equation 4.3. However, the built frame needs to be trimmed with the boundary of a design domain. To realize this step, the following algorithm is developed.

Algorithm 4-2: lattice frame trimming algorithm

1) Suppose p_1 and p_2 are the endpoints of a strut l.

2) If p_1 and p_2 are both outside the FV, strut l is removed.

3) If p_1 and p_2 are both inside the FV, strut l is preserved.

4) If p_1 and p_2 are on opposite sides of the FV boundary, strut l is trimmed. To do this, strut l is intersected with the FV boundary, and split into two sub-struts l_1 and l_2. The sub-strut that is outside the FV is removed.

The result of this step is shown in Figure 4-18(f). By combining the frame of totally internal kernel points and the frame of boundary kernel points and removing the duplicate struts, the frame of uniform lattice structures is built which is shown in Figure 4-18(g).

4.3.2 Conformal lattice structures

The workflow of lattice frame generation method for conformal lattice is shown in Figure 4-19. It is mainly divided into three sub-steps, and will be discussed in details in the following contents.

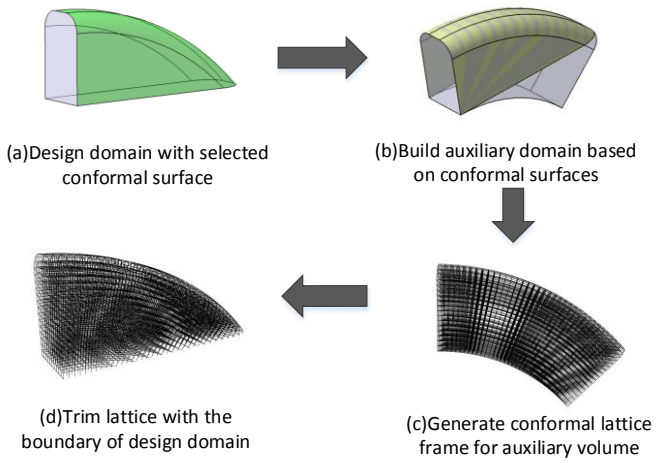

Figure 4-19 Conformal lattice frame generation

The first sub-step is to build auxiliary domain based on the conformal surfaces selected by designers. To guarantee the generated conformal lattice frame can adapt to the selected conformal surface, the generated auxiliary design domain should satisfy the following criteria:

Criteria 4-1: Criteria for auxiliary design domain of a conformal lattice structure

1) The generated auxiliary domain should include its original design domain

2) Conformal surfaces of the original design domain should also be the boundary of its related auxiliary domain.

3) The generated auxiliary domain should be in a mapped shape or can be split into a mapped shape.

The concept of mapped shape used in this thesis is directly adapted from one of volumetric mesh technique called “sweeping”[201]. This technique extrudes 2D mesh into a general third dimension. However, it has a strong requirement on the regularity of a design domain. Generally, the mapped shape is defined as a geometric body which contains two opposing faces (source and destination) and faces that directly connect the source and destination (along faces) [202]. An example of mapped shape body is shown in Figure 4-20. For any given design domain, there might be more than one auxiliary design domains which satisfies the Criteria 4-1. Generally, different auxiliary design domain may generate different lattice frames. In a trivial case, if the design domain itself is in a mapped shape, the auxiliary design domain equals to its original design domain. The generated lattice frame of this type of design domain must be a volume conformal lattice, since all cells keep integrity on the entire boundary of the design domain.

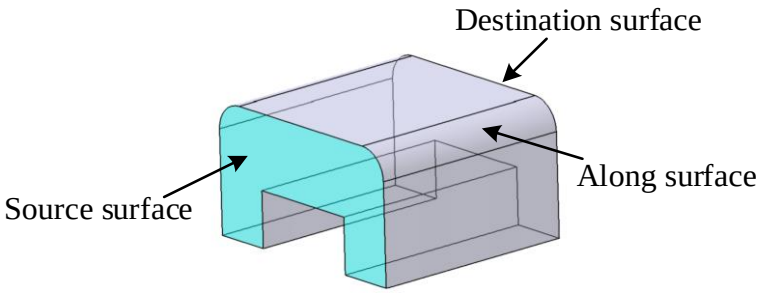

Figure 4-20 An example of mapped shape

Based on the auxiliary design domain obtained from last sub-step, the hexahedron primitives are obtained by meshing the generated auxiliary domain based on the volumetric mesh technique called “sweep” [201]. The obtained hexahedron primitives defined in the auxiliary design domain are generally considered as the primitive cells for conformal lattice structures. The cell of each hexahedron primitive is built based on lattice topology model and the mapping function described in Equation 4.9. Specifically, the lattice nodes inside each hexahedron primitive cell are calculated by Equation 4.9 and its 8 corner points. Based on the lattice topology data model, the struts are

constructed for the certain pairs of nodes, and saved in the edge set E_c. This process will be repeated cell by cell until the frame of all the hexahedron primitive cells are generated. By removing the duplicate nodes and struts, the frame of conformal lattice is obtained and its example is shown in Figure 4-19(c).

The last step of lattice frame generation for conformal lattice is the trimming process. Like uniform lattice structures, the cells which are located on the non-conformal surfaces need to be trimmed. For this step, Algorithm 4-2 presented for uniform lattice structures is applied. An example of the result of this step is shown in Figure 4-19(d).

4.3.3 Randomized lattice structures

Compared to uniform and conformal lattice structures, the topology of randomized lattice structures is difficult to be directly controlled. The position and orientation of each cell is not uniformly distributed inside the design domain. Like the uniform and conformal lattice structures, the first step of lattice frame construction for randomized lattice structures is to generate its primitive cells inside the design domain. Since designers cannot directly control the frame topology in each primitive cell of randomized lattice structures, the edges of primitive cells will be directly converted to the frame of lattice structures.

For tetrahedron based randomized lattice structures, the unstructured meshing techniques [203] which generate the tetrahedron elements inside a given design domain are mature. Among these techniques, the algorithm based on constrained Delaunay triangulation technique [204] is the most suitable one for the lattice frame generation because the distribution of cell size can be easily controlled by designers in a given design domain to satisfy given design requirements. Moreover, this algorithm can generate boundary conformal Delaunay tetrahedron cells. These cells satisfy the condition for the volume conformal lattice. Thus, the tetrahedron based randomized lattice

structures are also considered as a special type of conformal lattice structures in the some literatures[107, 120]. For more on the constrained Delaunay triangulation techniques, readers can refer to these cited references[203, 204].

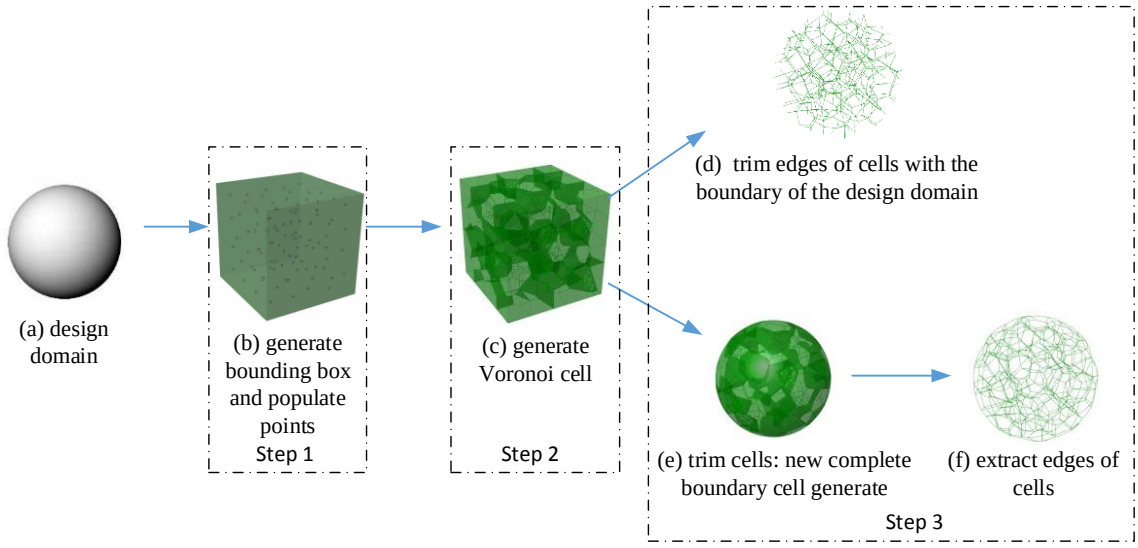

Figure 4-21 Frame generation of Voronoi based randomized lattice structures

As to a Voronoi cell based randomized lattice structure, its frame generation process is mainly divided into three steps, which are shown in Figure 4-21. The first step is to generate the randomly distributed points inside the bounding box of the design domain, which is shown in Figure 4-21(b). These points will be considered as the centers of Voronoi cells. Based on the populated points, the Voronoi polyhedrons which are shown in Figure 4-21(c) are generated based on the Voronoi tessellation algorithm inside the design domain. The edge of Voronoi cell will be regarded as the frame of Voronoi cell. At the end, the frame will be trimmed with the boundary of the design domain. The result is shown in Figure 4-21(d). It should be noted that the cell of trimmed frame will be incomplete after the trimming process like uniform lattice structures. To get the complete cell frame on the boundary of a design domain, the new completed polyhedron cells are built by cutting the boundary cells with the boundary of a design domain, which is shown in Figure 4-21(e). To replace those incomplete cells with newly built complete cell, the lattice frame with smooth

boundary is generated. In this thesis, the Voronoi based randomized lattice structure with the incomplete cell struts located on the boundary is referred to as nonsmoothed Voronoi based randomized lattice structures, while its counterpart is denoted as a smooth or conformal Voronoi based lattice structure.

To control the average size of Voronoi based randomized lattice structures, the number of populated points should be controlled. Generally, the number of points populated in the design domain is calculated based on the average cell size with the following Equation:

$$N_p = \lfloor V_D / l^3 \rceil \tag{4.13}$$

Where N_p denotes the number of center points for Voronoi cells; l is the preferred average cell size; V_D is the volume of a given design domain. It should be noted that Equation 4.13 is derived directly from the definition of Voronoi cell size in Section 4.1.2. To minimize the deviation of cell size, Lloyd's algorithm [205] is suggested to be applied after the initial points population process to evenly distribute the points in the bounding box. The standard deviation of cell sizes is significantly reduced after applying the Lloyd's algorithm on randomized populated points [206].

To further control the distribution of cell size inside the design domain, a unique points population method is proposed in this thesis. The major steps of this method are graphically presented in Figure 4-22. Its first step is to segment the bounding box of design domain into several sub-boxes. In each sub-box, a specific value of average cell size is predefined by designers. Based on the predefined cell size, Equation 4.13 is used to calculate the number of points for each sub-box. Then, the point population method discussed above will be applied to populate points in each sub-box. After that, Lloyd's algorithm will be applied on the entire bounding box of a design domain to smooth the distribution of points. This algorithm can update the position of Voronoi cell to locally reduce the size difference between neighbored cells. To keep the gradient of points

distribution which is predefined by designers, Lloyd's algorithm should only be applied for n_l iterations, where n_l is suggested to be smaller than 3. If the number n_l is too large, it will make the cell size evenly distribute inside the design domain again. At the end, the Voronoi cells are built based on the smoothed points, and the frame of Voronoi based randomized lattice structures are obtained. As it is shown in Figure 4-22(f), the cell size of generated lattice frame is gradually changed along Z axis. By controlling the total number of points, designers can control the average cell size inside the entire design domain.

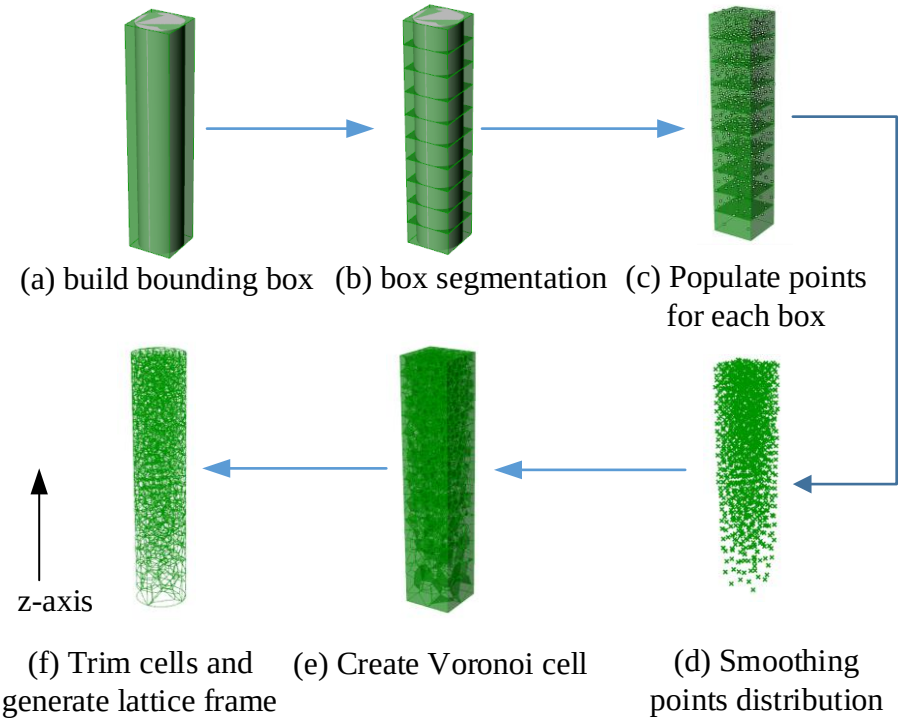

Figure 4-22 Point population method to control the cell size distribution inside the design domain

4.4 Construction of geometric and material distribution function

Based on the generated frame of lattice structures, the implicit functions are built to describe the geometry of each strut. The material distribution functions are established to represent the distribution of each material composition inside the designed lattice structures. In this section,

these two types of functions will be discussed respectively in the following two sub-sections.

4.4.1 Implicit function for geometry

To represent a solid strut defined in a lattice structure, the implicit modeling technique will be used. Specifically, a regular geometric set, which contains all the points inside solid struts, is described by a general function as:

$$S_t = \{P(x,y,z) | f(x,y,z) > 0, P \in \mathbb{R}^3\} \tag{4.14}$$

Where f is the implicit function defined for a given strut of lattice frame. Generally, there are several different ways to define the implicit functions for different purposes [207]. In this thesis, the implicit function is defined based on the generated lattice frame. For any strut e_i defined in the generated lattice frame, its implicit function is defined based on the Gaussian function:

$$f_{ei}(r) = ae^{-br^2} - c \tag{4.15}$$

Where r is defined as:

$$r = min\|P - P_e\|_p, P_e \in e_i \subset \mathbb{R}^3, P \in \mathbb{R}^3 \tag{4.16}$$

Where $\|\cdot\|_p$ denotes a p-norm defined in 3D Euclidean space. In Equation 4.15, a, b are two parameters which are used to control the shape of Gaussian function. *c* is generally referred to as a thresh hold of defined implicit function. By controlling the values of these parameters, the size of strut is varied. Specifically, in this thesis, both *a* and *c* are predefined by designers and kept as the constant during the strut solidification process. To get a solid strut, *a* should always be larger than *c*. As to parameter b, its value is determined based on the size of lattice strut. For a circular cross sectional shape strut, the value of parameter b is calculated by following equation:

$$b = \frac{1}{R^2} ln \frac{a}{c} \tag{4.17}$$

Where R is the radius of a strut. To further control the cross-sectional shape of strut, the value of p defined in Equation 4.16 can be changed. If p equals to 2, the defined cross-sectional shape is

the circle whose radius is the constant R. If p is infinitive, the cross-sectional shape of strut is the square whose edge length is $2R$. If p equals to the certain value which is defined from two to infinitive, the cross-sectional shape of strut will be in a transitional shape from a circle to a square. Several implicit surfaces of struts with different p values are shown in Figure 4-23.

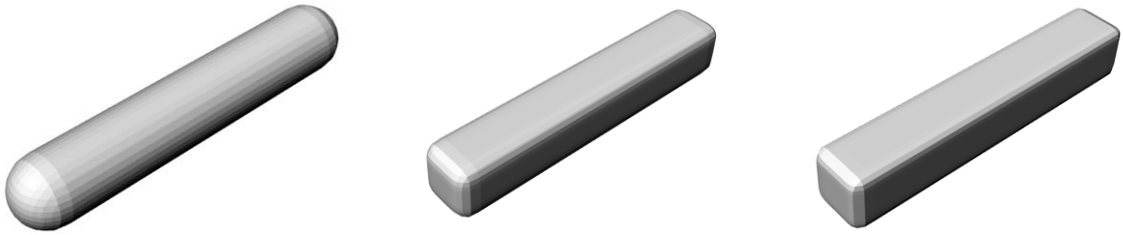

P=2 P=3 P=10

Figure 4-23 Implicit surface of a single solid strut with different p values

It is computationally expensive to directly evaluate the function defined in Equation 4.15 due to this function contains the exponential term. To approximate the function defined in Equation 4.15, a piecewise quadratic function has been used. The form of this function is expressed as:

$$f_{ei}(r) = \begin{cases} a\left(1 - \frac{3r^2}{b^2}\right) - c & 0 \le r < \frac{b}{3} \\ \frac{3a}{2}(1 - \frac{r}{b})^2 - c & \frac{b}{3} \le r \le 3 \\ -c & r \ge b \end{cases} \tag{4.18}$$

Equation 4.18 is in the same form as the well-known metaball function proposed by Nishimura [208]. However, it should be noted that the r defined in Equation 4.18 represents the measure of distance between a point to a strut which is defined in Equation 4.16. Like the Equation 4.15, *a* and *c* are also be predefined by users as a constant. To control the cell size, the parameter *b* defined in Equation 4.18 is calculated by the equation given below:

$$b = \begin{cases} \sqrt{\frac{3a}{a-c}}R, \frac{c}{a} > \frac{2}{3} \\ \frac{R}{1-\sqrt{\frac{2c}{3a}}}, \frac{c}{a} \le \frac{2}{3} \end{cases} \tag{4.19}$$

Where *R* denotes the size of strut cross section. Specifically, it is a radius of circular cross sectional

strut or half-length of a cubic cross-sectional shape.

Those functions introduced above can be used to build solid body for every lattice strut defined in lattice frame. However, it should be noted that there must exist some points which satisfy the condition defined in Equation 4.14 for several different struts simultaneously. The set of these points are defined as the conjunction region of lattice struts. To join the independently solidified lattice struts into a single solid structure, the union of lattice implicit functions for a lattice frame with *n* struts is defined as:

$$f(P) = \max\left(f_{e_i}(r)\right), i = 1,2,3,\dots,n \tag{4.20}$$

Where r is defined as the distance between the point P to strut e_i according to Equation 4.16. An example of solidified implicit surface of a given uniform lattice structure is shown in Figure 4-24.

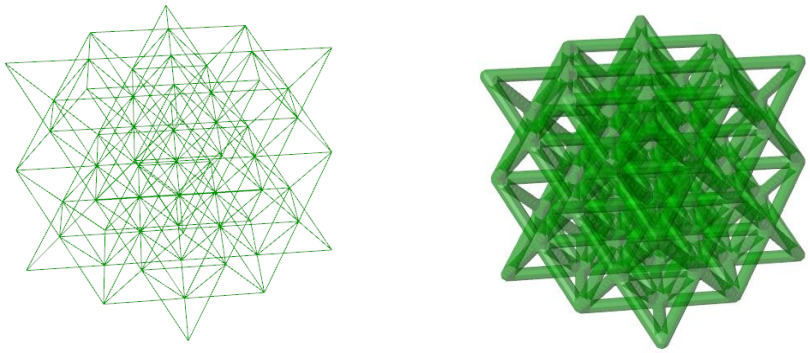

(a) lattice frame

(b) solidified lattice strut represented by implicit functions

Figure 4-24 An example of defined implicit function for the solidification of lattice frame

4.4.3 Material distribution function

Besides the geometric shape of lattice strut, material distribution function also needs to be built to describe the distribution of material compositions inside the design domain. The general form of material distribution function is expressed as:

$$A_m = f_m(P), A_m \in \mathbb{R}^n, P \in S_l \subset \mathbb{R}^3 \tag{4.21}$$

Where A_m is attribute vector to describe the material compositions at each point in the design domain. S_l represents a set of points in the lattice struts. The components of A_m is expressed as:

$$A_m = (m_1, m_2, \dots, m_n) \in \mathbb{R}^n, 0 \leq m_i \leq 1 \tag{4.22}$$

$$\sum_{i=1}^{n} m_i = 1 \tag{4.23}$$

Where m_i is the volume fraction of ith primary material. In a trivial case, the entire lattice structure is made of a single material. This function is considered as the constant function whose value equals to one over the entire solid region of lattice. For non-trivial cases, there are usually more than one types of materials. To describe the multi-material distribution inside the design domain, two general types of functions are used in this thesis. They are the macroscale material distribution function and mesoscale material distribution function. The former one is defined based on the global coordinate system of a design domain, while the later one is defined based on local coordinate of each strut. These two types of material distribution functions will be discussed respectively.

On macroscale, the material distribution can be directly defined based on the coordinate of the design domain of lattice structures. Thus, it can be independently modeled without considering the geometric details of the generated lattice structures. Some existing modeling methods [119] can be used to define the material distribution function on the design domain. One of them is to define a discrete function for the design domain. Specifically, a design domain needs to be further decomposed into a set of sub-domains. In each sub-domain, the materials are uniformly distributed with the prescribed material distribution vector A_m in each sub-domain. A mapping function from sub-domain to material distribution vector can be considered as a discrete function. The limitation of discrete representation is the material compositions on the border between different sub-domains are not continuous. Thus, the sub-domain should be as small as possible. Besides discrete

representation method, some continuous explicit functional including exponential functional, polynomial functional, and trigonometric functional can all be applied in the 3D space to describe the materials distribution inside the design domain. Moreover, the materials distribution can also be implicitly defined based on some geometric elements on a macroscale. Those geometric elements can be generally referred to as control features. The material distribution function can be defined based on the distance between any point P and those control features. The detailed discussion of those available methods for material distribution function on a macroscale will not be detailed discussed in this thesis, since they have already been thoroughly studied and summarized in existing references [119, 158, 209]. Two examples of lattice structures with macroscale materials distribution are given in Figure 4-25. In this figure, lattice structures are composed of two materials which are denoted as α and β. Only the distribution of α material is given. The distribution of β can be easily calculated based on the distribution of α material.

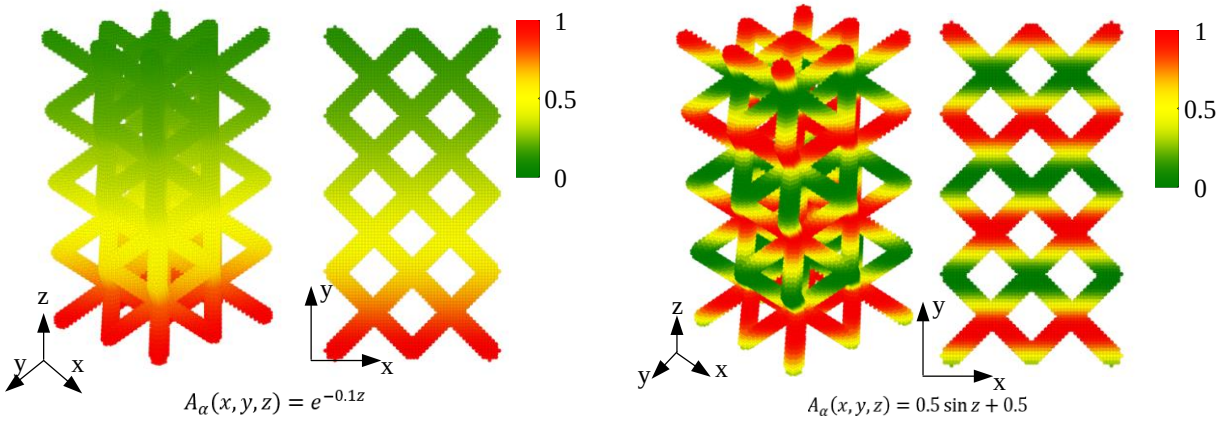

(a) Exponential function along Z

(b) Trigonometric function along Z

Figure 4-25 Material distribution function on a macroscale

On mesoscale, the materials distribution function is defined based on the local coordinate of struts. Thus, each lattice strut on mesoscale may have its own material distribution function. In this thesis, this material distribution function is defined locally based on the local coordinate of each

lattice strut which is expressed as:

$$A_m = f_{me_i}(r, t_{min}), 0 \leq r \leq R, 0 \leq t_{min} \leq 1 \quad (4.24)$$

Where A_m is the material distribution vector at any point P located in the i[th] solid strut of a lattice structure, $P \in S_{t_i}$; f_{me_i} is the material distribution function for the i[th] lattice strut defined in a lattice frame. r is described by Equation 4.16 as the minimal p-norm of the vector defined from the point P to any point P_e on the i[th] lattice strut in a lattice frame. R is the upper bound of r , which represents the size of lattice strut. The point on the lattice strut which can achieve the minimal value of p-norm on the defined vector in Equation 4.16 is regarded as P_{min}. t_{min} denotes a parameter corresponding to point P_{min} in the parametric equation of the i[th] strut. In this thesis, the normalized parametric equation is used to describe each strut in the lattice frame. To construct this equation, the start and end points of each lattice strut need to be determined at first. These two points are directly obtained from the data structure of lattice frame. But its sequence should be decided based on their coordinates. A rule is given to sort the sequence of strut nodes for the parametric equations used in this thesis. Specifically, the node with smaller coordinate value with respect to lexicography order along x, y, z axes is considered as the start node. Otherwise it is considered as the end node. Once the sequence of nodes is determined, the normalized parametric equation can be easily determined.

Practically, the general function f_{me_i} defined in Equation 4.24 for each lattice strut is rewritten into the form of compound function as:

$$f_{me_i}(r, t_{min}) = g\big(r, h(t)\big) = g \circ h \quad (4.25)$$

Where function $h(t)$ is used to describe the material distribution along each strut axis; function g(r) is used to describe the material distribution along the radius direction of strut axis. These two functions can be determined by designers independently and be integrated as the compound

function described in Equation 4.25. An example of material distribution function for a lattice strut shown in Figure 4-26 is given. This image is obtained by slicing the strut along its axis. For this lattice strut, it is supposed to be made of two materials α and β which are heterogeneously distributed inside the lattice strut. The material distribution function of α material can be explicitly defined by designers with the compound of the linear function and the exponential function which is given below:

$$f_{\alpha_{e_i}}(r, t_{min}) = e^{-r}(0.3 + 0.2t_{min}) \tag{4.26}$$

Based on this function, the function of material β can be simply defined as:

$$f_{\beta_{e_i}}(r, t_{min}) = 1 - f_{\alpha_{e_i}}(r, t_{min}) = 1 - e^{-r}(0.3 + 0.2t_{min}) \tag{4.27}$$

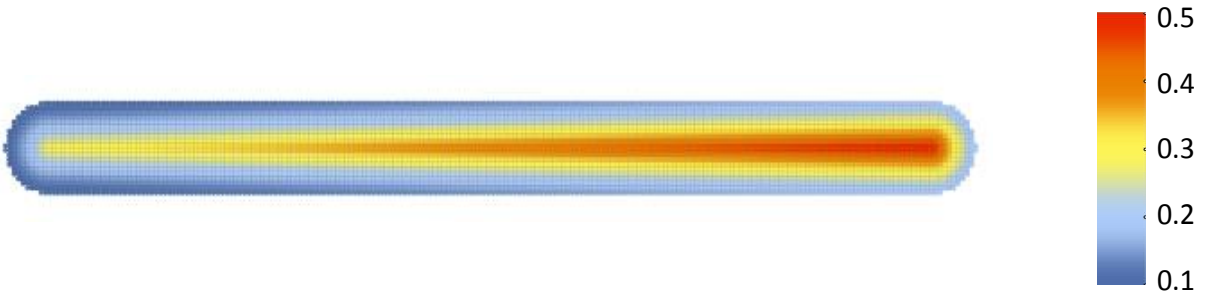

Figure 4-26 Distribution of α material in a single strut

Generally, the Equation 4.24 can be used only for those points that belongs to a single strut in the lattice frames. For other points located at the conjunction region of several lattice struts, an additional material blending function needs to be used. The general form of a weight factors based blending function is expressed as:

$$A_m(P) = \sum_{i=1}^{i=n} W_i(r_i) A_{me_i}(P) \ , \sum_{i=1}^{i=n} W(r_i) = 1 \ , 0 \le r_i \le R_i \tag{4.28}$$

Where $A_m(P)$ is the vector of material compositions at point P. $A_{me_i}(P)$ is the vector of material compositions calculated by its ith related strut at Point P. $W_i(r_i)$ is the weight factor function for ith related strut. r_i is the p-norm of the vector defined in Equation 4.16 which represents the

distance between point P to the i[th] strut. Since point P belongs to i[th] strut, r_i should be smaller or equals to the size of i[th] strut which is denoted as R_i is the Equation 4.28.

It is obvious that the key of blending function for material distribution at the conjunction region of struts is its weight factor equation. Inverse distance based weight function is the mostly widely used weight function for material blending [119]. Its detailed form is expressed as:

$$W_i(r_i) = \frac{\prod_{j=1,j\neq i}^{n} r_i}{\sum_{i=1}^{n}\prod_{j=1,j\neq i}^{n} r_i} \tag{4.29}$$

The weight function defined in Equation 4.29 states the closer point P to the i[th] strut is, the more influence of i[th] strut will have on the materials distribution on point P. However, this function has an obvious shortcoming when it applies to mesoscale lattice structures which usually contain a large number of struts. If it is only applied on the conjunction region, the material will be discontinuously distributed between the conjunction region and other regions of each lattice strut. This is mainly because the material distribution functions used to describe different regions are different. If the blending function is applied to the entire design domain, it will be computationally expensive to evaluate the weighting factor function in Equation 4.29, since no cutting-off is defined in this equation. The distance and material distribution vectors of point P with respect to every strut around it need to be evaluated. To avoid this issue, another weight factor function is proposed in this thesis, which is expressed as:

$$W_i(r_i) = \frac{[1-\frac{r_i}{aR_i}]_+^q}{\sum_{i=1}^{n}[1-\frac{r_i}{aR_i}]_+^q}, a > 1, q \in z^+, q \geq 1 \tag{4.30}$$

Where $[x]_+$ is max (0, x); R_i is the size of i[th] lattice strut, a and q are two parameters defined in Equation 4.30 which are used to control the shape of weight distribution function. In Equation 4.30, parameter a is used to control the size of blending region. The concept of blending region is defined as the conjunction region of lattice struts with struts' cross-sectional size as the vector

which is expressed as:

$$R = (aR_1, aR_2, \dots, aR_n) \tag{4.31}$$

In the extreme case, when a equals to one, the blending region strictly equals to the conjunction region of a given set of struts. On the point whose distance to all related struts are equal to the vector defined in Equation 4.31, the denominator of right hand side of Equation 4.30 will equal to zero. Thus, this point is the singularity point which lead the discontinuity of material distribution at that point. To avoid this issue, parameter a should be larger than 1, which is considered as an amplification coefficient defined between the conjunction region and material blending region. Only material in the blending region needs to be evaluated by the blending function defined in Equation 4.30. This function is continuous on the boundary of blending region, since the weighting function of i^{th} approaches to zero on the surface of blending region defined by this strut.

Besides blending functions discussed above which are based on the weight factors, maximum and minimum function are also applied to calculate the material compositions at the conjunction region of lattice struts. Its general formulation is defined as:

$$A_m(P) = \max\left(A_{me_i}(P)\right) i = 1,2,3 \dots, n \tag{4.32}$$

Where $\max(\cdot)$ is defined as a maximum function which is based on lexicographic order of $\mathbb{R}^n$ .Compared to the weight factor based blending functions, Equation 4.32 can save the computational time, since it does not need to calculate the weight factor of each strut. For lattice struts who may have the same material distribution on the conjunction region, the distribution of material compositions calculated by Equation 4.32 is continuous. However, when the different lattice struts have different material compositions on the same lattice node, the material distribution function will be discontinuous at the border between two struts. A comparison is given in Figure 4-27 to show the difference between two different types of blending functions. Like other lattice

struts discussed in this sub-section, the lattice struts in Figure 4-27 are also made of two materials α and β. In Figure 4-27 (a) and (b), two types of blending functions are used for lattice struts with different material distribution functions. The discontinuous edge is observed in Figure 25(a) which takes the maximum blending function defined in Equation 4.32. The edge is blurred by the blending function defined in Equation 4.30. Thus, the material composition changed continuously in the design domain. Figure 4-27 (b) and Figure 4-27 (c) show lattice struts with the same materials distribution function. Both blending functions provide continuous material distributions inside the design domain. Compared to the weight factor based blending function, the maximum blending function defined in Equation 4.32 is more smooth.

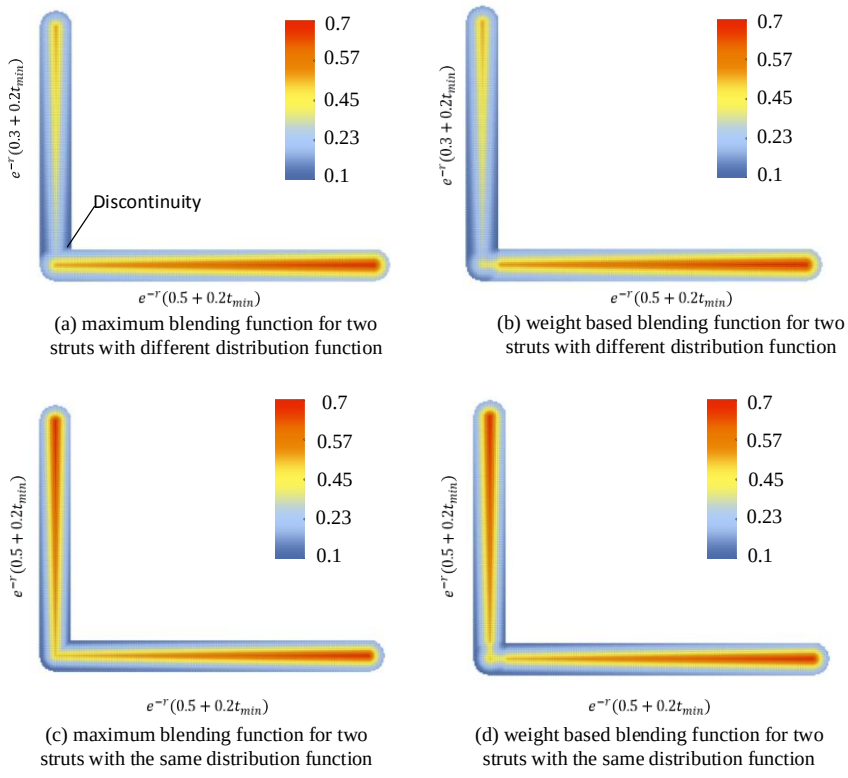

(a) maximum blending function for two struts with different distribution function

(b) weight based blending function for two struts with different distribution function

(c) maximum blending function for two struts with the same distribution function

(d) weight based blending function for two struts with the same distribution function

Figure 4-27 Different blending functions for lattice struts at conjunction regions for a certain material composition

Besides these two types of functions which are used to control materials distribution on macroscale and mesoscale independently, designers can also integrate these functions to control

the material distribution inside lattice structures on different design scales simultaneously. Like the compound function defined in Equation 4.25, to simultaneously control the materials distributions on both macro scale and mesoscale, designers can take the compound function of two types of functions discussed above. Its specific expression is given as:

$$f = f_{macro} \circ f_{meso} \tag{4.33}$$

Where f_{macro} and f_{meso} are materials distribution functions defined on macro and meso scale respectively. Material compositions of each point inside the design space are determined by its local and global coordinates. An example of controlling material distribution on both macro and mesoscale is given in Figure 4-28. In this example, an exponential function is applied to control the material distribution locally for every strut. A quadratic function is applied to control material distribution globally for each point.

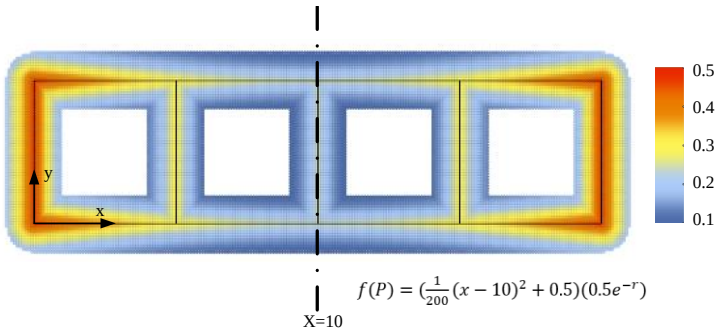

Figure 4-28 An example of multiscale material distributions

4.5 Voxelization

The last step of geometric modeling process is to convert the functions defined in the second step discussed in Section 4.4 into the voxel representation which can be directly used for Additive Manufacturing process. This process is referred to as voxelization process in the proposed method. In general, a voxel represents a value of a certain point of a regular grid defined in 3D space. This value can be defined in different data types including integer, Boolean float, even vectors for different purposes. In this thesis, to represent the geometry of lattice structure, the float number is

used to describe the value of implicit function at certain grid point. It can be easily converted to binary voxel which can be directly used for AM processes. For multi-material case, a material distribution vector is used. The component of this vector represents the volume fraction of material on the grid point. It should be noted that both voxels for geometry and material compositions should be defined on the same grid for a single design case.

To further describe the grid defined for voxelization process, several parameters are introduced in this paragraph. In this thesis, the grid point is assumed to be uniformly distributed in the design space. The grid spacing is denoted as a vector (dx, dy, dz). This vector is also called as voxel size in this paper. If voxel is defined in a cube where $dx = dy = dz$. The size of vector is described by a single scalar dv where $dv = dx = dy = dz$. Based on the spacing vector, each grid point's coordinate is calculated:

$$G_{ijk} = P(i,j,k) = P_0 + (i \cdot dx, j \cdot dy, k \cdot dz), i = 1, \dots, n_x, j = 1, \dots, n_y, k = 1, \dots, n_z \quad (4.34)$$

Where (i,j,k) is the index of grid point. P_0 is the coordinate of the grid point whose index is (0,0,0). (n_x, n_y, n_z) represents the number of grid points in each direction of a coordinate system. The total length of grid is calculated based on the equation defined below:

$$\left(l_x, l_y, l_z\right) = (n_x \cdot dx, n_y \cdot dy, n_z \cdot dz) \quad (4.35)$$

Where $\left(l_x, l_y, l_z\right)$ represents the total length of grid on each direction.

The voxelization process is divided into two sub-steps: grid construction and voxel value calculations. In the first sub-step, a bounding box of design domain of lattice structures is obtained. Then, the grid spacing vector are determined by designers according to the resolution of selected AM process and lattice struts' diameters. Based on the selected spacing vector and the size of bounding box, the number of grid points along each axis is calculated using Equation 4.35.

The second step is to calculate the voxel value of each point inside the defined grid. Generally,

this thesis provides two different methods to calculated the voxel value of each grid points. They are point-wise voxelization and strut-wise voxelization. The detailed working flow of these two different voxelization processes are provided in Figure 4-29 and Figure 4-30 respectively. In point-wise voxelization process, voxel values are evaluated point by point in the grid defined for a given design domain. For each point, the distance between points to all lattice struts needs to be evaluated. Then, based on the evaluated distance vectors the implicit function for geometry and materials distribution functions are evaluated. It should be noted that the point-wise voxelization process is usually more time consuming, as the distances between a grid point to every strut in the lattice frame need to be evaluated. Compared to geometry and material functions, evaluation of distance functions takes more time. Thus, this method is only suitable for lattice structures with a small number of struts.

Compared to point-wise voxelization process, the strut-wise voxelization does not require the evaluation of every point inside the grid of a design domain. It only requires to evaluate grid points inside a bounding box of struts. To construct this bounding box, a specialized algorithm is proposed as below:

Algorithm 4-3: Algorithm to construct strut oriented bounding box in grid for voxelization

1) Construct the bounding box B for selected strut. The diagonal corner of bounding box is represented as (P_{min}, P_{max})

2) Enlarge the constructed bounding box to the bounding box whose diagonal corner is $(P_{min} - (mR, mR, mR), P_{max} + (mR, mR, mR))$, where m is the magnification factor which is larger than one, and R represents the radius of the lattice strut;

3) Calculate the grid points inside the enlarged bounding box obtained from the previous step.

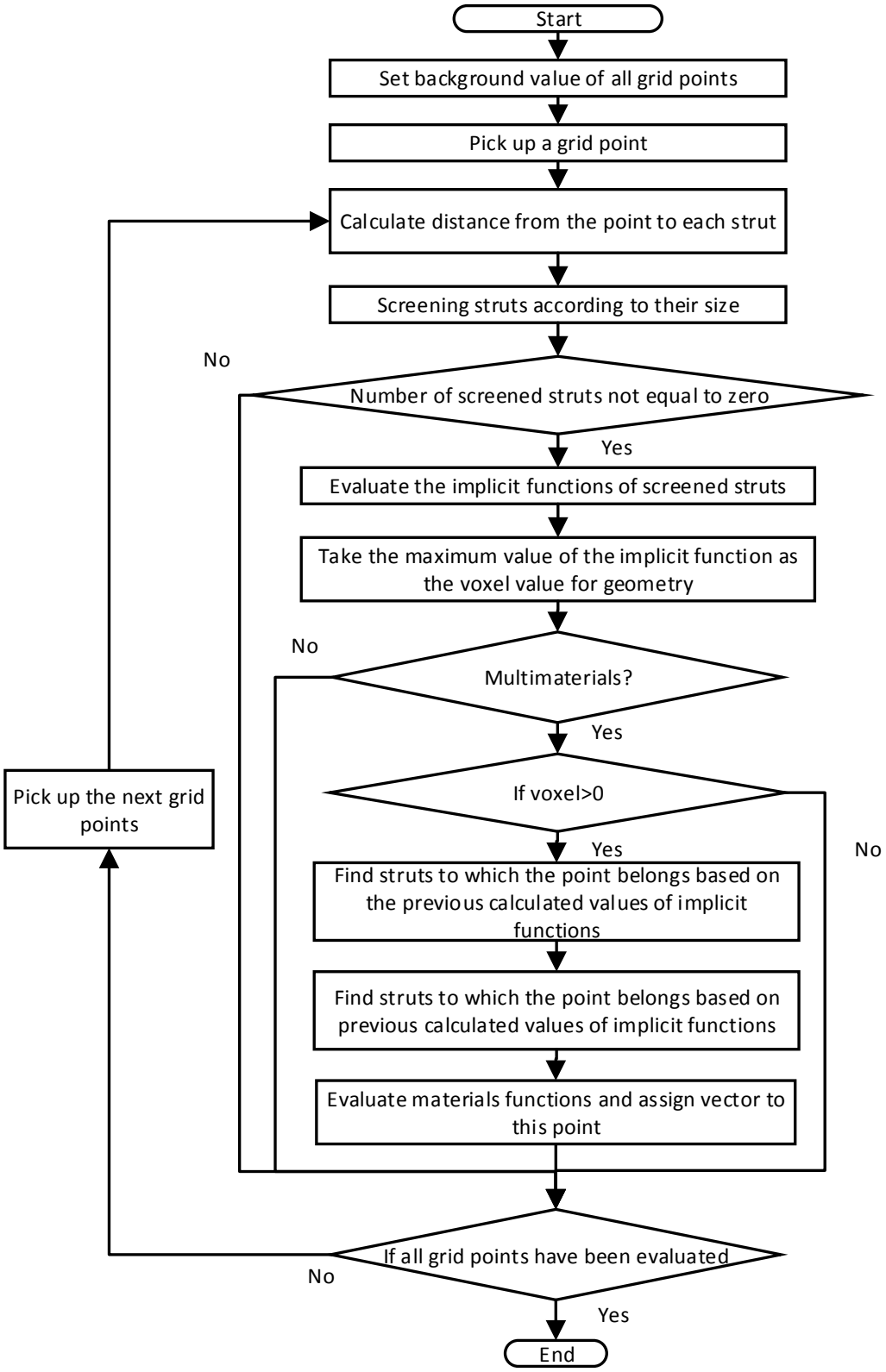

Figure 4-29 Working flow of point-wise voxelization process

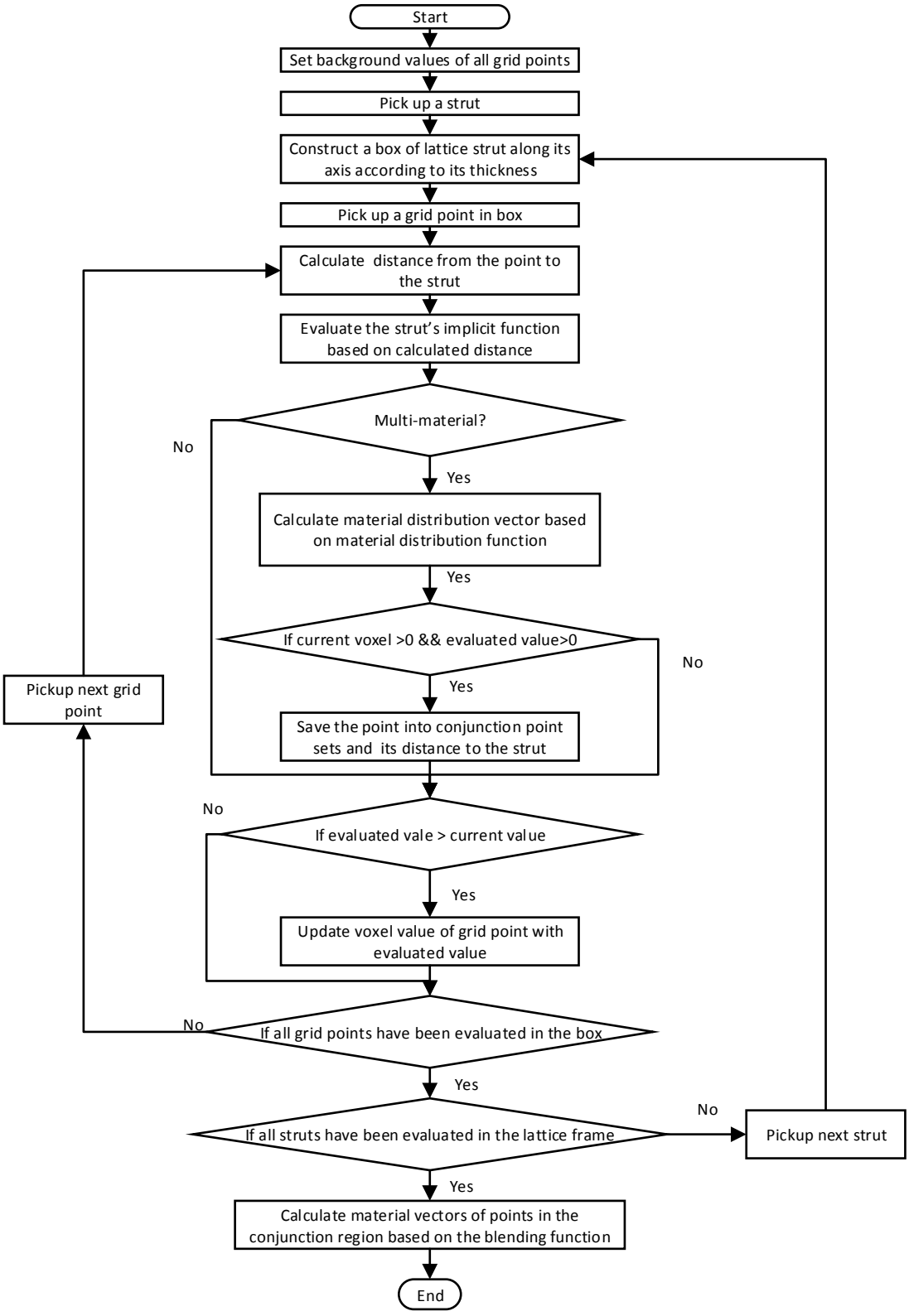

Figure 4-30 Working flow of strut-wise voxelization process

For each grid point defined in the bounding box of the lattice strut, only the distance from this grid point to the given lattice strut needs to be evaluated. Based on this distance and other calculated parameters, the geometric and material functions are evaluated. Since the bounding box of lattice struts may overlap, some grid points in the overlapped region may be evaluated more than one time. The volume of overlapping region will increase when the struts become thicker. Thus, it generally takes longer time to voxelize high relative density lattice structures with thicker struts. Compared to the point-wise voxelization method, the strut-wise voxelization can avoid the large amount of calculation of distance functions. Moreover, this method can also speed up the voxelization process by avoiding the evaluation of grid points which are not close to any struts. Thus, the strut-wise voxelization method is selected in this thesis for the voxelization process. A numerical experiment is provided to compare the speed of these two different voxelization processes. In this example, a lattice structure with 64 lattice struts has been used and shown in Figure 4-31. Two different methods have been implemented in Rhino® which is a CAD platform. Different struts' radius is applied for the same lattice frame. It should be noted only geometric implicit function is considered in this experiment. The running time of different voxelization methods is recorded and summarized in Table 4-1. Compared to the point-wise lattice voxelization method, strut-wise lattice voxelization method can significantly shorten the computational time. Furthermore, the increasing of strut thickness will increase the voxelization time of strut-wise method, since more grid points at conjunction regions need to be evaluated. However, there is no significant variation of the voxelization time of point-wise method. Generally, the speed of this method is independent to the struts' thickness. The result of this numerical result further prove that the strut-wise method is much faster than the point-wise method especially when the lattice struts' thickness is small.

Table 4-1 A comparison between the speed of two different voxelization methods

	R=0.2mm	R=0.5mm	R=0.8mm
Strut-Wise	931ms	1414ms	1868ms
Point-Wise	4401ms	4398ms	4388ms

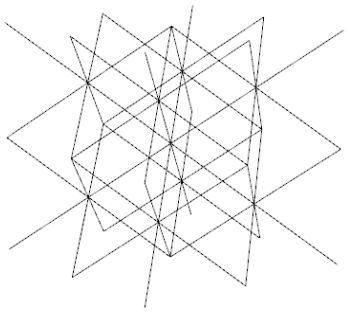

(a) Lattice frame for voxelization

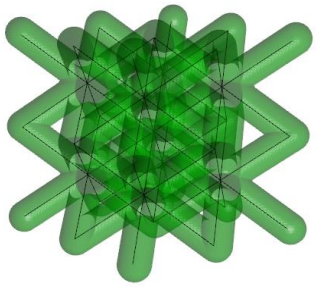

(b) Voxelized lattice represented by its boundary surface

Figure 4-31 Numerical experiments of lattice voxelization speed for two different voxelization processes

After the voxelization process, the voxels of generated lattice structure are obtained. It can be easily converted to the image of each sliced layers. For the processes with single material, the black and white image is used. For the fabrication process of multi-materials, the colored gradient image is used. These layer images can be directly fabricated by those Digital Light Projection (DLP) based printing technologies. For other types of printers, the image needs to be further converted to contours based on image sharping algorithm which can recognize the edge of the pattern on the image. In this thesis, the process of converting the voxel data to machine readable inputs is called as the postprocessing of geometric modeling. Different machines and AM process may require different types of input data. They are mainly divided into two major categories: slice images and slice contours. The voxel data generated by the proposed method is easily converted into these two types of data requested by the corresponding AM process. An example is provided in Figure 4-32 to illustrate the postprocessing.

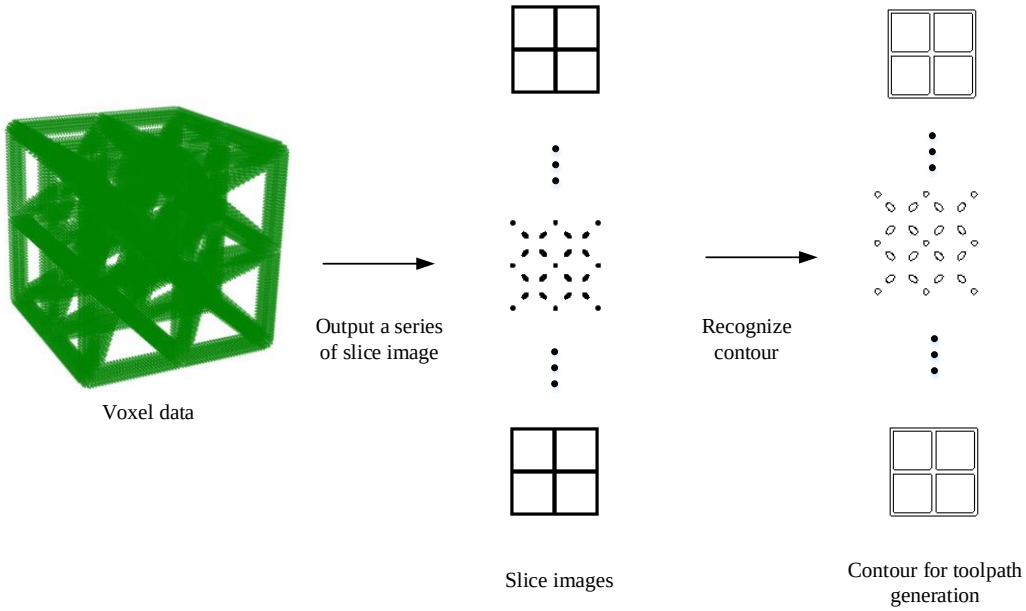

Figure 4-32 Postprocessing of voxel data

4.6 Case studies and discussion

The proposed multiscale geometric modeling method has been implemented. To save the memory and disk space during the lattice generation process, the open-source C++ library called OpenVDB® [210] is used for the efficient storage and manipulation of sparse Volumetric data discretized on 3D grids. This library is original developed and maintained by DreamWorks Animation® for use in volumetric applications in film production. Unless otherwise stated, all the computational experiments have been done in this section is on the computer with Intel® Core™ i7-4710 MQ CPU and 12 GB memory.

In this section, several different types of lattice structures have been generated based on the implemented lattice generation tool. Figure 4-33 shows the design domain of lattice structures. It is the L4 vertebra of human obtained from the Computerized Tomography (CT) images by the medical image segmentation tool called VTK-Snap[211] and smoothed by the software called Meshlab[212]. To graphically view the generated lattice structures, the voxel data have been

converted into a polygon mesh model and rendered. Besides converting voxel data to polygon mesh, it can also be directly rendered by the ray casting technique[213].

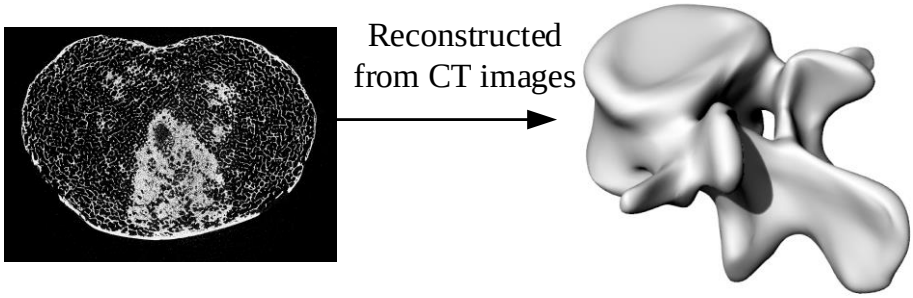

Figure 4-33 Design domain of lattice structures

The results of generated randomized lattice structures are shown in Figure 4-34. The modeling time for each type randomized lattice structures is summarized in Table 4-2. In this process, the lattice struts' diameter is set as 1 mm, and voxel size is fixed as 0.2 mm. From Table 4-2, it can be concluded that the most time-consuming process of randomized lattice generation is to construct lattice frame.

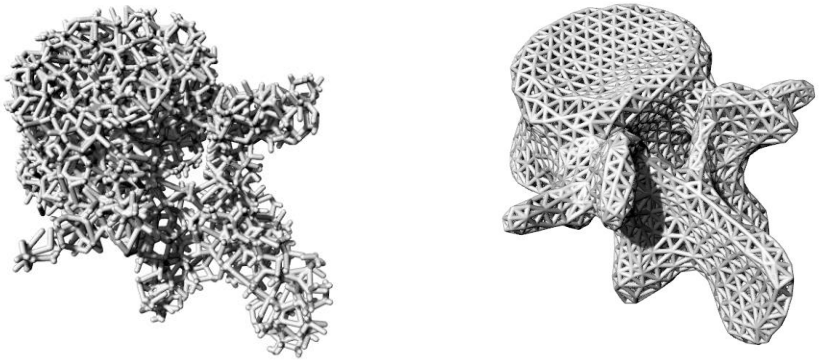

(a) Voronoi based randomized lattice structures, average cell size 5mm, strut's diameter 1.2mm

(b) Tetrahedron based randomized lattice structures, average cell size 5mm, strut's diameter 1.2mm

Figure 4-34 Voronoi based randomized lattice structure

Table 4-2 Geometric modeling time for randomized lattice structures with the same cell size

Lattice type	Time of frame generation/ms	Time of voxelization/ms	No. of struts
Voronoi lattice	1.13E+05	7.23 E+02	5822
Tetrahedron lattice	1.8E+05	1.04E+03	10065

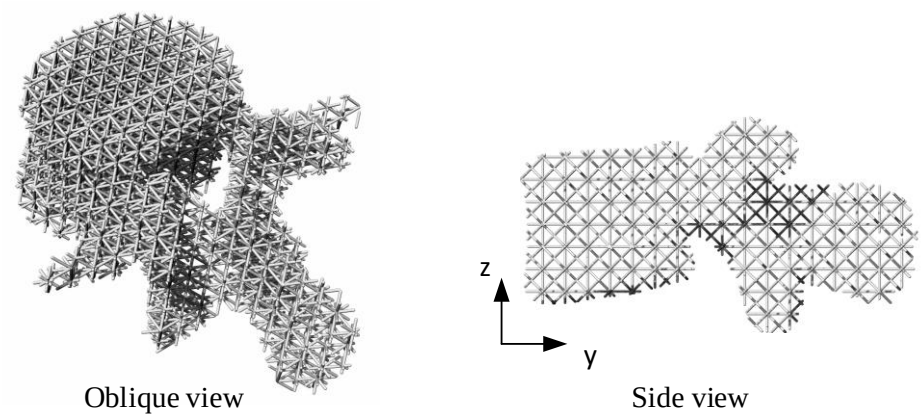

Oblique view Side view

(a) Uniform lattice, size 5x5x5 mm, strut diameter 0.6mm, topology: body-center cubic center

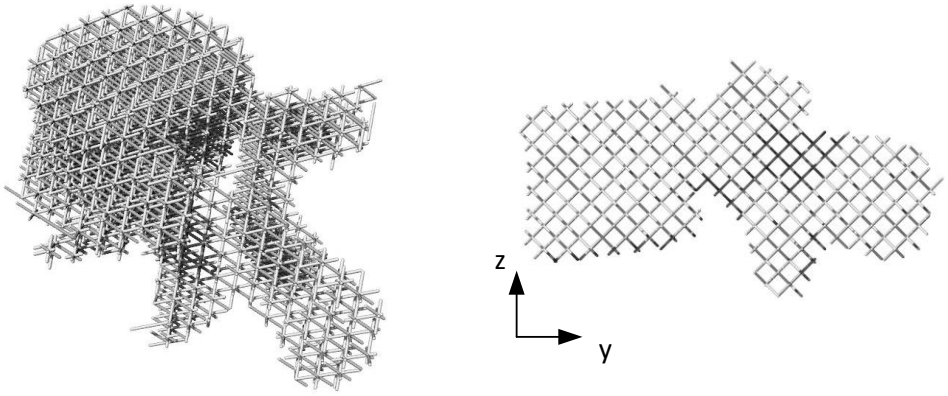

Oblique view Top view

(b) Uniform lattice, size 5x5x5 mm, strut diameter 0.6mm, topology: “cross” shape

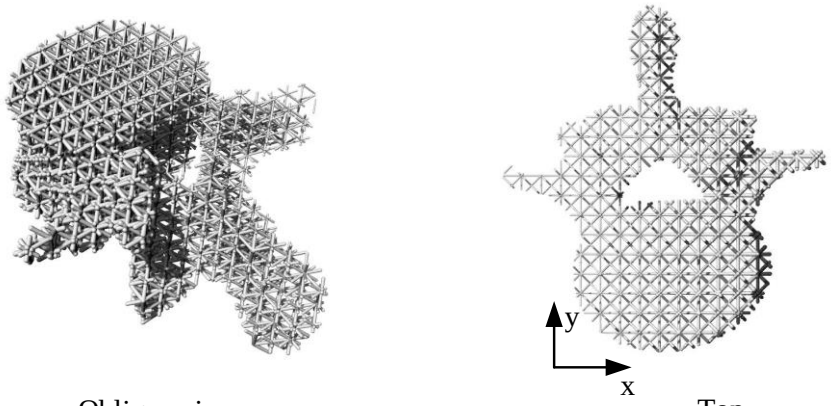

Oblique view Top

(c) Uniform lattice, size 5x5x5 mm, strut diameter 0.6-1.2mm linear distributed along x axis, topology: body-center cubic

Figure 4-35 Uniform lattice structures

Compared to randomized lattice structures, the speed of frame generation for uniform lattice structures is much faster as the cell is periodically located in the design domain. The result of generated uniform lattice with two different cell topologies, body-center cubic and cross cells, are shown in Figure 4-35 (a) and (b) respectively. Both two uniform lattice structures are homogeneous structures whose struts' diameter is a constant value (0.6mm) inside the design domain. Figure 4-35 (c) presents a heterogeneous lattice structure whose struts' diameter is linearly distributed along x axis from 0.6 mm to 1.2 mm. To evaluate the geometric modeling speed of uniform lattice structures, several geometric modeling experiments have been done to show the effects of geometric parameters of lattice structures on its generation speed. In these experiments, the body-center cubic cell is selected as the benchmark topology, and the size of each voxel is set as 0.1mm. The results of these experiments are summarized in the bar graphs presented in Figure 4-36.

In Figure 4-36(a), only the size of lattice cell is changed for different uniform lattice structures. The result shows both the time of frame generation and voxelization process significantly increase when the cell size become smaller. There are two major reasons for this. First, as the cell size decrease, the number of struts increase. Thus, it takes more time to generate and trim struts with the design boundary. This is the major reason for the increase of frame generation time. Secondly, the increase of strut number increases the volume of conjunction regions. As discussed in Section 4.5, the increase of the volume of conjunction regions generally increases the total number of grid points needed to be calculated during the voxelization process.

To compare the geometric modeling time of lattice structures with different struts' diameters, three different lattice structures are generated with the same cell size (5mm). Their geometric modeling time is summarized in the Figure 4-36(b). Based on this result, it can be concluded that the larger struts' diameter is, the longer voxelization time it takes. While the frame generation time

keeps unchanged. The reason for this phenomenon is mainly due to the increased number of grid points needs to be evaluated during voxelization process. However, since the cell size is unchanged, the generated frame is kept as the same while the struts' diameter increase.

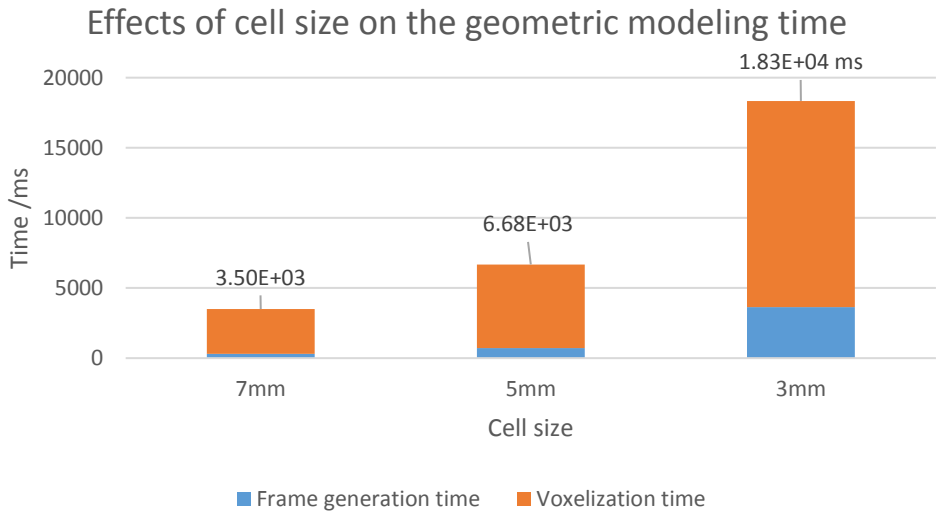

(a) The lattice generation time for "body-center cubic" lattice with different cell size

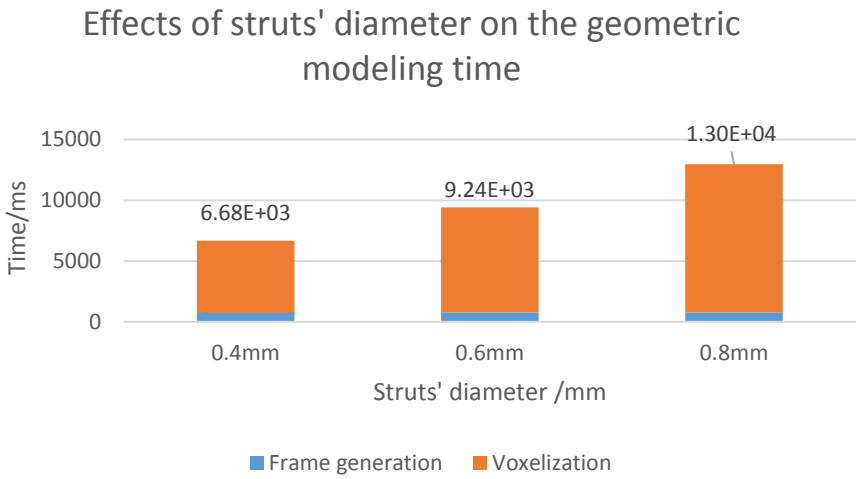

(b) The lattice generation time for "body-center cubic" lattice with different strut diameters

Figure 4-36 Effects of geometric parameters on the generation time of uniform lattice structures

Besides geometric parameters of lattice structures, the resolution of grid points for voxels also

have a significant impact on the lattice generation speed. This is simply due to the number of grid points which needs to be evaluated during the voxelization process. The increase of grid resolution will both increase the size and generation time of geometric model. To prove this proposition, an experiment has been done to compared the modeling time and size of the geometric model of uniform lattice structures with different voxel size. The result is summarized in Table 4-3. Based on this result, designers are suggested to select the bigger voxel size to reduce both computational time and disk space for the voxel data. However, it should also be noted that the increase of voxel size also causes the coarse and unsmoothed strut's surface. The struts with same diameter but different voxel size have been generated and shown in Figure 4-37. In this figure, marching cube algorithm [214] is used to generate the triangular mesh of lattice struts based on the voxel data. This generated mesh represents the smoothness of voxel data. Based on the result of this experiment, the voxel size is suggested to be smaller than one fifth of strut's diameter to keep the struts' smooth.

Table 4-3 Uniform lattice generation speed with respect to voxel size

Voxel size/mm	Lattice generation time/ms	Size of voxel file/MB
0.05	7.54E+04	149.1
0.1	6.66E+03	37.1
0.2	1.64E+03	9.1

(a)Voxel size 0.2mm (b)Voxel size 0.1mm (c)Voxel size 0.05mm

Figure 4-37 0.6 mm lattice struts with different voxel sizes

Compared to uniform lattice structures and randomized lattice structures, the design domain of conformal lattice structures should be inside the mapped-shape as discussed before. Thus, the half of a solid torus is selected as the design domain for conformal lattice structures, which is shown in Figure 4-38 (a). Two different of cell topologies are selected for this case study. The generated conformal lattice structures are shown in Figure 4-38(b) and (c).

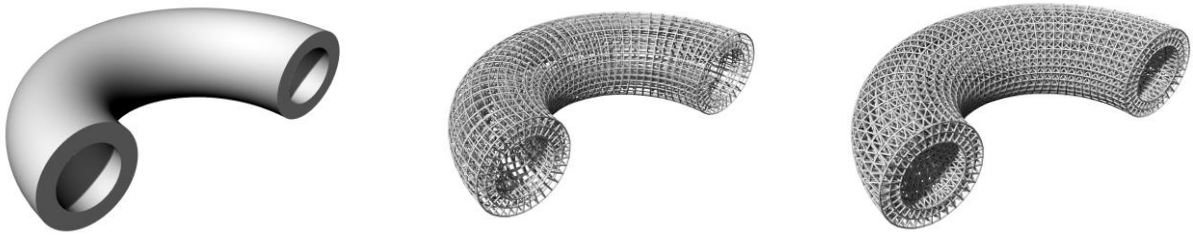

(a) Design domain for conformal lattice structure

(b) Generated conformal lattice structure with "cubic" cell topology

(c) Generated conformal lattice structure with "body-center" cell topology

Figure 4-38 Conformal lattice structures for the torus design domain

(a) Design domain

(b) Generated uniform lattice structures

Figure 4-39 Benchmark part used to compare the efficiency of two geometric modeling methods of lattice structures

Besides those presented cases for different types of lattice structures mentioned above, a further comparison of lattice generation speed between the proposed method and existing P-HGM (Prefabricated-Hybrid Geometric modeling) method [118] is made. The results of P-HGM method have been obtained by emulated its algorithm on a commercial available CAD software platform Rhino. To compare these two types of methods, uniform homogeneous lattice structures are generated in a standard cylinder with diameter of 30mm and length of 100mm. The design domain

and generated lattice structures are shown in Figure 4-39. To generate uniform lattice structures in this design domain, lattice cell with "cubic" topology is used. The diameter of lattice struts is set as the constant value which equals to 0.6mm. For the proposed method, the voxel size is set as 0.1mm.

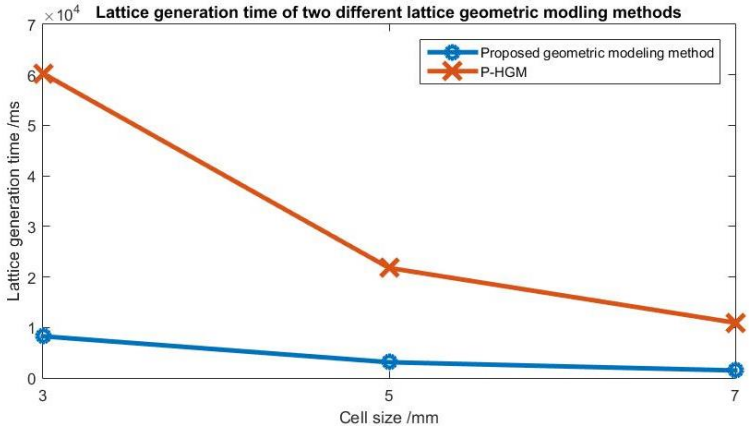

(a) A comparison between total generation times for uniform lattice structures with different cell size

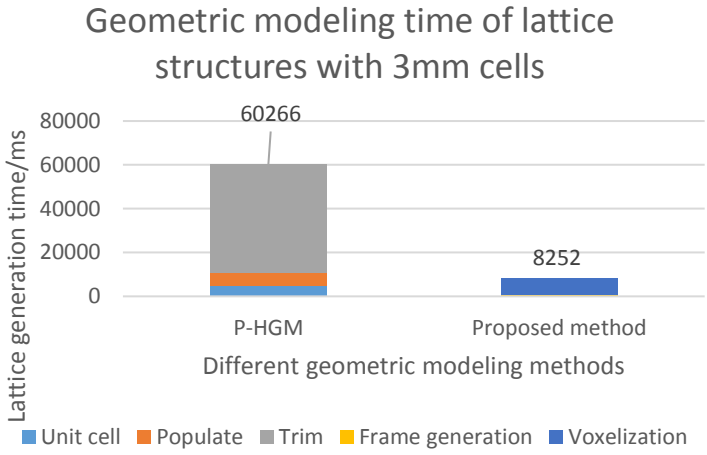

(b) A comparing between the time consumptions of major steps of two lattice geometric modeling method on uniform lattice structures with 3mm cells

Figure 4-40 Comparisons between the time consumptions of two different lattice geometric modeling methods

The time consumptions for two different geometric modeling methods are summarized and shown in Figure 4-40. As it is shown in Figure 4-40(a), the proposed method takes less time for

all lattice structures with different cell sizes. When the cell size decreases, both methods take longer time. However, the time consumption of P-HGM method increases faster than that of proposed method. The major reason is that the P-HGM method spend more time to trim generated lattice frame with respect the boundary of design domain. To further illustrate this point, a comparison of time consumptions of major steps of two lattice geometric modeling methods is given in Figure 4-40(b). From this figure, it can be concluded that the most time-consuming portion of P-HGM method is the trimming process, since the trimming process needs to be done for millions of triangles when the lattice cell size decreases.

4.7 Summary

In this chapter, an innovative multiscale geometric modeling method for mesoscale lattice structures is proposed. It consists of three major steps. They are lattice frame generation, construction of geometric, and material functions and voxelization. To introduce each step of the proposed method, several basic concepts and their related data structure are presented at the beginning of this chapter. Then the general working flow and detailed steps of the proposed method are carefully discussed. At the end of this chapter, several design cases of different types of lattice structures are presented. The major factors which effect the generation speed of proposed geometric method are investigated by a set of numerical experiments. Moreover, a comparison between the proposed method and existing P-HGM method is made. The result shows that the proposed method exhibits a better efficiency when the number of cells increases.

To compare with other existing geometric modeling methods, the proposed method has following advantages:

1 The proposed method is flexible to generate different types of lattice structures including uniform lattice structures, conformal lattice structures, and randomized lattice structures.

2 The proposed method enables a great design freedom for designers to control the geometric structures on multiscale. On macroscale, designers can fit the lattice structures in a complex design domain and control the variation of cell shape and size by selecting a set of conformal surfaces. On mesoscale, cell topologies, thickness of struts and its cross-sectional shape can all be changed and controlled for tailored properties.

3 The proposed method can realize multiscale material distributions. Material distributions functions can be used by designers to control the multi-material distributions on both macro and mesoscale simultaneously. It further extends the design freedom for designers.

4 A large number of lattice struts are efficiently generated by the proposed method with less time compared to the existing lattice geometric modeling method. Moreover, the proposed method can directly generate the slice files for AM fabrications. It saves the time in slicing process compared to traditional geometric modeling methods for lattice structures.

Chapter 5 Initial Design

In this chapter, the detailed processes and techniques used in the initial design stage will be discussed. The general purpose of initial design stage is to construct the initial design space of lattice structures for the design optimization stage. Generally, the design process of the initial design stage is divided into three steps: functional analysis, construction of FSs and FVs and generation of initial design space. Each of them will be carefully introduced in the first three sections of this chapter. Besides these three major steps, the manufacturability analysis model of AM processes on mesoscale lattice structures will also be discussed in Section 5.4. This model is used at the last step of initial stage to identify the range of design parameters of lattice structures. At the end, this chapter is wrapped up with a summary. The overall structure of this chapter is shown in Figure 5-1.

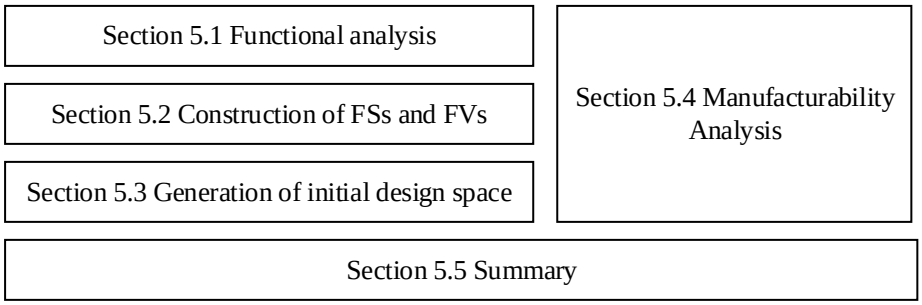

Figure 5-1 The overall structure of chapter 5

5.1 Functional analysis

The first step of initial design stage is to analyze the function based on the input functional descriptions as well as the related design requirements. The major goal of functional analysis is to build a set of functional entities which are considered as the blueprints for the subsequent design process. More specifically, each functional entity constructed at this step should be embodied by a certain physical entity at the end of design. This physical entity should achieve all the required

functions of the functional entity, and satisfy all the prescribed design requirements. To achieve this purpose, the detailed steps of functional analysis are summarized and presented in Figure 5-2.

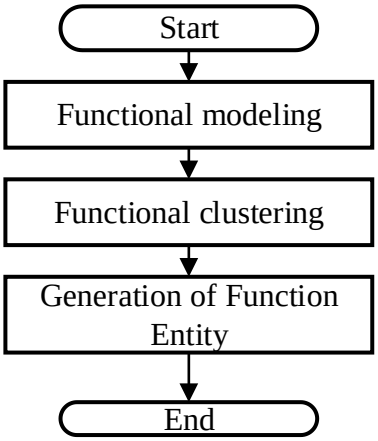

Figure 5-2 Three sub-steps of functional analysis

Functional analysis starts from the functional modeling procedure which uses a formal structured method to represent complex relations between all the defined functions of a design task. Techniques related to functional modeling process are mature and have already been thoroughly investigated. Thus, it will not be discussed in detail here. For more information about functional modeling processes, readers can refer to the following references [200, 215-217].

After functional modeling process, a structured representation of functions of the designed product is obtained. Based on the obtained functional model, designers need to cluster the defined functions in the functional model into several groups. Each group is used to construct a functional entity at the end of the functional analysis process. To help designers cluster functions in the functional model, there are a number of design guidelines summarized in the existing literatures [218] which can be directly used here. However, it should be noted that these guidelines all have certain limitations. Designers should be cautious when they follow these guidelines which usually neglect the design possibility enabled by AM processes. Thus, to overcome this limitation, two rounds of functional clustering process are suggested. At the beginning, the functional clustering

process is done based on the existing design guidelines [218]. The initial function groups are generated. Then, a second round of clustering process is conducted to decide whether these function groups are further merged by considering the AM enabled functional features and its related manufacturing costs. This process is generally referred to as AM enabled functional clustering in this thesis. To support the second round of functional clustering, AM enabled functional features database [219] is needed.

Specifically, in the AM enabled functional clustering process, the function groups can be further merged in two different ways. The first way is to directly combine physical entities for different function groups into a single physical entity. To ease the manufacturing difficulty as well as cost, some function groups are suggested to be embodied with different physical entities and assembled together. For example, functions which request two different types of materials usually are assigned to different physical entities. To further reduce the part's count, these two physical entities are integrated into a single entity and fabricated by a AM process. Thus, their corresponding functions are merged. A case of the prosthetic arm [220, 221] shown in Figure 5-3 has been used to illustrate this type functional clustering. Traditionally, this product consists two major part: plastic arm body and electric wire. Since these two parts use different materials, they should be fabricated separately and assembled together at the end. Based on the design freedom provided by AM process, these two separate parts are merged into one part and fabricated by a select AM process. Thus, the functions of these two parts are incorporated into a single functional entity. The integrated part can achieve functions including electric conduction and load bearing. In this thesis, this type of functional clustering is referred to as physical integration.

Instead of directly combining the physical entities, a totally new physical entity is needed to embody the merged function groups for the second type of AM enabled functional clustering. This

new developed physical entity can achieve all the requested functions through a new mechanism enabled by AM technologies. For example, the gripper which is shown in Figure 5-4 is fabricated by an AM process. This gripper can grasp objects by controlling its temperature. Traditionally, primary function "grip objects" needs to be decomposed into several sub-functions. Each sub-function will be implemented independently. For instance, a motor needs to provide movement, and a sensor is necessary for detecting temperature changes. Thus, the original design must have multiple functional entities. However, by the AM process, a shape memory polymer can be printed with a certain materials distribution. This special capability of the AM process enables the design of gripper in one part to achieve all sub-functions simultaneously. The physical entity used to achieve the merged groups of functions cannot be considered as the simple combination of its original physical entities. In this thesis, this type of AM enabled functional clustering is referred to as functional integration.

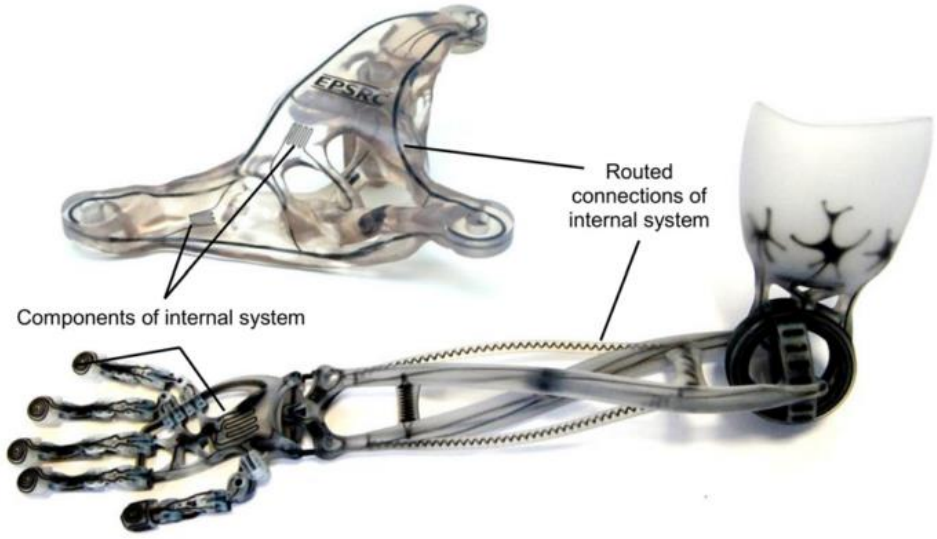

Figure 5-3 An example of physical integration enabled by a AM process [220]

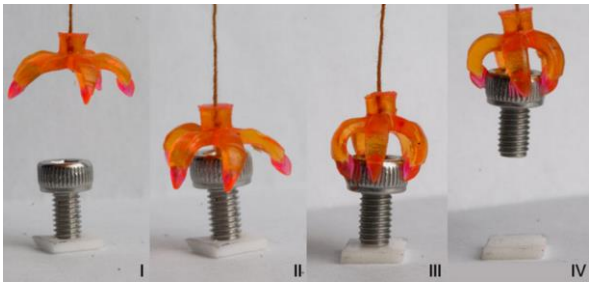

Figure 5-4 Multi-material gripper without traditional actuators [29]

After the functional clustering process, the function groups are obtained. Based on these function groups, the functional entity can be easily constructed. Specifically, the functions defined in each function group are regarded as the target functions for each functional entity. Besides functions, the design requirements also need to be assigned for each function entity in this step. According to the classification methods of design requirements discussed in Chapter 3, those function related design requirements are directly assigned to functional entities according to their related functions. As to non-functional related design requirements, such as weight, cost and volume, it should be carefully considered by designers to assign them into each functional entity. After that, the functional entities for a given design product are obtained.

It should be noted that the process of functional analysis discussed above mainly focuses on the innovative design where the functional descriptions are the only design input. For the redesign cases, the original design configurations are used as a reference for designers during functional clustering and construction of functional entities. It can simplify these two sub-steps during the functional analysis process, since designers can make decisions based on the original design by linking the functions to existing physical entity. Like those design cases of innovative design, AM enabled functional features are considered during the functional clustering sub-step to identify function groups which can be potentially merged. However, by using the original design as a reference it is potentially dangerous for designers to neglect other possible design configurations

at the functional level that can achieve better functional performance.

5.2 Construction of FSs and FVs

The second step of initial design stage is to construct FSs and FVs for each generated functional entity. These FSs and FVs can characterize a rough shape and position of the physical entity. For different design scenarios, the methods to construct FSs and FVs are different.

For innovative design or new design cases, due to the lack of sufficient information, FS needs to be built based on functional interface including material, energy and information flows between the focused functional entity and its connected functional entities. Based on the generated FSs, the FVs of a design case are constructed. It should be noted that the shape and position of FSs during this process largely depend on the required functions for each functional entity as well as the designers' previous knowledge on the designed product. Thus, even for the same functional entity, different designers may generate different FSs and FVs.

Compared to the innovative design cases, the construction of FSs and FVs for the redesign process is much easier and straightforward. The key surfaces can be directly extracted from the corresponding physical entity in the original design for each functional entity. In some design cases, these key surfaces are directly considered as FSs for a given physical entity. To generate more generalized FSs and FVs, designers need to reconstruct those extracted key surfaces based on its corresponding functions. An example is given in Figure 5-5 to show the reconstruction of FSs based on the extracted key surfaces from the original design. In this example, four surfaces tagged in yellow color in Figure 5-5(a) are firstly extracted as the key surfaces which link the designed triple clamp with the steering handle of motorcycle. Based on the analyzed functions of these surfaces, it can be concluded that the linked surface between triple clamp and steering handle should be in a cylindrical shape and positioned along the axis of the steering handle. Based on this

information, two cylindrical surfaces tagged in green color in Figure 5-5 (b) is reconstructed. These two reconstructed surfaces are considered as the FSs of designed physical entity. After obtaining all the FSs, the FV of this design case is easily generated by designers to connect the obtained FSs. It shows the geometric boundary of a given physical entity.

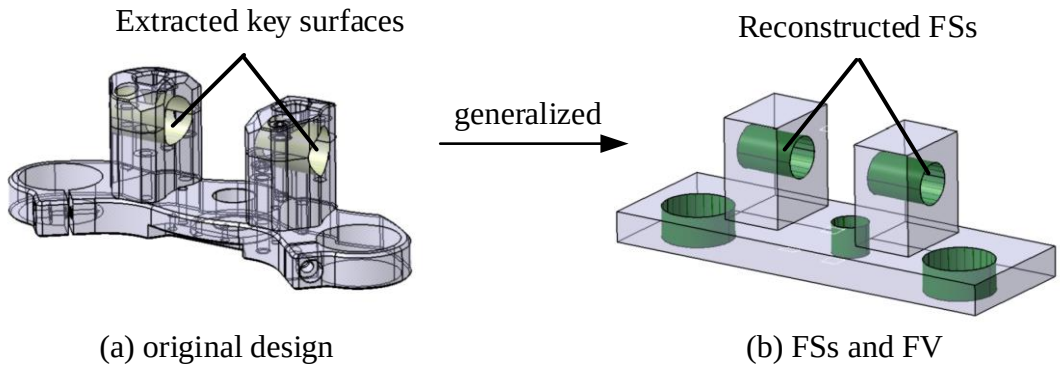

Figure 5-5 An example of construction of FSs based on the original design

5.3 Generation of initial design space

The last step in the initial design stage is to construct the design space that is used for the following design optimization process. This step plays a key role as a link between initial design stage and design optimization stage. Moreover, as discussed in Section 3.1.3, different design spaces may yield different optimal result. Thus, the design freedom considered inside the design space is crucial to the final performance of products. The process which is used to construct initial design space is proposed and shown in Figure 5-6. This process is divided into three sub-steps. Each of them will be discussed in detail in the following three sub-sections.

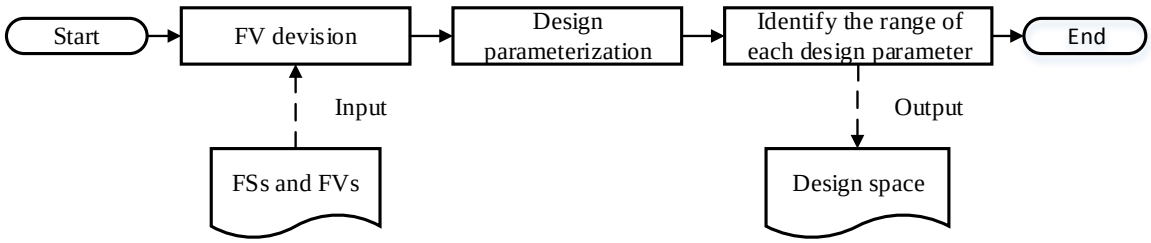

Figure 5-6 The process of the generation of initial design space

5.3.1 FV division

Traditionally, a FV is always filled with a single type of structure or materials. Specifically, it is filled with either solid materials or lattice structures. Thus, there is no need to further decompose them. The entire FV is directly considered as the geometry boundary of design space. Those design optimization methods on macroscale, such as topology optimization techniques [50], can be directly applied on the obtained FV and generate the optimized result. However, this situation has been changed by AM technologies, hybrid solid-lattice structures can be directly fabricated by AM processes. Compared to the FVs with a single type of structure, the hybrid FV may achieve better performance [12]. To consider this design freedom, the obtained FVs from the previous design step is further divided into several sub-FVs, if necessary. In each sub-FVs, either lattice structures or solid material can be used. The major purpose of FV division is to determine the type of structures which is used for each local region of initial FV.

At the beginning, a decision should be made to identify the region for solid or lattice from the initial FV. To support this decision making process, the material charts [222] which offer both effective properties of mesoscale lattice structures and solid materials can be used as a reference. Besides material chart, two general methods are introduced in this thesis which help designers divide FVs. The first method mainly focuses on the design for structural performance. This method takes the stress analysis on the obtained FV at first. In the stress analysis, the entire initial FVs are filled with solid materials, and the loading condition is directly applied on the initial FVs. Based on the stress distribution, the initial FVs are divided into two regions: low stress region and high stress region. Generally, these two regions correspond to two types of sub-FVs. Lattice is porous and less stiff. Thus, it is suggested to be used for low stress place. Otherwise, solid material is used for high stress region. A design case of an aircraft engine bracket is used to further illustrate this

method. In this design case, the aircraft engine bracket (shown in Figure 5-7(a)) is redesigned under the given loading condition shown in Figure 5-7 (b). The initial stress analysis has been done on this bracket, and its result is shown in Figure 5-8. Based on this result, the initial FV of engine bracket is further divided into two sub-FVs. Lattice structures and solid materials are used for these two sub-FVs respectively. To further connect these two sub-FVs, an additional FS is added between them. The result of FV division process for this example is shown in Figure 5-8.

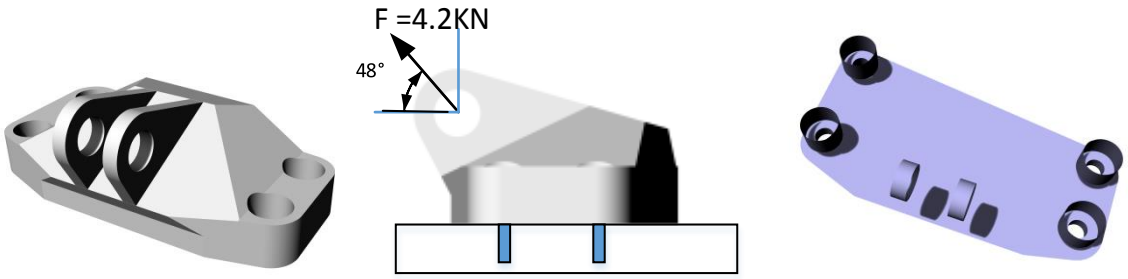

(a)Original design (b) loading condition (c) Functional Surfaces

Figure 5-7 An example of aircraft engine bracket [223]

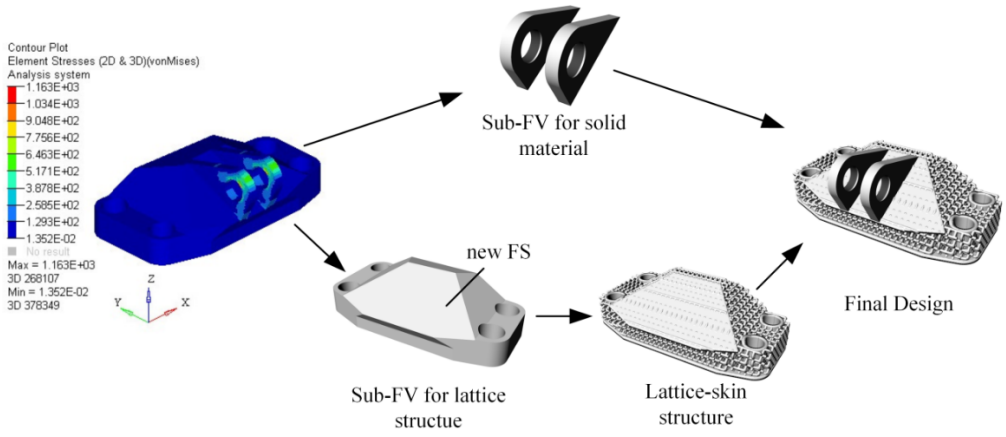

Figure 5-8 Example of FV division on the aircraft engine bracket

Besides stress analysis, topology optimization method is another option which can be applied to help designers to divide the initial FVs into several sub-FVs. Like the proposed method for multi-material optimization [224], density based topology optimization method is directly applied

on the obtained FVs with a given loading condition. Based on the optimal relative density, the clustering algorithm [225] is applied by designers to divide the initial FVs into several sub-FVs. According to the average relative density in each sub-FVs, designers can make a decision on which type of structure should be used to fill the decomposed sub-FV. Compared to the first method used for FV division, the second method generally requests more computational resources, since several optimization iterations need to be done for the topology optimization process. However, it can be applied to more complex design when the stress distribution is not the only factor that needs to be considered during the initial design stage. Besides the structural performance, the second method can be further applied to other design objectives by using different penalty functions to represent the effective properties of lattice structures.

Table 5-1 The comparison between different types of lattice structures

Lattice Type	Advantages	Disadvantages
Uniform lattice	(a) The effective properties can be obtained based on a single lattice unit cell; (b) Inverse homogenization technique can be applied to design cell topology for a certain desired physical property;	(a) Cells on the boundary may not be complete; therefore, boundary surface is not smooth; (b) All the cells in a lattice structure are in the same orientation;
Conformal lattice	(a) Cell orientations can be controlled by the selected conformal surface; (b) Cells can keep integrity on the selected conformal surface; (c) By carefully selecting the conformal surface, designers can align cells along the principal stress direction to achieve a better structural stiffness;	(a) Homogenization methods cannot be applied to evaluate its effective properties (b) Conformal lattice structure cannot be generated in a FV with any arbitrary shape and its related conformal surfaces
Randomized lattice	(a) By using a tetrahedron based randomized lattice structures, cell can keep complete on the boundary of the FV with irregular shape; therefore, it can achieve a relatively smooth boundary surface. (b) The size of cells can be smoothly varied in a FV to achieve a certain gradient of desired properties.	(a) The RVE (Represent Volume Element) which contains a considerable number of unit cells are needed; (b) The cell topology cannot be changed by the designers to obtain the desired properties

After determining which region to use lattice structures, designers should select suitable type of lattice structures to fill in each sub-FV. To facilitate designers to make a sound decision, the

comparison between different types of lattice structures is made and summarized in Table 5-1.

Instead of only using one type of lattice structures or a single cell topology for the entire FV of lattice structures, each FV of lattice structures can be further divided into several sub-FVs for different types of lattice structures or lattice cells with different topologies. The following design guidelines are proposed to help designers to make this decision.

Design Guideline 5-1: Guidelines for FV division

(a) For structural design, if the principal stress directions of local points in the FV are dramatically changed, this FV can be further divided into several sub-FVs which contain lattice structures with different cell topologies or in different orientations.

(b) Inside the FV of lattice structures, if materials in different region are supposed to have different physical properties, it is suggested to divide this FV into several different sub-FVs and each is filled with different type of lattice cells.

(c) The FV of a lattice structure which contains the neck region is suggested to be further divided into several sub-FVs. The neck region of original FV is supposed to be filled with solid materials to connect the decomposed sub-FVs.

Among these three guidelines, the first guideline mainly focuses on structural design. Unlike solid materials, lattice structures exhibit anisotropic effective properties on macroscale. The effective elastic properties of three different cell topologies are given and compared in Figure 5-9. It is manifested that the value of the normalized elastic modulus varies with respect to the orientation angles. Thus, in the different region of a FV, lattice structures are designed with different orientation angles. To achieve this purpose, the original FV of lattice structures are further divided into several sub-FVs. In each sub-FV, a lattice structure with different orientation angle is used. To connect the sub-FV of lattice structures with different orientation angles, additional FSs

which are implemented by a thin layer of solid materials should be added on the border between two sub-FVs. A specific algorithm [226] has been developed by author to optimize the distribution of lattice orientation angles. Compared to the lattice structure with uniform orientation angle, the variation of orientation angle can further improve the stiffness of designed lattice structures without increasing its weight. To further illustrate this method, a design example of a cantilever beam is given in Figure 5-10. In this example, the original FV of a lattice structure has been uniformly divided into six sub-FVs. Then the orientation angles of sub-FVs are considered as the design variables in the design optimization process. The detailed information of design optimization for orientation angles of lattice structures is discussed in the published paper [226]. A comparison between lattice structures with uniform orientation angle and optimal orientation angles is given and summarized in Table 5-2. From this result, it can be concluded that the non-uniform oriented lattice achieves a better stiffness than its uniform counter-part.

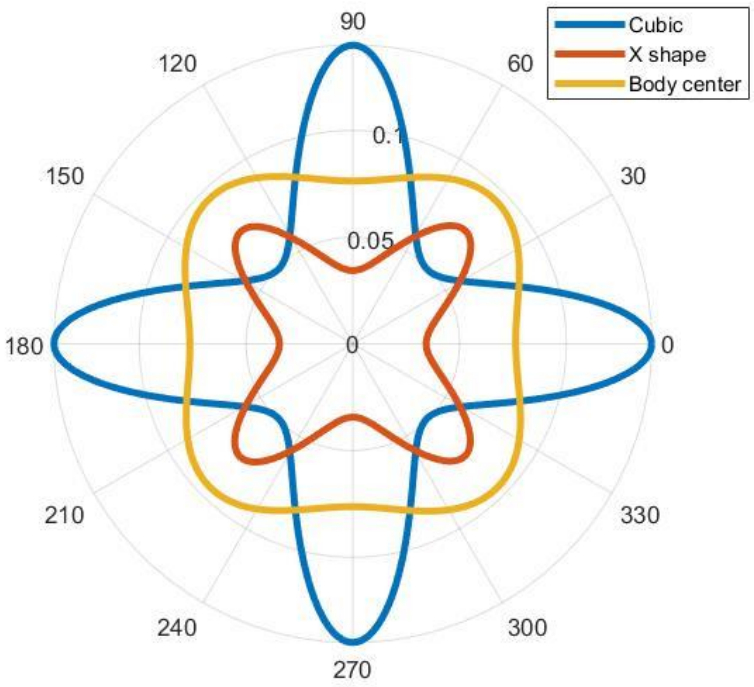

Figure 5-9 Normalized effective elastic modulus three different lattice cells with the same relative density $\rho^* = 0.3$

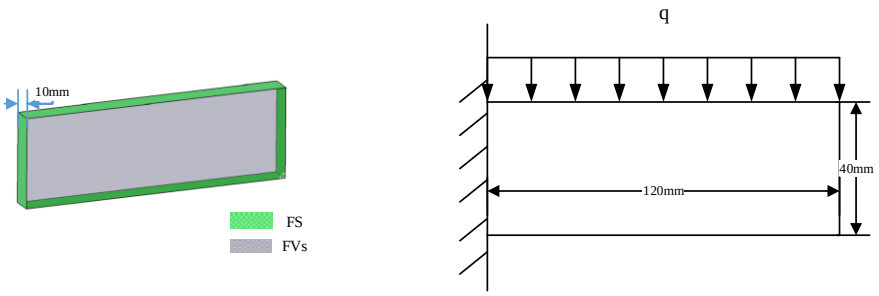

(a) FV, FSs and loading condition

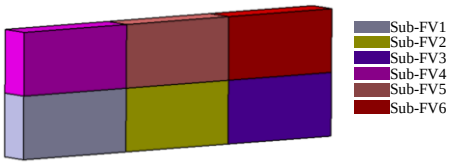

(b) Decomposition of FV into sub-FVs

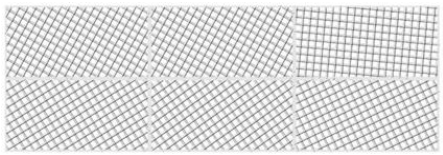

(c) Optimal distribution of lattice orientation

Figure 5-10 An example of FV division for lattice orientation optimization

Table 5-2 The comparison between lattice structures with uniform and non-uniform orientation distribution

Design configuration	Strain energy/kJ	Volume of total materials/mm^3
Uniform lattice orientation	11.5	7088.68
Non-uniform lattice orientation	7.6	7088.60

Besides the optimization of lattice structures' orientation, different lattice cell topologies can also be selected by designers to fill in a single FV. To divide the FV of lattice structures for different lattice cell topologies, the initial analysis needs to be done first. Based on the principal stress directions on each local point of a FV, the FV is further divided into several sub-FV by clustering algorithm [225]. Specifically, the observation point x_i is defined for each point P_i in the FV based on its principal stress directions as:

$$x_i = max(l \cdot e_x, l \cdot e_y, l \cdot e_z) \tag{5.1}$$

Where l is the unit directional vector of the principle stress with maximum 2-norm of point P_i. e_x, e_y, e_z are the unit directional vector of global design space. The FV is divided into n sub-FVs by applying k-mean clustering algorithm based on observation points defined above. This process can be mathematically stated as:

$$\arg min \sum_{i=1}^{n} \sum_{x \in S_i} ||x - \mu_i||^2 \tag{5.2}$$

Where S_i represents the i[th] sub-FV and μ_i denotes the mean of points in S_i. By solve the center value μ_i in Equation 5.2, the sub-FV which contains the point with similar orientation of principal stress is obtained. Based on the principal stress orientation in each sub-FV, a suitable lattice cell topology is selected. A design case for this type of FV division method is given and shown in Figure 5-11. In this design case, the initial FV of design has been divided into two sub-FVs based on the aforementioned method. In sub-FV1, the major stress component is the normal stress along the axis direction of the cantilever beam. Thus, the cubic shaped lattice cell topology which shows a better stiffness along x direction is used. In sub-FV2, the major stress component is the shear stress. The body-center cubic lattice cell which shows better shear stiffness is used. Since these two types of cell topologies share the same nodes on its boundary, there is no need to establish additional connections between them. The detailed connection criteria will be discussed at the end of this sub-section. Both hybrid lattice and pure lattice are designed and optimized by the proposed BESO based optimization method discussed in Chapter 6. The detailed boundary condition and optimization parameters for this design case is provided in Section 6.5. The summary of optimization result is summarized in Table 5-3. It is manifested that the hybrid lattice can achieve a better stiffness than either "cubic" shaped lattice or "body-center cubic" lattice.

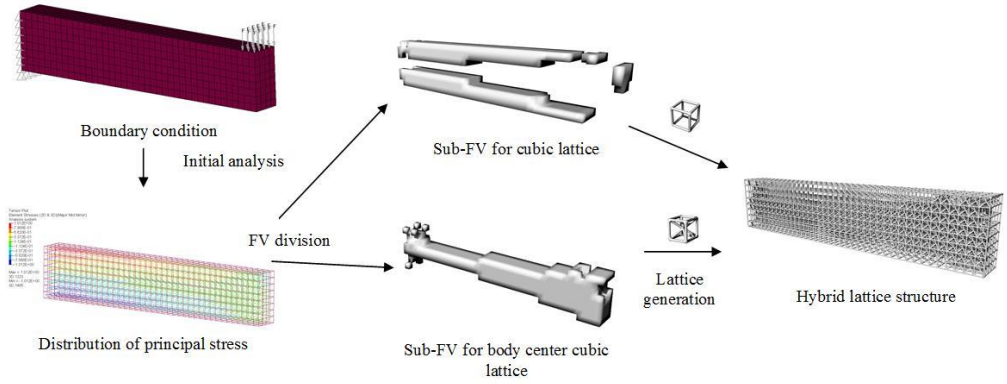

Figure 5-11 FV division for lattice structures

Table 5-3 The comparison between pure lattice and hybrid lattice

Type	Maximum displacement/mm	Compliance/mJ	Weight /kg
Hybrid lattice	0.145	5.20	0.46
Pure “cubic” lattice	0.206	7.50	0.46
Pure “body-center cubic” lattice	0.194	6.93	0.46

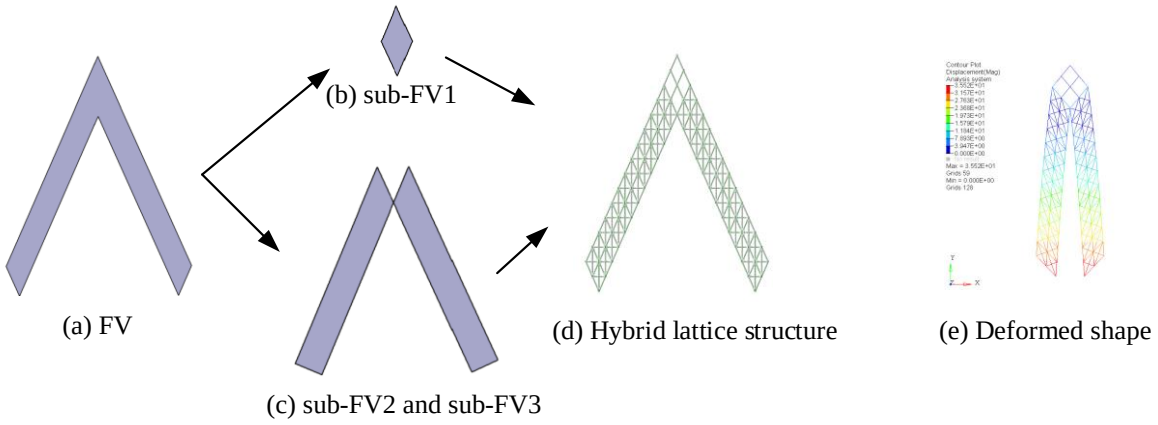

Figure 5-12 Design of a hybrid lattice structure for gripper

Comparing to Design guideline 5-1(a), Design guideline 5-1(b) can be applied to a broader range of applications. But it needs the information which shows the desired physical properties on each local region of an initial FV. In Design guideline 5-1(a), this information can be obtained by the initial structural analysis or topology optimization. As to other design applications considered in Design guideline 5-1(b), designers need to obtain this information by themselves. Based on this information, different cell topologies can be used for different sub-FVs. A design case of lattice gripper is used to illustrate this design guideline. The FV of this lattice gripper is shown in Figure 5-12(a). It is further divided into three sub-FVs since the desired elastic properties in different sub-FVs are different. The lattice cells in the sub-FV1 should have low shear modulus, which enables the large deformation in that region when the two arms of the gripper are closed. Thus, the rhomboid shaped lattice cell is used in this sub-FV. Compared to the lattice structure in sub-FV1, the lattice structures in sub-FV2 and sub-FV3 should be stiff enough under gripping force without

significant local deformation. Thus, triangular lattice cell is used in those two sub-FVs. The generated hybrid lattice structure with two different types of lattice cells is shown in Figure 5-12(d). The designed hybrid lattice structures can achieve the desired deformation, which is presented in Figure 5-12(e).

The Design guidelines 5-1(a) and (b) mainly divide the FV of lattice structures from functional point of view. Thus, their general purpose is to improve the functional performance of designed lattice structures. The purpose of Design guideline 5-1(c) is different from those two guidelines. It mainly focuses on the connectivity of generated lattice structures, and relates to the manufacturability of designed lattice structure. In Design guideline 5-1(c), the concept named as neck region is used. This concept origins from the CNC machining, and indicates the narrow region which combines two open area and cannot be accessed by the large cutting tool [227]. In this thesis, this concept is extended to 3-dimensional space, and indicates the three-dimensional narrow region which is used to connect to solid broad region in FV. Like the two-dimensional case for CNC tool path generation, skeleton frame for three-dimensional model [228] is used to help designers to automatically recognize the neck region. To characterize the dimension of a neck region, the diameter of the biggest ball which can pass through the neck region is defined as its size in this thesis. If the FV of a lattice structure consists the neck region whose size is equal or smaller than the cell size, the generated lattice structure may lose connectivity at the neck region.

To illustrate Design guideline 5-1(c), an example is given and shown in Figure 5-13 (a) and (b). In the FV of this design case, there is a neck region located at the center of FV. There are two methods which can generate the fully connected lattice structures. In the first method, designer can further decrease the size of cells. As it is shown in Figure 5-13 (c), when the cell size is set as 4 mm which is smaller than size of neck region, the generated lattice structure is fully connected.

However, this is not recommended when the size of cells is already in a small number. The decrease of lattice cell size will bring the issue to its fabrication process. The second way is to follow the Design guideline 5-1(c) which divide initial FV into two sub-FVs and connected by a new generated solid structure at the neck region (shown in Figure 5-13(d)). Since the volume of neck region is small compared to other regions of FV, it will not significantly increase the weight of the entire structure.

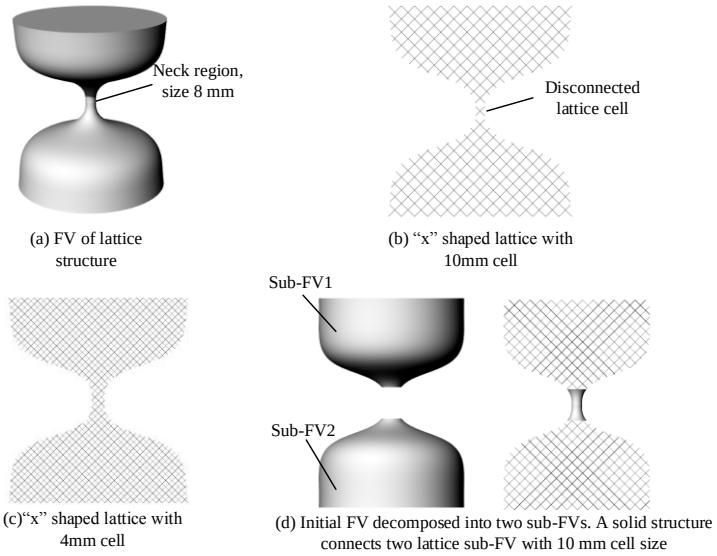

Figure 5-13 An example of FV division due to the neck region

After FV division, different types of lattice structures are selected to fill in the different sub-FVs. To keep the connections between different types of lattice on the boundary of neighboring sub-FVs. Several approaches are summarized in this sub-section. The most general way is to add a thin layer of solid material which is considered as skin at the boundary between two adjacent sub-FVs. This method can be used to connect different types of lattice structures. Its example is shown in Figure 5-10 where the uniform lattice structures with different orientations have been connected. There is one disadvantage of this method that additional weight will be added for the new generated skin structures. To solve this issue, some specific connection methods for certain

types of lattice structures are proposed. Among them, if the two neighboring sub-FVs are both uniform lattice structure with the same orientation and cell size but different topologies, they are naturally connected without any additional structures if two lattice cell topologies are compatible. The definition of compatibility of lattice cell topologies is given as following:

Definition 5-1: Geometric compatibility of lattice cell topology

Suppose $G_1(E_1, P_1)$ and $G_2(E_2, P_2)$ are two cell topologies for lattice cell defined in the cubic parametric space D $[-1,1]^3$, where E_1 , E_2 are their edge sets and P_1, P_2 are their nodes set; For any boundary face F of cube D, if $P_1 \bigcap P_2 \bigcap F \neq \emptyset$, then G_1 and G_2 are compatible to each other.

Based on this definition, it can be easily proved that for any two uniform lattice cells with the same size and orientation, if their topologies are compatible, then they can be connected without any additional structures. For any set of cell topologies, if any two cell topologies in this set are compatible to each other, then this set of cell topologies is named as the compatible topology set. When designers select the lattice topologies for two adjacent sub-FVs, it is suggested to select lattice topologies from the compatible set, since they can be easily connected to each other. In Figure 5-14, a set of compatible cell topologies is presented.

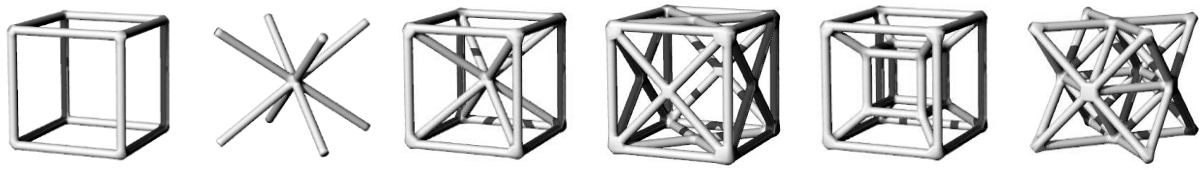

(a) Cubic (b)'x' shaped (c) body-center (d) face- centered (e) tesseract (f) octed

Figure 5-14 A set of compatible lattice cell topologies

Besides uniform lattice structures, the sub-FV with tetrahedron based randomized lattice structures can also be easily connected to other types of lattice structures including uniform and conformal lattice structures without any additional linking structures. To achieve this purpose, the frame of conformal and uniform structures needs to be built first. Then, the node of conformal and

uniform lattice structures on the shared face between two sub-FVs can be used as the node points to build the frame of tetrahedron based lattice structures. This method can guarantee the constructed lattice structures between two sub-FVs are fully connected.

5.3.2 Design parameterization

The second sub-step is to determine the design parameters which are used in the design optimization stage to further improve the functional performance of the designed part. This sub-sections mainly focuses on the design parameters for FVs with lattice structures. As to FVs with solid materials, its size, shape and topology can be generally considered as the design parameters, which have already been investigate on those macroscale design methods reviewed in Chapter 2. Thus, they are not future discussed in this chapter.

Generally, different parameters are used to describe the FV of different types of lattice structures. The names of parameters for three different types of lattice structures focused in this paper are summarized in the three tables presented below. For the detailed explanation of each parameters, readers can refer Chapter 4 in this thesis.

Table 5-4 Available parameters for uniform lattice structures

Parameter Name	Symbol	Distribution type
Cell size	$l(l_x, l_y, l_z)$	constant
Strut's cross-section	c	Strut-wise
Thickness of strut	t	Strut-wise
Relative density	ρ^*	Spatial distribution
Cell topology	G	Constant
Cell orientation	(α, β, γ)	Constant
Material distribution	A_m	Spatial distribution

Table 5-5 Available parameters for conformal lattice structures

Parameter Name	Symbol	Distribution type
Average cell size	l	constant
Strut's cross-section	c	Strut-wise
Thickness of strut	t	Strut-wise
Cell topology	G	Constant
Material distribution	A_m	Spatial distribution

Table 5-6 Available parameters for randomized lattice structures

Parameter Name	Symbol	Distribution type
Average cell size	l	Spatial distribution
Strut's cross-section	c	Strut-wise
Thickness of strut	t	Strut-wise
Average relative density	ρ^*	Spatial distribution
Material distribution	A_m	Spatial distribution

For each FV of lattice structures, designers need to select a group of parameters which can be used for the following design optimization stage. These parameters are referred to as design parameters in this thesis. The selection of design parameters mainly depends on the available design optimization methods for different type of mesoscale lattice structures. In this thesis, the proposed design optimization methods mainly focus on the distribution of relative density. Thus, those relative density related parameters including relative density ρ^* and the thickness of strut can be considered as the design parameters. It should be noted these two parameters are correlated to each other. Once the strut thickness, cell size and cell topology is determined, the relative density of a unit cell can be explicitly calculated. Thus, designers only need to select one of them as the design parameter. Besides relative density related design parameters, the distributions of material compositions A_m can be also considered during the optimization stage with other available multi-material lattice optimization method [229].

Apart from the design parameters selected by designers mentioned above, other listed parameters also need to be determined by designers on the initial design stage. They are generally denoted as non-design parameters in this thesis. The non-design parameters will be kept as constants during the following design optimization stage. The general sequence of determination of non-design parameters of lattice structures is given in Figure 5-15. The base materials of lattice structures are suggested to be determined first, since it significantly affects the effective properties

of structures as well as its related manufacturing methods. Then, cell topology of lattice structures can be selected. During this process, material chart contains the homogenized effective properties of different cell topologies can be used. After that, the cross-sectional shape of a lattice strut is suggested to be considered by designers. In most cases, the circular cross-sectional shape is suggested to be select to reduce the stress concentration on the sharp edge of lattice strut. The last parameter needs to be decided is the lattice cell size. Generally, the cell size is suggested to be bigger than the minimum feature size FV of lattice structures. If the size is too big, then a certain region of FV cannot be fully filled with lattice cells. If the cell size is too small, there is a manufacturability issue for low relative density lattice, since the lattice strut is too thin to be fabricated.

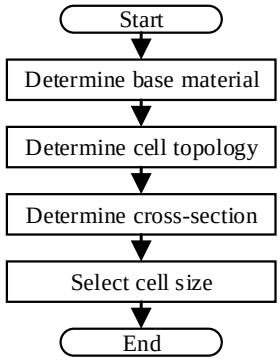

Figure 5-15 The suggested sequence of determination of non-design parameters of lattice structures

5.3.3 Identify the range of design parameters

To generate the initial design space for a given design, the last step is to identify the range of design parameters. In another word, the constraints for each design parameters need to be determined. These constraints mainly come from the manufacturing limitations of the selected AM process. Thus, it is necessary for designers to select a suitable AM process method based on the base materials of FVs. In this step, several existing AM process selection method [230, 231] can be applied. Based on the selected AM process, a quick process planning needs to be done to

identify the printing orientation based on recognized FSs and FVs. After determination of printing orientation, the cell orientation of lattice structures in the manufacturing coordinate system is calculated. Then, the Manufacturable Elements (MEs) of the designed lattice structure are built. The concept of MEs is used in this thesis to link the design and manufacturing process of lattice structures. This concept is originally defined by Rosen [13] as a predefined, parametrized decomposition of a volumetric region of a part. Based on this original concept and the characteristics of lattice structures focused in this thesis, a ME of lattice structure is defined as a lattice strut with its related geometry, material and process information. To parametrically represent each ME of lattice structures in the proposed design method, a data structure of ME is developed and its graphic view is shown in Figure 5-16.

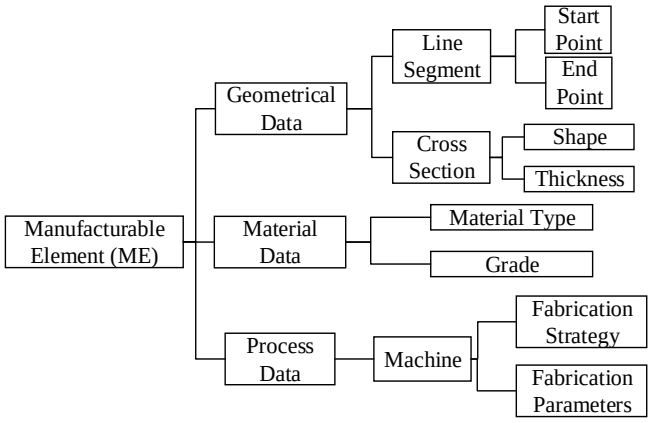

Figure 5-16 A graphic view of the data structure of ME

In current stage, the values of those non-design parameters have been fixed. Only the design parameters will be varied during the future optimization process. To identify the range of these design parameters, a set of MEs are constructed to cover the full range of design parameters. Then, the manufacturability of these MEs will be evaluated by the proposed manufacturability model. Then, based on the feedback of manufacturability model, the ranges of design parameters are obtained. The detailed information of manufacturability model will be discussed in the next

section of this chapter. After this step, the generated initial design space is output for the design optimization stage.

5.4 Manufacturability model of AM process

To describe the manufacturability of different AM processes for lattice structures, a manufacturability model needs to be developed. The general function of this model is described by the block diagram shown in Figure 5-17. It is manifest that the major function of manufacturability model is to decide whether the input ME is manufacturable or not based on predefined success criteria. It should be noted for different applications the success criteria may be different. For example, if designers more care on the geometric shape of fabricated lattice structures, parameters which are used to describe the geometric deviation between the designed lattice and fabricated lattice can be used as the success criterion. If the designed lattice structures play a critical role for the structural performance. Mechanical properties of fabricated struts are more important. Thus, the mechanical properties of fabricated lattice struts should be generally considered as success criteria for the manufacturability model.

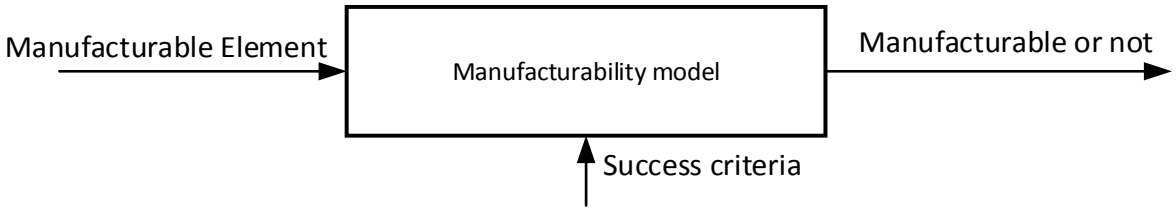

Figure 5-17 Functional diagram of manufacturability model

To realize the defined function of manufacturability model described above, there are three general methods. The first method is to construct the model based on a large number of experiments which can cover the entire design space of lattice structures. This method is the most accurate but impractical, since it is expensive and time consuming. The second method is to do a manufacturing simulation for each ME inside the design space. Compared to the experimental

method, simulation method can save a lot of experimental cost. However, the accuracy is hard to be guarantee, since some simplified model may be used in the simulation process for time saving. Even though the simplified simulation model is used, it still takes a very long time for the simulation since the design space of lattice structures usually contains a large number of design points. The last method is to construct a meta-model of the selected AM process based on experimental data. Specifically, a set of points inside the design space is pre-selected. The experiments need to be done to test focused properties of fabricated MEs with pre-defined design parameters. Based on obtained experimental data, a meta-model is built to describe the relation between parameters defined in ME and its fabricated properties. Based on this relation, it is easier to judge any given ME located in the design space. Compared to pure experiment based methods, the meta-model can significantly reduce the number of experiments. Moreover, once meta-model is built, it can immediately predict whether the input MEs is manufacturable or not. It is faster than simulation based method. More importantly, at the end of a design process, the fabricated design can be also used as the training data which can further improve the accuracy of developed meta-model. Due to those reasons mentioned above, the meta-model based method is selected to model the manufacturability of the selected AM process in the proposed design methodology.

To further illustrate the detailed steps which are used to construct the manufacturability model of AM process on lattice structures, one of AM processes called Fused Deposition Process (FDM) is used as an example in this section. In this example, lattice struts are supposed in a circular shape and fabricated by a certain machine with a given set of process parameters. Thus, the only thing changes the MEs is its geometric data. To describe the relations between geometric data of MEs and geometric deviation of fabricated lattice struts, a set of test parts are designed with lattice struts with different thickness and orientation angles. These tests parts are divided into two groups based

on their tool paths shown in Figure 5-18. They are horizontal struts and inclined struts. The vertical strut is considered as a special case of an inclined strut when the inclined angle equals to 90 degrees. The reason to cause manufacturing errors for horizontal struts (shown in Figure 5-19) and vertical struts (shown in Figure 5-20) are different. Thus, these two groups of struts are investigated separately in the developed meta-model. The focused geometric parameters for horizontal struts are its overhang length L and strut diameter D. As to the inclined struts, they are inclined angle θ and strut diameter D. To represent the geometric quality of fabricated lattice strut, the geometric deviation ratio R_s for horizontal struts is defined as:

$$\mathrm{R}_h = \frac{D_f}{D} \times 100\% \tag{5.3}$$

Where D_f is the deflection and D is the nominal diameter of the horizontal strut. For inclined struts, the geometric deviation ratio R_s is defined as:

$$R_s = \left(\frac{|t_b - D|}{D}\right) \times 100\% \tag{5.4}$$

Where t_b is the thickness shown in Figure 5-20, D is the nominal diameter of lattice strut.

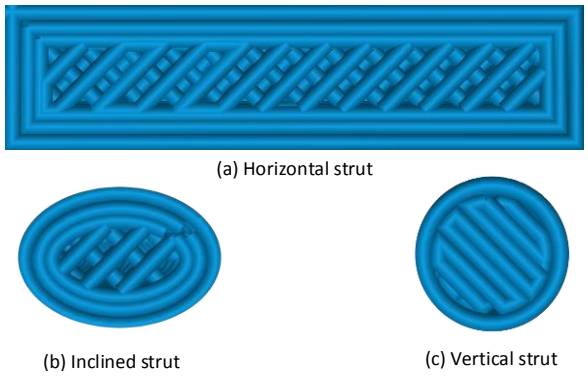

Figure 5-18 Toolpath for lattice struts with different orientation

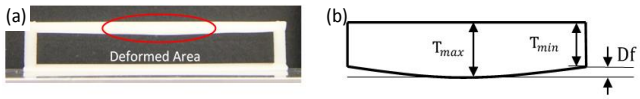

Figure 5-19 Manufacturing defect of horizontal strut

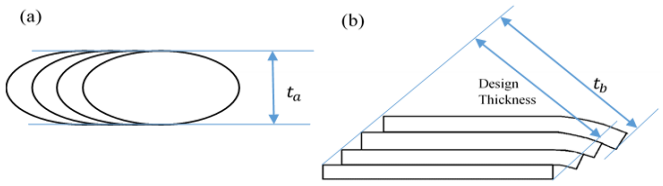

Figure 5-20 Manufacturing defect of inclined strut

To represent the relation between the defined geometric deflection ratio and design parameters of MEs, the Artificial Neural Network (ANN) is used in this example. ANN is a massively parallel distributed processor consists of simple processing units. Due to large scale of parallel distributed structure as well as the ability to learn and generalize, ANN has computing power to solve complex problems that are currently intractable [232]. Moreover, ANN is a non-linear model, and it is often used when the relationship between the input and output variables is not completely understood or even unknown. Therefore, it is suitable for this research to build the non-linear relationship between the deflection ratio and geometrical parameters. And this model can analyze more input parameters without much effort so that if designers want to consider the influence of process parameters as well as design parameters the ANN model is also valid to predict the result. Another advantage of ANN is that when new data are obtained in the later fabrication, it can be imported to the network to improve the performance.

Based on the trained ANN models, the relation between the geometric data of MEs and geometric deviation ratio is established. Two response surfaces are constructed and shown in Figure 5-21 for horizontal lattice struts and inclined lattice struts respectively.

Based on this relation and the predefined criterion of geometric deflection ratio, it is easier to determine whether a ME is manufacturable or not. For detailed data and experimental steps of this meta-model, readers can further refer to the published paper [233].

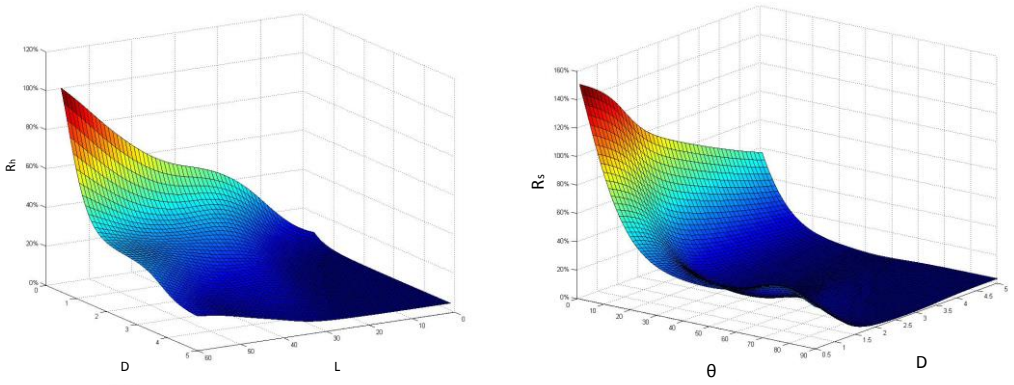

(a) Horizontal struts (b) Inclined struts

Figure 5-21 Response surfaces for geometric deflection ratio with respect to geometric data of MEs for two different types of lattice struts

5.5 Summary

In this chapter, the detailed process and techniques used in the initial design stage is introduced. The main purpose of this design stage is to construct the initial design space which is the foundation of the design optimization process discussed in the next Chapter. To construct the initial design space, there are three steps: functional analysis, construction of FSs and FVs and generation of initial design space. The techniques and methods which are used in each step are presented. In functional analysis step, the input informal functional description and design requirements need to be formalized and represented by a structural representation method which is also known as a functional model. Based on the functional model, different functions or sub-functions are clustered into several groups. Each group of functions is realized by a single physical entity. Based on the group of functions and their related design requirements, the functional entity is built. The second step of the initial design stage is to construct FSs and FVs which roughly describe the geometrical position and shape of designed physical entity. Based on the obtained FSs and FVs, the third step is to construct the initial design space. In this step, there are three sub-steps. In the first sub-steps, FV needs to be further divided into several sub-FVs if necessary. Several guidelines and design

cases are provided. The design result illustrates the functional performance of lattice structures is further improved through FV division. The second sub-step is to identify the design parameters of lattice structures for the optimization stage. Besides design parameters, a detailed procedure is summarized to help designers to figure out the value of those non-design parameters. The last sub-step is to identify the range of design parameters. To achieve this purpose, a definition of ME is proposed. Based on this concept, manufacturability model of AM process for lattice structures is used to identify the fabrication limitations of each lattice strut in the lattice frame. The detailed introduction of the constructed manufacturability model is also presented at the end of this chapter. In the developed model, the meta-model is used to link the MEs with its fabricated quality. Based on this meta-model, designers can easily figure out whether the designed lattice structures are fabricatable or not.

Generally, the proposed methods and techniques in this chapter can be used by designers to prepare the design space for the next optimization stage. Thus, it is the foundation for the following design process.

Chapter 6 Design Optimization

After the initial design stage, the design optimization process is needed to further improve the functional performance of designed products by tuning the selected design parameters. In this chapter, three different design optimization methods for mesoscale lattice structures are proposed. They are BESO based optimization method, heuristic optimization method, and generalized relative density based optimization method. Each has its own merits. Among these three design optimization methods, the first two methods are developed only for the optimization of structural performance. Compared to heuristic optimization method, BESO based method can generally achieve better structural performance. However, it also requests longer computational time when the number of struts is large. Compared to the first two optimization methods, the third method is more general, which can be used for multifunctional design. Thus, if designer has a design case related to multifunctional purposes, he or she should select the third method. It should be noted that the third method can also be applied for the design of a single function. However, if the third method only applies to the optimization of structural performance, it cannot achieve the same optimal performance and BESO based method, since some assumptions used in this method limit the design freedom in the optimization process.

To help designers choose a suitable optimization method, the relation between functions and selected design parameters is analyzed at first. This relation might be simple and straightforward for those structural optimization problems. However, when it comes to multifunctional design cases, the performance and the selected design parameters may be coupled. To identify those relations, the F-P-P-D model discussed in Chapter 3 is suggested to be constructed at first. Based on this model, designers can select a suitable optimization algorithms for mesoscale lattice

structures. Moreover, this model also provides a tool for designers to analyze the coupled relations during design optimization process of lattice structures for multifunctional purposes. It is the key to the proposed simulation infrastructure of the generalized relative density based optimization method.

To introduce the detailed process and techniques used in the design optimization stage, the structure of this chapter is organized as followed. In Section 6.1, an example is used to illustrate the detailed process of construction of F-P-P-D model. Based on the constructed F-P-P-D model, the most suitable optimization method is selected by designers at this design stage. This method is applied to determine the value of selected design parameters in the initial design space. In the following three sections, three different proposed optimization methods are introduced respectively. Then several case studies are presented in Section 6.5 to further validate the proposed design optimization methods. Moreover, a comparison is made between them. Guidelines are summarized to help designers choose the appropriate design optimization method for different design cases. Finally, a summary is made at the end of this chapter in Section 6.6.

6.1 Construction of F-P-P-D model

As illustrated in Figure 3-4, the first step of design optimization is to construct a F-P-P-D model. The detail information of a F-P-P-D model has been already discussed in Chapter 3. Here, a design case is used to illustrate the application of the F-P-P-D model for multiple functional purposes. In this example, the FV which contains heterogeneous uniform lattice structure is designed for two major functions: heat transfer and load bearing. The performance parameters related to these two functions are summarized in Figure 6-1. Among them, two performance parameters: structural compliance and rate of heat flow are directly used to evaluate the load bearing function and heat transfer function. Thus, these two parameters belong to the first category

of performance parameters. During the design process of this case study, a light weight is desired by customers to save material. Thus, the weight of the structure is categorized into the third type of performance parameters. Besides these parameters mentioned above, there are three other performance parameters that exist in the performance domain. They are structural displacement distribution, temperature distribution and thermal stress. These three parameters are not directly linked to the defined functions. However, they are critical to structural compliance and rate of heat flow on the given surface. Hence, these three parameters are regarded as the second type of performance parameters.

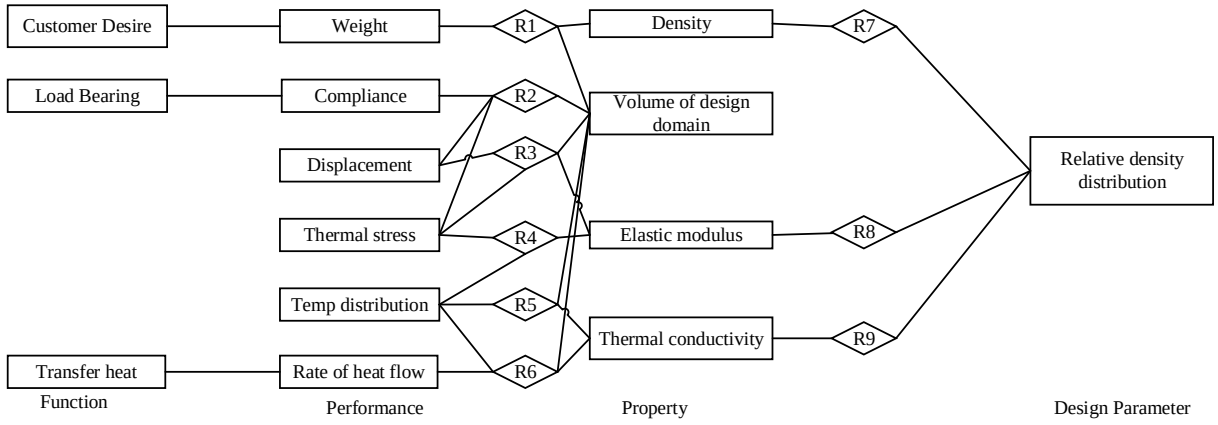

Figure 6-1 The F-P-P-D of the given multifunctional design example

To achieve the desired performance parameters, a set of critical properties that is directly linked to performance parameters is listed in the property domain shown in Figure 6-1. They are density of structure, volume of the design domain, elastic modulus, thermal expansion coefficient and thermal conductivity. The relationship between performance parameters and property parameters is described by six given relations R1-R6 presented in Figure 6-1. Among them, relation R2 is defined to link structural compliance with displacement, thermal stress and volume of design domain based on the equation shown below:

$$l = \frac{1}{2}\int_{\Omega} p_i\, u_i\, d\Omega + \frac{1}{2}\int_{\Gamma_t} t_i u_i\, ds + \frac{1}{4}\int_{\Omega} \sigma_{ij}^{t}(u_{i,j} + u_{j,i})\, d\Omega \tag{6.1}$$

Where p_i is the body force distributed inside the design domain Ω, and t_i is the boundary tractions on the traction part $\Gamma_t \subset \Gamma = \partial\Omega$; u represents the displacement; σ_{ij}^t is the thermal stress tensor. Since both p_i and t_i are provided based on the loading condition of a structure. Thus, compliance of a structure only depends on its displacement distribution, thermal stress and the volume of design domain. Meanwhile, relation R1 links the weight of a structure to its density distribution. The equation representing this relation can be expressed as:

$$m = \int_\Omega \rho \, d\Omega \tag{6.2}$$

Where m is the weight of structure; ρ denotes the density distribution inside the design domain. To calculate the structural displacement, the equilibrium equation and elastic constitutive equation have been written in the weak form as:

$$\int_\Omega E_{ijkl}\varepsilon_{ij}(u)\varepsilon_{kl}(v)d\Omega = \int_\Omega p_i \, v_i \, d\Omega + \int_{\Gamma_t} t_i v_i \, ds + \int_\Omega \sigma_{ij}^t \varepsilon_{ij}(v) \, d\Omega \tag{6.3}$$

Where E_{ijpq} is the elasticity tensor, which is a variable over the design domain; p_i, t_i are the body force and boundary tractions respectively; σ_{ij}^t denotes the thermal stress tensor. v is the arbitrary admissible virtual displacement; u is the displacement of the designed structure; ε_{ij} is the strain tensor. For a small displacement problem, it is expressed as:

$$\varepsilon_{ij}(u) = 1/2(u_{i,j} + u_{j,i}) \tag{6.4}$$

In Equation 6.3, only elasticity tensor distribution and thermal stress may vary during the design optimization process. Thus, based on the Equation 6.3, the relation R3 is defined to link the displacement distribution to the thermal stress as well as the elastic properties of lattice structures. To calculate the thermal stress, the following equations can be applied.

$$\sigma_{ij}^t = E_{ijkl}\varepsilon_{kl}^t \tag{6.5}$$

$$\varepsilon_{kl}^t = [\alpha_T(T - T_{ref}) \quad \alpha_T(T - T_{ref}) \quad \alpha_T(T - T_{ref}) \quad 0 \quad 0 \quad 0] \tag{6.6}$$

Where ε_{kl}^t is the thermal strain caused by the thermal expansion. Its value can be calculated by

Equation 6.6. In this equation, α_T represents the thermal expansion coefficient. This value is fixed once the base material of lattice structures is determined. T represents the temperature at a given point, and T_{ref} is its reference temperature. Equations 6.5 and 6.7 represent the relation between thermal stress, elastic modulus and temperature distribution. This relation is denoted as R4 in the F-P-P-D model shown in Figure 6-1.

To calculate the temperature distribution inside the design domain, the governing equation of steady thermal conduction is established based on Fourier heat transfer theorem and energy conservation theorem, which is shown below.

$$\frac{\partial}{\partial x}\left(\kappa_x \frac{\partial T}{\partial x}\right) + \frac{\partial}{\partial z}\left(\kappa_y \frac{\partial T}{\partial z}\right) + \frac{\partial}{\partial z}\left(\kappa_z \frac{\partial T}{\partial z}\right) + Q = 0 \tag{6.7}$$

Where $\kappa_x, \kappa_y, \kappa_z$ are effective thermal conductivities along x, y, z axis respectively. Q is the heat generated by a heat source. If the boundary condition and the internal heat source of Equation 6.7 are given, the temperature of designed structures only relies on the thermal conductivity distribution. This relation is represented as R5 in Figure 6-1.

Once the temperature distribution is given, the rate of heat flow q_s on the given boundary is calculated by the equation listed below.

$$q_s = -\int_s (\kappa_x \frac{\partial T}{\partial x} n_x + \kappa_y \frac{\partial T}{\partial y} n_y + \kappa_x \frac{\partial T}{\partial z} n_z) ds \tag{6.8}$$

Where (n_x, n_y, n_z) is the norm of the boundary surface. Based on this equation, it is concluded that the rate of heat flow on given surfaces depends on the temperature distribution and the heat conductivity of structure. Thus, R6 is defined in Figure 6-1 to represent this relation.

The properties summarized in the property domain of Figure 6-1 is controlled by the design parameters of lattice structures. Generally, the physical properties of lattice structures are determined by unit cell topology and its relative density. In this design example, the relative density distribution is selected as the design parameters. Other parameters of lattice structures including

cell topologies are determined in the initial design stage. Its detailed process is discussed in Section 5.3.2. Thus, there is only one design parameter in the design parameter domain for this case study.

Based on a homogenization technique, the effective elastic modulus distribution and heat conductivity coefficient are calculated based on relative density distribution. R8 and R9 are used in Figure 6-1 to represent these relations respectively. The exact density of lattice structures ρ is easily calculated by the equation shown below.

$$\rho = \rho_m \rho_c \tag{6.9}$$

Where ρ_m is the density of the base material of lattice structures; ρ_c is its local relative density. To represent the relation between relative density and its exact density, relation R7 is defined in the F-P-P-D model shown in Figure 6-1.

Based on the constructed F-P-P-D model discussed above, designers can select a suitable design optimization method. For the specific design case discussed in this section, it involves more than one functions, and the relations between functional performances of two functions are coupled. Thus, the generalized relative density based optimization method is suggested to be used.

As to those applications which only relates to the design optimization of structural performance, their F-P-P-D model is simple and straight forward. An example of F-P-P-D for a typical structural design optimization problem is shown in Figure 6-2. In this model, the stiffness of a structure is the major design objective in the performance domain. It links to the effective stiffness of lattice structures which is represented as the function of relative density of lattice structures. Other performance parameters including the weight of structure are considered as the design constraints during the design optimization methods. For those design cases whose F-P-P-D model like the one shown Figure 6-2, the proposed BESO based optimization method and heuristic optimization method are suggested to be used.

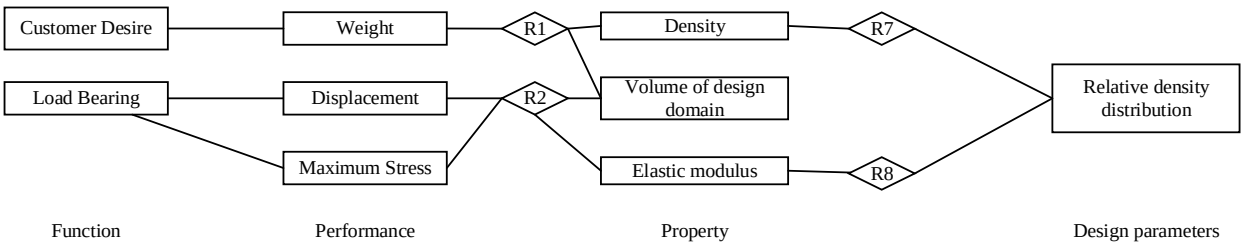

Figure 6-2 The F-P-P-D model for the design optimization of structural performance

6.2 BESO based optimization method for lattice structures

BESO method is a finite element based topology optimization method, where inefficient material is iteratively removed from a structure while efficient material is simultaneously added to the structure. Compared to Evolutionary Structural Optimization (ESO) which is limited to material removal only, the BESO method is much more efficient. This method was first proposed by Querin et al. [47, 234] to enhance the optimization results and the speed of the ESO algorithm. Later, a modified version of the BESO algorithm was presented by Huang and Xie [235] to solve non-convergence and mesh-dependency problems associated with earlier version BESO algorithms.

In this research a modified BESO algorithm is proposed to optimize thickness of lattice struts on mesoscale. Instead of directly removing or adding elements as in the conventional BESO method, the thickness of each strut is updated during the optimization iteration to redistribute material in the design space. This optimization is designed to emulate the remodeling process of bone which is known as Wolff's law [236]. The material will be removed in low stress areas and formed in the high stress areas. The volume of material removed is equal to material added, which keeps the total volume unchanged. The mathematical representation of the proposed optimization problem for lattice structures is expressed as:

$$\text{To Find: } \mathbf{t} = (t_1, t_2, \dots, t_n) \tag{6.10}$$

$$\text{Minimize: } PI = \left(\sum_{i=1}^{i=n} \sigma_{VM_i} V_i\right)/FL$$

$$\text{S.T.: } Ku - P = 0$$

$$\sum_{i=1}^{i=n} V_i \leq V_{const}$$

$$t_{min}^i \leq t_i \leq t_{max}^i$$

Where $\mathbf{t}$ is the n-dimensional vector that contains the size of each strut t_i in the generated lattice frame. *PI* is the performance indicator of a structure to measure how well the overall structure is performing against an idealized fully stressed design [234]. $\sigma_{VM_i}$and V_i represent the maximum Von-Mises stress of the ith strut and its related volume respectively. *F* and *L* are two parameters used to describe an idealized load case, where *F* is a representational force and *L* is a reference length. Their values are predefined by designers based on the size of FV and its related loading condition. During the optimization process, the values of these two parameters are kept unchanged. *K* is the global stiffness matrix of the lattice structure which is regarded as a function of design parameter $\mathbf{t}$ in this problem. u is the vector of nodal displacement in lattice structures and *P* is the nodal load vector. V_{const} is the value of volume constraint which is predefined by designers based on the design requirements. $V_i(t_i)$ is a function to calculate the volume of ith strut inside the lattice structure. The form of this function may vary depending on the cross-sectional shape of the strut and its length. $t^i{}_{min}$ and $t^i{}_{max}$ represent the lower and upper bound of the thickness of lattice struts. Their values are determined in the initial design stage, which is discussed in Section 5.3.3.

To solve the problem defined in Equation 6.10, the BESO based optimization method for mesoscale lattice structures is developed. Its main work flow is shown in Figure 6-3. The overall logic of this proposed algorithm is to relocate struts' material or volume according to struts' stress distribution calculated from FEA. In this optimization algorithm, the key is the volume relocation

process. In this process, the volume of struts whose maximum Von-Mises stress is lower than the given volume is reduced by a certain percentage and the total removed volume is redistributed according to struts' stress distribution. Based on this volume relocation process, the updated structure gradually adapts to the given external load. The detailed description of main steps of proposed optimization algorithm is given as follows:

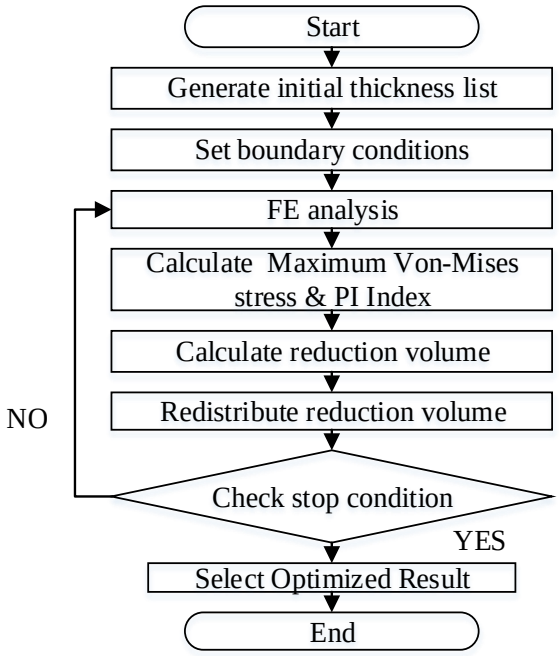

Figure 6-3 General working flow of BESO based lattice optimization algorithm

Algorithm 6-1: BESO based optimization algorithm for mesoscale lattice

Step1: Set up FEA model. In this model, the Timoshenko beam element is used to describe mechanical behavior of each lattice strut. The triangle 2D-shell element is used to model the skin structure on the FSs. Moreover, the FVs with solid material are meshed with 4 nodal tetrahedron elements.

Step2: Generate thickness list of lattice struts.

Step3: Apply all kinematic boundary constrains, loads, element properties, etc.

Step4: Carry out a linear static finite element analysis of the structure.

Step5: Calculate maximum Von Mises stress σ_{VM_i} of each lattice strut in the lattice frame.

Step6: The thickness of lattice is reduced if the strut satisfies the following rule:

Rule 6-1: Material removal rule

Suppose σ_{VM_i} is the maximum Von Mises stress of lattice strut s_i, t_i is the thickness of lattice strut s_i, σ_{VMMax} is the maximum Von Mises stress of all struts in lattice frame, if $(\sigma_{VM_i} \leq RR \times \sigma_{VMMax}) \wedge (t_i > t_{Min})$, then the material will be removed from the lattice s_i which is denoted as $s_i \in S_r$.

In Rule 6-1, RR is known as rejection ratio: $0 \leq RR \leq 1$. RR initially equals to 0.01.

Step7: The reduced thickness t_{r_i} of each lattice strut is calculated by

$$t_{r_i} = RT \times t_i \tag{6.11}$$

Where RT is known as thickness remove ratio. If $t_i - t_{r_i} < t_{min}$, then the reduced thickness $t_{r_i}$is recalculated by

$$t_{r_i} = t_i - t_{min} \tag{6.12}$$

Based on calculated t_{r_i}, the thickness of reduced strut is updated.

Step8: The total removed volume V_{rtotal} is calculated by

$$V_{rtotal} = \sum_{i=1}^{i=n} (A(t_i) - A(t_i - t_{r_i}))l_i \tag{6.13}$$

Where A is the function of struts cross section area with respect to its thickness; l_i is the length of strut t_i.

Step9: Redistribute the removed volume to non-reduced struts whose thickness is lower than the maximum thickness. The added volume for strut s_i is calculated by:

$$V_{Add_i} = (\sigma_{VM_i} / \sum_{i=1}^{i=k} \sigma_{VM_i}) \times V_{rtotal} \tag{6.14}$$

Where k is the number of added volume struts. If $V_{Add_i} + V_i > A(t_{max})l_i$, the added volume will

be recalculated by:

$$V_{Add_i} = (A(t_{max}) - A(t_i))l_i \tag{6.15}$$

The residual volume V_{rs_i} in the adding process of this strut is expressed as:

$$V_{rs_i} = (\sigma_{VM_i} / \sum_{i=1}^{i=k} \sigma_{VM_i}) \times V_{rtotal} - (A(t_{max}) - A(t_i))l_i \tag{6.16}$$

The same method will be used to redistribute residual volumes into the remaining struts until the total residual volume equals to zero.

Step10: Based on the calculated V_{Add_i}, the updated thickness of added volume struts is calculated by:

$$t_i' = A^{-1}(A(t_i) + V_{Add_i}/l_i) \tag{6.17}$$

Where A^{-1} is the inverse function of A.

Step11: if $|PI_{i-1} - PI_i| < c_s$ or $i \geq i_{max}$, algorithm stop, else update RR by:

$$RR = RR + ri \tag{6.18}$$

Where *ri* is known as the rejection ratio incremental value.

Step12: Repeat step4-11, when condition in Step11 is not met.

Finally, the optimized design parameters are selected during the history of the optimization process. After the optimization process, the thickness of each lattice strut is determined. Based on this data and lattice frame, geometric model of lattice structures for a given FV is constructed. Detailed techniques used to build the geometric model of lattice structure have already been discussed in the Chapter 4 of this thesis.

6.3 Heuristic optimization method for mesoscale lattice structures

One of the major difficulties of the optimization of mesoscale lattice structures is the large number of design parameters. In most cases, FVs with lattice structures may contain numerous lattice cells and lattice struts. It is necessary to locally control the change of the relative density or

thickness of these structures to achieve the optimal performance. The process is usually computational expensive. To solve this issue, a heuristic optimization method for mesoscale lattice structures is developed in this thesis. In this method, the distribution of relative density obtained from a topology optimization method has been considered as a clue to decide the thickness of lattice's struts in different regions of FVs. This method assumes that the result of density based topology optimization can represent the importance of each local region to the structural performance of overall structure. Based on this assumption, a specific mapping function is developed to distribute materials inside a FV. Compared to the existing topology optimization based lattice optimization algorithm [50, 237], the developed method considers both the optimal relative density distribution as well as the principal stress directions at each local point. It can further improve the overall stiffness of a structure without the increase of its weight. The general flow of the proposed heuristic optimization has been summarized in Figure 6-4. Detailed process of this optimization method is carefully discussed in the rest of this section.

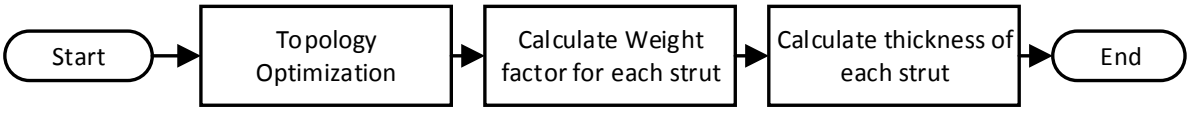

Figure 6-4 General flow of proposed heuristic optimization method for lattice structures

The mathematical representation of the proposed heuristic optimization method is expressed as:

$$\text{To Find: } \mathbf{t} = (t_1, t_2, \dots, t_n) \tag{6.19}$$

$$\text{Minimize: } P = f^T u$$

$$\text{S.T.: } Ku - f = 0$$

$$\sum_{i=1}^{i=n} V_i = V_{const}$$

$$t_{min}^i \leq t_i \leq t_{max}^i$$

Where $\mathbf{t}$ is a vector of lattice struts' thickness. It is regarded as the design parameter in this optimization method. P is the overall compliance of the designed structure. f and u are load and displacement vectors. K is the stiffness matrix. V_i is the volume of ith strut. V_{const} is the maximum volume of the structure. It is controlled and predefined by designers. t_{min}^{i} and t_{max}^{i} are the minimum and maximum struts thickness. Their value is obtained from the initial design stage discussed in Section 5.3.3.

To solve the optimization method defined in Equation 6.19, its related SIMP based topology optimization problem needs to be solved first. The mathematical formulation of this topology optimization problem is expressed as:

$$\begin{aligned} \text{To Find:} \quad & \boldsymbol{\rho}^* = (\rho_1^*, \rho_2^*, \dots, \rho_m^*) \\ \text{Minimize:} \quad & P = f^T u \\ \text{S.T.:} \quad & K(\boldsymbol{\rho}^*)u - f = 0 \\ & E_i = (\rho_1^*)^n E \\ & \textstyle\sum_{i=1}^{i=m} V_i \rho_i^* \leq V_{const} \\ & \rho_{min}^* \leq \rho_i^* \leq 1 \end{aligned} \tag{6.20}$$

Where $\boldsymbol{\rho}^*$ is a vector which contains the relative density for each element inside a FV. P represents the structural compliance. f and u are load and displacement vectors. K is the global stiffness matrix. It is the function of relative density distribution. E_i is penalized elastic modulus of ith element inside the FV. E is the elastic modulus of a base material, and n is the penalty factor. The value of the penalty factor is selected by designers depends on the cell topologies. V_i is the volume of ith element and V_{const} is the maximum allowable volume.

The topology optimization problem stated in Equation 6.20 can be easily solved by the SIMP based topology optimization method. During its solving process, the density filter is utilized to

avoid the checkerboard phenomenon. After solving the problem, the optimal relative density distribution is obtained. It is mathematically described by the density vector $\boldsymbol{\rho}^*$ of element. Beside $\boldsymbol{\rho}^*$, the stress distribution of the optimal design under a given load condition is also obtained. This stress distribution is described by a vector $\mathbf{s}$:

$$\mathbf{s} = (\sigma_1, \sigma_2, \dots, \sigma_m) \tag{6.21}$$

Where $\sigma_i, i = 1,2, \dots, m$ is the stress tensor for the ith element. In the proposed optimization method, both vector $\boldsymbol{\rho}^*$ and $\mathbf{s}$ are used to calculate the thickness of each strut based on defined mapping function. This mapping function is established based on the previous assumption that the result of topology optimization indicates the importance of material in different region for structural perfor. The general form of this mapping function is expressed as:

$$t_i(\boldsymbol{\rho}^*, \mathbf{s}, t_{max}) = t_{min}^i + \frac{w_i(\boldsymbol{\rho}^*, \mathbf{s}) - w_{max}}{w_{max} - w_{min}}(t_{max} - t_{min}^i) \tag{6.22}$$

Where t_i is the thickness of ith strut. t_{min}^i is the minimum strut thickness of ith strut. t_{max} is maximum thickness of struts. Its value is a constant to all the struts inside the FV. It is used to control the overall volume of designed lattice structures. To guarantee the designed lattice structures is manufacturable, t_{max} should satisfy the following condition:

$$t_{max} < t_{max}^i, \forall i = 1,2, \dots, n \tag{6.23}$$

In Equation 6.22, w_i is defined as the weight coefficient of ith strut. Its value is calculated based on the topology optimization result $\boldsymbol{\rho}^*$ and $\mathbf{s}$. w_{max} and w_{min} are the maximum and minimum value of weight coefficients for all the lattice struts inside the FV.

To calculate the strut thickness from Equation 6.22, the key is to calculate the weight coefficient of each strut. During its calculation procedure, two factors need to be considered. The first factor is called as density based factor. It is calculated from the relative density distribution $\boldsymbol{\rho}^*$ which is obtained from topology optimization process. It represents the importance of the

material in the local region to the overall structural performance. The strut in the region with high relative density should have a thicker cross section. Instead of directly using the relative density of the closest element to the strut, a weighted average function is used to generally consider the effects of all the surrounded elements. The function to calculate density based factor is defined as:

$$w_d^j = \frac{\sum_{i=1}^{m} \rho_i^* / r_i^2}{\sum_{i=1}^{m} 1/r_i^2} \tag{6.24}$$

Where w_d^j is the density based factor of jth strut. ρ_i^* is the relative density of ith surrounded element; r_i is the distance from the centroid of the element to the center of the strut. m is the number of surrounded elements of the strut. The value of m is controlled by the surrounded distance d_e. Only those elements whose distance to the strut is smaller than d_e are considered as the surrounded elements. Thus, the smaller the d_e, the smaller the number of elements in the surrounded elements set. When the relative density changes dramatically, it will cause unsmooth distribution of struts' thickness. Thus, d_e is usually larger than the size of a unit cell.

The second factor which needs to be considered is called as stress based factor. The value of this factor is mainly determined by the stress components in the local stress tensor for each region. It follows the assumption that the strut which is aligned with the direction of major principal stress should be thicker than those struts in other orientations. This assumption is summarized based on the observation of thickness distribution of trabeculae inside a femur head [238]. Particularly, the thickness of trabeculae varies following the paths of principal compressive and tensile stresses they carry. It can achieve the greatest strength with the minimum of material. Based on this assumption, the function to calculate the importance factor for lattice orientation is proposed, and expressed as:

$$w_o^j = \frac{|\mathbf{P_1}|}{\sum_{i=1}^{i=3} |\mathbf{P_i}|} \left(\vec{h} \cdot \vec{l}\right)^2 + \frac{|\mathbf{P_2}|}{\sum_{i=1}^{i=3} |\mathbf{P_i}|} \left(\vec{h} \cdot \vec{m}\right)^2 + \frac{|\mathbf{P_2}|}{\sum_{i=1}^{i=3} |\mathbf{P_i}|} \left(\vec{h} \cdot \vec{n}\right)^2 \tag{6.25}$$

Where w_o^j is stress based factor for the j[th] strut. Its value is determined by the stress tensor of its closest element; $\mathbf{P_1}, \mathbf{P_2}, \mathbf{P_3}$ are three principle stresses of the nearest element of strut. $\vec{l}, \vec{m}, \vec{n}$ are their related unit direction vectors. $\vec{h}$ is the direction vector of the axis of strut.

Those two factors mentioned need to be simultaneously considered during the calculation of lattice strut's thickness by Equation 6.22. Thus, a weighted-sum function is constructed to calculate the weight coefficient of each strut. This function is expressed as:

$$w^j = u_1 w_d^j + u_2 w_o^j \, , u_1 + u_2 = 1, u_1 \geq 0, u_2 \geq 0 \tag{6.26}$$

Where u_1, u_2 are two weight coefficients corresponding to two different weight factors introduced above. For a general design case, these two coefficients are suggested to be equal. Based on those equations discussed above, the function to calculate the thickness of each strut is obtained. This function only takes t_{max} as an independent variable. Based on this function, the total volume of the lattice structures can also be represented by a function on t_{max}. By solving the volumetric constraint defined in Equation 6.19, the value of t_{max} is calculated. Then, based on this value, the thickness of each strut is obtained. The calculated struts' thickness is used to build the geometric model of heterogeneous lattice structures during the geometric modeling stage.

6.4 Generalized relative density based optimization method for lattice structures

The two optimization methods discussed above are both developed to improve the stiffness of designed lattice structures. For those applications where lattice structures play multifunctional roles, the multifunctional design optimization method is needed. In this thesis, a generalized relative density based optimization method is developed for multifunctional lattice structures. To introduce this innovative optimization method, this section is further divided into three sub-sections. In Sub-section 6.4.1, the general multifunctional optimization model is introduced. After that, the multifunctional simulation infrastructure which is used to evaluate the multifunctional

performance of mesoscale lattice structures is discussed in Sub-section 6.4.2. At the end of this section, the solution of the constructed optimization formulation and its related post-process are presented.

6.4.1 Multifunctional optimization model

To deal with multiple functions and their coupled functional performance, the compromise Decision Support Programming (DSP) template [239] is used in this thesis to formulate the multifunctional optimization model. This template is a hybrid formulation which incorporates characteristics from both traditional mathematical programming and goal programming. Similarly, to the goal programming, the multiple objectives are formulated as system goals and the deviation function is defined which is solely a function of goal deviation variables. Moreover, the concepts of system constraints and bounds from the traditional mathematical programming are also incorporated in this formulation, which makes it more suitable for engineering design applications. The detailed description of this formulation can be found elsewhere [239].

The compromise DSP formulation used in this thesis for the multifunctional design of heterogeneous lattice structures is presented in Formulation 6-1. In this optimization formulation, the relative density distribution of heterogeneous lattice structures is considered as the design parameter. Specifically, the FV of lattice structures has been discretized into several sub-regions. The relative densities of all the sub-regions inside the FV constitutes the vector **X** which is regarded as a design parameter in the proposed optimization method. The upper and lower bound of local relative density $x_{l,L}$ and $x_{l,U}$ for l^{th} region are given to guarantee the manufacturability of the generated lattice structures.

Formulation 6-1 compromise DSP formulation template for multifunctional design of lattice structures

Given

n	number of relations between performance domain and property domain
m	number of relations between property domain and design parameter domain
p	number of system goals
q	number of the discretized sub-regions inside design space
s	number of system inequality constraints
P_f	A vector of performance parameters
P_r	A vector of property parameters
G_k	Targets, $k = 1,2,3, \dots, p$
$f_i(P_f, P_r)$	system constraint equation describes the relations between performance domain and property domain, $i = 1,2,3, \dots, n$
$h_j(P_r, X)$	system equation describes the relations between property domain and design parameter domain, $j = 1,2,3, \dots, m$
$c_t(P_r)$	system constraint equation for inequality constraint on performance parameter, $t = 1,2,3, \dots, s$

Find

$X = (x_1, x_2, \dots, x_q)$	a design vector consists the relative density of lattice structures in each discretized sub-region inside the entire design space
d_k^-, d_k^-	Deviation variables, $k = 1,2,3, \dots, p$

Satisfy

Constraints

$$f_i(P_f, P_r) = 0, i = 1,2,3, \dots, n \quad (6.27)$$

$$h_j(P_r, X) = 0, j = 1,2,3, \dots, n \quad (6.28)$$

$$c_t(P_r) \geq 0 \quad (6.29)$$

Goals

$$A_k(P_f(X)) + d_k^- - d_k^+ = G_k \; k = 1,2,3, \dots, p \quad (6.30)$$

Bounds

$$x_{l,L} < x_l < x_{l,U} \quad (6.31)$$

$$d_k^- \cdot d_k^+ = 0; d_k^-, d_k^+ \geq 0 \quad (6.32)$$

Minimize

$$Z = \sum W_i(d_k^- + d_k^+); \sum W_i = 1, W_i > 0 \quad (6.33)$$

In the compromise DSP formulation for the heterogeneous lattice structure shown in Formulation 6-1, the system goals are selected from the performance parameters in the performance domain. In most cases, these goals are from the first or third category of performance

parameters which are directly related to the defined functions or can quantitatively represent the non-functional related performance of the designed structure. For example, in the design of structured part for load bearing purpose, the structural compliance is usually regarded as the goal of design optimization process. It should be noted that not all the performance parameters in the first and third categories need to be considered as the goals. In some special cases, some performance parameters can also be considered as the system constraints $c_t(P_r)$ rather than goals, since there are strict requirements which those performance parameters must satisfy. To represent the selected performance parameters for the system goals, the k^{th} achievement function for i^{th} performance parameter defined in the domain of performance parameters is expressed as:

$$A_k(P_r) = e_i^T P_r \tag{6.34}$$

Where e_i denotes the vector with one in the i^{th} component and zero elsewhere. It should be noted the performance parameters can also be regarded as the function of design parameters based on the relations defined in the F-P-P-D model. Thus, the achievement function defined in Equation 6.34 is also the function of design parameters. However, it is usually difficult to directly obtain the explicit relations between design parameters and structure's performance. Thus, in this thesis, two sets of equations $f_i(P_f, P_r) = 0$ and $h_j(P_r, X) = 0$ are given to implicitly define the relations between performance parameters and design parameters. Each of these functions represent one relation defined in the F-P-P-D model. By solving the two sets of functions described above, the values of performance parameters are obtained. In addition to achievement functions, the deviation variables d_k^-, d_k^+ are given to measure the extent to which each goal target g_k is under or over-achieved the value. It should be noted that deviation variables defined in Formulation 6-1 are associated to system goals, and their range of values depends on the goal itself. To normalize the deviation variables is necessary to avoid some goals with large numerical value dominating the

optimization process. A summary of normalization rules for different types of goals are shown in Table 6-1.

Table 6-1 Normalize rules for goals[239]

Goal Type	Normalization Rule
Maximize $\boldsymbol{A_k(P_f)}$	$A_k(P_f)/G_k + d_k^- - d_k^+ = 1$, $d_k^+ = 0$, G_k is larger than maximum expected value of $A_k(P_f)$
Minimize $\boldsymbol{A_k(P_f)}$ to non-zero	$G_k/A_k(P_f) + d_k^- - d_k^+ = 1$, $d_k^+ = 0$, G_k is smaller than minimum expected value of $A_k(P_f)$
Minimize $\boldsymbol{A_k(P_f)}$ to zero	$A_k(P_f)/A_{kmax} + d_k^- - d_k^+ = 0$, $d_k^- = 0$, A_{kmax} is the upper bound of $A_k(P_f)$
$\boldsymbol{A_k(P_f)}$ approach to $\boldsymbol{G_k}$ from below	$A_k(P_f)/G_k + d_k^- - d_k^+ = 1$
$\boldsymbol{A_k(P_f)}$ approach to $\boldsymbol{G_k}$ from above	$G_k/A_k(P_f) + d_k^- - d_k^+ = 1$
$\boldsymbol{A_k(P_f)}$ approach to $\boldsymbol{0}$	$A_k(P_f)/A_{kmax} + d_k^- - d_k^+ = 1$

The objective function of the compromise DSP template is defined as a linear weighted combination of deviation variables for each goal. The weight coefficient for each of goal is determined by the designers based on its significance. During the design process, both target values and weights of goals can be varied to generate a series of solutions. Tradeoffs are made by designers to choose the 'optimal' solution at the end of design process.

6.4.2 Multifunctional design simulation of lattice structures

To solve the optimization model defined in Formulation 6-1, multifunctional simulation infrastructure needs to be built to evaluate the performance parameters with respect to given design parameters. This simulation infrastructure is further divided into two parts. In the first part, asymptotic homogenization technique is applied to calculate the effective properties of lattice structures in each sub-region. Based on the obtained properties, the equations which describe the relations between performance and properties will be solved numerically by FEA method. In the following contents of this sub-section, the detailed steps of each part will be illustrated based the multifunctional design case discussed in Section 6.1.

In each discrete sub-region, the lattice structures are assumed to be homogeneous and periodic.

To evaluate the properties of lattice structures for a given sub-region, asymptotic homogenization technique [240] is applied. This technique can calculate the macroscopic effective properties of composite or lattice structures based on an asymptotic expansion of the governing equations in different disciplines. The mathematic theory behind this technique has been summarized in detail in previous research work [240]. A comparison between asymptotic homogenization technique and other homogenization technique has also been made by Arabnejad and Pasini [80]. It shows that asymptotic homogenization technique can be applied to predict the effective properties of lattice structures in a wide range of relative densities. Moreover, compared to other available homogenization techniques like energy based method [241], asymptotic homogenization technique is also able to calculate different types of effective properties including elastic modulus, heat conductivity, fluid permeability. Due to these reasons, this technique is selected in the proposed design method.

To introduce the detailed steps of applying homogenization technique on lattice structures for multifunctional purposes, the design case introduced in Section 6.1 is used again. In this design case, both effective elastic modulus tensor E_{ijkl}^{H} and effective conductive tensor k_{ij}^{H} need to be calculated for each sub-region. According to the theory of asymptotic homogenization, effective elastic tensor E_{ijkl}^{H} can be calculated by the equation presented below.

$$E_{ijkl}^{H} = \frac{1}{|V|}\int_{V} E_{pqrs}(\varepsilon_{pq}^{0(ij)} - \varepsilon_{pq}^{(ij)})(\varepsilon_{rs}^{0(kl)} - \varepsilon_{rs}^{(kl)})dV \tag{6.35}$$

Where $|V|$ denotes the volume of unit cell of a lattice structure; E_{pqrs} is the elastic tensor of its base material; $\varepsilon_{pq}^{0(ij)}$ are set of prescribed macroscopic strain fields; $\varepsilon_{pq}^{(ij)}$ is locally varied strain fields under a given macroscopic strain field. Its value is calculated based on the displacement distribution inside unit cell by equations defined below.

$$\varepsilon_{pq}^{ij} = \frac{1}{2}(u_{p,q}^{ij} + u_{q,p}^{ij}) \tag{6.36}$$

Where u^{ij} denotes microscopic displacement for a given macroscopic strain $\varepsilon_{pq}^{0(ij)}$. Its value is solved by the weak formulation defined below.

$$\int_V E_{ijpq}\varepsilon_{ij}(v)\varepsilon_{pq}(u^{kl})dV = \int_V E_{ijpq}\varepsilon_{ij}(v)\varepsilon_{pq}^{0(kl)}\, dV \tag{6.37}$$

Where v is the virtual displacement field. Usually, Equation 6.37 can be solved numerically by FEA technique. The obtained displacement distribution is applied to calculate the effective elastic tensor based on Equations 6.35 and 6.36. Likewise, according to homogenization theory, the effective heat conductivity k_{ij}^H can be calculated by the equation expressed below.

$$k_{ij}^H = \frac{1}{|V|}\int_V (T_{,l}^{0(i)} - T_{,l}^{(i)})k_{lm}(T_{,m}^{0(j)} - T_{,m}^{(j)})\, dV \tag{6.38}$$

Where $|V|$ denotes the volume of unit cell; k_{lm} is the heat conductivity tensor of the selected base material. $T_{,l}^{0(i)}$ is a given macroscopic temperature field;T^i is a microscopic temperature field. To obtain the microscopic temperature field, like elastic tensor, the weak form of Fourier law needs to be solved, which is shown below.

$$\int_V v_{,i}k_{ij}T_{,j}^k dV = \int_V v_{,i}k_{ij}T_{,j}^{0(k)} dV \tag{6.39}$$

Where v is the virtual temperature field. Like Equation 6.37, this equation can also be solved by FEA method to obtain the microscopic temperature distribution for a given macroscopic temperature field.

The analytical solutions for both E_{ijkl}^H and k_{ij}^H are hard to deduce. In most cases, only numerical solutions are available for Equation 6.37 and Equation 6.39. Thus, interpolation functions are used in this thesis to approximate the derivative of effective properties with respect to the relative density of lattice structures. To preserve the shape of the data and respect monotonicity, the monotone piecewise cubic interpolation function proposed by Fritsch and

Carlson [242] has been applied to interpolate the discrete data from numerical calculation. This interpolation function can guarantee a continuous first derivatives as well the monotonicity on each subinterval. Compared to piecewise cubic spline interpolation, it has no overshoot and less oscillation. In this section, two typical 2-dimensional lattice cells, 'square' and 'cross', are used as the example. The domain of relative density (0 to 1) has been evenly partitioned into 20 intervals having 21 nodes. The normalized effective elastic modulus and thermal conductivity on each node has been numerically evaluated. Based on the results, their interpolation functions have been constructed and shown in Figure 6-5. Since both 'square' and 'cross' cells are symmetrical with respect to the orthogonal axes that pass through their center, their effective elastic modulus and thermal conductivity along these two symmetric axes should also be equal. Thus, Figure 6-5 only shows the properties along one symmetric axis. The properties along the other symmetric axis should be the same. By comparing these two different cell topologies, it is concluded that square cell achieves better elastic modulus than cross cell with the same relative density. However, the cross cell shows a better performance with respect to shear modulus. As to effective heat transfer properties, the difference between two different cells are relatively small especially in the range of low relative density area. Generally, the square cell shows slightly better performance than the cross cell when the relative density of cell increases.

Based on the asymptotic homogenization technique, the effective properties of lattice structures in each discrete sub-region are calculated. These results are used to evaluate the value of performance parameters based on the defined relations between performance domain and property domain. Each of these relations is expressed by its corresponding system equations. A set of system equations defined by these relations needs to be solved during this process.

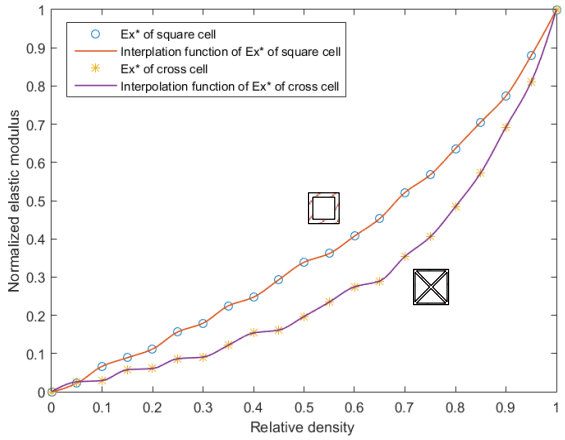

(a) Normalized effective elastic modulus with respect to cell's relative density

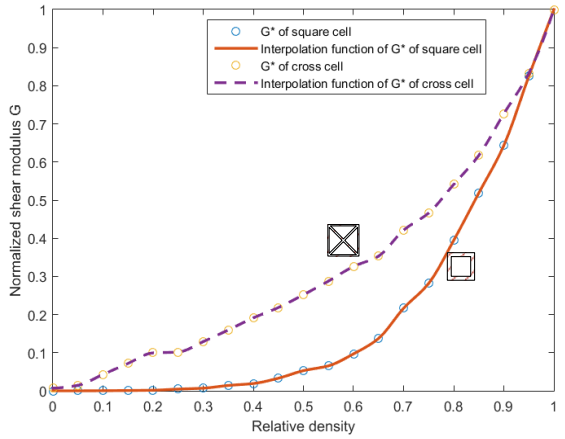

(b) Normalized effective shear modulus with respect to relative density

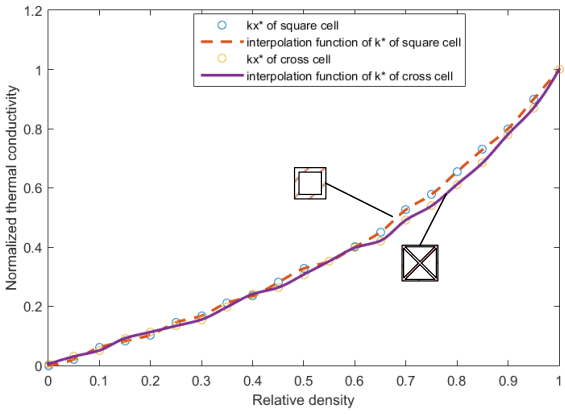

(c) Normalized effective thermal conductivity with respect to relative density

Figure 6-5 effective material properties of 'square' and 'cross' cells.

In this thesis, FEA method has been applied to solve the set of system equations defined between performance domain and properties domain. Particularly, Equation 6.1 is rewritten into the discrete form as:

$$C = \frac{1}{2}(P^0 + P^{th})^T U \tag{6.40}$$

Where P^0 is the nodal load vector and P^{th} is the nodal thermal load vector. U is the nodal displacement vector. To obtain the displacement distribution, Equation 6.3 is also rewritten into the discrete form as:

$$K(E)U = P^0 + P^{th} \tag{6.41}$$

Where K is the stiffness matrix of a designed structure. It depends on the distribution of effective elastic tensor E. The nodal load vector P^0 is determined once boundary condition is given. However, the value of P^{th} needs to be calculated based on the Equation 6.5 and Equation 6.6. For ith element, its equivalent discrete nodal heat load vector is calculated by:

$$P_i^{th} = \alpha(x_i) \int_\Omega {B_i}^T D_i(E(x_i))(T(x) - T_{ref})\phi^T d\Omega \tag{6.42}$$

Where P_i^{th} is the thermal load vector on the node of ith element; $\alpha(x_i)$ is the thermal expansion coefficient of the material in the ith element; B_i and D_i are element strain-displacement matrix and elasticity matrix respectively. Among them, D_i is regarded as the function of material elastic properties inside the design domain. $T(x)$ is temperature distribution inside the element. T_{ref} is reference temperature; ϕ is [1100] for a two-dimensional problem and [111000] for a three-dimensional problem.

As to the Equation 6.7 defined in relation R5, it represents the governing equation of heat conduction. Its discrete form is rewritten into the equation shown below:

$$(K_t(k) + H_t)T = q_t + q_h \tag{6.43}$$

Where K_t is the thermal conductivity matrix. Like stiffness matrix, if the shape of design domain

and elements are given, this matrix only depends on the distribution of conductivity coefficient k. H_t is the boundary convection matrix. q_t, q_h are heat flux vector and boundary convection vector. To further evaluate the rate of heat flow Q on the given boundary surface, the Equation 6.8 is rewritten as:

$$Q = H(k)T \tag{6.44}$$

Where $H(k)$ is a heat flow-temperature matrix defined for a given boundary surface. It is a function of heat conductivity coefficient.

To solve the set of equations listed above, the performance parameters are obtained. The order of solving these equations is important. To get the right order of equation solving, the adjacent matrix R which has n rows and $p+q$ columns is constructed to represent the complex relationship between performance and properties. Here n is the number of relations defined between two domains, and p, q are the number of performance parameters and property parameters respectively. In this matrix, each row represents a defined relation between performance and property, while its columns represent parameters in both performance domain and property domain. If the jth parameter is linked with the ith relation, the element r_{ij} equals to one, else r_{ij} equals to zero. Based on this rule, the adjacent matrix for the design example discussed in Section 6.1 is constructed and shown in Table 6-2.

Table 6-2 Adjacent matrix for relations between performance and properties

	Weight	Compliance	Displacement	Thermal stress	Temp	Heat flow	Density	Volume	Elastic modulus	Thermal expansion coefficient	Thermal conductivity
R1	1	0	0	0	0	0	1	1	0	0	0
R2	0	1	1	1	0	0	0	1	0	0	0
R3	0	0	1	1	0	0	0	1	1	1	0
R4	0	0	0	1	1	0	0	0	1	1	0
R5	0	0	0	0	1	0	0	1	0	0	1
R6	0	0	0	0	1	1	0	1	0	0	1

The adjacent matrix shown in Table 6-2 is rewritten into a block matrix in the form shown

below:

$$R = [C \quad D] \tag{6.45}$$

Where C is $n \times p$ submatrix which only contains the columns related to performance parameters. D is $n \times q$ submatrix which only contains the columns related to property parameters. Based on the property of submatrix C, the design cases are further divided into three categories. If the submatrix C can be converted to identity matrix by interchanging its rows or columns, all the performance parameters can be solved independently. This type of design problem is called functional uncoupled design. If the submatrix C can be converted to triangular block by interchanging its rows or columns, all the performance parameters can be sequentially solved. The solving order can be easily obtained from the converted triangular block. This type of design problem is denoted as functional decoupled design. Elsewise, if C can neither be converted to triangular or identity matrix, the design problem is fully functional coupled. To calculate the performance parameters of this type of design problems, Multidisciplinary Analysis (MDA) strategy such as Gauss-Seidel MDA [243] can be applied. For the design case discussed in this thesis, its submatrix C is reorganized into C^* shown in Table 6-3.

Table 6-3 adjacent matrix C* for functional performance

	Weight	Compliance	Displacement	Heat flow	Thermal stress	Temp
R1	1	0	0	0	0	0
R2	0	1	1	0	1	0
R3	0	0	1	0	1	0
R6	0	0	0	1	0	1
R4	0	0	0	0	1	1
R5	0	0	0	0	0	1

The matrix C^* defined in Table 6-3 is an upper triangular matrix. To evaluate the performance parameter for this design problem, Equation 6.43 of relation R5 is firstly solved to obtain the temperature distribution. Its result is fed into Equations 6.5 and 6.6 which represent relation R4.

By solving these two equations, the thermal stress distribution is calculated. Meanwhile, the temperature distribution is used to calculate the heat flow by solving Equation 6.44 which represents relation R6. To calculate the displacement distribution, Equations 6.41 to 6.43 are used which represent relation R3. Based on the calculated displacement distribution and thermal stress, the structural compliance is obtained based on Equation 6.40 defined in relation R2. Finally, the total mass of structure is easily calculated by Equation 6.2, since this value is independent to other performance parameters. Based on the performance parameters calculated above, the value of objective function is easily obtained.

6.4.3 Solution of optimization model

To solve the compromise DSP formulation defined in Section 6.4.1, gradient based non-linear optimization methods including SQP and Method of Moving Asymptotes (MMA) can be applied. These methods all request the evaluation of objective function' gradient. Thus, to calculate the gradient is the key to solve the defined optimization formulation. Generally, the gradient of objective function of compromise DSP problem defined above can be calculated based on the chain rule expressed as:

$$\frac{dz}{dX} = \sum\left(w_k \frac{d\left(d_k^- + d_k^+\right)}{dA_k(X)} \cdot \frac{dA_k(X)}{dP_f} \cdot \frac{dP_f}{dX}\right) \tag{6.46}$$

In Equation 6.46, the derivative of deviation with respect to the achievement function can be easily evaluated for different types of normalize rules discussed in Table 6-1. In most cases, the achievement function is directly defined based on the linear combination of performance parameters. Thus, the derivative of the achievement function with respect to the performance parameters is also easy to be obtained.

Compared to the first two derivatives on the right-hand side of Equation 6.46, the last term is usually difficult to be directly evaluated, since the performance parameters and their related

properties are coupled. To evaluate the derivative of each performance parameters with respect to design parameters, adjoint method is used in this thesis. This is because the number of design parameter is much larger than the number of performance parameters. The detailed calculation steps for the design case introduced in the Section 6.1 is attached in the Appendix C. During the calculation process, the derivatives of property parameters with respect to the design parameters are easily obtained from the interpolation function discussed in the previous sub-section.

Besides the gradient of objective functions, the gradients of constraint functions also need to be calculated. In the defined optimization formulation, the equality constraints are all from the system governing equations. These constraints must be strictly satisfied. Thus, there is no need to calculate their gradients. It is only necessary to calculate the gradient of non-equality constraints $c_t(P_f)$. Like the objective function, this value can also be evaluated based on the chain rule mentioned above. It will not be discussed in detail here.

Based on the calculated gradient of objective function as well as the constraints function, gradient based non-linear optimization solver is applied. By solving the defined compromise DSP formulation, the distribution of lattice structures' relative density is obtained. This distribution is used to build the heterogeneous lattice structures. Specifically, cells are supposed to have the same relative density in each sub-region. Thus, the relative density for each cell is calculated. Based on this result, the geometric model of heterogeneous lattice structures is built. In this thesis, the process which is used to convert the optimization result to the parameters needed for geometric modeling process is referred as the post-process.

Besides the post-process, it is also necessary to do another round of simulation to evaluate the performance of generated heterogeneous structures. This round of simulation is called as performance checking. During the performance checking, fine elements whose size is smaller than

the thickness of cell's struts or walls are used. Thus, this round of simulation can capture the stress and strain distribution on mesoscale. Moreover, it provides more accurate result than the simulation model used in the optimization process. However, fine elements also lead to a significant increase of computational cost. Thus, this analysis model with fine elements is only used during performance checking process at the end of optimization process. If the calculated performance cannot satisfy the design requirements, some constraints or weight-coefficient parameters defined in the compromise DSP formulation needs be modified and another round of optimization needs to be done, otherwise the final design result is output for geometric modeling process.

6.5 Case studies and discussion

In this section, several design cases are provided to validate the efficiency of those proposed optimization methods for mesoscale structures lattice structures proposed in this chapter. At the end of this section, a comparison between three different optimization methods is made. It helps designers to select a suitable method for their design cases.

To validate the proposed BESO based optimization method and heuristic optimization method, the same design case used to illustrate the FV division for hybrid lattice structures discussed in Section 5.3.1 is used in this section. The dimensions of the FV and its loading condition are given in Figure 6-6. In this design case, lattice struts' thickness is chosen as the design parameter. It should be noted that the thickness of strut in this design case represents the its diameter, since its cross section is in a circular shape. Besides struts' thickness, other parameters of the design lattice structures are decided in the initial design stage discussed in Chapter 5. In this section, the values of these parameters are summarized in Table 6-4 and Table 6-5.

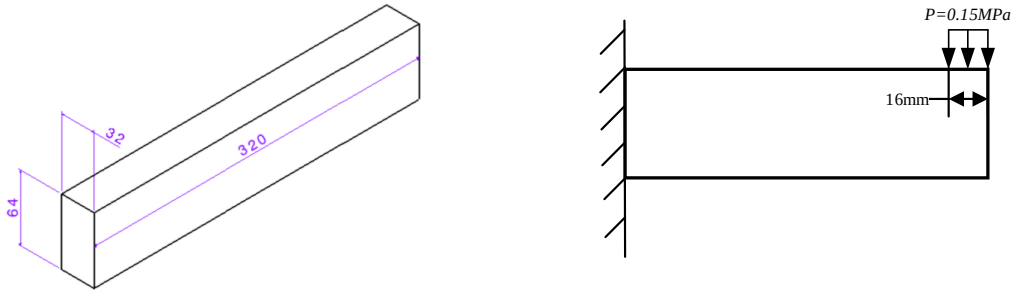

(a) Dimensions of FV for lattice structures /mm (b) loading condition

Figure 6-6 Dimensions of the FV and its loading condition

Table 6-4 Mechanical properties of base material of lattice structures

Material Name	Elastic modulus	Poisson ratio	Yield Strength	Density
316 Stainless Steel	192 GPa	0.3	290MPa	8.0 kg/m^3

Table 6-5 The parameters of lattice structures determined in the initial design stage

Lattice type	Cell size	Cell topology	Cross-section shape	Cell orientation
Uniform lattice	8mm	"body center cubic" and "Cubic" shape	Circular shape	(0,0,0)

Based on the FV division process discussed in Chapter 5 and those determined parameters summarized above, the initial design space of this FV is generated and its frame is shown in Figure 6-7. In this initial design space, the thickness of struts in the FV is considered as design parameters. The thickness each lattice struts is constrained by the manufacturability of the selected AM process. For this design case, a commercial Selective Laser Melting (SLM) machine, Renishaw AM400, is supposed to use for the fabrication process. To guarantee the designed lattice structure is fabricatable, the minimum strut thickness is set as 0.8mm. To keep the designed lattice structure to be porous, the maximum strut thickness is set as 1.6 mm.

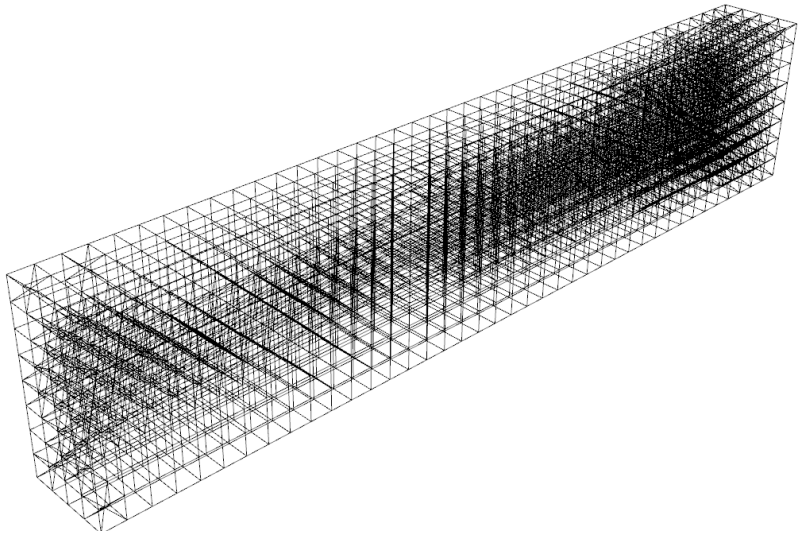

Figure 6-7 Hybrid lattice frame

The initial design space discussed above have been optimized by two different lattice optimization methods discussed above to compare results. For both methods, the volume of designed lattice structure is fixed as the constraint during the optimization process.

The parameters used for the proposed BESO based optimization is summarized in Table 6-6. After 34 iterations, the algorithm stops due to the difference of PI values between two iterations are smaller than the given value predefined in Table 6-6. Besides PI values, the maximum displacement and maximum Von-Mises stress of iterations are recorded during the design optimization process. The trends of their values are summarized in Figure 6-8. Based on this optimization result, the geometrical model of optimized heterogeneous lattice structure is built and shown in Figure 6-9.

Table 6-6 Values of parameters used in BESO based optimization algorithm

RT	Ri	c_s	i_{max}	F	L
0.2	0.01	0.001	50	75 N	320 mm

A comparison of structural performance between the optimized heterogeneous lattice structures and the original homogeneous lattice structures is made and shown in Table 6 7. It is

manifested that the optimized heterogeneous lattice structure significantly improves the structural stiffness under the given loading condition. It minimizes both maximum Von-Mises stress and maximum displacement. This result validates the efficiency of the proposed BESO based lattice optimization method.

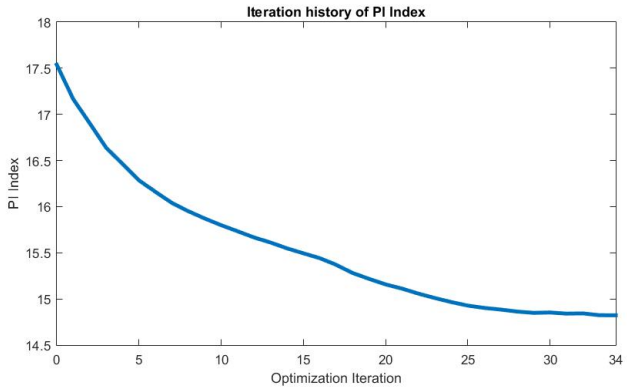

(a) Iteration history of PI Index

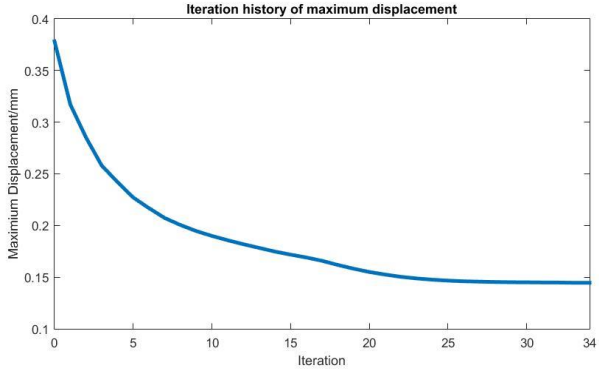

(b) Iteration history of maximum displacement

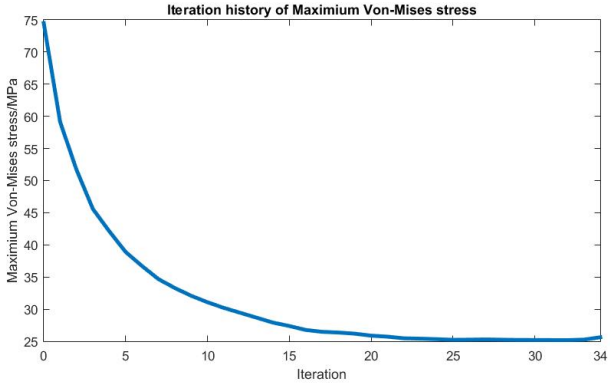

(c) Iteration history of maximum displacement

Figure 6-8 Optimization history of BESO based optimization method for lattice structures

Table 6-7 Performance of lattice structures designed by different optimization methods

Optimization method	Structural compliance/ mJ	Maximum displacement/ mm	Maximum Von-Mises stress/ MPa	Total Volume/mm^3
Original homogeneous lattice structure	13.722	0.378	74.51	58748
Heterogeneous lattice structure (BESO based method)	5.207	0.145	25.83	58748
Heterogeneous lattice structure (Heuristic optimization)	8.432	0.237	53.39	58748
Heterogeneous lattice structure (Heuristic optimization without considering principal stress direction)	9.377	0.260	66.862	58748

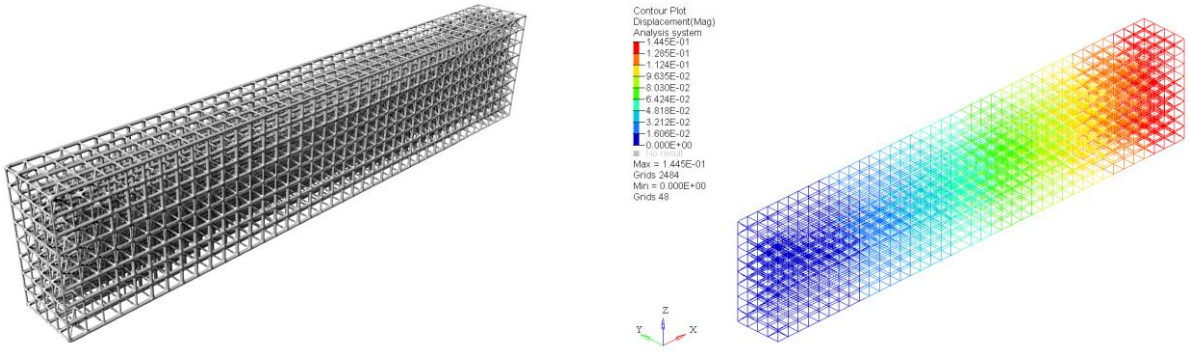

(a) Optimized heterogeneous lattice structure

(b) Displacement distribution of optimized lattice structure

Figure 6-9 Optimized heterogeneous lattice structure of BESO based lattice optimization method

To further investigate the effects of the two parameters Ri and RT on the convergent speed of the proposed BESO based method, a set of numerical experiments has been done. At first, the RT value is fixed. Different Ri value is used in the proposed BESO based method for the same design case. The number of iterations is recorded in Table 6-8. This result shows that the larger Ri value is, the faster convergent speed it is achieved. However, when this value is too big, it will cause the oscillation at the end of optimization process. The number of iterations will reach the maximum value defined in Table 6-6. An example is given and shown in Figure 6-10. In this case, Ri is set as 0.08. The large value of this parameter cause the oscillation which prevent the algorithm

converging. Thus, the Ri value cannot be too big.

Besides Ri, the value of RT is also changed from 0.1 to 0.4. Its effect on the rate of convergence is shown in Table 6-9. Like Ri, the increase of RT will also decrease the number of iterations. However, the rate of convergence of the proposed method is less sensitive to this parameter comparing to Ri.

Table 6-8 The number of iterations needed for different Ri values (RT=0.2)

Ri = 0.01	Ri = 0.02	Ri = 0.04
34	22	10

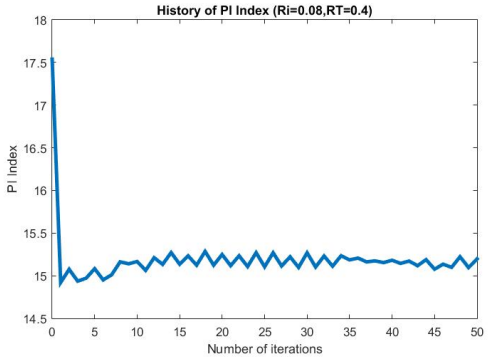

Figure 6-10 Iteration history of PI index Ri = 0.08, RT=0.2

Table 6-9 The number of iterations needed for different RT values (Ri = 0.01)

RT= 0.1	RT = 0.2	Ri = 0.4
36	34	30

A parallel comparison of using the developed heuristic optimization method for mesoscale lattice structures is also conducted on the same initial design space. The optimized result and its displacement distribution are shown Figure 6-11. The structural performance of the optimized lattice structure resulted from heuristic optimization is also summarized in Table 6-7. Compared to the homogeneous lattice structures without optimization, it is shown that the optimized heterogenous lattice structure has a better structural performance with respect to lower maximum displacement and Von-Mises stress. Moreover, by comparing the developed method with other similar methods which do not consider the effect of principle stress, it is concluded that the

proposed method can further improve the structural stiffness without increasing its weight.

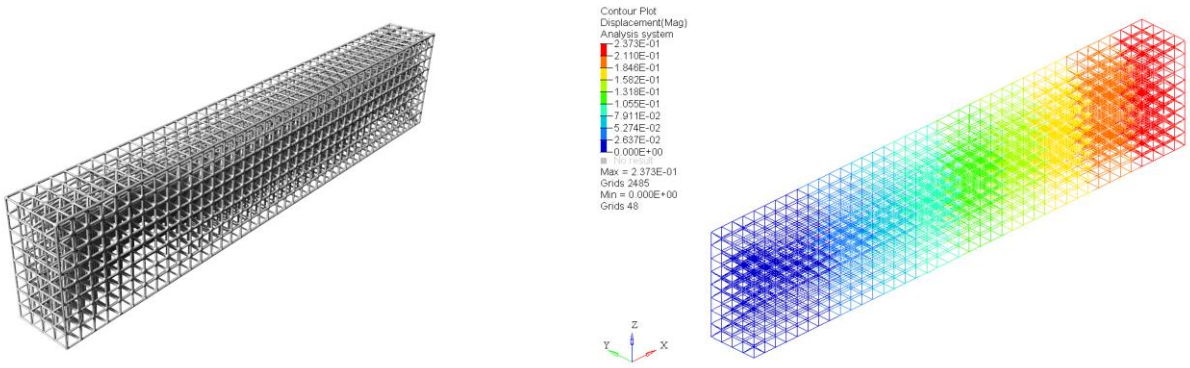

(a) Optimized heterogeneous lattice structures

(b) Displacement distribution

Figure 6-11 Optimized heterogeneous lattice structure of the developed heuristic optimization method

The optimization results summarized in Table 6-7 shows that both proposed methods can improve the stiffness and strength of designed lattice structures. Moreover, BESO based method can achieve a better structural performance than the heuristic optimization method. Comparing to heuristic optimization method, BESO method provides more degrees of freedom to accurately control the thickness of each strut. Thus, it can achieve better structural performance. However, it should also be noticed that the better performance of lattice structure is at the cost of longer optimization time for BESO based optimization method. In this case study, both methods have been implemented on the same computer with Intel Core I7-4710MQ CPU and 12 GB memory. The commercial FEA solver called OptiStruct [59] is used for both methods. The computational time is recorded and shown in Table 6-10. In this table, the time consumption of BESO based method is calculated based on the optimized Ri and RT which only takes 10 iterations for convergence. It is concluded that the BESO based method generally takes longer time than the developed heuristic method. There are two major reasons. Firstly, heuristic optimization can directly use the topology optimization result for struts' thickness calculation. If this optimization process has already done at the initial design stage, it can save the computational time. Secondly,

the number of elements considered in the topology optimization process is much smaller than the number of elements used in the BESO based optimization method. Generally, the solid element used in topology optimization is bigger than the size of cell. Thus, each element may contain several cells, each cell contains several struts. Thus, to solve topology optimization problem is computationally cheaper than to solve the BESO based optimization method. The computational time will significantly increase for a lattice structure that contains numerous cells and struts. Thus, designers are suggested to select heuristic optimization method when lattice structures contain a large number of struts. However, if designers care more about the performance of designed lattice structures, the BESO based method is a better choice.

Table 6-10 Comparison of time consumptions between two different methods

	Time for topology optimization	Time for algorithm	Total time
BESO based method	-	50 s	50s
Heuristic optimization method	20s	19.2s	39.2s

To validate the third proposed optimization method on the lattice structures for multifunctional purposes, the design case discussed in Section 6.1 is used. Its FV with uniform 2-dimensional lattice is designed for multifunctional purposes. The working condition of the design case is shown in Figure 6-12. Its related parameters are summarized in Table 6-11. Two functions of this design case are required and summarized below:

a) to design a structure which can withstand the given structural load;

b) to design a structure which can conduct heat from the heating surface to the other side of the gas.

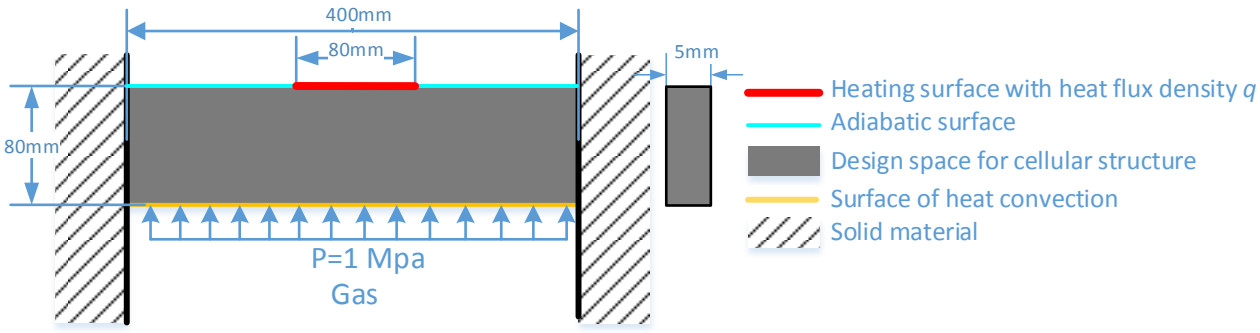

Figure 6-12 Working condition of multifunctional lattice

Table 6-11 Related parameters for the multifunctional design case

T_{gas}	T_{solid}	T_{ref}	q	k	h	E	Nu	ρ
$35°C$	$35°C$	$30°C$	$50W/mm^2$	$73W/°C$	$40W/°C$	210GPa	0.3	$7.9kg/m^3$

To quantitatively measure these two functions described above, two functional performance parameters: structural mean compliance and heat flow rate of the bottom surface of the FV are considered in this design case. Since the functions and their related performance parameters are the same to the design case discussed in Section6.2, the F-F-P-D model shown in Figure 6-1 can also be used for this design case. Based on its F-F-P-D model, the compromise DSP formulation for this design case is formulated and summarized in Formulation 6-2.

Formulation 6-2 Compromise DSP formulation for the given design case

Given

A_{cmax}	The upper bound of structural mean compliance.
G_t	The target of the heat flow rate on the bottom of designed structure
m_{max}	The maximum weight of structure
$A_c = \frac{1}{2}P^T U$	Achievement function to calculate the structural mean compliance
$A_t = H(k)T$	Achievement function to calculate the heat flow rate
$m_s = \rho \sum_1^q x_i v_i$	The weight function to calculate the weight of designed structure

$E^e = E^e(x)$ The homogenized elastic properties with respect to relative density of cellular structure

$k^e = k^e(x)$ The homogenized heat transfer coefficient with respect to relative density

Find

$X = (x_1, x_2, \dots, x_q)$ A design parameter vector contains the relative density of cellular structure in each sub-region

d_1^+, d_2^- Deviation variables for two achievement function

Satisfy

Constraints

$$K(E^e)U = P = P^0 + P^{th} \quad (6.47)$$

$$(K_t(k^e) + H_t)T = q_t + q_h \quad (6.48)$$

$$P_i^{th} = \alpha(x_i) \int_\Omega {B_i}^T D_i(E(x_i))(T - T_{ref})\phi^T d\Omega \quad (6.49)$$

$$m_s < m_{max} \quad (6.50)$$

Goals

$$A_c/A_{cmax} - d_1^+ = 0 \quad (6.51)$$

$$A_t/G_t + d_2^- = 1 \quad (6.52)$$

Bounds

$$x_{l,L} < x_l < x_{l,U} \quad (6.53)$$

Minimize

$$Z = W_1 d_1^+ + W_2 d_2^-, W_1 + W_2 = 1 \quad (6.54)$$

Due to the symmetry of both loading condition and geometric shape, only half of FV is considered in the proposed optimization formula. The half of FV has been discretized into 20×8 sub-regions whose size is $10\times10\times10$ mm. The relative densities of the lattice structure in those

sub-regions are considered as the design parameters in the proposed optimization formulation. Each design parameter is bounded by two values. The upper bound $x_{l,U}$ equals to 1 for all sub-regions. The value of lower bound $x_{l,L}$ is determined by the minimal thickness of fabricatable wall or struts. Suppose the minimal fabricatable wall thickness is t_{min}, the lower bound of relative density is calculated by the following equations:

$$x_{l,L} = \rho_r(t_{min}), \text{ if } x_l \in X_{boundary} \tag{6.55}$$

$$x_{l,L} = \rho_r(t_{min}/2), \text{ if } x_l \in X_{internal} \tag{6.56}$$

Where ρ_r is the function to calculate the relative density of each cell. Its formulation depends on the cell topologies. $X_{boundary}$ is a set of sub-regions which are located on the boundary of the design space. $X_{internal}$ is a set of sub-regions which are located on the internal of the FV. It is clear from Figure 6-13 that wall located on the internal of design space is composed of two cell walls. Thus, the minimal thickness of each cell wall should be only half of the fabricatable wall thickness. Particularly for this design case, the cell size l and the minimal fabricatable wall thickness t_{min} are summarized in Table 6-12.

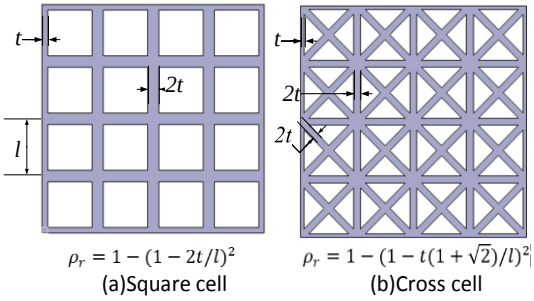

Figure 6-13 Relationship between relative density and wall thickness of 2-dimensional lattice structures

Besides the bounds for design parameters, target parameters including A_{cmax} and G_t also need to be predefined before the optimization process. For this design case, the value of A_{cmax} is estimated based on the mean compliance of initial homogeneous lattice structures. To guarantee

the d_1^+ is non-negative during the optimization process, A_{cmax} is suggested to be five to ten times larger than initial compliance. As to the maximum heat flow rate, it should be smaller or equal to the total input energy of the whole system. Based on these criteria, A_{cmax} and G_t are determined and their value are summarized in Table 6-12

Table 6-12 Parameters of optimization formulation

A_{cmax}	G_t	l(cell size)	t_{min}	m_{solid}
8000mJ	100kW	5mm	0.15mm	1.264kg

Besides those parameters listed in Table 6-12, other parameters of compromise DSP formulation including maximum mass, lattice structure topology and weight coefficient for each deviation coefficient should be predefined in the initial design stage. However, in this chapter, to investigate their impact on the final performance of designed lattice structure, the values of these parameters are varied during the design optimization process.

To validate the efficiency and accuracy of the proposed generalized relative density based method, the "cross" cell has been selected as the benchmark in this thesis. By solving the optimization formulation listed in Formulation 6-2, the optimal relative density distribution of the lattice structure is obtained with respect to given mass constraint $m_{max} = 0.3m_{solid}$ and weight coefficient $W_1 = W_2 = 0.5$. Its result is shown in Figure 6-14(a).

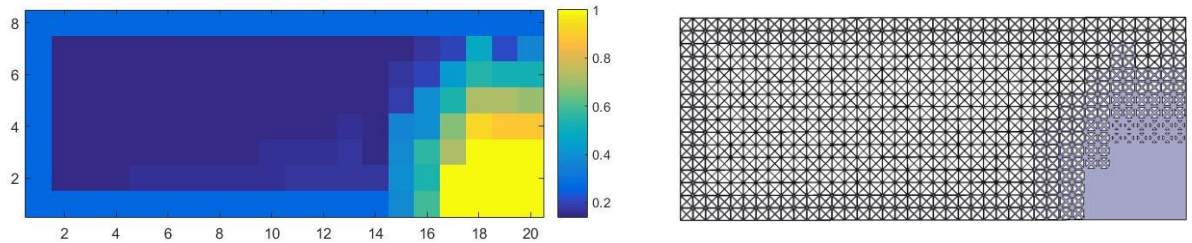

(a)Relative density distribution

(b)Optimized heterogeneous cellular structure

Figure 6-14 Optimization result of cellular structure with "cross" topology ($m_{max} = 0.3m_{solid}, W_1 = W_2 = 0.5$)

Based on this result, the heterogeneous lattice structures are built which is shown in Figure 6-14(b). FEA simulation has been done to evaluate the performance of optimized structure. To validate the accuracy of proposed simulation infrastructure on the heterogeneous lattice structures, the FEA model with fine volumetric mesh whose size is smaller than the thickness of cell wall has been used in this thesis. Its result is given in Figure 6-15.

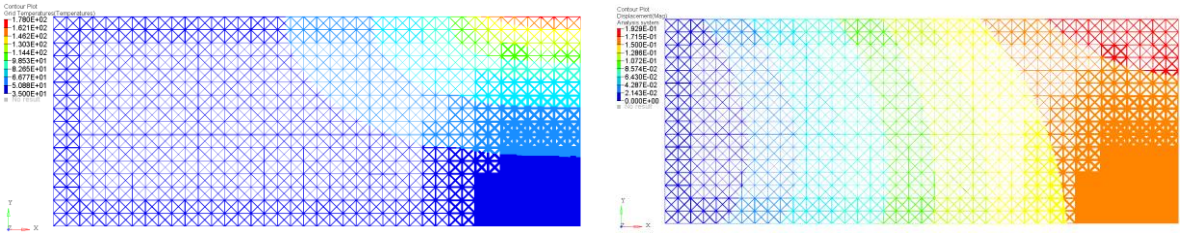

(a) Temperature distribution: T_{max} = 178℃ (b) Displacement distribution U_{max} = 0.193mm

Figure 6-15 Simulation result of heterogeneous lattice with fine volumetric mesh

Meanwhile, the proposed simulation infrastructure has also been utilized to calculate the performance of the optimized heterogeneous lattice structures. The simulation results of the proposed simulation infrastructure are shown in Figure 6-16.

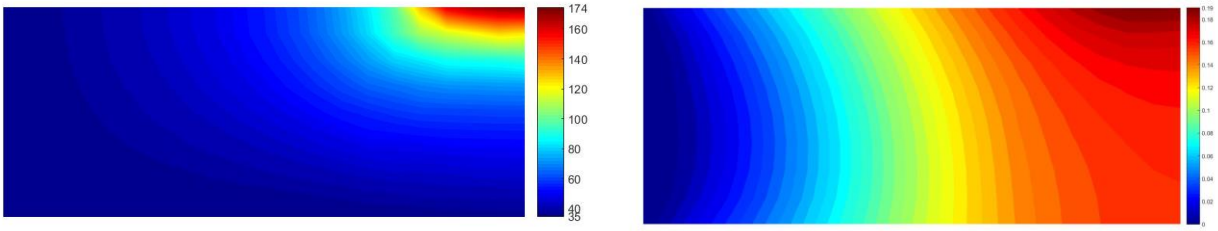

(a) Temperature distribution Tmax = 174.4℃ (b) Displacement distribution Umax = 0.191mm

Figure 6-16 Simulation result of heterogeneous lattice based on proposed simulation infrastructure

By comparing these two simulation results, it is identified that both displacement and temperature distribution obtained from the proposed simulation infrastructure is in accordance with the result obtained from FEA model with fine volumetric mesh. The deviations of maximum displacements and temperatures between two results are within 3%. The accuracy of proposed simulation infrastructure has been validated.

To verify the efficiency of the proposed optimization method, a comparison between optimized lattice structures and its original homogeneous lattice structures has been made and summarized in Table 6-13.

Table 6-13 A comparison of structural performance between homogeneous and optimized heterogeneous lattice structure (m_{max}=0.3m_{solid},W_1 =W_2=0.5)

	Homogeneous lattice structure	Heterogeneous lattice structure
Cross cell	$A_c = 1151.3\ mJ, A_t = 94.1$Kw	$A_c = 469.0\ mJ, A_t = 98.1$Kw
Square cell	$A_c = 1615.7 mJ, A_t = 94.4$Kw	$A_c = 900.68 mJ, A_t = 98.5$Kw

The result in Table 6-13 shows that the proposed optimized method can improve both structural performance and thermal performance according to design requirements. Meanwhile, the "square" cell has also been used for this design case, since it shows better effective heat conductivity than "cross" on macroscale from Figure 6-5. Its optimized relative density distribution and performance are summarized in Figure 6-17 and Table 6-13 respectively. It is obvious that both cell topologies have a similar trend of relative density distribution which the material tends to concentrate on the bottom right corner where the temperature is relative low. Generally, this redistribution of material can reduce the generated thermal stress. When it comes to the performance, it is shown that both homogeneous and heterogeneous cellular structures with cross exhibits a better structural performance than the counterparts with "square" topology. The main reason is "cross" cell generally shows a better mechanical performance under shear stress compared to "square" cell, which has been shown in Figure 6-5. However, as to the thermal performance, "square" cell shows a slightly better performance than the "cross" cell. Thus, designers need to decide on which cell to choose based on other specifications of design case.

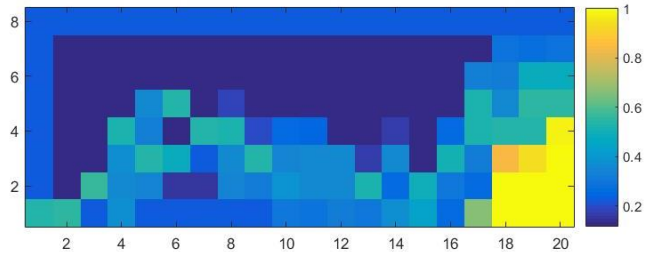

(a) relative density distribution

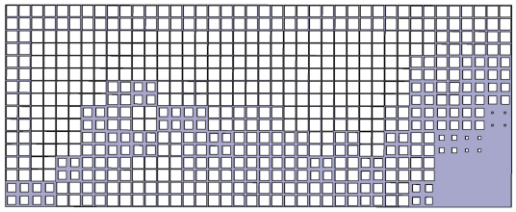

(b) optimized heterogeneous cellular structure

Figure 6-17 Optimization result of cellular structures with "square" topology ($m_{max} = 0.3m_{solid}, W_1 = W_2 = 0.5$)

To further investigate the effects of weight coefficient on the performance of optimized cellular structures. A group of numerical experiments have been done and their results have been summarized in Table 6-14. By tuning the weight coefficient, designers can control the optimal performance for different functions. With the increase of W_1, the optimal structural compliance decreases a lot. However, this also causes the drop of optimal heat flow rate.

Table 6-14 optimal performance of heterogeneous cellular structures under different weight coefficients (m_{max}=0.3m_{solid},cross cell)

$W_1 = 1$ $W_2 = 0$	$W_1 = 0.75$ $W_2 = 0.25$	$W_1 = 0.5$ $W_2 = 0.5$	$W_1 = 0.25$ $W_2 = 0.75$	$W_1 = 0$ $W_2 = 1$
$A_c = 406.4mJ$ $A_t = 97.8$Kw	$A_c = 414.1mJ$ $A_t = 98.0$Kw	$A_c = 469.0mJ$ $A_t = 98.1$Kw	$A_c = 475.0mJ$ $A_t = 98.8$Kw	$A_c = 886.1$mJ $A_t = 99.1$Kw

In addition to weight coefficients, the effect of mass constraint on the optimal performance of heteronomous lattice structures has also been investigated by varying its value from $0.3m_{solid}$ to $0.7m_{solid}$ with $0.2m_{solid}$ interval. The results are summarized in Table 6-15. This table shows both two functional performances have been enhanced with respect to increase the mass constraints. However, the increasing of materials will mainly affect the structural performance. As to thermal performance, the increment is significant when the mass constraint changes from $0.3m_{solid}$ to $0.5m_{solid}$. However, when this value reaches to $0.7m_{solid}$, there is no increasing on the thermal

performance. It can also be concluded that the optimal structural compliance is less sensitive when the mass constraint is larger than $0.5m_{solid}$.

Table 6-15 effects of mass constraint on the performance of optimized cellular structure with cross topologies (W_1 =W_2=0.5)

$m_{max} = 0.3m_{solid}$	$m_{max} = 0.5m_{solid}$	$m_{max} = 0.7m_{solid}$
$A_c = 469.0$mJ $A_t = 98.1$Kw	$A_c = 280.2$mJ $A_t = 99.5$Kw	$A_c = 235.3$mJ $A_t = 99.5$Kw

Based on the result of this design case, it is concluded that the proposed simulation infrastructure can capture the response of designed heterogeneous structure. Based on this simulation infrastructure, the proposed design and optimization method for lattice structures can consider different types of functional performance simultaneously. The optimized heterogeneous lattice structures can achieve better performances for both functions: heat transfer and load bearing. Moreover, the optimal performance for each function can be tuned by changing several different types of parameters used in the proposed method including cell type, weight coefficient for different achievement parameters and mass constraints.

Based on the design cases introduced above, a comparison between different optimization methods developed in this thesis is made and summarized in Table 6-16. Based on this comparison, several guidelines are summarized to help designers select a suitable optimization method for different cases.

Guideline 6-1: Design guidelines for the selection of optimization method

a) If the designed lattice structure only plays a structural role and contains a small number of cells and struts, it is suggested to use BESO based optimization method.

b) If the designed lattice structure only plays a structural role and contains a large number of cells and struts, the heuristic optimization method can be used, which could save computational time.

c) If the structural stiffness is critical during the design process, BESO based optimization method is suggested to use, since it can achieve better stiffness

d) In the design case where lattice structures play multifunctional purposes, generalized relative density based method is suggested to use.

Table 6-16 A comparison between three different optimization methods for lattice structures discussed in this thesis

	Advantage	Disadvantage
BESO based optimization method	1 It can achieve the best structural stiffness comparing to other two methods; 2 It is easy to be implemented based on commercial FEA solver, since it does not request calculation of gradient;	1 The algorithm is slow when there are a large number of cells and struts inside FV. 2 The length-diameter ratio should be smaller than 5 for every lattice strut, since beam elements are used for simulation. 3 It can only be used for structural performance
Heuristic optimization method	1 It can efficiently calculate the thickness of lattice struts based on topology optimization result; 2 It can be used for different types of lattice structures; 3 It does not have the limitation on strut's length-diameter ratio like BESO based optimization method;	1 The optimal stiffness obtained by this method is smaller than that calculated by BESO based method;
Generalized relative density based method	1 It can deal with multiple functions and their coupled relations 2 It does not have the limitations on the strut's length-diameter ratio;	1 If this method is used only for structural performance, its optimal structural stiffness is smaller than that calculated by BESO based method; 2 It is only available for uniform lattice structures

6.6 Summary

In this chapter, the developed optimization methods which can be used in the design optimization stage are introduced. At the beginning, the process of construction F-P-P-D model is illustrated by a multifunctional design case. Then, three different design optimization methods for heterogeneous lattice structures are introduced respectively. Among them, BESO based optimization method and heuristic optimization are mainly developed for the structural performance of the designed lattice structures. Different optimization schemes are used in these

two different methods. However, their goal is the same that is to increase the structural stiffness by redistributing materials inside the FV of lattice structures. Besides those two design optimization methods for structural performance, another general optimization method is proposed for multifunctional lattice structures. In this method, the FV of lattice structures are further divided into sub-regions. In each region, the relative densities of lattice cells are assumed to be equal. Based on the proposed simulation infrastructure and existing Compromise DSP template, this optimization method can consider functional performance parameters defined for different functions simultaneously. To further illustrate three proposed methods and validate their efficiency. Two design cases are given at the end of this chapter. The results of these design cases validate the effective and efficiency of the proposed design optimization methods for lattice structures. The comparison between these three methods is made at the end of this chapter. Based on this comparison, several guidelines are summarized to help designers select an appropriate design optimization method for different design cases.

Chapter 7 Implementation

Based on the proposed design methodology for mesoscale lattice structures discussed in the previous chapters, a computer-aided design tool called Intralattice has been developed in this research. This tool is developed as a plug-in to a commercial CAD software Rhino® [244] with utilization of the commercial FEA solver called OptiStruct®[59]. Its main purpose is to provide supports for designers to generate the optimized mesoscale lattice structures. This chapter first introduces the development environment of Intralattice. And then, the detailed framework and the operation flow of this developed software are discussed.

At the end of chapter, a design case has been carried out to further illustrate the general design flow enabled by Intralattice. The result of this case study also proves the effectiveness of developed software. Finally, a summary is made and several future developing works are pointed out.

7.1 Software development environments and tools

Intralattice is developed as a plug-in to the commercial CAD software Rhino in the Microsoft® Visual Studio Integrated Development Environment (IDE) with C# language. Classes and methods from Microsoft® .NET framework [245] is used for the development of User Interface (UI) and data access. To access and manipulate the geometric modeling kernel of CAD software, RhinoCommon [244] which is the cross-platform .NET Software Development Kit (SDK) for Rhino is used. Moreover, to efficiently deal with matrix computation in the developed design tool, functions from ALGLIB library [246] are used to handle mathematical and matrix calculations. The detailed introduction of those tools and libraries used for Intralattice is not going to be covered in this thesis. For more information about those tools and libraries, readers can further refer to these cited references[244-247].

7.2 Prototype of Intralattice

Based on the development environment and tools discussed above, the prototype of Intralattice is developed. In this section, the overall framework of Intralattice is firstly introduced, which is followed by the detailed discussion on functions and moduli of each layer in the framework. Then, the main operation flow of Intralattice is presented in Section 7.2.2.

7.2.1 Framework

The framework of the developed Intralattice software is presented in Figure 7-1. This framework is developed based on a classic three-tier architecture. The entire software is divided into three layers. They are layer of user interface, logic layer, and data access layer. These three layers are developed based on the CAD interface with Rhino. Specifically, some objects defined in RhinoCommon SDK are used in these three layers when they need to exchange data with CAD software.

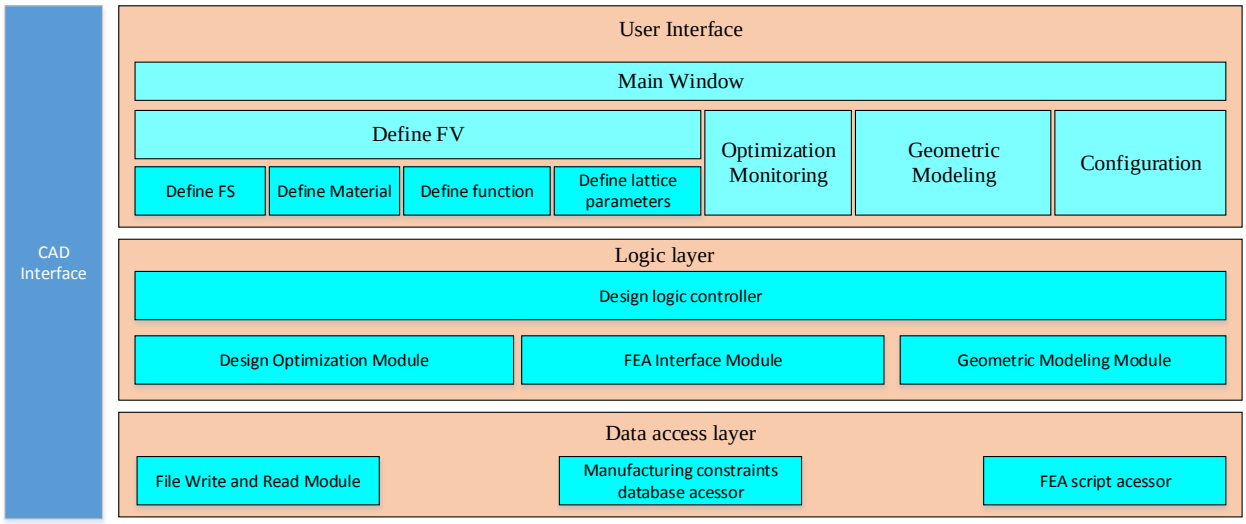

Figure 7-1 The overall framework of developed design tool

Among these three layers, UI layer is a bridge between designers and Intralattice. In this layer, a set of hieratical Windows Form components are developed to receive users' input and display the design progress and its related parameters. In these components, the main window (shown in

Figure 7-2) is developed to guide designers to follow the proposed design flow in this thesis. It contains three group boxes which represent three design stages of the proposed design methodology respectively. In the initial design stage, designers need to determine the FVs and its related FSs of the designed products. Based on the defined FVs and FSs, the initial design space of lattice structures is constructed. This process is done by the component called "Define FV" and its related sub-components. Based on the constructed initial design space, the next step is to do design optimization. In this stage, the "Optimization monitoring" component can view the trend of optimization iterations. Moreover, configuration component is used to set the file path for the FEA script which is used to evaluate the performance of designed lattice structures. At the end of the entire design process, the geometric model of optimized lattice structures is generated. In the geometric modeling component, the parameters which are related to geometric modeling process such as voxel size and mesh size are defined by the designers. Detailed images of these Windows Form components are summarized in the Appendix C of this thesis.

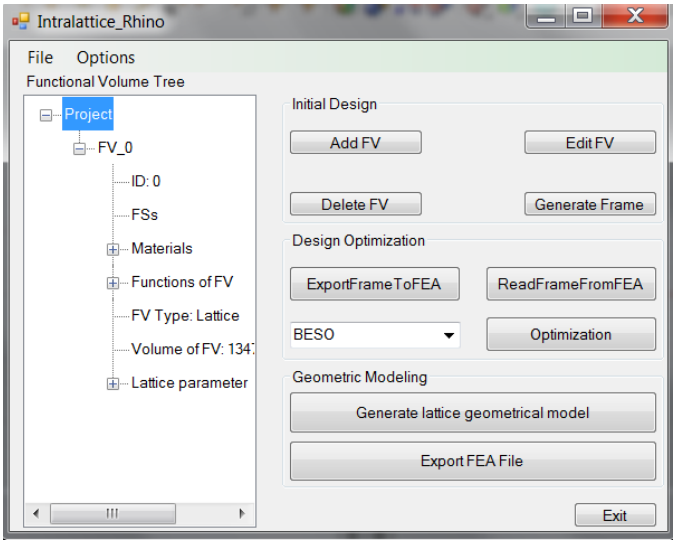

Figure 7-2 Image of main window of Intralattice

The second layer of the developed design tool is the logic layer. In this layer, there are four moduli: design logic controller, design optimization module, FEA interface module, geometric

modeling module. Among these four moduli, the design logic controller is the module to control the design process and information flow both interlayer and intralayer. Under the logic controller, the design optimization module is developed to implement three different design optimization algorithms which are used to improve the functional performance of designed lattice structures. Among them, BESO based optimization algorithm and heuristic optimization algorithm are directly developed based on .NET® platform inside the Intralattice. As to the generalized relative density optimization algorithm, the optimization and simulation codes are implemented in a scientific computational platform called MATLAB® [248] which provides a flexible environment for customized simulation codes. In the design optimization module, an interface is developed for this design optimization algorithm which directly reads the result from MATLAB platform, and interprets them into the data for geometric modeling process.

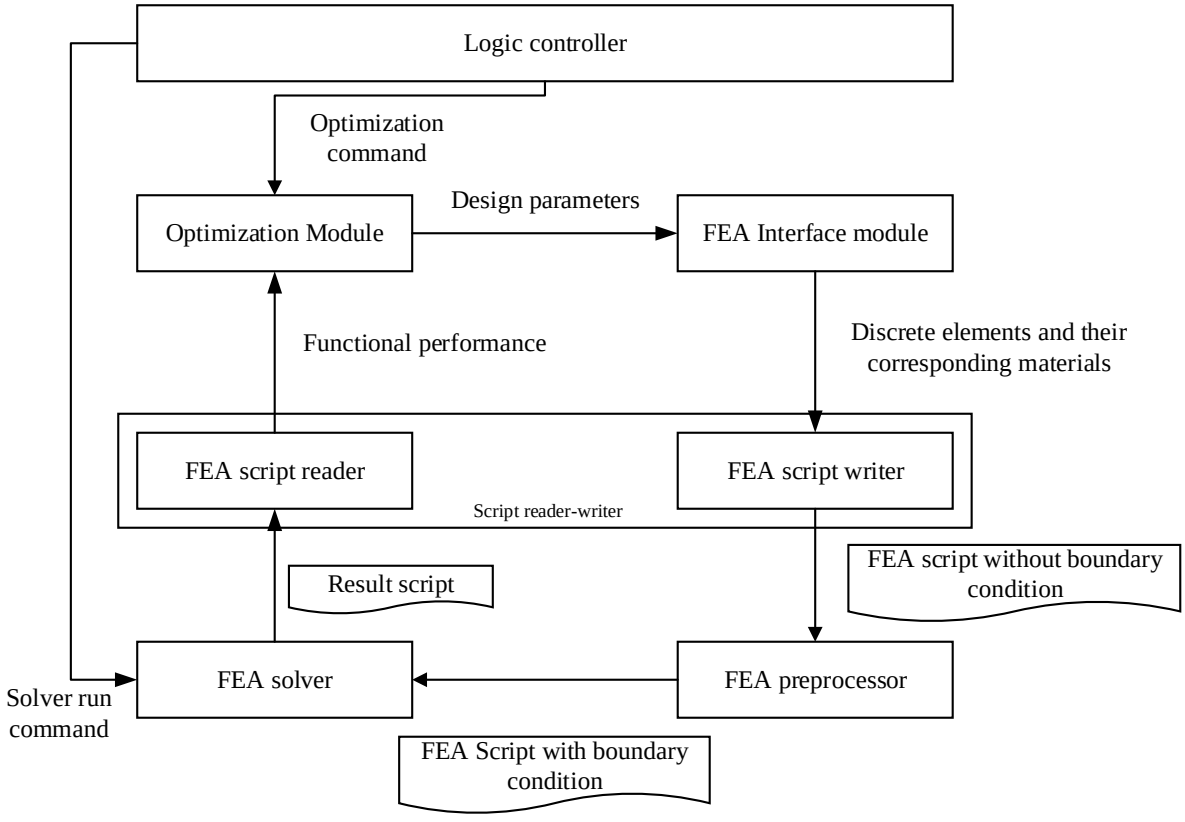

Figure 7-3 Connection mechanism between Intralattice and FEA solver

During the design optimization process of BESO based algorithm, the structural performance need to be evaluated. Thus, FEA interface module is developed in the logic layer to link the design optimization module to the existing FEA solvers. The detailed connection mechanism between Intralattice and a FEA solver is described in Figure 7-3. Particularly, FEA interface module is used to prepare the elements data and materials data for FEA solver. As to the boundary condition and other necessary information for the FEA simulation model, they need to be interactively defined by designers with the existing preprocessor of FEA solvers. For the current version of Intralattice, it accepts the files from Hypermesh® which is the preprocessor of FEA solver OptiStruct®. In most cases, these types of information are not going to be changed during the design optimization process. Thus, they only need to be defined at the beginning of the optimization process.

After the generation of FEA script, logic controller sends a command to the FEA solver. FEA solver reads the generated FEA script and run the simulation. Its simulation result is read by FEA script reader. The script reader does the post-processing work for FEA solver and output the feedback to optimization module. This connection mechanism enables the decoupling between FEA interface module and specific FEA solver. FEA interface module is developed for different FEA solvers for different types of simulations. The only work needs to be done for adding a new FEA solver is to add codes in FEA script reader and writer module in the data access layer to recognize different FEA script format.

The last module in the logic layer is the geometric modeling module. In this module, the proposed geometric modeling algorithm is implemented. It efficiently generates the geometric model for the optimized lattice structures.

The last layer of Intralattice software is the data access layer. The function of this layer is mainly for data reading and writing. According to the specific functions of each components, this

layer is divided into three moduli. Among them, the first one is a general file read/write module. This module inherits the standard Input/Output (IO) functions from .NET framework. It is mainly developed for the text file read and write. The second module is the accessor for manufacturing constraints database. This module takes lattice frame as the input, based on the lattice frame and selected fabrication process, the manufacturing constraints are returned as the feedback. These constraints are used during the lattice design optimization process to guarantee the designed lattice is fabricatable. The third module is FEA script read-write module. The function of this module has already been discussed in Figure 7-3. Thus, it will not be detailed discussed here.

7.2.2 Operation flow of Intralattice

The general operation flow of the developed Intralattice design tool is summarized in Figure 7-4. Like the proposed design methodology, the operation of Intralattice is divided into three stages: initial design, design optimization and geometric modeling.

Among these three stages, the operations in the initial design stage mainly focus on the data input of the generated initial design space of FVs. Designers can construct geometric models of FSs and FVs for each functional entity based on the CAD platform. Then, these types of information are interactively input into the developed design tool in the developed UI. Based on the summarized design guidelines in Chapter 5, designers can decide whether to further divide the constructed FVs. The developed design tool enables designers to do modification on the existing FVs and FSs by clicking “Edit FV” button on the main window of software shown in Figure 7-2. After the division of FVs, parameters which are not selected as design variables in the optimization process should be determined. These parameters are attached to those FVs for lattice structures in the FV editing window. Based on these parameters, the lattice frame is generated by Intralattice. This information feeds to the manufacturing constraint model where the manufacturing limitation

of each lattice strut can be automatically obtained.

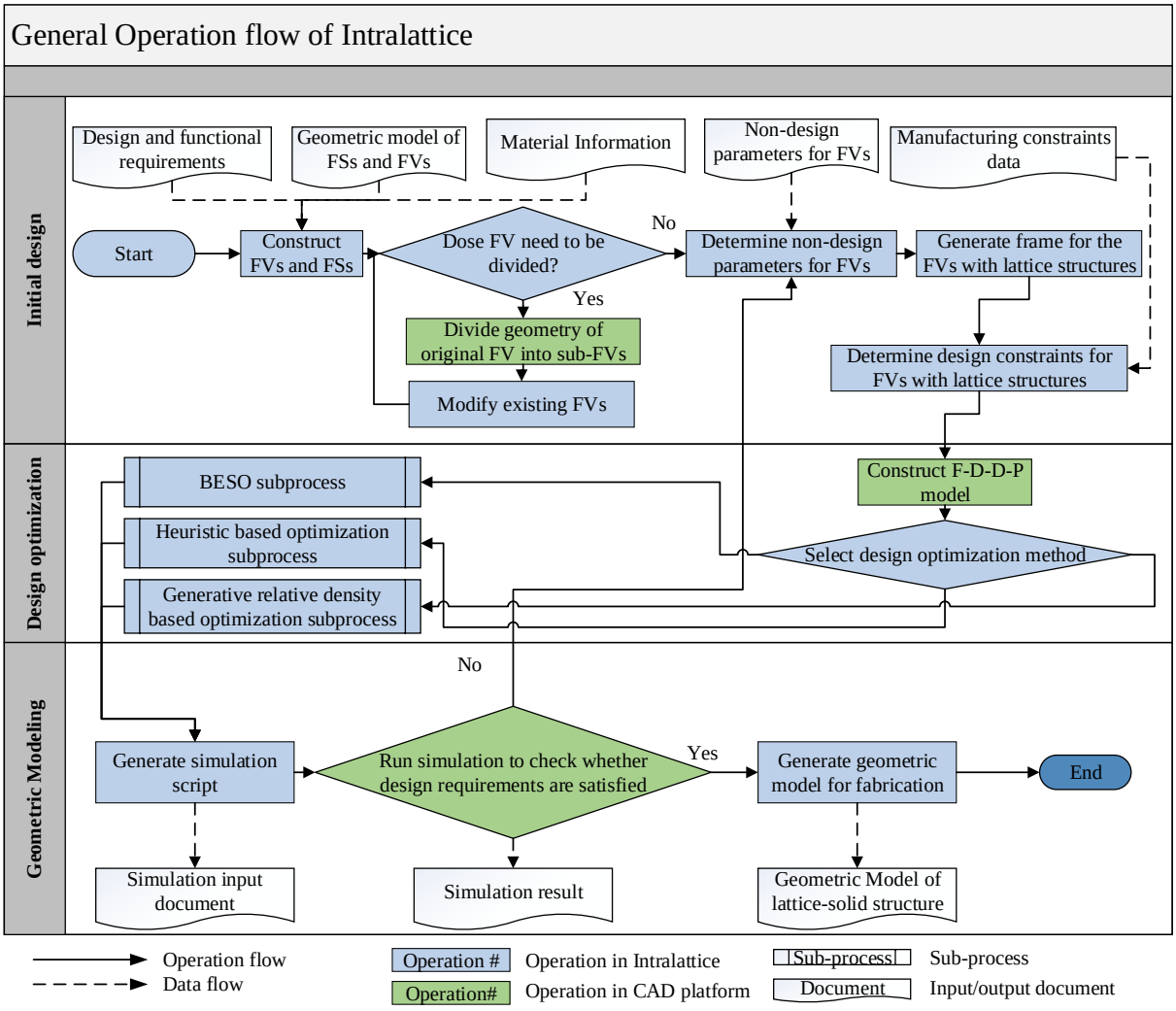

Figure 7-4 Operation flow of the developed Intralattice software

After the initial design, the F-P-P-D model of the design should be constructed. Based on the F-P-P-D model and summarized guideline in Chapter 6, a suitable design optimization method needs to be selected. Based on designers' decision, the sub-process of the selected optimization method is conducted. Three sub-processes of proposed design optimization methods are summarized in Figure 7-5.

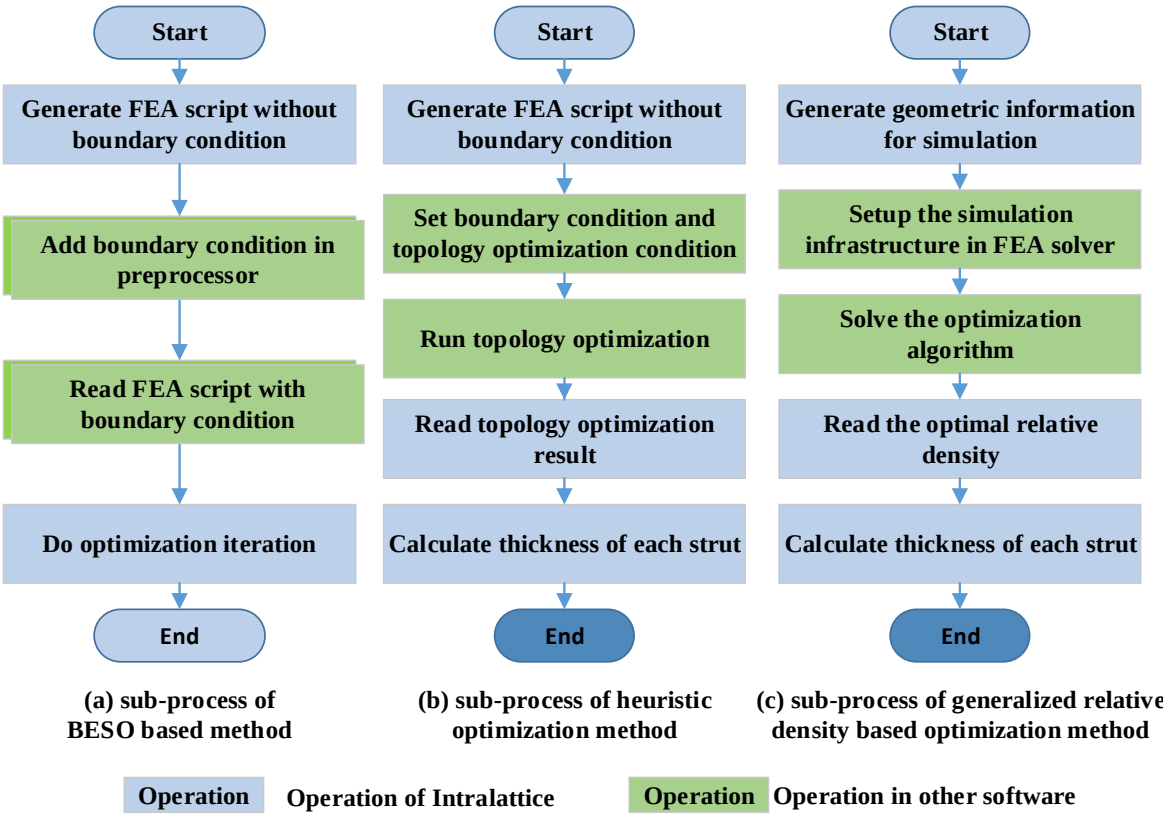

Figure 7-5 Sub-processes of different optimization methods

These three sub-processes cannot run independently without feedback of simulation result. Different algorithms requests different types of simulation results. As to BESO based optimization method, the stress distribution of each beam element is needed during the optimization process. To achieve this purpose, the connection mechanism described in Figure 7-3 is applied. Unlike BESO based optimization method, the heuristic method based optimization algorithm takes the topology optimization result as the input directly. Thus, the developed FEA script reader module can also directly read the topology optimization result from Optistruct®. Compared to the first two optimization methods, the last one is more complex since it involves the multifunctional optimization. The simulation infrastructure usually needs to be built by designers according to the specific design case. In the current version of Intralattice, a problem-specific MATLAB® code is developed to do the multifunctional analysis as well as optimization. The developed design tool

only reads the result of external optimization solver and simulation infrastructure. Based on this result, the thickness of each strut is calculated, and the geometric model is finally built.

After the design optimization, optimized parameters of FVs with lattice structures is obtained. Based on its result, the simulation model of optimized design is generated for validation purpose. If the optimized design satisfies all the design and functional requirements, designers can click "generate geometric model" button on the main window to obtain the digital model of designed lattice-solid structure for fabrication. If the optimized design cannot satisfy all the design and functional requirements, designers needs to go back to the initial design stage to modify defined FVs, and then do the design optimization again. This design process will be terminated until all the functional and design requirements are satisfied.

7.3 Case study

To validate the developed Intralattice and illustrate its major operation flow, a design case of quadcopter arm is given in this section. Its original design and loading condition are shown in Figure 7-6.

The major function of this part is to transfer the lifting force from the propeller to the main frame of quadcopter. To achieve this function, four design requirements which are summarized based on the general design and fabrication guidelines of quadcopter [249, 250] are listed below:

(1) The maximum displacement at point c should be smaller than 7 mm under given load condition;

(2) The maximum stress should be smaller than the yield stress of selected materials;

(3) The total mass of part should be smaller or equal to 33 g;

(4) The main body of the arm should be porous to minimize the drag force when the air passes through it vertically.

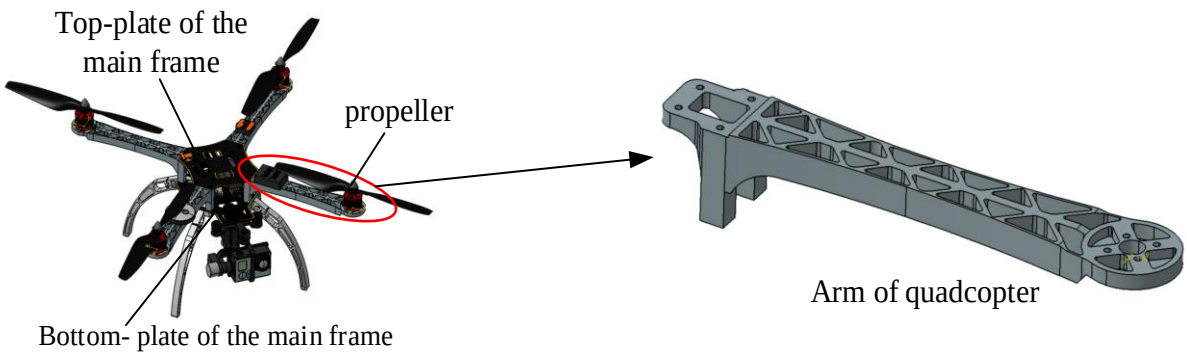

(a) Original design of the arm of a quadcopter

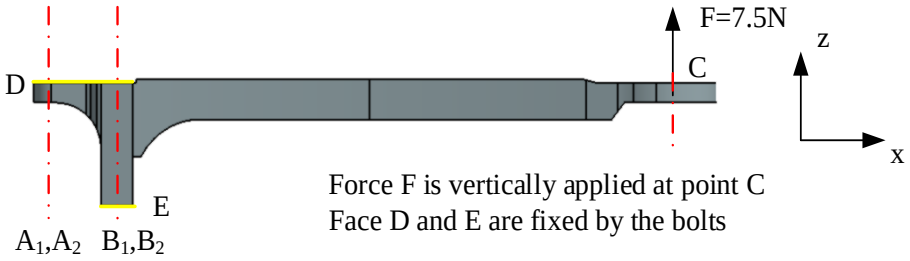

(b) Loading condition of the arm of a quadcopter

Figure 7-6 Arm of quadcopter and its loading condition

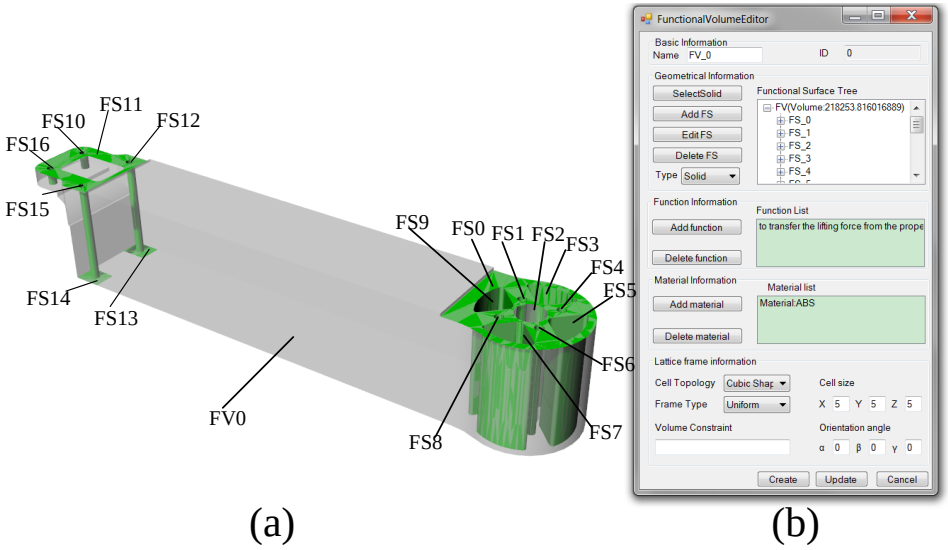

(a) (b)

Figure 7-7 FVs and FSs of the arm of a quadcopter

Based on the functional description and design requirements mentioned above, seventeen FSs have been extracted (shown in Figure 7-7) from its original design. Among these FSs, FS1, FS4, FS6 and FS8 are defined as cylindrical surfaces for the connection bolts between a motor and the

designed arm. FS2 is the surface which provides a space for the center hole to fit the bottom of a motor. FS3, FS5, FS7, FS9 are designed for the heat dissipation purpose. The air passes through these surfaces to cool the motor when it is working. FS0 plays a role as horizontal supporting surface for the motor. On the other side of the designed arm, those FSs are mainly working as connection surfaces between the arm and a main frame of quadcopter. Among them, FS12, FS15, FS16 and FS10 are cylindrical surfaces for bolt connections. FS11 is designed to support the top plate of the main body, while FS13 and FS14 are in the same horizontal plane and used to connect the bottom plate of this main body.

Based on the FSs described above, an initial FV is constructed in CAD software and indicated in Figure 7-7. This FV is used to link all the FSs defined above to assist these FSs to achieve their related functions. The constructed FSs and FV are interactively defined in Intralattice by the "FV Editor" window shown in Figure 7-7(b).

A further examination of the generated FSs and FV in last step shows that the initial FV is decomposed into three sub-FVs. According to the design requirements of this part, the main body of the arm should be porous to reduce the drag force during the flight. Thus, a lattice structure is preferred for this part. However, the geometric shape of two ends of the generated FV contains some neck regions. These regions are formed due to the constraints from their related FSs. Thus, those two portions are not suitable for lattice structures. Due to these reasons and the design guideline 5-1(c) discussed in Chapter 5, the initial FV shown in Figure 7-7 is further divided into three sub-FVs shown in Figure 7-8. In this figure, sub-FV0 and sub-FV2 are filled with solid materials, while a lattice structure is used in sub-FV1. To connect the divided sub-FVs, the connection surfaces between neighbored sub-FVs are added as the new FSs for each sub-FV. Since the volume of sub-FV1 is small compared to fabricatable size of a lattice cell, this sub-FV is not

going to be further decomposed in this design case.

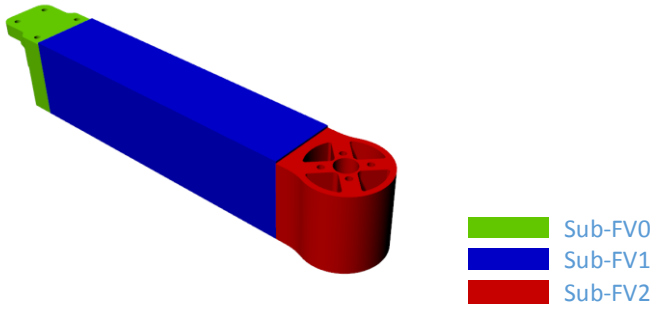

Figure 7-8 Sub-FVs after FV division

Besides the geometric information of FSs and FVs discussed above, other information, such as material parameters and the parameters of lattice structures for sub-FV1, also needs to be determined before the design optimization stage. In this design case, one of the most widely used thermoplastic material called Acrylonitrile-Butadiene-Styrene (ABS) is selected due to its lightweight and high impact resistance. The mechanical properties of printed ABS materials are obtained based on tensile testing followed by ASTM D638 standard. The result is summarized in Table 7-1. In addition to material information, lattice parameters of sub-FV1 also need to be decided. For this sub-FV, a uniform lattice structure is applied since the shape of this FV is regular. As to the topology of the lattice unit cell, a body-center cubic lattice cell is selected due to its stretching-dominant properties [5]. The cell size is selected based on the overall dimension of the FV. Specifically, for this design case, it is selected to keep the integrity of all the cells on its boundary. The size of cell is summarized in Table 7-2. As to cell orientation, it is selected as the original orientation of global coordinate system of design. Its orientation angle is represented as (0,0,0). By lining up cells in this orientation, it guarantees the cell in the location of maximum stress place shows best stiffness along the local major principal stress direction.

Table 7-1 Material properties of ABS

Elastic Modulus	Poisson Ratio	Yield Stress	Density
2070MPa	0.35	38Mpa	1 g/cm^3

Table 7-2 The dimension of the unit cell

X	Y	Z
16mm	24mm	18.5mm

In addition to lattice parameters, design constraints for different sub-FVs also need to be determined in this stage to generate initial design space. To distribute the mass constraint which is defined on the overall structure to each divided sub-FV, the topology optimization is conducted on the generated sub-FVs. During the topology optimization process, the properties of solid material listed in Table 7-1 are used for all sub-FVs. The mass constraint of the overall structure is applied. The result is shown in Figure 7-9.

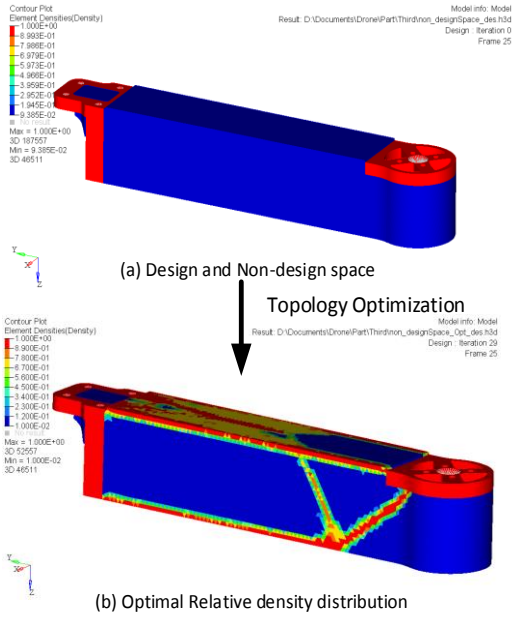

Figure 7-9 Topology optimization for the division of FV

Based on the topology optimization result, the mass distributed in each sub-FV for the optimal design are calculated. These values are considered as the mass constraints for each sub-FVs. The result is summarized in Table 7-3.

Table 7-3 The Constraints of mass for each sub-FV

	Sub-FV0	Sub-FV1	Sub-FV2	Total
Mass/mg	7951.48	19777.92	5270.60	33000

Besides the calculation of mass constraints for each sub-FV, the result of topology optimization is also used to update the shape of sub-FV0 and sub-FV2 which are filled with solid materials to make them satisfy the mass conditions listed in Table 7-3. As to sub-FV1, its shape is also changed to adapt to the variation of sub-FV2, while other parameters keep the same. Updated geometric shape of FV is shown in Figure 7-10 to 7-12.

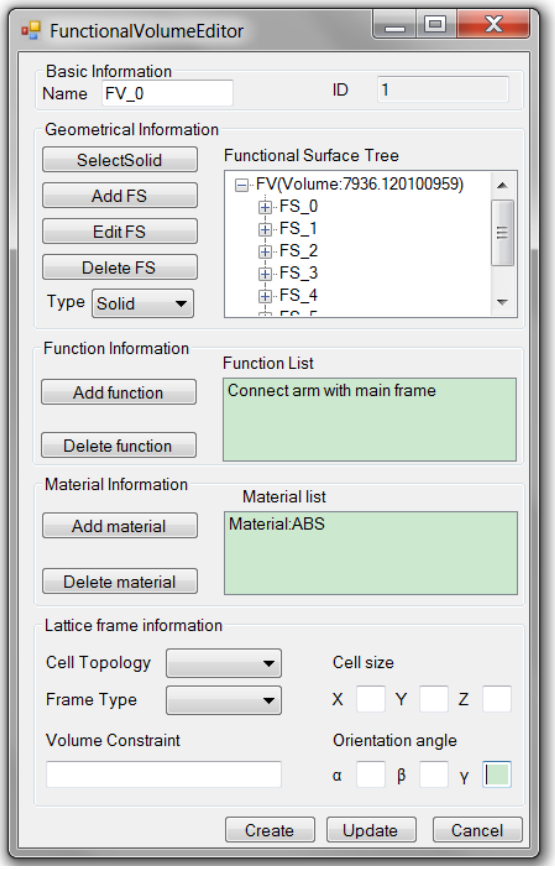

Figure 7-10 The FV editor of sub-FV0

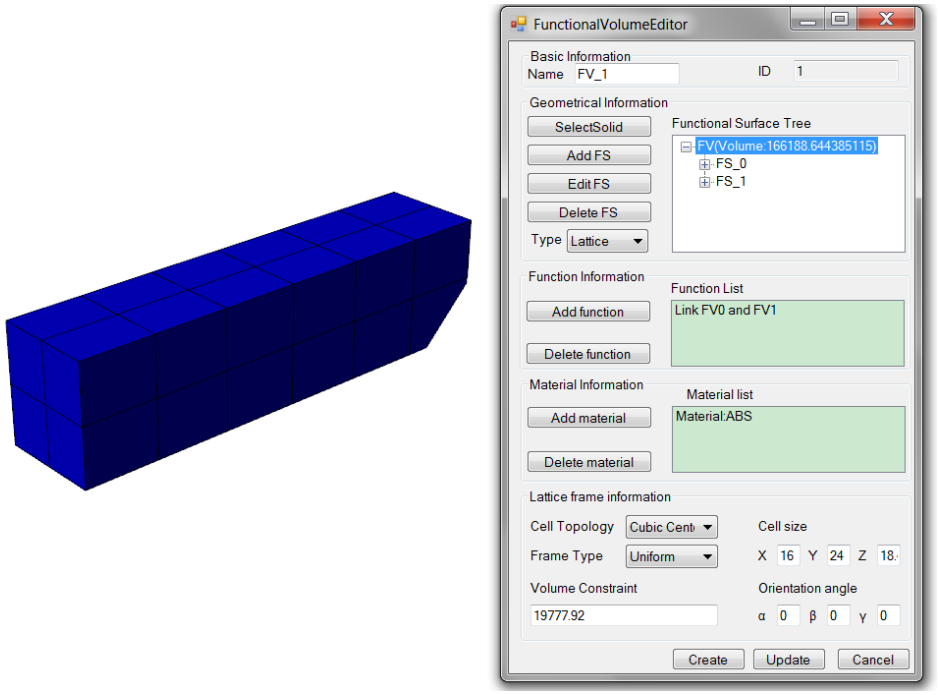

Figure 7-11 The FV editor of sub-FV 1

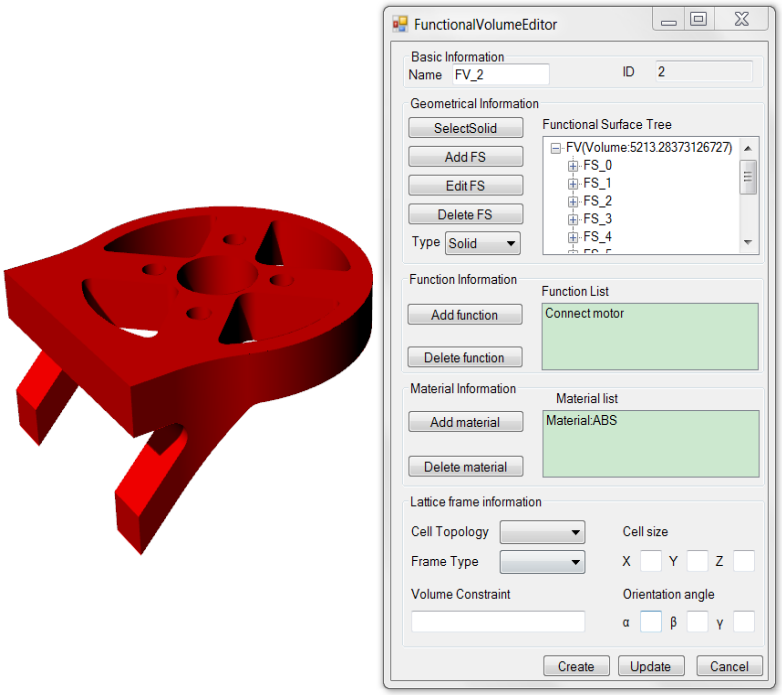

Figure 7-12 The FV editor of sub-FV 3

The result of the initial design stage is manually input into the developed software. After this step, the FV tree is constructed. The result of the constructed FV tree is shown in Figure 7-13.

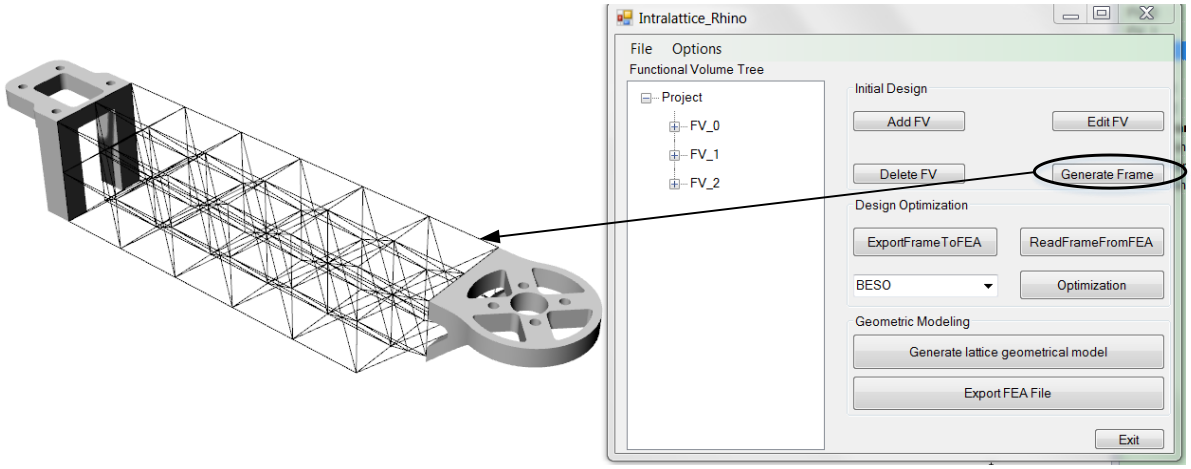

Figure 7-13 The result of initial design

Based on those parameters of lattice structures discussed above, the lattice frame for sub-FV1, is generated by clicking "frame generation" button. The generated lattice frame is shown in Figure 7-13. The last step of the initial design stage is to determine the manufacturing constraints of each lattice strut of the generated lattice frame. To achieve this purpose, the additive manufacturing process and its related process parameters need to be predefined. In Intralattice software, designers can set the process related information under "Configuration-Manufacturing Process Selection" dropdown menu. The window which is used to set manufacturing information for this design case is presented in Figure 7-14. In this window, a few available AM machines are listed in the combo list. For each machine, its related parameters are predefined with different sets, as the manufacturability model for these parameters sets are available in the database. To view the detailed of parameters of each group, designers can click "view parameter" button. In addition to manufacturing related parameters, designers also need to define the printing orientation according to the generated FSs and FVs. To define the printing orientation, the XOY plane of global coordinate system in CAD software is considered as the printing plate, and its Z axis is regarded as the vertical axis of the printing machine. Based on the reference coordinate system defined above, designers can rotate the FSs and FVs accordingly in the CAD software. The printing

orientation of this design case is shown in Figure 7-15. There are two major reasons for choosing this printing orientation. Firstly, it guarantees the printing quality of FS1, FS4, FS6, FS8, FS10, FS12, FS15 and FS16. These FSs are designed for assembly bolt. Thus, they need to be printed vertically to achieve higher dimensional accuracy. Moreover, this printing orientation also minimizes the support structures that are need to support the solid sub-FVs. For this design case, no support structure is needed to print those solid sub-FVs.

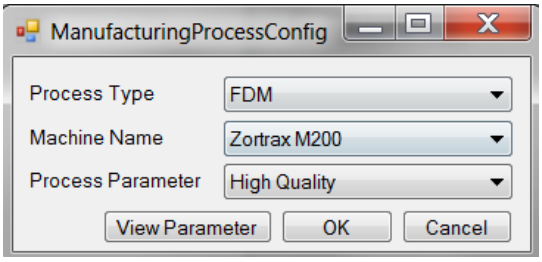

Figure 7-14 Configuration window for manufacturing information

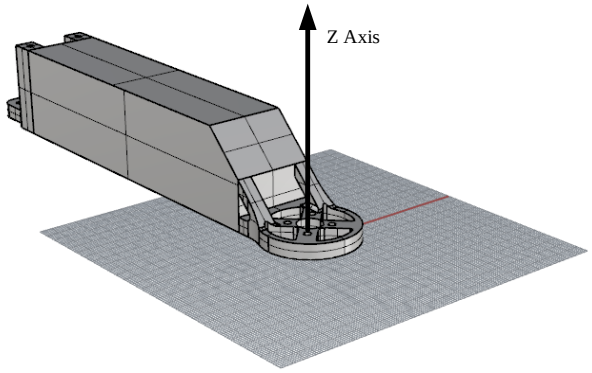

Figure 7-15 Printing orientation of the designed case

Based on the input manufacturing information, manufacturing constraint for each strut is automatically obtained from manufacturability model of the selected AM process. Designers can do further modification if any other special requirements they may have. For this design case, these constraints are summarized in Table 7-4. In this table, all the struts of the lattice frame are divided into two groups. They are horizontal struts and slants struts. For horizontal struts, they are further divided into two sub-groups for different lengths. Similarly, slant struts are also divided into two

sub groups for the different orientation angles of its axis. The manufacturing constraint of the struts in each sub-group are the same. It should be noted that the AM manufacturing constraints model used for this design case only provides the lower bound of struts' diameter. The upper bound of the diameter is generally determined by the porosity constraint of lattice structures. If this value is too big, the designed lattice structures cannot be considered as porous structures.

Table 7-4 Manufacturing constraints on the diameter of struts

Manufacturable Elements	Constant geometric data	Lower bound	Upper bound
Horizontal strut	L = 16mm	0.9mm	5mm
	L = 25mm	1.5mm	5mm
Slanted strut	$\theta = 90°$	0.9mm	5mm
	$\theta = 31°$	1.9mm	5mm

After obtaining manufacturing constraints of lattice struts, designers can start to do design optimization. In the design optimization stage, designers are suggested to firstly build F-P-P-D model to analyze the relationship between performance parameters and the selected design parameters. For this design case, its F-P-P-D model is shown in Figure 7-16. In the performance domain, there are two general performance parameters which need to be considered. They are the mass of a structure and its displacement at point C. The mass of a structure depends on the overall porosity of the sub-FV with lattice structures as well as the volume of that sub-FV. In the design optimization process, the volume of sub-FV is fixed. Thus, the mass constraint is converted to the constraints on the overall porosity of the lattice region. The displacement is considered as the objective of the optimization process. It only links to the design parameter of lattice struts' thickness distribution. Based on this F-P-P-D model, the BESO based optimization method is selected for two reasons. Firstly, this design optimization problem only relates to structural performance. Secondly, the total number of cells is small. Thus, it does not take a long time to for each optimization iteration.

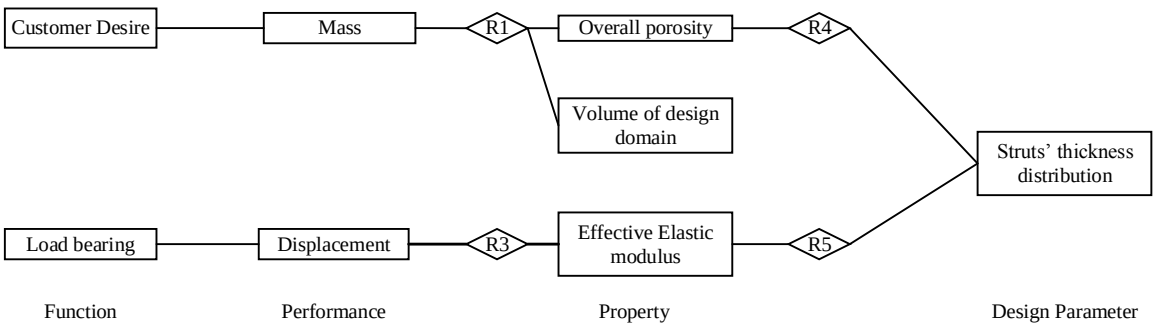

Figure 7-16 The F-P-P-D model for the given design case

According to sub-process presented in Figure 7-5(a) for BESO based optimization, a FEA script without boundary condition needs to be firstly generated for the FEA solver. This process is easily done by clicking the "ExportFrameToFEA" button on the main window of Intralattice. Then, the FEA solver script file with frame elements are generated in the given folder. The directory of the folder is predefined by designers under "Configuration-Folder Setting" drop down menu. By opening the generated script file in the preprocessor of FEA solver, designers can add boundary conditions for the designed structures. For this design case, the simulation model with boundary conditions is shown in Figure 7-17. In this model, the solid FVs are meshed with volumetric tetrahedron elements, while the lattice structure is modeled with 1-D beam element. To link these two types of elements in different FVs, Rigid Body Elements (RBEs) are applied.

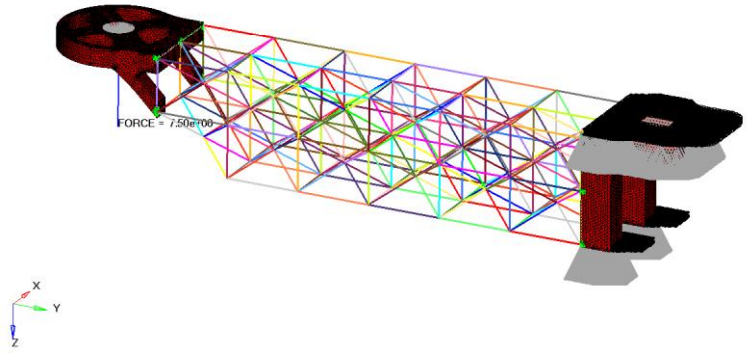

Figure 7-17 FEA model with boundary conditions for the given design case

After generating the FEA script with boundary conditions, designers can click

"ReadFEAScript" button. The boundary condition is read into the developed software. The last step of the design optimization stage is to optimize the generated lattice frame with the selected optimization method. Designers can predefine the parameters of each selected optimization method under "Configuration- Optimization Option" drop down menu. For this design case, the parameters used for BESO based optimization method are summarized in Table 7-5. After setting the optimization parameters, designers can click "Optimization" button, the frame is automatically optimized under the given loading condition. The PI index with respect to optimization iterations is displayed during the optimization process. For this design, the trend of PI index with respect to optimization iterations is presented in Figure 7-18 which shows the design optimization process of this design case is converged after 53 iterations.

Table 7-5 Value of parameter used in the optimization algorithm

RT	Ri	F	L	I_{max}	c
0.1	0.01	7.5 N	165 mm	100	0.001

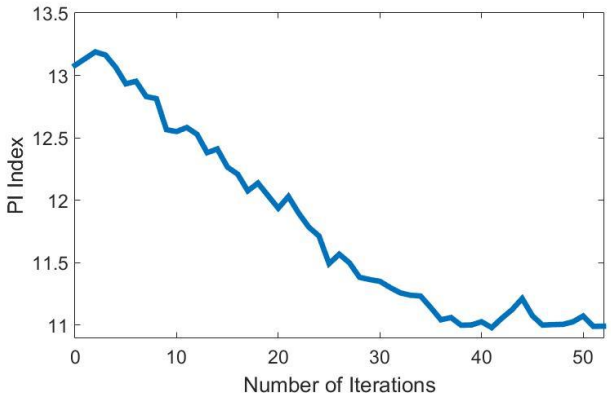

Figure 7-18 The trend of PI index with respect to optimization iterations

After design optimization, the FEA model of optimized part is generated by clicking the "Generate FEA model" button on the main window of Intralattice. Based on the generated FEA model, the simulation of optimized part can be done. The result is shown in Figure 7-19 (a).

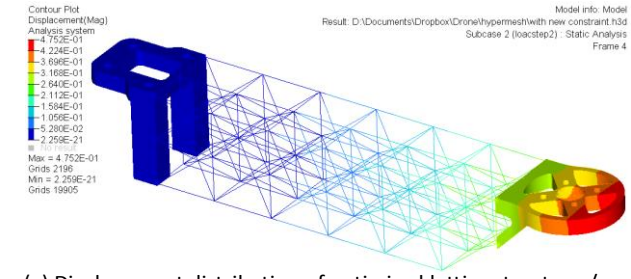

(a) Displacement distribution of optimized lattice structure /mm

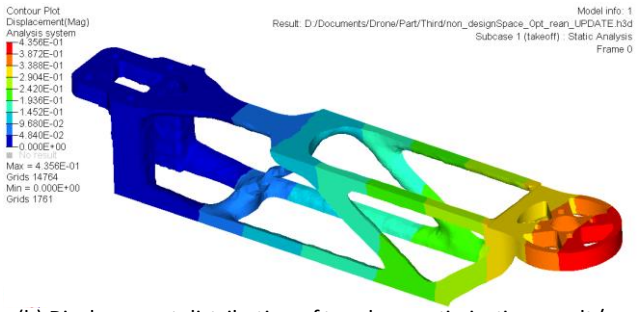

(b) Displacement distribution of topology optimization result/mm

Figure 7-19 Comparison between the simulation results between optimized lattice structures and topology optimization result

Table 7-6 The comparison of simulation results and physical results

	Optimization with constraints	Optimization with uniform constraint	Homogenous Lattice	Topology optimization	Original design
Volume (mm^3)	31277	32534	32375	33905.15	33376
Displacement at Point C – Simulation (mm)	0.375	0.319	0.875	0.354	4.834
Displacement – Physical tests (mm)	0.454	Not Available	0.78	Not Available	4.807
Max Von Mises (MPa)	1.857	1.690	4.351	2.42	15.11
Manufacturability	Yes	No	Yes	No	Yes

Since the material used in this design case is ABS which is a ductile material, Von Mises yield criterion [251] is used to determine whether the designed lattice structure can sustain given load without plastic deformation. The maximum Von-Mises stress of the optimized lattice structures is summarized in Table 7-6. By checking these values, it is manifested that all the design requirements listed at the beginning of this section are satisfied. Then, by clicking "Generate geometric model" button, the geometric model of the designed lattice-solid hybrid structure is generated and shown in Figure 7-20(a). Based on the generated geometric model, the part is

fabricated by the selected AM machine, the fabrication result is shown in Figure 7-20(b). It illustrates that the optimized lattice structure is fabricatable for the selected AM machine under the given process parameters.

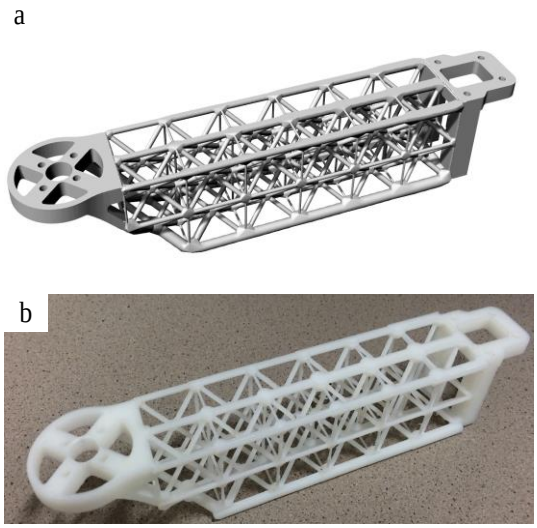

Figure 7-20 Geometric model of optimized lattice structures and its fabrication result

To compare the design result with other existing design methods and its original design, the simulation results of different types of design configurations are summarized in Table 7-6. Compared to the original design and the design of a homogeneous lattice structure, it is obvious that the optimized heterogeneous lattice structure significantly improves the structural stiffness without increasing its weight. To further verify this conclusion, physical tests on both homogeneous lattice and optimized heterogeneous lattice have been done. In the physical tests, a tensile test machine (ADMET MicroEP series with 45N load sensor) is used to apply the given load and measure the displacement on the end of arm. A clamp is used to fix the other end of arm. The experimental setup used in this design case is shown in Figure 7-21. The results of physical tests have also been summarized in Table 7-6. It shows a small deviation (less than 0.1mm) between simulation results and physical testing results. This deviation is mainly caused by the anisotropic material properties of printed ABS material which has not been considered in the

current research. However, both simulation and physical testing data show a clear trend that the designed lattice structure significantly improves the structural stiffness compared to its original design and homogeneous lattice structures.

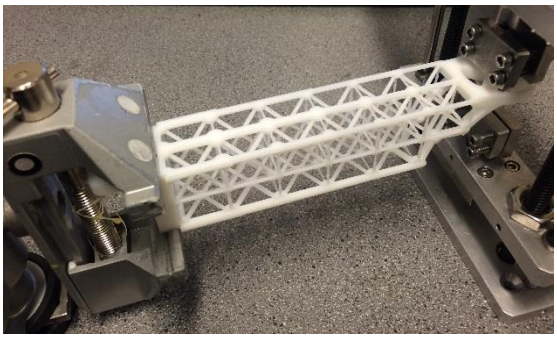

Figure 7-21 Physical test of optimized lattice structures

To further evaluate the efficiency of the proposed lattice design and optimization method, the part (shown in Figure 7-19(b)) directly obtained from traditional topology optimization routine (SIMP) has also been considered as a benchmark part in this paper. The displacement contours of optimized lattice structures and topology optimization result are compared and shown in Figure 7-19(b). Even though the topology optimization result achieves slightly better stiffness, the large area of the overhang region in the topology optimized part makes it difficult to be directly fabricated without support structures. Moreover, as it is shown in Table 7-6, optimized lattice structures may achieve a smaller maximum Von-Mises stress compared to topology optimization result.

Another interesting fact which is observed from Table 7-6 is that the optimized lattice with uniform constraint achieves a better stiffness than that of non-uniform constraints obtained from the model of manufacturing constraints as well as the result of topology optimization. In this research, the uniform constraint refers smallest cylinder that is recognized by the machine's slicing software [252]. Its value is 0.6mm for the selected machine. This constraint is uniformly applied to all the struts during the optimization process. Compared to the optimized lattice with non-

uniform constraints, the uniform constraints provide a larger design freedom for designers. Thus, the structure is further optimized to achieve better performance. However, this structure cannot be fabricated with the selected machine, since the dimension of optimized struts violates the constraints obtained from manufacturing constraints model. Based on this fact, it is inferred that if the process related parameters, such as printing strategy and process parameters, can be optimized to alleviate the existing manufacturing constraints, the performance of parts can be further improved by the proposed design method.

7.4 Summary

This chapter describes the development work of the software called Intralattice, which is the implementation of the proposed design methodology. It is developed in C# programming language under the .NET framework. To connect with CAD software Rhino, RhinoCommon SDK is also used in this software.

The overall framework of Intralattice is mainly divided into three layers. The major module and components of each layer are discussed in detail. In addition to the framework, the overall operation flow of the developed software is also introduced in this chapter. It gives designers a guide on how to take advantage of the developed software during their design process.

At the end of this chapter, a design case is provided to further illustrate the design process enabled by the developed software. In this case study, an arm of quadcopter is redesigned for a better stiffness without increasing its weight. The entire design process of this case study has been illustrated in this chapter with detailed introduction on the operation procedures of Intralattice. The geometric model of design result is generated at the end of the design process and fabricated by the selected AM machine. To evaluate the performance of optimized design, both FEA simulation and physical testing have been done. The results show the optimized result exhibits a better

stiffness than its original design as well as the homogeneous lattice structures without optimization. Moreover, by comparing the optimized lattice structures with topology optimization result, it shows the stiffness of two different design configurations is almost the same. However, the optimized lattice structure shows a better fabricability, since it can be fabricated without support structures which are hard to remove in the intricate portion.

The current version of Intralattice is only a prototype. Thus, some additional functions and features need to be added. The future development work of this software is listed below:

1 In the current version of Intralattice, only very few available cell topologies can be selected by designers. The lattice cell topology module will be added in future which enables designers to define their own desired lattice topologies for certain properties;

2 Currently, F-P-P-D model cannot be directly constructed in the developed software. Other software like Microsoft Visio needs to be used to help designers to build this model. In the future version, this function can be integrated into the developed software;

3 More types of database, such as materials database, manufacturing information database and mesoscale lattice topologies database, should be linked to Intralattice. It will make the software more intelligent to provide a recommendation for designers when they use lattice structures in their design.

Chapter 8 Conclusions and Future Work

The design freedom enabled by AM technologies largely expands the application of mesoscale lattice structures. To take full advantage of unique capabilities of AM processes on mesoscale lattice structures, the design methods which can consider both design freedom and constraints of AM processes are needed.

A comprehensive literature review has been done in this thesis to summarize the existing design methods for additive manufacturing and mesoscale lattice structures. The result of this review shows most existing methods for AM only focus on a single design scale or a single function. Very little research has been devoted on developing multiscale and multifunctional design method for lattice structures. Moreover, it also indicates that lack of efficient lattice geometric modeling tool is another obstacle for designers to take full advantage of lattice structures. Most existing geometric modeling methods used in commercial CAD software cannot efficiently generate lattice with a large number of cells to fit the domain with complex macro shape. In addition to that, the gap between geometric model and simulation model prevents designers from further optimizing and simulating the generated lattice structures easily.

To solve those issues summarized from the literature review, a multiscale and multifunctional design methodology for lattice structures is proposed. This innovative design methodology mainly focuses on the mesoscale lattice structures. It aims to provide a general design flow and several detailed design optimization methods for lattice structures. The general flow of the proposed design methodology can be divided into three stages: initial design, design optimization and geometric modeling.

In the initial design stage, functional analysis method is developed to help designers to

integrate multifunction into a single physical entity, which can further reduce the overall part's count. Several design guidelines for FV division are provided to enable designers to consider both solid and lattice structures during the design process. A manufacturability model of lattice structures is developed which can guarantee the optimized lattice structures are fabricatable.

In the design optimization stage, the F-P-P-D model is created to analyze and represent two levels of coupling relations during the multifunctional design of mesoscale lattice structures. Besides this model, three different optimization methods for mesoscale lattice structures are developed. Among them, BESO based method and heuristic optimization method are mainly developed for structural performance. The last one is developed to deal with multifunctional optimization. The effectiveness and efficiency of proposed optimization methods are verified by several case studies. A comparison between different optimization methods is made. Base on this comparison, a guideline is provided in this thesis to help designers to select a suitable optimization method for the specific design case.

In the geometric modeling stage, a hybrid multiscale geometric modeling method is proposed. This method combines the advantages of frame-based modeling, implicit function modeling and voxel based modeling, which enables the fast generation of the digital model for a lattice structure with multiscale complexities. Moreover, the proposed geometric modeling method also supports the design of lattice structures with multi-material or functional graded material. It enables designers to consider the material distribution inside lattice structures on both macro and mesoscale.

At the end of this thesis, a software prototype, Intralattice, is discussed as the implementation of the proposed design methodology. The developed software is a plug-in to the commercial CAD platform called Rhino. A case study of the arm of quadcopter is used to illustrate how to use the

developed software and verify its effectiveness.

Generally, it is concluded that the multiscale design freedom provided by AM technologies enables designers to further improve the functional performance of lattice structures. The proposed design methodology can take benefit of this design freedom and assist designers to obtain the optimized lattice structures during the design process. The effectiveness and efficiency of the proposed methodology have been proved by several case studies given in this thesis. This research provides the foundation for the wide application of mesoscale lattice structures in the future.

However, it should be noted that the current research still has some limitations. For example, deviations of geometric shape as well as material properties caused by AM manufacturing processes are not considered. To solve these issues, future research can be carried out in the following areas:

1) In this thesis, the effects of a manufacturing process on the geometric dimensions and material properties of printed mesoscale lattice structures are not considered. These values may vary with respect to lattice strut's thickness as well as strut's orientations. Thus, in the future, these effects should be considered in the simulation infrastructure during the optimization process.

2) The optimization methods which can simultaneously consider the lattice relative density distribution and its base-material distribution are needed. Comparing to lattice structures with a single material, multi-material lattice provides more design freedom to further improve its functional performance.

3) Currently, FV division needs to be done manually by designers based on the proposed design guidelines. Further research is needed to develop a computer-aided tool which can automatically divide FV into several sub-FV according to functional and manufacturing requirements.

Reference

[1] Merriam-Webster, 2017, "Design," https://www.merriam-webster.com/dictionary/design.

[2] Olexa, R., 2001, "The father of the second industrial revolution," Manufacturing Engineering, 127(2).

[3] Merriam-Webster., 2016, "lattice," http://www.merriam-webster.com/dictionary/lattice.

[4] Schaedler, T. A., and Carter, W. B., 2016, "Architected Cellular Materials," Annual Review of Materials Research, pp. 187-210.

[5] Deshpande, V., Fleck, N., and Ashby, M., 2001, "Effective properties of the octet-truss lattice material," Journal of the Mechanics and Physics of Solids, 49(8), pp. 1747-1769.

[6] Lehman, J., and Lakes, R., 2013, "Stiff lattices with zero thermal expansion and enhanced stiffness via rib cross section optimization," International Journal of Mechanics and Materials in Design, 9(3), pp. 213-225.

[7] Yang, L., Cormier, D., West, H., Harrysson, O., and Knowlson, K., 2012, "Non-stochastic Ti-6Al-4V foam structures with negative Poisson's ratio," Materials Science and Engineering A, 558, pp. 579-585.

[8] Zhang, Q., Han, Y., Chen, C., and Lu, T., 2009, "Ultralight X-type lattice sandwich structure (I): Concept, fabrication and experimental characterization," Science in China, Series E: Technological Sciences, 52(8), pp. 2147-2154.

[9] Heinl, P., Müller, L., Körner, C., Singer, R. F., and Müller, F. A., 2008, "Cellular Ti–6Al–4V structures with interconnected macro porosity for bone implants fabricated by selective electron beam melting," Acta Biomaterialia, 4(5), pp. 1536-1544.

[10] Bose, S., Vahabzadeh, S., and Bandyopadhyay, A., 2013, "Bone tissue engineering using 3D printing," Materials Today, 16(12), pp. 496-504.

[11] Emmelmann, C., Scheinemann, P., Munsch, M., and Seyda, V., 2011, "Laser Additive Manufacturing of Modified Implant Surfaces with Osseointegrative Characteristics," Physics Procedia, 12, pp. 375-384.

[12] Tang, Y., Kurtz, A., and Zhao, Y. F., 2015, "Bidirectional Evolutionary Structural Optimization (BESO) based design method for lattice structure to be fabricated by additive manufacturing," Computer-Aided Design, 69, pp. 91-101.

[13] Rosen, D. W., 2007, "Computer-aided design for additive manufacturing of cellular structures," Computer-Aided Design & Applications, 4(5), pp. 585-594.

[14] Ozdemir, Z., Hernandez-Nava, E., Tyas, A., Warren, J. A., Fay, S. D., Goodall, R., Todd, I.,

and Askes, H., 2016, "Energy absorption in lattice structures in dynamics: Experiments," International Journal of Impact Engineering, 89, pp. 49-61.

[15] Lehman, J., and Lakes, R. S., 2014, "Stiff, strong, zero thermal expansion lattices via material hierarchy," Composite Structures, 107, pp. 654-663.

[16] Brooks, H., and Brigden, K., 2016, "Design of conformal cooling layers with self-supporting lattices for additively manufactured tooling," Additive Manufacturing, 11, pp. 16-22.

[17] Fantini, M., Curto, M., and De Crescenzio, F., 2016, "A method to design biomimetic scaffolds for bone tissue engineering based on Voronoi lattices," Virtual and Physical Prototyping, 11(2), pp. 77-90.

[18] Wadley, H. N., Fleck, N. A., and Evans, A. G., 2003, "Fabrication and structural performance of periodic cellular metal sandwich structures," Composites Science and Technology, 63(16), pp. 2331-2343.

[19] Wang, J., Evans, A. G., Dharmasena, K., and Wadley, H. N. G., 2003, "On the performance of truss panels with Kagomé cores," International Journal of Solids and Structures, 40(25), pp. 6981-6988.

[20] Deshpande, V., and Fleck, N., 2001, "Collapse of truss core sandwich beams in 3-point bending," International Journal of Solids and Structures, 38(36), pp. 6275-6305.

[21] Wadley, H. N., 2006, "Multifunctional periodic cellular metals," Philosophical Transactions of the Royal Society A: Mathematical, Physical and Engineering Sciences, 364(1838), pp. 31-68.

[22] Kruth, J.-P., 1991, "Material incress manufacturing by rapid prototyping techniques," CIRP Annals-Manufacturing Technology, 40(2), pp. 603-614.

[23] ASTM, 2012, "F2792. 2012.Standard Terminology for Additive Manufacturing Technologies," ASTM international, West Conshohocken, PA,US.

[24] Chu, C., Graf, G., and Rosen, D. W., 2008, "Design for additive manufacturing of cellular structures," Computer-Aided Design and Applications, 5(5), pp. 686-696.

[25] Gaynor, A. T., Meisel, N. A., Williams, C. B., and Guest, J. K., 2014, "Multiple-Material Topology Optimization of Compliant Mechanisms Created Via PolyJet Three-Dimensional Printing," Journal of Manufacturing Science and Engineering, 136(6), p. 061015.

[26] Obielodan, J., Ceylan, A., Murr, L., and Stucker, B., 2010, "Multi-material bonding in ultrasonic consolidation," Rapid prototyping journal, 16(3), pp. 180-188.

[27] Rutz, A. L., Hyland, K. E., Jakus, A. E., Burghardt, W. R., and Shah, R. N., 2015, "A multimaterial bioink method for 3D printing tunable, cell‐compatible hydrogels," Advanced Materials, 27(9), pp. 1607-1614.

[28] Tang, Y., Yang, S., and Zhao, Y. F., 2016, "Sustainable Design for Additive Manufacturing

Through Functionality Integration and Part Consolidation," Handbook of Sustainability in Additive Manufacturing: Volume 1, S. S. Muthu, and M. M. Savalani, eds., Springer Singapore, Singapore, pp. 101-144.

[29] Ge, Q., Sakhaei, A. H., Lee, H., Dunn, C. K., Fang, N. X., and Dunn, M. L., 2016, "Multimaterial 4D printing with tailorable shape memory polymers," Scientific Reports, 6.

[30] Wang, Q., Jackson, J. A., Ge, Q., Hopkins, J. B., Spadaccini, C. M., and Fang, N. X., 2016, "Lightweight Mechanical Metamaterials with Tunable Negative Thermal Expansion," Physical Review Letters, 117(17), p. 175901.

[31] Tang, Y., Dong, G., Zhou, Q., and Zhao, Y. F., 2017, "Lattice Structure Design and Optimization With Additive Manufacturing Constraints," IEEE Transactions on Automation Science and Engineering, PP(99), pp. 1-17.

[32] Angrish, A., "A critical analysis of additive manufacturing technologies for aerospace applications," Proc. Aerospace Conference, 2014 IEEE, pp. 1-6.

[33] Jardini, A. L., Larosa, M. A., Filho, R. M., Zavaglia, C. A. d. C., Bernardes, L. F., Lambert, C. S., Calderoni, D. R., and Kharmandayan, P., 2014, "Cranial reconstruction: 3D biomodel and custom-built implant created using additive manufacturing," Journal of Cranio-Maxillofacial Surgery.

[34] Bourell, D. L., Leu, M. C., and Rosen, D. W., 2009, "Roadmap for additive manufacturing: identifying the future of freeform processing," The University of Texas, Austin.

[35] Bendsøe, M. P., 2003, Topology optimization: theory, methods and applications, Springer.

[36] Borrvall, T., and Petersson, J., 2003, "Topology optimization of fluids in Stokes flow," International Journal for Numerical Methods in Fluids, 41(1), pp. 77-107.

[37] Dühring, M. B., Jensen, J. S., and Sigmund, O., 2008, "Acoustic design by topology optimization," Journal of Sound and Vibration, 317(3-5), pp. 557-575.

[38] Deng, Y., Liu, Z., Liu, Y., and Wu, Y., 2013, "Combination of topology optimization and optimal control method," Journal of Computational Physics, 257(PA), pp. 374-399.

[39] Frandsen, L. H., Harpøth, A., Borel, P. I., Kristensen, M., Jensen, J. S., and Sigmund, O., 2004, "Broadband photonic crystal waveguide 60° bend obtained utilizing topology optimization," Optics Express, 12(24), pp. 5916-5921.

[40] Bendsøe, M. P., Ben-Tal, A., and Zowe, J., 1994, "Optimization methods for truss geometry and topology design," Structural optimization, 7(3), pp. 141-159.

[41] Dorn, W. S., Gomory, R. E., and Greenberg, H. J., 1964, "Automatic design of optimal structures," Journal de mecanique, 3(1), pp. 25-52.

[42] Bendsøe, M. P., and Kikuchi, N., 1988, "Generating optimal topologies in structural design

using a homogenization method," Computer methods in applied mechanics and engineering, 71(2), pp. 197-224.

[43] Rozvany, G., Zhou, M., and Birker, T., 1992, "Generalized shape optimization without homogenization," Structural Optimization, 4(3-4), pp. 250-252.

[44] Allaire, G., Jouve, F., and Toader, A.-M., 2002, "A level-set method for shape optimization," Comptes Rendus Mathematique, 334(12), pp. 1125-1130.

[45] Wang, M. Y., Wang, X., and Guo, D., 2003, "A level set method for structural topology optimization," Computer Methods in Applied Mechanics and Engineering, 192(1–2), pp. 227-246.

[46] Xie, Y., and Steven, G. P., 1993, "A simple evolutionary procedure for structural optimization," Computers & structures, 49(5), pp. 885-896.

[47] Young, V., Querin, O., Steven, G., and Xie, Y., 1999, "3D and multiple load case bi-directional evolutionary structural optimization (BESO)," Structural optimization, 18(2-3), pp. 183-192.

[48] Wang, S. Y., and Tai, K., 2005, "Structural topology design optimization using Genetic Algorithms with a bit-array representation," Computer Methods in Applied Mechanics and Engineering, 194(36–38), pp. 3749-3770.

[49] Chen, Z., Gao, L., Qiu, H., and Shao, X., "Combining genetic algorithms with optimality criteria method for topology optimization," Proc. Bio-Inspired Computing, 2009. BIC-TA'09. Fourth International Conference on, IEEE, pp. 1-6.

[50] Brackett, D., Ashcroft, I., and Hague, R., "Topology optimization for additive manufacturing," Proc. 22nd Annual international solid freeform fabrication symposium, pp. 348-362.

[51] Rozvany, G. I., 2009, "A critical review of established methods of structural topology optimization," Structural and Multidisciplinary Optimization, 37(3), pp. 217-237.

[52] Namasivayam, U. M., and Seepersad, C. C., 2011, "Topology design and freeform fabrication of deployable structures with lattice skins," Rapid Prototyping Journal, 17(1), pp. 5-16.

[53] Lin, J., Luo, Z., and Tong, L., 2010, "Design of adaptive cores of sandwich structures using a compliant unit cell approach and topology optimization," Journal of Mechanical Design, Transactions of the ASME, 132(8), pp. 0810121-0810128.

[54] Aremu, A., Ashcroft, I., Wildman, R., Hague, R., Tuck, C., and Brackett, D., 2013, "The effects of bidirectional evolutionary structural optimization parameters on an industrial designed component for additive manufacture," Proceedings of the Institution of Mechanical Engineers, Part B: Journal of Engineering Manufacture, 227(6), pp. 794-807.

[55] Leary, M., Merli, L., Torti, F., Mazur, M., and Brandt, M., 2014, "Optimal topology for additive manufacture: A method for enabling additive manufacture of support-free optimal structures," Materials and Design, 63, pp. 678-690.

[56] Gardan, N., and Schneider, A., 2014, "Topological optimization of internal patterns and support in additive manufacturing," Journal of Manufacturing Systems.

[57] Brackett, D., Panesar, A., Ashcroft, I., Wildman, R., and Hague, R., "An optimization based design framework for multi-functional 3D printing," Proc. 24th International SFF Symposium - An Additive Manufacturing Conference, SFF 2013, pp. 592-605.

[58] Panesar, A., Brackett, D., Ashcroft, I., Wildman, R., and Hague, R., 2014, "Design Optimization Strategy for Multifunctional 3D Printing," 24th International SFF Symposium - An Additive Manufacturing Conference, SFF 2014Austin Texas, US.

[59] Inc, A. E., 2013, "Optistruct User's Guide V12.0," Altair Engineering Inc.

[60] Chang, K. H., and Tang, P. S., 2001, "Integration of design and manufacturing for structural shape optimization," Advances in Engineering Software, 32(7), pp. 555-567.

[61] Lynch, M. E., Gu, W., El-Wardany, T., Hsu, A., Viens, D., Nardi, A., and Klecka, M., 2013, "Design and topology/shape structural optimisation for additively manufactured cold sprayed components: This paper presents an additive manufactured cold spray component which is shape optimised to achieve 60% reduction in stress and 20% reduction in weight," Virtual and Physical Prototyping, 8(3), pp. 213-231.

[62] Rengier, F., Mehndiratta, A., von Tengg-Kobligk, H., Zechmann, C. M., Unterhinninghofen, R., Kauczor, H.-U., and Giesel, F. L., 2010, "3D printing based on imaging data: review of medical applications," International journal of computer assisted radiology and surgery, 5(4), pp. 335-341.

[63] Chulvi, V., Cebrian-Tarrasón, D., Sancho, Á., and Vidal, R., 2013, "Automated design of customized implants," Revista Facultad de Ingeniería, 1(68), pp. 95-103.

[64] D'Urso, P. S., Effeney, D. J., Earwaker, W. J., Barker, T. M., Redmond, M. J., Thompson, R. G., and Tomlinson, F. H., 2000, "Custom cranioplasty using stereolithography and acrylic," British Journal of Plastic Surgery, 53(3), pp. 200-204.

[65] Singare, S., Liu, Y., Li, D., Lu, B., Wang, J., and He, S., 2007, "Individually prefabricated prosthesis for maxilla reconstruction," Journal of Prosthodontics.

[66] Dai, K.-R., Yan, M.-N., Zhu, Z.-A., and Sun, Y.-H., 2007, "Computer-aided custom-made hemipelvic prosthesis used in extensive pelvic lesions," The Journal of arthroplasty, 22(7), pp. 981-986.

[67] Faur, C., Crainic, N., Sticlaru, C., and Oancea, C., 2013, "Rapid prototyping technique in the preoperative planning for total hip arthroplasty with custom femoral components," Wiener klinische Wochenschrift, 125(5-6), pp. 144-149.

[68] Xiong, S., Zhao, J., Jiang, Z., and Dong, M., 2010, "A computer-aided design system for foot-feature-based shoe last customization," The International Journal of Advanced Manufacturing Technology, 46(1-4), pp. 11-19.

[69] Ariadi, Y., and Rennie, A., 2008, "Templates for consumer use in designing customised products."

[70] Ariadi, Y., Campbell, R. I., Evans, M. A., and Graham, I. J., "Combining additive manufacturing with computer aided consumer design," Proc. 23rd Annual International Solid Freeform Fabrication Symposium - An Additive Manufacturing Conference, SFF 2012, pp. 238-249.

[71] Zhou, W., Wu, D., Ding, X., and Rosen, D. W., "Customer co-design of computer mouse for mass customization without causing mass confusion," Proc. Proceedings - 2010 International Conference on Manufacturing Automation, ICMA 2010, pp. 8-15.

[72] Acher, M., Baudry, B., Barais, O., and Jézéquel, J. M., 2014, "Customization and 3D printing: A challenging playground for software product lines," ACM International Conference Proceeding Series, 1, pp. 142-146.

[73] Industries, M., 2017, "Thinkiverse," https://www.thingiverse.com/.

[74] Merriam-Webster., 2004, Merriam-Webster's collegiate dictionary, Merriam-Webster.

[75] Gibson, L. J., and Ashby, M. F., 1999, Cellular solids: structure and properties, Cambridge university press.

[76] Evans, A. G., Hutchinson, J. W., Fleck, N. A., Ashby, M. F., and Wadley, H. N. G., 2001, "The Topological Design of Multifunctional Cellular Metals," Progress in Materials Science, 46(3–4), pp. 309-327.

[77] Gibson, L. J., 2005, "Biomechanics of cellular solids," Journal of Biomechanics, 38(3), pp. 377-399.

[78] Varanasi, S., Bolton, J. S., Siegmund, T. H., and Cipra, R. J., 2013, "The low frequency performance of metamaterial barriers based on cellular structures," Applied Acoustics, 74(4), pp. 485-495.

[79] Hosseini, S. M. H., Willberg, C., Kharaghani, A., and Gabbert, U., 2014, "Characterization of the guided wave propagation in simplified foam, honeycomb and hollow sphere structures," Composites Part B: Engineering, 56, pp. 553-566.

[80] Arabnejad, S., and Pasini, D., 2013, "Mechanical properties of lattice materials via asymptotic homogenization and comparison with alternative homogenization methods," International Journal of Mechanical Sciences, 77, pp. 249-262.

[81] Ashby, M. F., and Cebon, D., 1993, "Materials selection in mechanical design," Le Journal de Physique IV, 3(C7), pp. C7-1-C7-9.

[82] Sigmund, O., 1994, "Materials with prescribed constitutive parameters: an inverse homogenization problem," International Journal of Solids and Structures, 31(17), pp. 2313-2329.

[83] Sigmund, O., 1995, "Tailoring materials with prescribed elastic properties," Mechanics of Materials, 20(4), pp. 351-368.

[84] Neves, M., Rodrigues, H., and Guedes, J., 2000, "Optimal design of periodic linear elastic microstructures," Computers & Structures, 76(1), pp. 421-429.

[85] Almeida, H. D. A., and da Silva Bártolo, P. J., 2010, "Virtual topological optimisation of scaffolds for rapid prototyping," Medical Engineering and Physics, 32(7), pp. 775-782.

[86] Huang, X., Radman, A., and Xie, Y., 2011, "Topological design of microstructures of cellular materials for maximum bulk or shear modulus," Computational Materials Science, 50(6), pp. 1861-1870.

[87] Radman, A., Huang, X., and Xie, Y. M., 2013, "Topological optimization for the design of microstructures of isotropic cellular materials," Engineering Optimization, 45(11), pp. 1331-1348.

[88] Zhou, S., and Li, Q., 2008, "Computational design of multi-phase microstructural materials for extremal conductivity," Computational Materials Science, 43(3), pp. 549-564.

[89] Zhou, S., Li, W., Sun, G., and Li, Q., 2010, "A level-set procedure for the design of electromagnetic metamaterials," Optics express, 18(7), pp. 6693-6702.

[90] Challis, V., Roberts, A., and Wilkins, A., 2008, "Design of three dimensional isotropic microstructures for maximized stiffness and conductivity," International Journal of Solids and Structures, 45(14), pp. 4130-4146.

[91] Torquato, S., Hyun, S., and Donev, A., 2003, "Optimal design of manufacturable three-dimensional composites with multifunctional characteristics," Journal of Applied Physics, 94(9), pp. 5748-5755.

[92] Guest, J. K., and Prévost, J. H., 2006, "Optimizing multifunctional materials: design of microstructures for maximized stiffness and fluid permeability," International Journal of Solids and Structures, 43(22), pp. 7028-7047.

[93] Seepersad, C. C., Allen, J. K., McDowell, D. L., and Mistree, F., 2008, "Multifunctional Topology Design of Cellular Material Structures," Journal of Mechanical Design, 130(3), pp. 031404-031404.

[94] Deshpande, V. S., and Fleck, N. A., 2001, "Collapse of truss core sandwich beams in 3-point bending," International Journal of Solids and Structures, 38(36-37), pp. 6275-6305.

[95] Wicks, N., and Hutchinson, J. W., 2001, "Optimal truss plates," International Journal of Solids and Structures, 38(30-31), pp. 5165-5183.

[96] Wicks, N., and Hutchinson, J. W., 2004, "Performance of sandwich plates with truss cores," Mechanics of Materials, 36(8), pp. 739-751.

[97] Rathbun, H., Zok, F., and Evans, A., 2005, "Strength optimization of metallic sandwich panels

subject to bending," International journal of solids and structures, 42(26), pp. 6643-6661.

[98] Liu, J.-S., and Lu, T. J., 2004, "Multi-objective and multi-loading optimization of ultralightweight truss materials," International Journal of Solids and Structures, 41(3), pp. 619-635.

[99] Liu, T., Deng, Z., and Lu, T., 2006, "Design optimization of truss-cored sandwiches with homogenization," International Journal of Solids and Structures, 43(25), pp. 7891-7918.

[100] Lu, T., Valdevit, L., and Evans, A., 2005, "Active cooling by metallic sandwich structures with periodic cores," Progress in Materials Science, 50(7), pp. 789-815.

[101] Hutchinson, R., Wicks, N., Evans, A., Fleck, N., and Hutchinson, J., 2003, "Kagome plate structures for actuation," International Journal of solids and structures, 40(25), pp. 6969-6980.

[102] Liu, T., Deng, Z., and Lu, T., 2007, "Bi-functional optimization of actively cooled, pressurized hollow sandwich cylinders with prismatic cores," Journal of the Mechanics and Physics of Solids, 55(12), pp. 2565-2602.

[103] Rezaie, R., Badrossamay, M., Ghaie, A., and Moosavi, H., 2013, "Topology Optimization for Fused Deposition Modeling Process," Procedia CIRP, 6, pp. 522-527.

[104] Sundararajan, V. G., 2011, "Topology optimization for additive manufacturing of customized meso-structures using homogenization and parametric smoothing functions," Master, The University of Texas at Austin.

[105] Wang, H. V., and Rosen, D., 2001, "Computer-aided design methods for the additive fabrication of truss structure," Master, School of Mechanical Engineering, Georgia Institute of Technology.

[106] Wang, H., and Rosen, D. W., "Parametric modeling method for truss structures," Proc. 22nd Computers and Information in Engineering Conference, pp. 759-767.

[107] Wang, H. V., 2005, "A unit cell approach for lightweight structure and compliant mechanism," Doctor, Georgia Institute Of Technology, Georgia,Atlanta.

[108] Nguyen, J., Park, S. I., and Rosen, D., 2013, "Heuristic Optimization Method for Cellular Structure Design of Light Weight Components," Int J Precis Eng Man, 14(6), pp. 1071-1078.

[109] Chen, Y., 2007, "3d texture mapping for rapid manufacturing," Computer-Aided Design & Applications, 4(6), pp. 761-771.

[110] Brackett, D., Ashcroft, I., and Hague, R., "A dithering based method to generate variable volume lattice cells for additive manufacturing," Proc. 22nd Annual International Solid Freeform Fabrication Symposium, Austin, TX, Aug, pp. 8-10.

[111] Teufelhart, S. R., G, 2012, "Optimization of Strut Diameters in Lattice Structures," Proceedings of the 23 rd Solid Freeform Fabrication (SFF) Symposium.

[112] Reinhart, G., and Teufelhart, S., 2011, "Load-Adapted Design of Generative Manufactured Lattice Structures," Physics Procedia, 12, Part A(0), pp. 385-392.

[113] Reinhart, G., and Teufelhart, S., "Optimization of mechanical loaded lattice structures by orientating their struts along the flux of force," Proc. 8th CIRP International Conference on Intelligent Computation in Manufacturing Engineering, ICME 2012, pp. 175-180.

[114] Aremu, A. O., Brennan-Craddock, J. P. J., Panesar, A., Ashcroft, I. A., Hague, R. J. M., Wildman, R. D., and Tuck, C., 2017, "A voxel-based method of constructing and skinning conformal and functionally graded lattice structures suitable for additive manufacturing," Additive Manufacturing, 13, pp. 1-13.

[115] Pasko, A., Fryazinov, O., Vilbrandt, T., Fayolle, P.-A., and Adzhiev, V., 2011, "Procedural function-based modelling of volumetric microstructures," Graphical Models, 73(5), pp. 165-181.

[116] Fryazinov, O., Vilbrandt, T., and Pasko, A., 2013, "Multi-scale space-variant FRep cellular structures," Computer-Aided Design, 45(1), pp. 26-34.

[117] Wang, H., Chen, Y., and Rosen, D. W., "A hybrid geometric modeling method for large scale conformal cellular structures," Proc. ASME 2005 International Design Engineering Technical Conferences and Computers and Information in Engineering Conference, American Society of Mechanical Engineers, pp. 421-427.

[118] Vongbunyong, S., and Kara, S., 2016, "Rapid generation of uniform cellular structure by using prefabricated unit cells," International Journal of Computer Integrated Manufacturing, pp. 1-13.

[119] Kou, X. Y., and Tan, S. T., 2007, "Heterogeneous object modeling: A review," Computer-Aided Design, 39(4), pp. 284-301.

[120] Tang, Y., Sheng, Y., and Zhao, Y. F., 2016, "DESIGN METHOD FOR CONFORMAL LATTICE-SKIN STRUCTURE FABRICATED

BY AM TECHNOLOGIES," ASME 2016 International Design Engineering Technical Conferences and Computers and Information in Engineering Conference, ASME, Charlotte, NC, USA.

[121] Pasko, A., Adzhiev, V., Sourin, A., and Savchenko, V., 1995, "Function representation in geometric modeling: concepts, implementation and applications," The Visual Computer, 11(8), pp. 429-446.

[122] Singh, J. M., and Narayanan, P., 2010, "Real-time ray tracing of implicit surfaces on the GPU," IEEE transactions on visualization and computer graphics, 16(2), pp. 261-272.

[123] Ferry, M., Paul Severin, W., David, W., Mark, B., Fook Rhu, O., Woon Shin, C., Dietmar Werner, H., and Jan-Thorsten, S., 2011, "CAD/CAM-assisted breast reconstruction," Biofabrication, 3(3), p. 034114.

[124] Vongbunyong, S., and Kara, S., 2016, "Development of Software Tool for Cellular Structure Integration for Additive Manufacturing," Procedia CIRP, 48, pp. 489-494.

[125] Muller, P., Mognol, P., and Hascoet, J.-Y., 2012, "Modeling and control of a direct laser powder deposition process for Functionally Graded Materials (FGM) parts manufacturing," Journal of Materials Processing Technology.

[126] Torquato, S., Hyun, S., and Donev, A., 2002, "Multifunctional composites: optimizing microstructures for simultaneous transport of heat and electricity," Physical review letters, 89(26), p. 266601.

[127] Kang, H., Lin, C.-Y., and Hollister, S. J., 2010, "Topology optimization of three dimensional tissue engineering scaffold architectures for prescribed bulk modulus and diffusivity," Structural and Multidisciplinary Optimization, 42(4), pp. 633-644.

[128] Sigmund, O., and Torquato, S., "Design of materials with extreme thermal expansion using a three-phase topology optimization method," Proc. Smart Structures and Materials' 97, International Society for Optics and Photonics, pp. 52-60.

[129] Dobson, D. C., and Cox, S. J., 1999, "Maximizing band gaps in two-dimensional photonic crystals," SIAM Journal on Applied Mathematics, 59(6), pp. 2108-2120.

[130] de Kruijf, N., Zhou, S., Li, Q., and Mai, Y. W., 2007, "Topological design of structures and composite materials with multiobjectives," International Journal of Solids and Structures, 44(22-23), pp. 7092-7109.

[131] Chen, Y., Zhou, S., and Li, Q., 2010, "Multiobjective topology optimization for finite periodic structures," Computers & Structures, 88(11), pp. 806-811.

[132] de Kruijf, N., Zhou, S., Li, Q., and Mai, Y.-W., 2007, "Topological design of structures and composite materials with multiobjectives," International Journal of Solids and Structures, 44(22), pp. 7092-7109.

[133] Cadman, J. E., Zhou, S., Chen, Y., and Li, Q., 2013, "On design of multi-functional microstructural materials," Journal of Materials Science, 48(1), pp. 51-66.

[134] Rodrigues, H., Guedes, J. M., and Bendsoe, M., 2002, "Hierarchical optimization of material and structure," Structural and Multidisciplinary Optimization, 24(1), pp. 1-10.

[135] Lin, C.-Y., Hsiao, C.-C., Chen, P.-Q., and Hollister, S. J., 2004, "Interbody fusion cage design using integrated global layout and local microstructure topology optimization," Spine, 29(16), pp. 1747-1754.

[136] Liu, L., Yan, J., and Cheng, G., 2008, "Optimum structure with homogeneous optimum truss-like material," Computers & Structures, 86(13–14), pp. 1417-1425.

[137] Deng, J., Yan, J., and Cheng, G., 2013, "Multi-objective concurrent topology optimization of thermoelastic structures composed of homogeneous porous material," Structural and

Multidisciplinary Optimization, 47(4), pp. 583-597.

[138] Yan, X., Huang, X., Zha, Y., and Xie, Y., 2014, "Concurrent topology optimization of structures and their composite microstructures," Computers & Structures, 133, pp. 103-110.

[139] Guo, X., Zhao, X., Zhang, W., Yan, J., and Sun, G., 2015, "Multi-scale robust design and optimization considering load uncertainties," Computer Methods in Applied Mechanics and Engineering, 283, pp. 994-1009.

[140] Khoda, A. K. M. B., and Koc, B., 2013, "Functionally heterogeneous porous scaffold design for tissue engineering," CAD Computer Aided Design, 45(11), pp. 1276-1293.

[141] Podshivalov, L., Gomes, C. M., Zocca, A., Guenster, J., Bar-Yoseph, P., and Fischer, A., "Design, analysis and additive manufacturing of porous structures for biocompatible micro-scale scaffolds," Proc. 1st CIRP Conference on BioManufacturing, pp. 247-252.

[142] Rajan, T., and Pai, B., 2014, "Developments in Processing of Functionally Gradient Metals and Metal–Ceramic Composites: A Review," Acta Metallurgica Sinica (English Letters), 27(5), pp. 825-838.

[143] Kaysser, W. A., and Ilschner, B., 1995, "FGM Research Activities in Europe," MRS Bulletin, 20(01), pp. 22-26.

[144] Vel, S. S., and Batra, R. C., 2002, "Exact Solution for Thermoelastic Deformations of Functionally Graded Thick Rectangular Plates," AIAA Journal, 40(7), pp. 1421-1433.

[145] Zhou, S., and Li, Q., 2008, "Design of graded two-phase microstructures for tailored elasticity gradients," Journal of Materials Science, 43(15), pp. 5157-5167.

[146] Radman, A., Huang, X., and Xie, Y., 2013, "Topology optimization of functionally graded cellular materials," Journal of Materials Science, 48(4), pp. 1503-1510.

[147] Radman, A., Huang, X., and Xie, Y. M., 2014, "Maximizing stiffness of functionally graded materials with prescribed variation of thermal conductivity," Computational Materials Science, 82(0), pp. 457-463.

[148] Nadeau, J. C., and Ferrari, M., 1999, "Microstructural optimization of a functionally graded transversely isotropic layer," Mechanics of Materials, 31(10), pp. 637-651.

[149] Cho, J. R., and Ha, D. Y., 2002, "Volume fraction optimization for minimizing thermal stress in Ni–Al2O3 functionally graded materials," Materials Science and Engineering: A, 334(1–2), pp. 147-155.

[150] Na, K.-S., and Kim, J.-H., 2010, "Volume fraction optimization for step-formed functionally graded plates considering stress and critical temperature," Composite Structures, 92(6), pp. 1283-1290.

[151] Cho, J. R., and Ha, D. Y., 2002, "Optimal tailoring of 2D volume-fraction distributions for

heat-resisting functionally graded materials using FDM," Computer Methods in Applied Mechanics and Engineering, 191(29–30), pp. 3195-3211.

[152] Hu, Y., Blouin, V. Y., and Fadel, G. M., 2008, "Design for Manufacturing of 3D Heterogeneous Objects With Processing Time Consideration," Journal of Mechanical Design, 130(3), pp. 031701-031701.

[153] Kou, X. Y., Parks, G. T., and Tan, S. T., 2012, "Optimal design of Functionally Graded Materials using a procedural model and Particle Swarm Optimization," CAD Computer Aided Design, 44(4), pp. 300-310.

[154] Na, K. S., and Kim, J. H., "Volume fraction optimization of functionally graded composite plates for stress reduction and thermo-mechanical buckling," Proc. AIP Conference Proceedings, pp. 706-711.

[155] Ootao, Y., Kawamura, R., Tanigawa, Y., and Imamura, R., 1999, "Optimization of material composition of nonhomogeneous hollow sphere for thermal stress relaxation making use of neural network," Computer Methods in Applied Mechanics and Engineering, 180(1–2), pp. 185-201.

[156] Elishakoff, I., Gentilini, C., and Viola, E., 2005, "Three-dimensional analysis of an all-round clamped plate made of functionally graded materials," Acta Mechanica, 180(1-4), pp. 21-36.

[157] Huang, J., Fadel, G. M., Blouin, V. Y., and Grujicic, M., 2002, "Bi-objective optimization design of functionally gradient materials," Materials & Design, 23(7), pp. 657-666.

[158] Biswas, A., Shapiro, V., and Tsukanov, I., 2004, "Heterogeneous material modeling with distance fields," Computer Aided Geometric Design, 21(3), pp. 215-242.

[159] Nemat-Alla, M., 2003, "Reduction of thermal stresses by developing two-dimensional functionally graded materials," International Journal of Solids and Structures, 40(26), pp. 7339-7356.

[160] Hedia, H., Shabara, M., El-Midany, T., and Fouda, N., 2004, "A method of material optimization of cementless stem through functionally graded material," International Journal of Mechanics and Materials in Design, 1(4), pp. 329-346.

[161] Hua, J., He, Y., and Qin, H., "Multiresolution heterogeneous solid modeling and visualization using trivariate simplex splines," Proc. Proceedings of the ninth ACM symposium on Solid modeling and applications, Eurographics Association, pp. 47-58.

[162] Martin, W., and Cohen, E., "Representation and extraction of volumetric attributes using trivariate splines: a mathematical framework," Proc. Proceedings of the sixth ACM symposium on Solid modeling and applications, ACM, pp. 234-240.

[163] Cho, J. R., and Shin, S. W., 2004, "Material composition optimization for heat-resisting FGMs by artificial neural network," Composites Part A: Applied Science and Manufacturing, 35(5), pp. 585-594.

[164] Vel, S. S., and Pelletier, J. L., 2007, "Multi-objective optimization of functionally graded thick shells for thermal loading," Composite Structures, 81(3), pp. 386-400.

[165] Zhang, X. D., Hong, Y. L., and Li, A. H., 2012, "Optimization of axial symmetrical FGM under the transient-state temperate field," International Journal of Minerals, Metallurgy and Materials, 19(1), pp. 59-63.

[166] Fereidoon, A., Sadri, F., and Hemmatian, H., 2012, "Functionally graded materials optimization using particle swarm-based algorithms," Journal of Thermal Stresses, 35(4), pp. 377-392.

[167] Parashkevova, L., Ivanova, J., and Bontcheva, N., 2004, "Optimal design of functionally graded plates with thermo-elastic plastic behaviour," Comptes Rendus Mécanique, 332(7), pp. 493-498.

[168] Chen, F., and Jie, W., 2007, "Finite element design of MgO/Ni system functionally graded materials," Journal of Materials Processing Technology, 182(1-3), pp. 181-184.

[169] Mozafari, H., Abdi, B., and Ayob, A., 2012, "Optimization of temperature-dependent functionally graded material based on Colonial Competitive Algorithm," Applied Mechanics and Materials, pp. 4575-4580.

[170] Xu, Y., Zhang, W., Chamoret, D., and Domaszewski, M., 2012, "Minimizing thermal residual stresses in C/SiC functionally graded material coating of C/C composites by using particle swarm optimization algorithm," Computational Materials Science, 61, pp. 99-105.

[171] Noh, Y. J., Kang, Y. J., Youn, S. J., Cho, J. R., and Lim, O. K., 2013, "Reliability-based design optimization of volume fraction distribution in functionally graded composites," Computational Materials Science, 69, pp. 435-442.

[172] Goupee, A. J., and Vel, S. S., 2007, "Multi-objective optimization of functionally graded materials with temperature-dependent material properties," Materials and Design, 28(6), pp. 1861-1879.

[173] Turteltaub, S., 2002, "Functionally graded materials for prescribed field evolution," Computer Methods in Applied Mechanics and Engineering, 191(21–22), pp. 2283-2296.

[174] Turteltaub, S., 2002, "Optimal control and optimization of functionally graded materials for thermomechanical processes," International Journal of Solids and Structures, 39(12), pp. 3175-3197.

[175] Cho, J., and Park, H., 2003, "Effective volume‐fraction optimization for thermal stress reduction in FGMs using irregular h‐refinement," International journal for numerical methods in engineering, 58(5), pp. 749-770.

[176] Vel, S. S., and Goupee, A. J., "Multi-objective optimization of geometric dimensions and material composition of functionally graded components," Proc. AIP Conference Proceedings, pp. 610-615.

[177] Nemat-Alla, M., 2009, "Reduction of thermal stresses by composition optimization of two-dimensional functionally graded materials," Acta Mechanica, 208(3-4), pp. 147-161.

[178] Maciejewski, G., and Mróz, Z., 2013, "Optimization of functionally gradient materials in valve design under cyclic thermal and mechanical loading," Computer Assisted Mechanics and Engineering Sciences, 20(2), pp. 99-112.

[179] Lipton, R., 2002, "Design of functionally graded composite structures in the presence of stress constraints," International Journal of Solids and Structures, 39(9), pp. 2575-2586.

[180] Stump, F. V., Silva, E. C. N., and Paulino, G. H., "Topology optimization with stress constraints: Reduction of stress concentration in functionally graded structures," Proc. AIP Conference Proceedings, pp. 303-308.

[181] Batra, R. C., and Jin, J., 2005, "Natural frequencies of a functionally graded anisotropic rectangular plate," Journal of Sound and Vibration, 282(1), pp. 509-516.

[182] Rubio, W. M., Paulino, G. H., and Silva, E. C. N., 2011, "Tailoring vibration mode shapes using topology optimization and functionally graded material concepts," Smart Materials and Structures, 20(2).

[183] Qian, L. F., and Batra, R. C., 2005, "Design of bidirectional functionally graded plate for optimal natural frequencies," Journal of Sound and Vibration, 280(1–2), pp. 415-424.

[184] Rubio, W. M., and Silva, E. C. N., "Toward design of functionally graded piezoelectric ultrasonic motors using topology optimization," Proc. Proceedings - IEEE Ultrasonics Symposium.

[185] Carbonari, R. C., and Silva, E. C. N., 2010, "Integral piezoactuator system with optimum placement of functionally graded material-a topology optimization paradigm," Journal of Intelligent Material Systems and Structures, p. 1045389X10386129.

[186] Rubio, W. M., Buiochi, F., Adamowski, J. C., and Silva, E. C. N., "Topology optimized design of functionally graded piezoelectric ultrasonic transducers," Proc. Physics Procedia, pp. 891-896.

[187] Amigo, R. C. R., Vatanabe, S. L., and Silva, E. C. N., 2013, "Design, manufacturing and characterization of functionally graded flextensional piezoelectric actuators," Journal of Physics: Conference Series, 419(1).

[188] Carbonari, R. C., Silva, E. C. N., and Paulino, G. H., 2007, "Topology optimization design of functionally graded bimorph-type piezoelectric actuators," Smart Materials and Structures, 16(6), pp. 2605-2620.

[189] Lin, D., Li, Q., Li, W., Zhou, S., and Swain, M. V., 2009, "Design optimization of functionally graded dental implant for bone remodeling," Composites Part B: Engineering, 40(7), pp. 668-675.

[190] Lin, D., Li, Q., Li, W., and Swain, M., 2010, "Bone remodeling induced by dental implants

of functionally graded materials," Journal of Biomedical Materials Research Part B: Applied Biomaterials, 92(2), pp. 430-438.

[191] Sadollah, A., and Bahreininejad, A., 2011, "Optimum gradient material for a functionally graded dental implant using metaheuristic algorithms," Journal of the Mechanical Behavior of Biomedical Materials, 4(7), pp. 1384-1395.

[192] Bahraminasab, M., Sahari, B. B., Edwards, K. L., Farahmand, F., Hong, T. S., Arumugam, M., and Jahan, A., 2014, "Multi-objective design optimization of functionally graded material for the femoral component of a total knee replacement," Materials and Design, 53, pp. 159-173.

[193] Cui, C., and Sun, J., 2014, "Optimizing the design of bio-inspired functionally graded material (FGM) layer in all-ceramic dental restorations," Dental Materials Journal, 33(2), pp. 173-178.

[194] Gasik, M., Keski-Honkola, A., Bilotsky, Y., and Friman, M., 2014, "Development and optimisation of hydroxyapatite-ß-TCP functionally gradated biomaterial," Journal of the Mechanical Behavior of Biomedical Materials, 30, pp. 266-273.

[195] Hedia, H. S., and Fouda, N., 2014, "Design optimization of cementless hip prosthesis coating through functionally graded material," Computational Materials Science, 87, pp. 83-87.

[196] Chen, K.-Z., and Feng, X.-A., 2003, "Computer-aided design method for the components made of heterogeneous materials," Computer-Aided Design, 35(5), pp. 453-466.

[197] Chen, K.-Z., and Feng, X.-A., 2004, "CAD modeling for the components made of multi heterogeneous materials and smart materials," Computer-Aided Design, 36(1), pp. 51-63.

[198] Kumar, V., Burns, D., Dutta, D., and Hoffmann, C., 1999, "A framework for object modeling," Computer-Aided Design, 31(9), pp. 541-556.

[199] Zhang, H., 2014, "Topology of fiber bundles," Master, Kansas State University.

[200] Otto, K. N., and Wood, K. L., 2001, Product design : techniques in reverse engineering and new product development, Prentice Hall, Upper Saddle River, NJ.

[201] Whiteley, M., White, D., Benzley, S., and Blacker, T., 1996, "Two and three-quarter dimensional meshing facilitators," Engineering with computers, 12(3-4), pp. 144-154.

[202] Altair Engineering, I., 2013, "HyperWorks User's Guide," Altair Engineering, Inc.

[203] Owen, S. J., "A survey of unstructured mesh generation technology," Proc. IMR, pp. 239-267.

[204] Si, H., 2015, "TetGen, a Delaunay-Based Quality Tetrahedral Mesh Generator," ACM Trans. Math. Softw., 41(2), pp. 1-36.

[205] Lloyd, S., 1982, "Least squares quantization in PCM," IEEE transactions on information

theory, 28(2), pp. 129-137.

[206] Du, Q., Faber, V., and Gunzburger, M., 1999, "Centroidal Voronoi tessellations: Applications and algorithms," SIAM review, 41(4), pp. 637-676.

[207] Gomes, A., Voiculescu, I., Jorge, J., Wyvill, B., and Galbraith, C., 2009, Implicit curves and surfaces: mathematics, data structures and algorithms, Springer Science & Business Media.

[208] Nishimura, H., Hirai, M., Kawai, T., Kawata, T., Shirakawa, I., and Omura, K., 1985, "Object modeling by distribution function and a method of image generation," The Transactions of the Institute of Electronics and Communication Engineers of Japan, 68(Part 4), pp. 718-725.

[209] Dutta, D., and Shpitalni, M., 2000, "Heterogeneous solid modeling for layered manufacturing," CIRP Annals - Manufacturing Technology, 49(1), pp. 109-112.

[210] Museth, K., 2013, "VDB: High-resolution sparse volumes with dynamic topology," ACM Transactions on Graphics (TOG), 32(3), p. 27.

[211] Yushkevich, P. A., Piven, J., Hazlett, H. C., Smith, R. G., Ho, S., Gee, J. C., and Gerig, G., 2006, "User-guided 3D active contour segmentation of anatomical structures: significantly improved efficiency and reliability," Neuroimage, 31(3), pp. 1116-1128.

[212] Cignoni, P., Corsini, M., and Ranzuglia, G., 2008, "Meshlab: an open-source 3d mesh processing system," Ercim news, 73(45-46), p. 6.

[213] Levoy, M., 1990, "A hybrid ray tracer for rendering polygon and volume data," IEEE Computer graphics and Applications, 10(2), pp. 33-40.

[214] Lorensen, W. E., and Cline, H. E., "Marching cubes: A high resolution 3D surface construction algorithm," Proc. ACM siggraph computer graphics, ACM, pp. 163-169.

[215] Brown, D. C., 2003, "Functional, Behavioral and Structural Features," (37017b), pp. 895-900.

[216] Sticklen, J., and Bond, W. E., 1991, "Functional reasoning and functional modelling," IEEE Expert, 6(2), pp. 20-47.

[217] Hirtz, J., Stone, R. B., McAdams, D. A., Szykman, S., and Wood, K. L., 2002, "A functional basis for engineering design: reconciling and evolving previous efforts," Research in engineering Design, 13(2), pp. 65-82.

[218] Otto, K. N., 1992, "A formal representational theory for engineering design," California Institute of Technology.

[219] Maidin, S. B., Campbell, I., and Pei, E., 2012, "Development of a design feature database to support design for additive manufacturing," Assembly Automation, 32(3), pp. 235-244.

[220] Panesar, A., Brackett, D., Ashcroft, I., Wildman, R., and Hague, R., 2015, "Design

Framework for Multifunctional Additive Manufacturing: Placement and Routing of Three-Dimensional Printed Circuit Volumes," Journal of Mechanical Design, 137(11), pp. 111414-111414.

[221] Amos, M., Matthew, C., and Wimhurst, S., 2013, "3D Printed Prosthetic Arm," University of Nottingham, Nottingham, UK.

[222] Ashby, M. F., and Bréchet, Y. J. M., 2003, "Designing hybrid materials," Acta Materialia, 51(19), pp. 5801-5821.

[223] CRABCAD, 2014, "GE jet engine bracket challenge," https://grabcad.com/challenges/ge-jet-engine-bracket-challenge.

[224] Liu, K., Detwiler, D., and Tovar, A., 2016, "Machine Learning and Metamodel-Based Design Optimization of Nonlinear Multimaterial Structures," (50114), p. V02BT03A015.

[225] Michalski, R. S., Carbonell, J. G., and Mitchell, T. M., 2013, Machine learning: An artificial intelligence approach, Springer Science & Business Media.

[226] Tang, Y., and Zhao, Y., "Lattice-skin Structures Design with Orientation Optimization," Proc. Solid Freeform Fabrication.

[227] Zhou, M., Zheng, G., and Chen, Z. C., 2016, "An automated CNC programming approach to machining pocket with complex islands and boundaries by using multiple cutters in hybrid tool path patterns," The International Journal of Advanced Manufacturing Technology, 83(1-4), pp. 407-420.

[228] Ma, W.-C., Wu, F.-C., and Ouhyoung, M., "Skeleton extraction of 3d objects with radial basis functions," Proc. Shape Modeling International, 2003, IEEE, pp. 207-215.

[229] Stanković, T., Mueller, J., Egan, P., and Shea, K., 2015, "A generalized optimality criteria method for optimization of additively manufactured multimaterial lattice structures," Journal of Mechanical Design, 137(11), p. 111405.

[230] Zheng, P., Wang, Y., Xu, X., and Xie, S. Q., 2016, "A weighted rough set based fuzzy axiomatic design approach for the selection of AM processes," The International Journal of Advanced Manufacturing Technology, pp. 1-14.

[231] Mançanares, C. G., Zancul, E. d. S., da Silva, J. C., and Miguel, P. A. C., 2015, "Additive manufacturing process selection based on parts' selection criteria," The International Journal of Advanced Manufacturing Technology, 80(5-8), pp. 1007-1014.

[232] Haykin, S., 1998, Neural Networks: A Comprehensive Foundation, Prentice Hall PTR.

[233] Tang, Y., Dong, G., Zhou, Q., and Zhao, Y. F., 2017, "Lattice Structure Design and Optimization With Additive Manufacturing Constraints," IEEE Transactions on Automation Science and Engineering.

[234] Querin, O. M., Steven, G. P., and Xie, Y. M., 1998, "Evolutionary structural optimisation (ESO) using a bidirectional algorithm," Engineering Computations (Swansea, Wales), 15(8), pp. 1031-1048.

[235] Huang, X., and Xie, Y., 2007, "Convergent and mesh-independent solutions for the bi-directional evolutionary structural optimization method," Finite Elements in Analysis and Design, 43(14), pp. 1039-1049.

[236] Frost, H. M., 1994, "Wolff's Law and bone's structural adaptations to mechanical usage: an overview for clinicians," The Angle Orthodontist, 64(3), pp. 175-188.

[237] Rezaie, R., Badrossamay, M., Ghaie, A., and Moosavi, H., 2013, "Topology Optimization for Fused Deposition Modeling Process," Procedia CIRP, 6, pp. 521-526.

[238] Meyer, U., and Wiesmann, H. P., 2006, Bone and cartilage engineering, Springer Science & Business Media.

[239] Mistree, F., Hughes, O. F., and Bras, B., 1993, "Compromise decision support problem and the adaptive linear programming algorithm," Progress in Astronautics and Aeronautics, 150, pp. 251-251.

[240] Hassani, B., and Hinton, E., 1998, "A review of homogenization and topology optimization I—homogenization theory for media with periodic structure," Computers & Structures, 69(6), pp. 707-717.

[241] Hill, R., 1963, "Elastic properties of reinforced solids: some theoretical principles," Journal of the Mechanics and Physics of Solids, 11(5), pp. 357-372.

[242] Fritsch, F. N., and Carlson, R. E., 1980, "Monotone piecewise cubic interpolation," SIAM Journal on Numerical Analysis, 17(2), pp. 238-246.

[243] Lambe, A. B., and Martins, J. R., 2012, "Extensions to the design structure matrix for the description of multidisciplinary design, analysis, and optimization processes," Structural and Multidisciplinary Optimization, 46(2), pp. 273-284.

[244] Associates, R. M. a., 2016, "RhinoCommon SDK," http://developer.rhino3d.com/api/RhinoCommonWin/html/N_Rhino.htm.

[245] Microsoft, 2017, ".NET Framework Class Library," https://msdn.microsoft.com/en-us/library/gg145045(v=vs.110).aspx.

[246] Bochkanov, S., and Bystritsky, V., 2011, "ALGLIB-a cross-platform numerical analysis and data processing library," ALGLIB Project. Novgorod, Russia.

[247] Halvorson, M., 2013, Microsoft visual basic 2013 step by step, Pearson Education.

[248] Guide, M. U. s., 1998, "The mathworks," Inc., Natick, MA, 5, p. 333.

[249] Javir, A., Pawar, K., Dhudum, S., Patale, N., and Patil, S., 2015, "Design, Analysis and Fabrication of Quadcopter," Journal of The International Association of Advanced Technology and Science, 16(11).

[250] Gaponov, I., and Razinkova, A., "Quadcopter design and implementation as a multidisciplinary engineering course," Proc. Teaching, Assessment and Learning for Engineering (TALE), 2012 IEEE International Conference on, IEEE, pp. H2B-16-H12B-19.

[251] Boresi, A. P., Schmidt, R. J., and Sidebottom, O. M., 1993, Advanced mechanics of materials, Wiley New York.

[252] Zortrax, 2017, "Z-suite," https://zortrax.com/products/z-suite/.

Appendix A. Comparison between different types of AM processes

Category Name	Construction Method for Layer	Material Type	Raw material state	Main Applications	Main Advantages	Main Disadvantages	Support Structure Needed
Material jetting	Deposit droplet of build material	Wax, Polymer, Metal	Liquid or Solid	Prototypes, Casting Pattern, Injection molding	High accuracy, Multi-material fabrication	Material types limited	Yes
Binder jetting	Deposit droplet of binder to connect build material	Metal, Ceramics, Polymer, Sand, Glass, Composite	Powder	Prototypes, Green parts, Casting patterns, Molds and cores	Fast and cheap, widening set of materials is available	Limited mechanical properties	No
Material Extrusion	Extrude material through nozzle in a controlled manner	Polymer, Composite	Filament	Prototypes, Scaffolds, End-use part	Multi-material structure, Simple and cheap	Fabrication speed is very slow	Yes
Powder bed fusion	Fuse selective part of powder bed through thermal source	Metals, Ceramic and Polymer	Powder	Prototypes, Tools for injection mold, End-use Part	Good Material properties widening set of materials is available	Expensive, surface finish is limited, difficult to remove support structure	Polymer-No Other-Yes
Vat photopolymerization	Selectively cure photopolymer in vat by UV light	Photopolymer	Liquid	Prototypes, Casting pattern	Cheap, Good accuracy and surface finish	Limited material types and mechanical properties	Yes
Sheet lamination	Bond cut sheet into solid part	Metal or paper	Sheet or tape	Prototypes, End-use part	Relatively high speed, Multi-material part fabrication	Poor surface finish,	No
Directed Energy Deposition	Material is deposited and fused simultaneously for a solid part	Metal	Powder	Prototypes, End-use part, Part maintain	Multi-material fabrication, fix damaged part, less support needed	Expensive, difficult to remove support structure	Yes

Appendix B. Sensitive analysis of multifunctional design case

In this appendix, the detailed steps of calculating derivatives of performance parameters with respect to design parameters for the design problem introduced in Section 6.5 are given. For this design problem, its F-P-P-D model is given in Figure 6-1. It is clear that some of performance parameters are coupled by the defined relations between performance domain and property domain. To solve this coupled system, a typical multidisciplinary analysis method is applied.

Particularly for this design problem, two performance parameters: structural compliance and heat flow rate for a given surface are considered in the achievement functions. The explicit expression of these two performance parameters can be easily obtained based on governing equations of R1 and R6 respectively, which are given below.

$$C = \frac{1}{2}(P^0 + P^{th})^T U \tag{B-1}$$

$$Q = H(k)T \tag{B-2}$$

In this design problem, other performance parameters including displacement U, temperature distribution T, thermal stress P^{th} and property parameters elastic tensor and heat conductivity can be regarded as the state variables. The governing equations related to those state variables can be rewritten into the residual form as:

$$R_3 = K(E)U - P^t - P^0 \tag{B-3}$$

$$R_4 = P^t - \sum(\alpha(x_i) \int_\Omega {B_i}^T D_i(E)\left(T - T_{ref}\right)\phi^T d\Omega) \tag{B-4}$$

$$R_5 = (K_t(k) + H_t)T - q_t - q_h \tag{B-5}$$

$$R_8 = h_E(x) - E \tag{B-6}$$

$$R_9 = h_k(x) - k \tag{B-7}$$

Where h_E and h_k are the constructed interpolation function for homogenized properties discussed in Section 6.4.2. Based on the residual form of governing equations, the adjoint vector can be solved from two equations given below:

$$\mathrm{A}=\begin{bmatrix} \frac{\partial R_3}{\partial U}^T & \frac{\partial R_4}{\partial U}^T & \frac{\partial R_5}{\partial U}^T & \frac{\partial R_8}{\partial U}^T & \frac{\partial R_9}{\partial U}^T \\ \frac{\partial R_3}{\partial P^t}^T & \frac{\partial R_4}{\partial P^t}^T & \frac{\partial R_5}{\partial P^t}^T & \frac{\partial R_8}{\partial P^t}^T & \frac{\partial R_9}{\partial P^t}^T \\ \frac{\partial R_3}{\partial T}^T & \frac{\partial R_4}{\partial T}^T & \frac{\partial R_5}{\partial T}^T & \frac{\partial R_8}{\partial T}^T & \frac{\partial R_9}{\partial T}^T \\ \frac{\partial R_3}{\partial E}^T & \frac{\partial R_4}{\partial E}^T & \frac{\partial R_5}{\partial E}^T & \frac{\partial R_8}{\partial E}^T & \frac{\partial R_9}{\partial E}^T \\ \frac{\partial R_3}{\partial k}^T & \frac{\partial R_4}{\partial k}^T & \frac{\partial R_5}{\partial k}^T & \frac{\partial R_8}{\partial k}^T & \frac{\partial R_9}{\partial k}^T \end{bmatrix} \tag{B-8}$$

$$A\begin{bmatrix}\psi_3^C\\ \psi_4^C\\ \psi_5^C\\ \psi_8^C\\ \psi_9^C\end{bmatrix}=\begin{bmatrix}\frac{\partial C}{\partial U}\\ \frac{\partial C}{\partial P^t}\\ \frac{\partial C}{\partial T}\\ \frac{\partial C}{\partial E}\\ \frac{\partial C}{\partial k}\end{bmatrix} \tag{B-9}$$

$$A\begin{bmatrix}\psi_3^Q\\ \psi_4^Q\\ \psi_5^Q\\ \psi_8^Q\\ \psi_9^Q\end{bmatrix}=\begin{bmatrix}\frac{\partial Q}{\partial U}\\ \frac{\partial Q}{\partial P^t}\\ \frac{\partial Q}{\partial T}\\ \frac{\partial Q}{\partial E}\\ \frac{\partial Q}{\partial k}\end{bmatrix} \tag{B-10}$$

It should be noted some elements in the adjoint matrix A are equal to zero for this particular design since the relations between those functional performance and property parameters are not fully coupled. By solving Equation 33 and Equation 34, the adjoint vectors ψ^C and ψ^Q can be obtained. These two adjoint vector can be applied to calculate the derivatives of selected performance parameters with respect to design variables by the equations shown below:

$$\frac{dC}{dx_j} = -\psi_8^{C^T} \frac{\partial R_8}{\partial x_j} - -\psi_9^{C^T} \frac{\partial R_9}{\partial x_j} \tag{B-11}$$

$$\frac{dQ}{dx_j} = -\psi_8^{Q^T} \frac{\partial R_8}{\partial x_j} - -\psi_9^{Q^T} \frac{\partial R_9}{\partial x_j} \tag{B-12}$$

Appendix C. User Interface of Intralattice

In this appendix, the developed UI for Intralattice will be summarized. Its major function will be briefly introduced.

Figure C-1 shows the main window of the developed of Intralattice. The major function of this window is to manage the design flow of mesoscale lattice structures. It consists of three major parts. On the top, there is a typical drop-down menu bar. Under the menu "File", there are two sub-items: New and Save, which are shown in Figure C-2. These two sub-items are used to create a new project as well as saving an existing project. Under the menu "Options", there are three sub-items. The first one is called configuration. This sub-item can be used to set the parameters of a optimization algorithm as well as voxelization process. The dialogues which is used to set the parameters for BESO and heuristic based optimization algorithms are shown in Figure C-3. As to the dialogue of voxel size, it is shown in Figure C-4.

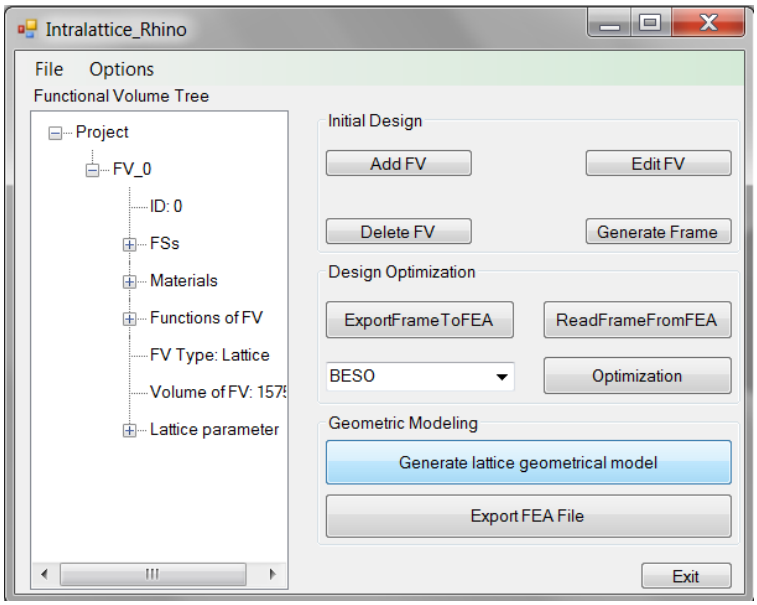

Figure C-1 Main window of Intralattice

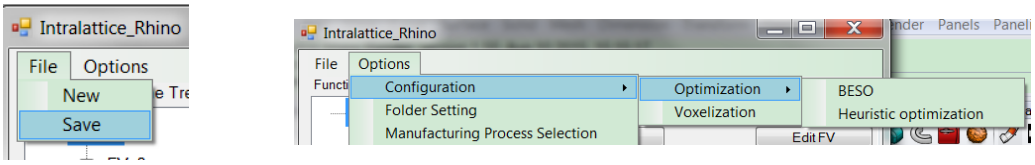

Figure C-2 The drop-down menu of main window of Intralattice

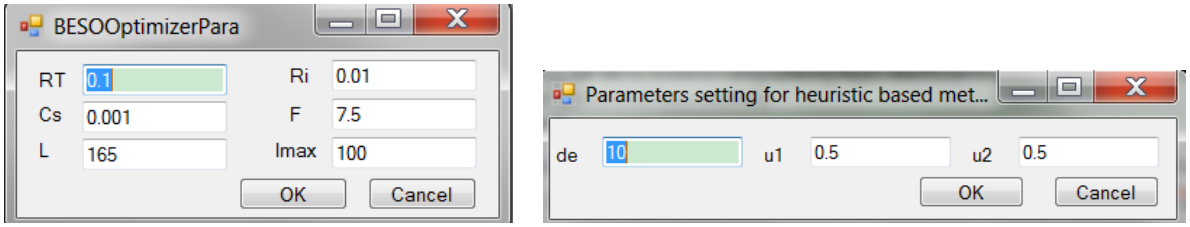

(a) Dialogue to set BESO optimization parameter (b) The dialogue to set heuristic based optimization parameter

Figure C-3 Dialogues to set the parameters of optimization algorithms

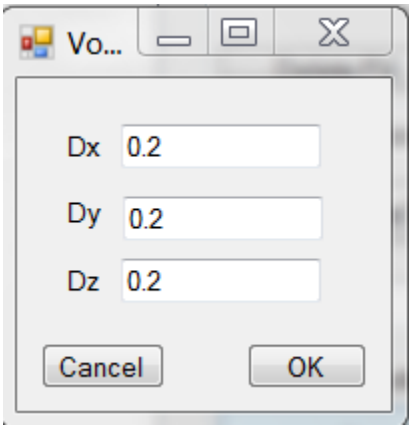

Figure C-4 Configuration window of voxel size

The second sub-item under "Options" drop-down menu is the Folder setting. The dialogue which can set input and output directory of the design tool is presented in Figure C-5. When the operation during the major design flow needs to read or output files, it will automate to search the given files in the pre-set file directory in this dialogue. The third sub-items under the "Options" drop down menu is the manufacturing process selection. The window corresponds this sub-item has been shown in Figure C-6. In this window, there are three pull-down lists in which designers can set manufacturing related parameters. In the current version of Intralattice, the

manufacturability database of lattice structures is only available for certain types of machines under certain groups of process parameters. Thus, designers can select available machine and its related process parameters from the drop-down lists. To view the details of process parameters, designers can click the “View Parameter” button.

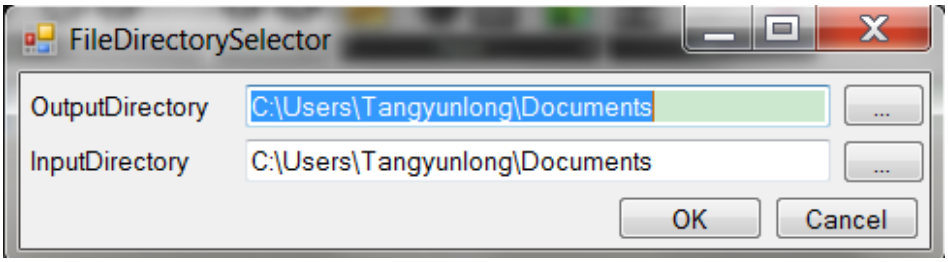

Figure C-5 The dialogue for file directory setting

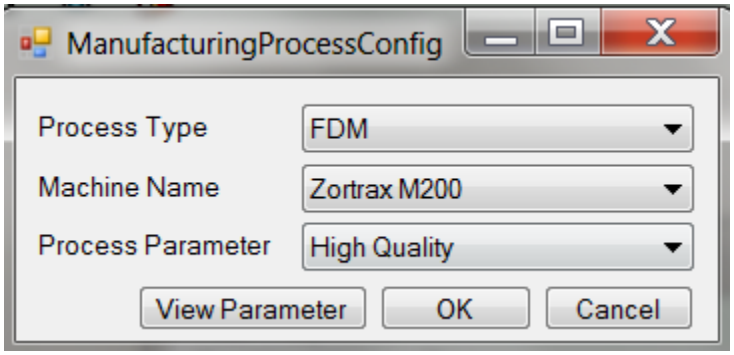

Figure C-6 Manufacturing process configuration

Besides the drop-down menu, on the left side of the main window of Intralattice, there is a structure tree which shows the defined FVs and its related information. In this tree structure, the FSs is viewed as child nodes under the FVs. This tree can help designers to review the information for those defined FVs.

On the right-hand side of the main window, there are several buttons which are organized into three group boxes. Each box represents one design stage. By clicking those buttons, the specific operation will be done to help designers to optimize and generate lattice structures.

To create FV and edit FV, the window of FV editor is developed and shown in Figure C-7. In

this window, the information of FV can be edited by the designers. This window consists of five group-boxes. In the first group-box, the basic information of FV can be edited. It should be noted that the ID of each FV is uniquely distributed by the software. Thus, it cannot be changed by designers. But designers can see it in the corresponding text-box in this window.

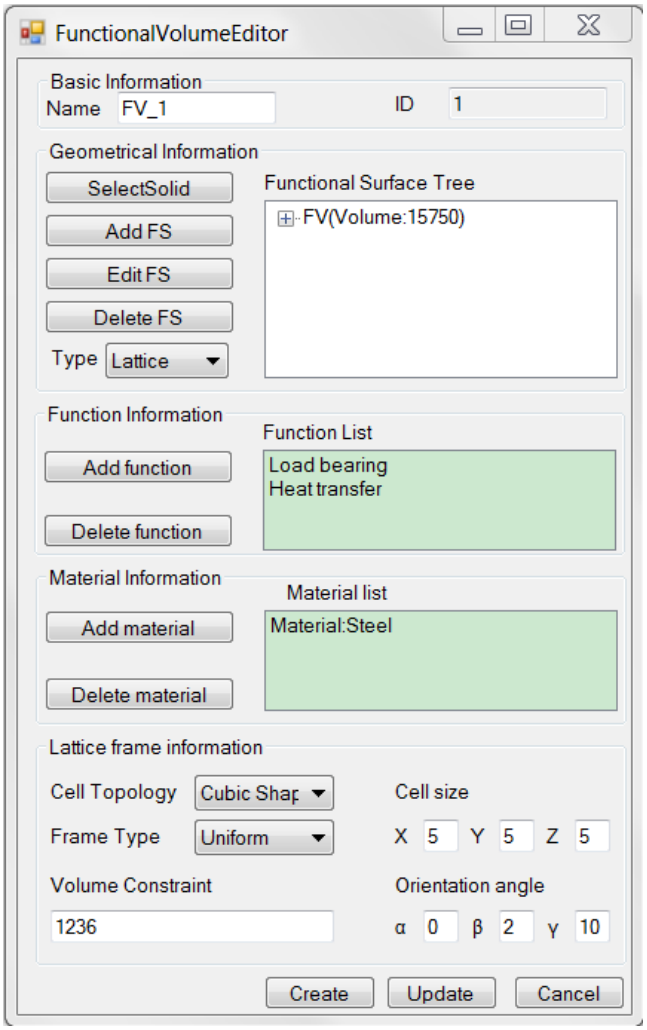

Figure C-7 The window of FV editor

The second group-box mainly focuses on the geometric information of FV. Designers can select a solid region as the boundary of FV in the CAD software by clicking the button called "SelectSolid". Information of FSs should also be defined in this group-box. There are three buttons in this group-box which represent the major operations on FV. By clicking "Add FV" button, the

new window of FSs editor will be open automatically. In this window, designers can define the geometric element of FSs as well as its major functions. In current version of Intralattice, FSs can be classified into three types. The first type of FS is defined void, which means there is no additional requirements on the lattice structures near this FSs. The second type of FS is defined as conformal. This type means the cell shape and size should be changed to adapt to the shape of selected surfaces according to the provided method discussed in Chapter 4 of this thesis. The last type of FS is the strictly trimmed boundary. On the boundary of this type FS, the lattice structures should be strictly trimmed.

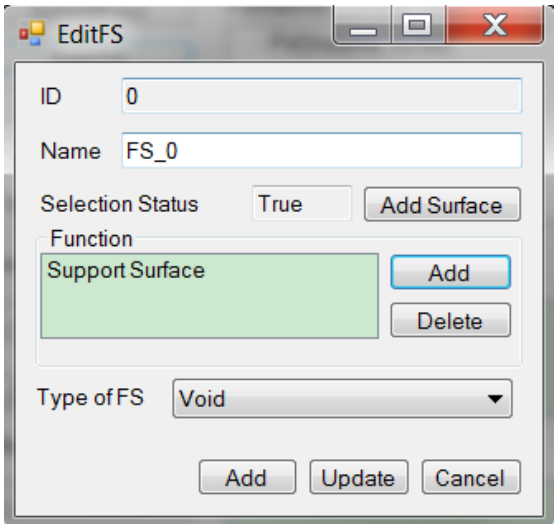

Figure C-8 The window of FSs editor

The third group-box of the FV editor window shown in Figure C-7 is related to functional information of designed FV. By clicking “Add Function” button, the function definition editor shown in Figure C-9 will be shown. In this window, designers can define the function of a FV.

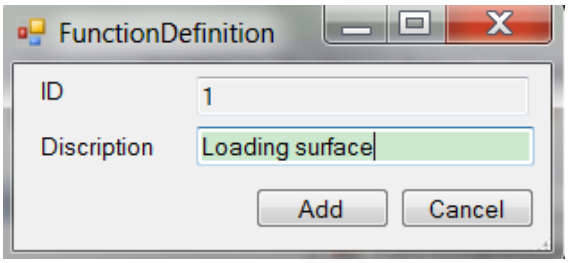

Figure C-9 Function definition editor

The fourth box-group in the FV editor is related to material information. By clicking "Add Material" button, the material editor shown in Figure C-10 will be displayed. In this window, designers can define the material properties of lattice structures.

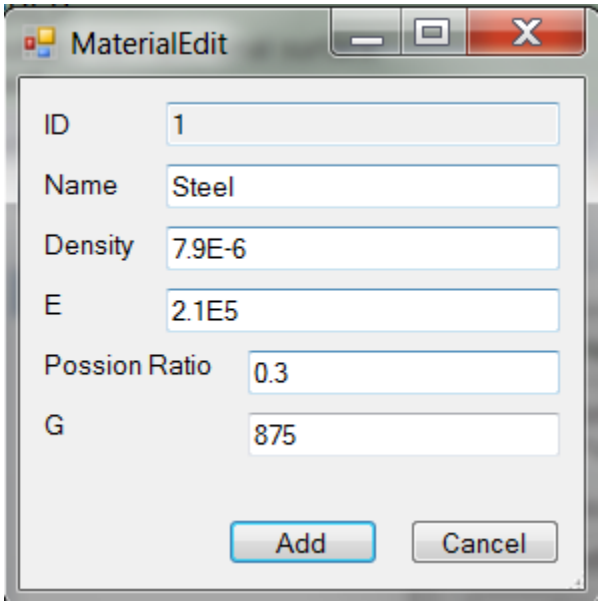

Figure C-10 Material properties editor

The last box-group in the FV editor shown in Figure C-7 is related to lattice parameters. If the FV is determined to fill with lattice structures. The parameters input in this region can be used to build the lattice frame. For those FV with solid material, the parameters defined in this region are useless.

Besides those windows discussed above which help designers to interactively define the FV and related FSs during the design process, there is another window which is developed in

Intralattice to show the optimization process. It is called as optimization monitoring window. In this window, several line graphs are displayed to show the convergence of the BESO based optimization algorithm. As it is shown in Figure C-11, the PI value, maximum Von-Mises stress and maximum displacement of a structure can be displayed in this window.

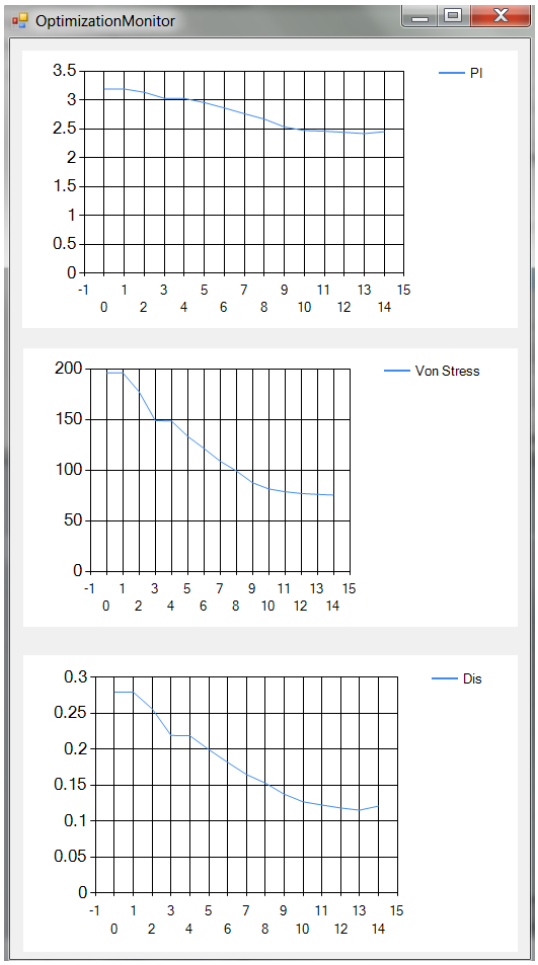

Figure C-11 The window of optimization process monitoring

Appendix D. List of publications

Journal Papers

[D1] **Tang, Y.,** Kurtz, A., and Zhao, Y. F., 2015, "Bidirectional Evolutionary Structural Optimization (BESO) based design method for lattice structure to be fabricated by additive manufacturing," Computer-Aided Design, 69, pp. 91-101.

[D2] **Tang, Y.,** Zhou, Y., Hoff, T., Garon, M., and Zhao, Y., 2016, "Elastic modulus of 316 stainless steel lattice structure fabricated via binder jetting process," Materials Science and Technology, 32(7), pp. 648-656.

[D3] **Tang, Y.,** and Zhao, Y. F., 2016, "A survey of the design methods for additive manufacturing to improve functional performance," Rapid Prototyping Journal, 22(3), pp. 569-590.

[D4] **Tang, Y.,** Mak, K., and Zhao, Y. F., 2016, "A framework to reduce product environmental impact through design optimization for additive manufacturing," Journal of Cleaner Production.

[D5] **Tang, Y.,** Dong, G., Zhou, Q., and Zhao, Y. F., 2017, "Lattice Structure Design and Optimization with Additive Manufacturing Constraints," IEEE Transactions on Automation Science and Engineering. doi: 10.1109/TASE.2017.2685643

[D6] **Tang, Y**, Zhao, Y. F., 2017, " Multifunctional Design of Heterogeneous Cellular Structures for Additive Manufacturing". Submitted to Structural and Multidisciplinary Optimization (Submitted under review)

[D7] Yang, S., **Tang, Y.,** and Zhao, Y. F., 2015, "A new part consolidation method to embrace the design freedom of additive manufacturing," Journal of Manufacturing Processes, 20, pp. 444-449.

[D8] Dong, G., **Tang, Y.,** and Zhao, Y. F., 2017, A Survey of Modeling of Lattice Structures Fabricated by Additive Manufacturing, Journal of Mechanical Design, (Accepted, under

publication process)

Book Chapter

[D9] **Tang, Y.,** Yang, S., and Zhao, Y. F., 2016, "Sustainable Design for Additive Manufacturing Through Functionality Integration and Part Consolidation," Handbook of Sustainability in Additive Manufacturing: Volume 1, S. S. Muthu, and M. M. Savalani, eds., Springer Singapore, Singapore, pp. 101-144.

Peer-reviewed Conference Papers

[D10] **Tang, Y.,** Hascoet, J.-Y., and Zhao, Y. F., "Integration of topological and functional optimization in design for additive manufacturing," Proc. ASME 2014 12th Biennial Conference on Engineering Systems Design and Analysis, American Society of Mechanical Engineers, pp. V001T006A006-V001T006A006, Copenhagen, Denmark, 2014 June.

[D11] **Tang, Y.,** and Zhao, Y. F., "Design Method for Lattice-Skin Structure Fabricated by Additive Manufacturing," Proc. ASME 2014 International Mechanical Engineering Congress and Exposition, American Society of Mechanical Engineers, pp. V02BT02A030-V002BT002A030, Montreal, Quebec, Canada, 2014 Nov.

[D12] **Tang, Y.,** and Zhao, Y., "Lattice-skin Structures Design with Orientation Optimization," Proc. Solid Freeform Fabrication, Austin, Texas, US, 2015 Aug.

[D13] **Tang, Y.,** Sheng, Y., and Zhao, Y. F., "Design Method for Conformal Lattice-Skin Structure Fabricated BY AM Technologies," ASME 2016 International Design Engineering Technical Conferences and Computers and Information in Engineering Conference, ASME, Charlotte, NC, USA, 2016 Aug.

[D14] Zhou, Y., **Tang, Y.,** Hoff, T., Garon, M., and Zhao, F. Y., 2015, "The Verification of the Mechanical Properties of Binder Jetting Manufactured Parts by Instrumented Indentation Testing,"

Procedia Manufacturing, 1, pp. 327-342. Charlotte, NC, USA, 2015 June.

[D15] Yang, F., **Tang, Y.**, and Zhao, Y. F., "Manufacturability of Overhang Structures Fabricated by Binder Jetting Process," Proc. ASME 2016 International Mechanical Engineering Congress and Exposition, American Society of Mechanical Engineers, pp. V002T002A063-V002T002A063, ASME, Phenoix, Arizona, 2016 Nov.

[D16] Yang, S., **Tang, Y**., and Zhao, Y. F., "Assembly-Level Design for Additive Manufacturing: Issues and Benchmark," Proc. ASME 2016 International Design Engineering Technical Conferences and Computers and Information in Engineering Conference, American Society of Mechanical Engineers, pp. V02AT03A028-V002AT003A028, Charlotte, NC, USA, 2015 June.

[D17] Zhou, Y., Chen, H., **Tang, Y.,** Gopinath, S., Xu, X., and Zhao, Y. F., "Simulation and optimization framework for additive manufacturing processes," Proc. Innovative Design and Manufacturing (ICIDM), Proceedings of the 2014 International Conference on, IEEE, pp. 34-40, Montreal, QC, Canada, 2014,Aug.

[D18] Luo, Z., Yang, F., Dong, G., **Tang, Y.**, and Zhao, Y. F., "Orientation Optimization in Layer-Based Additive Manufacturing Process," Proc. ASME 2016 International Design Engineering Technical Conferences and Computers and Information in Engineering Conference, American Society of Mechanical Engineers, pp. V01AT02A039-V001AT002A039, ASME, Charlotte, NC, USA, 2016 Aug.

Abstracts of major journal publications

Journal Publication D1

Computer-Aided Design 69 (2015) 91–101

Contents lists available at ScienceDirect

Computer-Aided Design

journal homepage: www.elsevier.com/locate/cad

Bidirectional Evolutionary Structural Optimization (BESO) based design method for lattice structure to be fabricated by additive manufacturing*

Yunlong Tang, Aidan Kurtz, Yaoyao Fiona Zhao *

Department of Mechanical Engineering, McGill University, 817 Sherbrooke Street West, Montreal, QC, Canada H3A 0C3

HIGHLIGHTS

- Both functional roles of solid volume and skin structure are considered.
- Lattice orientation is introduced that may be adjusted to improve performance.
- Increased speed of lattice frame generation.
- Structural stiffness is increased by the proposed optimization algorithm.

GRAPHICAL ABSTRACT

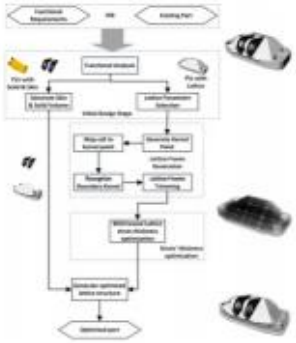

ARTICLE INFO

Keywords:
Additive manufacturing
Design method
Lattice structure
Optimization
Functional surface
Functional volume

ABSTRACT

Unlike traditional manufacturing methods, additive manufacturing can produce parts with complex geometric structures without significant increases in fabrication time and cost. One application of additive manufacturing technologies is the fabrication of customized lattice-skin structures which can enhance performance of products while minimizing material or weight. In this paper, a novel design method for the creation of periodic lattice structures is proposed. In this method, Functional Volumes (FVs) and Functional Surfaces (FSs) are first determined based on an analysis of the functional requirements. FVs can be further decomposed into several sub-FVs. These sub-FVs can be divided into two types: FV with solid and FV with lattice. The initial design parameters of the lattice are selected based on the proposed guidelines. Based on these parameters, a kernel based lattice frame generation algorithm is used to generate lattice wireframes within the given FVs. At last, traditional bidirectional evolutionary structural optimization is modified to optimize distribution of lattice struts' thickness. The design method proposed in this paper is validated through a case study, and provides an important foundation for the wide adoption of additive manufacturing technologies in the industry.

Abbreviations: AM, Additive Manufacturing; BESO, Bidirectional Evolutionary Structural Optimization; BNF, Backus Normal Form; DFAM, Design For Additive Manufacturing; ESO, Evolutionary Structural Optimization; FEA, Finite Element Analysis; FS, Functional Surface; FV, Functional Volume; RBE, Rigid Body Element; SMS, Size Matching and Scaling.

* This paper has been recommended for acceptance by C.L. Wang and Y. Chen.

* Corresponding author. Tel.: +1 514 398 2523; fax: +1 514 398 4476.

E-mail addresses: tang.yunlong@mail.mcgill.ca, tangyunlong2011@gmail.com (Y. Tang), aidan.kurtz@mail.mcgill.ca (A. Kurtz), yaoyao.zhao@mcgill.ca (Y.F. Zhao).

http://dx.doi.org/10.1016/j.cad.2015.06.001

1. Introduction

Additive Manufacturing is defined by ASTM as a "process of joining materials to make an object from 3D model data, usually layer upon layer, as opposed to subtractive manufacturing methodologies" [1]. Compared to traditional manufacturing methods, AM technologies have two remarkable advantages. Firstly, as opposed to casting or forging, customized manufacturing tools such as molds or dies are no longer needed, which significantly

Journal Publication D2

Elastic modulus of 316 stainless steel lattice structure fabricated via binder jetting process

Y. Tang[1], Y. Zhou[1], T. Hoff[1], M. Garon[2] and Y. F. Zhao*[1]

This study mainly evaluates the elastic modulus of 316 stainless steel lattice structures fabricated via binder jetting process. In this present research, both solid and lattice samples are designed and fabricated by binder jetting process for two different types of mechanical tests. Besides experimental study, a numerical model based on energy approach has been proposed to predict the effective elastic modulus of fabricated lattice samples. By comparing the calculated results of the proposed numerical model with the experimental results, the established model is proved to be validated. This numerical model can be used to determine the parameters of lattice structures fabricated by binder jetting process for desired mechanical properties. At the end, both advantages and disadvantages of the lattice structures fabricated by binder jetting process are analysed. Based on this analysis, the potential application and future research work are pointed out.

Keywords: Additive manufacturing, Lattice structure, Binder jetting process, Stainless steel

This paper is part of a Themed Issue on Additive manufacturing of metals for aerospace applications

Introduction

Cellular structure is a unique classification of the structure that is made up of an interconnected network of solid struts or plates that form the edge and faces of cells.[1] This kind of structure is common in nature, such as wood, animal bone and coral, which are able to bear a long term static or cyclical load. These natural cellular structures have been used by humans for centuries. Recently, some manmade cellular structures have been designed and fabricated for their multifunctionalities such as weight reduction, energy absorption, heat transfer, thermal protection and insulation.[1–5]

According to the geometrical configuration, cellular structures can be classified into many different types, such as foam, honeycomb and lattice structures. Among these different types of cellular structure, the lattice structure, which is a space truss structure composed of struts, nodes and other microelements with certain repeated arrangement in three-dimensional (3D) space, is the most attractive type of their inherent advantages. First, compared to those disordered cellular foam structures, only a small portion of lattice structures is needed to determine its properties for the high degree of order. Thus, this type of structure enables designers much more freedom to realise their design goals. Besides that, lattice structures can also be designed to be a stretching dominated structure for load bearing with high stiffness as well as a bending dominated structure for compliant mechanism with a large deformation. Because of the reasons mentioned above, lattice structures have high potential in a wide range of applications, such as automobile, aerospace, and medical devices and implants. However, the high manufacturing complexity is the biggest barrier for the wide application of lattice structures. Compared to those stochastic cellular foam structures, conventional fabrication processes of lattice structures, such as sheet metal forming, investment casting and metal wire bonding, are time and cost consuming. Moreover, because of manufacturing limitation, only the lattice structures with simple external geometry can be fabricated, which severely restricts the design freedom to achieve advanced functionalities.

Additive manufacturing (AM) is a material joining process whereby a product can be directly fabricated from its 3D model.[6] This innovative manufacturing technology enables the fabrication of parts with any shape, and thus has been used to fabricate the parts with both complex internal lattice and external geometry. Even though AM is a powerful manufacturing method with many unique capabilities, the qualification of additively manufactured parts is still one of the most serious hurdles for the wide adoption of this technology. To overcome this difficulty, significant research work has been done to improve the quality of parts fabricated by different types of AM processes. For example, some simulation and computational models have been proposed for different AM technologies such as fused deposition modelling[7–9] and powder bed fusion[10–12] to predict the quality factors of fabricated parts. Besides those simulation models, some research work has been done specifically focusing on the quality of lattice structures fabricated by different types of AM techniques. In the past few years, several different types of AM processes, such as electron beam melting (EBM),[13] selective laser melting (SLM),[14] direct laser metal sintering (DLMS)[15] and 3D printing (3DP),[16] have been employed to build metal lattice structure. These AM fabrication processes can be divided into two categories according to their fabrication principles. The first type is a powder bed fusion process where thermal energy is

[1]McGill University, Montreal, Canada
[2]Biomomentum Inc., Laval, Canada

*Corresponding author, email Yaoyao.zhao@mail.mcgill.ca

Journal Publication D3

A survey of the design methods for additive manufacturing to improve functional performance

Yunlong Tang and Yaoyao Fiona Zhao
Department of Mechanical Engineering, McGill University, Montreal, Canada.

Abstract

Purpose – This paper aims to provide a comprehensive review of the state-of–the-art design methods for additive manufacturing (AM) technologies to improve functional performance.

Design/methodology/approach – In this survey, design methods for AM to improve functional performance are divided into two main groups. They are design methods for a specific objective and general design methods. Design methods in the first group primarily focus on the improvement of functional performance, while the second group also takes other important factors such as manufacturability and cost into consideration with a more general framework. Design methods in each groups are carefully reviewed with discussion and comparison.

Findings – The advantages and disadvantages of different design methods for AM are discussed in this paper. Some general issues of existing methods are summarized below: most existing design methods only focus on a single design scale with a single function; few product-level design methods are available for both products' functionality and assembly; and some existing design methods are hard to implement for the lack of suitable computer-aided design software.

Practical implications – This study is a useful source for designers to select an appropriate design method to take full advantage of AM.

Originality/value – In this survey, a novel classification method is used to categorize existing design methods for AM. Based on this classification method, a comprehensive review is provided in this paper as an informative source for designers and researchers working in this field.

Keywords Design, Additive manufacturing, Review

Paper type Literature review

1. Introduction

Additive manufacturing (AM) is defined as a material joining process, whereby a product can be directly fabricated from its 3D model (ASTM, 2012). Compared to other manufacturing methods, such as machining or casting, the AM processes have the following unique capabilities. First, parts with an extremely complex shape can be built by the AM processes without increasing fabrication cost. Second, AM technologies are suitable for processing multiple materials either simultaneously or sequentially; therefore, parts with complex material compositions can be fabricated by this manufacturing method. Third, manufacturing preparation time can be substantially reduced, as the part is directly fabricated from its 3D model. These unique capabilities of AM technologies have brought great application potentials in several major industries such as aerospace (Angrish, 2014) and medical implants manufacturers (Jardini *et al.*, 2014). For example, in the aerospace industry, lightweight, strong and sometimes electrically conductive parts are more desired. The AM process can produce lightweight components by replacing solid material with lattice structures. Gradient electrical conductivity can also be achieved by changing the composition of materials at each fabrication point or each fabrication layer. Major airplane manufacturers such as Boeing, Airbus and Northrop Grumman have all identified AM to be an emerging and revolutionary manufacturing method (Bourell *et al.*, 2009).

However, it is also a challenge for most designers to take full use of the unique capabilities brought by AM for two main reasons. First, design rules or guidelines for traditional manufacturing methods are deeply rooted in designers' mind. These design rules and guidelines restrict designers to further improve the performance of products by designing an intricate part fabricated by AM processes. Second, lack of design and analysis tool for a complex structure is another obstacle for designers to take full use of the AM technologies. For example, even though the lattice structure fabricated by the AM process has been proved to have a better weight–stiffness ratio, it is difficult to model this type of structure with most existing feature-based computer-aided design (CAD) systems.

To overcome those difficulties mentioned above, the design methods to consider the unique capabilities of AM technologies are needed. These design methods are not only

The current issue and full text archive of this journal is available on Emerald Insight at: **www.emeraldinsight.com/1355-2546.htm**

Rapid Prototyping Journal
22/3 (2016) 569–590

[ISSN 1355-2546]
[DOI 10.1108/RPJ-01-2015-0011]

This paper is supported by National Sciences and Engineering Research Council of Canada Discovery Grant RGPIN 436055-2013, China Scholarship Council (201306020032)

Received 22 January 2015
Accepted 21 April 2015

Journal Publication D4

Journal of Cleaner Production 137 (2016) 1560–1572

Contents lists available at ScienceDirect

Journal of Cleaner Production

journal homepage: www.elsevier.com/locate/jclepro

A framework to reduce product environmental impact through design optimization for additive manufacturing

Yunlong Tang, Kieran Mak, Yaoyao Fiona Zhao*

Department of Mechanical Engineering, McGill University, Montreal, Canada

ARTICLE INFO

Article history:
Received 3 August 2015
Received in revised form
31 May 2016
Accepted 5 June 2016
Available online 10 June 2016

Keywords:
Sustainability
Environmental impact
LCA
Design optimization
Additive manufacturing
Binder-jetting

ABSTRACT

Additive Manufacturing (AM) also known as 3D printing technology has drawn increasing attention from the industrial world. It provides the capability of freeform fabrication to achieve high complexity as well as significant reduction of a supply chain which further enhances the profit margin for manufacturers. However, while claiming on the advantage on the environmental aspect, there is very limited research on the environmental impact of AM technologies. Most of existing environmental assessment models for AM processes are developed based on a general Life Cycle Assessment (LCA) framework. Due to the limited scope and boundary of these models, design results are usually taken as the input. These existing models may work well for traditional manufacturing processes. However, when it comes to AM process, these methods are no longer valid, since the design freedoms which may have a great impact on sustainability are always neglected. To deal with this issue, a general framework which can integrate a design stage in LCA for minimizing the product environmental impact of AM process in particular for binder-jetting process is proposed. The detailed description of each major stage of the proposed framework is presented. This framework has been applied to evaluate the environmental impact of fabricating an engine bracket by binder-jetting process. In this case study, a comparison of environmental impact between CNC and binder-jetting fabrication process is made. The result shows that binder-jetting consumes significantly less energy and produce less CO_2 to produce a topologically optimized part than CNC milling for the same product. This case study demonstrates a key role of design optimization in the proposed framework. This proposed framework can be further modified for other typical AM process in the future.

1. Introduction

In the past few decades, Additive Manufacturing (AM) also known as 3D printing technology has drawn increasingly attention from the industrial world. Compared with traditional subtractive manufacturing, AM has three main advantages. Firstly, AM provides the capability of freeform fabrication. It removes the traditional manufacturing restrictions and provides the design freedom for innovative product (Beaman et al., 1997). Secondly, AM can reduce the supply chain of fabrication and enhance the profit space for manufacturers (Huang et al., 2013; Morrow et al., 2007). Thirdly, AM technologies also provide a huge potential to reduce the environmental impact that normal manufacturing has (Luo et al., 1999).

Because of these promising characteristics AM has been applied in the industrial field for a long time and plenty of researches have been conducted on the aspect of process control, simulation and modeling. However, while claiming the advantage on the environmental aspect, there is very limited research on the sustainability aspect of this technology. Another issue is, because of the lack of well documented life-cycle data, it is difficult to conduct an accurate Life-Cycle Assessment (LCA) or sustainability analysis for AM technologies.

Most environmental impact assessment models or methods for AM is developed based on the general framework of LCA (shown in Fig. 1) (Rebitzer et al., 2004). With this method, quantified environmental impact data can be obtained based on new unit process models of various AM processes with different LCA boundaries and cut-offs. For example, a general process model and environmental evaluation method are proposed by Luo et al. (1999). Eco-indicator, collected and calculated by PRé Consultants of Netherlands is used to indicate the environmental impact of three different types of AM

* Corresponding author.
E-mail address: yaoyao.zhao@mcgill.ca (Y.F. Zhao).

http://dx.doi.org/10.1016/j.jclepro.2016.06.037
0959-6526/

Journal Publication D5

Lattice Structure Design and Optimization With Additive Manufacturing Constraints

Yunlong Tang, Guoying Dong, Qinxue Zhou, and Yaoyao Fiona Zhao

***Abstract*—Lattice structures with different desired physical properties are promising for a broad spectrum of applications. The availability of additive manufacturing (AM) technology has relaxed the fabricating limitation of lattice structures. However, manufacturing constraints still exist for AM-fabricated lattice structures, which have a significant influence on the printing quality and mechanical properties of lattice struts. In this paper, a design and optimization strategy is proposed for lattice structures with the consideration of manufacturability to ensure desired printing quality. The concept of manufacturable element is used to link the design and manufacturing process. A metamodel is constructed by experiments and the artificial neural network to obtain the manufacturing constraints. Sizes of struts are optimized by a bidirectional evolutionary structural optimization-based algorithm with these manufacturing constraints. An arm of quadcopter is redesigned and optimized to validate the proposed method. Its result shows that optimized heterogeneous lattice structures can improve the stiffness of the model compared to the homogeneous lattice structure and the original design. Both the Von-Mises stress and the maximum displacement are reduced without increasing the weight of designed part. And by considering the manufacturability constraints, the optimized design has been successfully fabricated by the selected additive manufacturing process.**

***Note to Practitioners*—Lattice structures might fail to be fabricated by the additive manufacturing technique if the designed model exceeds the processability of the machine. Our approach has the capability of considering the manufacturing constraints in the design and optimization process. We conducted experiments to investigate the manufacturability and proposed a method that can give the domain of the design variables for a selected manufacturing process. And we also designed an algorithm that can optimize the lattice structure inside the domain of design variables. It ensures that the lattice model can be successfully fabricated by the selected process and the performance is dramatically increased compared to the original design. Engineers can use our approach to optimize the lattice structure automatically without knowing the knowledge of optimization and manufacturability.**

***Index Terms*—Additive manufacturing (AM), design, lattice structure, manufacturing constraints.**

Manuscript received October 4, 2016; revised December 8, 2016; accepted January 23, 2017. This paper was recommended for publication by Associate Editor C. C. L. Wang and Editor Y. Chen upon evaluation of the reviewers' comments. This work was supported in part by the National Sciences and Engineering Research Council of Canada Discovery under Grant RGPIN 436055-2013, in part by the China Scholarship Council under Grant 201306020032, and in part by the Rio Tinto-Richard Evans Fellowship in Engineering. *(Corresponding author: Yaoyao Fiona Zhao.)*

The authors are with the Mechanical Engineering Department, McGill University, Montreal, QC H3A 0G4, Canada (e-mail: yaoyao.zhao@mcgill.ca).

Color versions of one or more of the figures in this paper are available online at http://ieeexplore.ieee.org.

Digital Object Identifier 10.1109/TASE.2017.2685643

I. Introduction

THE word "lattice" originally describes a framework or structure of crossed woods or metal strips and can be extended to regular geometrical arrangements of points or objects over an area and space [1]. In this paper, the lattice structure is defined as a mesoscale (0.1–10 mm) or microscale (<0.1 mm) truss-like structure which consists of interconnected struts and nodes with a certain repeated arrangement in 3-D space. In this sense, lattice structures can be regarded as a type of cellular structure on a mesoscale. Compared to other types of cellular structures including foams and honeycombs, lattice structures are more flexible to achieve a wide range of different desired physical properties, such as high stiffness-weight ratio [2], low thermal expansion coefficient [3], negative Poisson ratio [4], and high heat dissipation rate through active cooling [5]. Moreover, it can also be designed as a bioimplant to enhance the ossesointegration as well as alleviating stress-shielding effect. Due to its outstanding performance, lattice structures have been used in a broad spectrum of applications, including bone and dental implants [6]–[8], ultralight structures [9], [10], energy absorbers [11], low thermal expansion structures [12], and conformal cooling [13].

Traditionally, lattice structures can be fabricated via casting, sheet metal forming, or wire bonding processes [14]. However, manufacturing constraints of these processes severely restrict the complexity of designed lattice structures. These processes can only be applied to fabricate lattice structures with few simple unit cell topologies in a regular shape on a macroscale. This manufacturing limitation has been relaxed by using additive manufacturing (AM) to fabricate lattice structures. By fabricating a part layer by layer, AM enables the design of complex structures without significantly increasing the cost. Thus, the geometrical freedom provided by AM greatly enlarges the design space of lattice structures. Lattice structures with multiscale complexities can be easily fabricated for a better functional performance. For instance, on a macroscale, conformal lattice structures [15] can be produced to fit a complex macroshape with a relatively smooth surface boundary. On a mesoscale or microscale, complex lattice unit cells have been designed and fabricated to achieve a given gradient of elastic properties [16]. However, it should also be noted that every manufacturing process has limitations. AM is no exception. In particular, some recent research has observed and studied on the manufacturing constraints of lattice structures fabricated by different AM processes. The manufacturability of gyroid lattice structures made of 316L stainless steel